Antiferromagnetic phase transitions in [gamma] Mn alloys by alloying

Bayri, Ali

Award date:
1993

Awarding institution:
University of Bath

Antiferromagnetic Phase Transitions in γ-Mn Alloys by Alloying

submitted by Ali Bayri

for the degree of PhD

of the University of Bath

1993

*

A. Bayri

ProQuest LLC
789 East Eisenhower Parkway
P.O. Box 1346
Ann Arbor, MI 48106-1346

Contents.

List of Figures

Abstract

γ-Mn alloys show a host of antiferromagnetic phase transitions. In this thesis we show that these phase transitions in some aspects can be explained in terms of alloying. We solve the Classical Heisenberg Model for some sophisticated non-collinear spin states in the presence of a finite number of impurities. The results suggest that the impurities can trap a local non-collinear arrangement of spins. By studying theoretically the Magnetic Diffuse Scattering for the particular clusters, after the addition of impurities, we showed that the diffuse peaks are centred at the Bragg peaks of the non-collinear spin structure. Thus we concluded that the alloying causes these phase transitions. We applied our model to three particular materials: MnNi, Mn_3Pt, and MnCu. The results are in agreement with experiments.

Chapter One

1.1 Introduction

In this thesis we will mostly deal with antiferromagnetic materials. In other words we are dealing with magnetism in solids. In order to understand magnetism in solids we need to know about the magnetic properties of a free atom or ion, since the behaviour may be different. This is due to the fact that, when we are dealing with the atomic case, we generally consider an isolated atom with no influence from its surroundings. On the other hand, when a solid is considered the effects of the surroundings can become very important. Thus the atomic properties of an atom do not necessarily survive in a solid. Since the atomic physics is strongest (this is because an ion in a crystal would be effected by the surroundings), firstly we must know the magnetism of a free atom or ion then we can attempt to understand the magnetism of solids.

An atom derives its magnetic moment from electrons. There are two sources from which the electron can obtain its magnetic moment. The electrons can orbit around the nucleus therefore there can be a magnetic moment associated with each orbiting electron. Classically, the angular momentum of a particle is a property that depends on the particle's linear momentum $\mathbf{p}$ and its displacement $\mathbf{r}$ from some prescribed origin. It is given by $\mathbf{L} = \mathbf{r} \wedge \mathbf{p}$. The quantum mechanical operator $\mathbf{L}$ corresponding to this observable derives its definition directly from the classical expression above, with $\mathbf{p}$ replaced by its corresponding gradient operator. The second source of the magnetic moment of electrons is based on the spin of the electrons. In contrast to the angular momentum, spin angular momentum does

not relate to a particle's coordinates or momenta, nor are the eigenstates of spin dependent on boundary conditions imposed in coordinate space. Spin is an internal property of a particle, like mass or charge. It is an extra degree of freedom attached to a quantum mechanical particle. Spin angular momentum is denoted by the symbol **S**. The Cartesian components of **S**, being angular momentum components, obey the commutation rules $[\mathbf{S}_i, \mathbf{S}_j] = i\hbar\epsilon_{ijk}\mathbf{S}_k$. The spin magnetic moment of the electron has a constant magnitude. In a magnetic field the eigenstate of the spins can only be either parallel or antiparallel to the field. It may readily be shown that the spin is a consequence of the relativistic nature of the electron. Consider the Dirac equation, which describes the relativistic motion of an electron or positron by means of a wave function having four components. In the non-relativistic limit the electronic part of this equation may be separated by means of the Fold-Wouthuysen transformation to give an equation for the two component wave function describing the electron alone. In this limit the 4x4 γ matrices reduce to 2x2 Pauli spin matrices[1]. Now we can say that an atom derives its magnetic moment from electrons, which obtain their magnetic moment from two sources, called the spin and orbital angular momentum.

The resultant magnetic moment of an atom is then a special combination of these two magnetic moments (angular and spin). This combination is accomplished according to Hund's third rule in free atom and ions[2] (we will see later on that the Hund's rules are the consequences of the exchange interactions). However, when a solid is considered the situation is completely different. (Here one can look at some particular energies in free atom and in a crystal, in order to see that the situation does not remain unchanged. For examples: Intraatomic Coulomb repulsion U of Eq(1.11) is up to 10 eV whereas the energy per itinerant electron in a metal due to

Coulomb interaction is about 1 eV. Although intraatomic exchange energy is about 0.3 to 3 eV, direct inter atomic exchange energy is about 0.1 eV and 1 eV for 3d and 4f electrons respectively. And so on). The solid as a whole can have a net magnetic moment. In studying the magnetic properties of any solid, it is important to know which magnetic atoms are present and how they are situated in the lattice. One can then focus attention on each crystallographically different type. However the magnetic properties of a given atom are usually profoundly influenced by the electric fields of neighbouring atoms, so that it is not usually sufficient to know which atoms are present. It is necessary to know, also, the details of the environment of the atoms. In this study we mainly consider the case of transition metal alloys. Now we will try to understand the magnetism of these materials and see that the magnetism is not the same as in the atomic case.

These metals have partly filled 3d shells. The measured magnetic moments of these metals are very close to that given by the spin contribution alone. In order to understand this point we should review the wavefunction of electrons around a nucleus and take the crystal field into account. The wave function of a single electron under a central force is given by

$$\psi_{nlm} = R_{nl}(r)Y^m{}_l(\theta, \phi) \tag{1.1}$$

the first part of the right hand side of this equation is the radial part and its properties are beyond our scope, but it can be found in any quantum mechanical text book[3]. Our interest is in the second part which is known as the spherical harmonics in the literature. The d-electrons are of special interest here. The eigenfunctions of these electrons are those given in (1.1) with $n = 3$, $l = 2$, and they can be spec-

ified by a single index $m = m_l$, $m = 0, \pm 1, \pm 2$. The expressions for the spherical harmonics $Y_2{}^m$ will be of main interest to us here as follows:

$$Y_2{}^{\pm 2} = (\frac{1}{4})\sqrt{(\frac{15}{2\pi})} \sin^2\theta \exp(\pm i2\phi),$$

$$Y_2{}^{\pm 1} = \mp(\frac{1}{2})\sqrt{(\frac{15}{2\pi})} \sin\theta\cos\theta \exp(\pm i\phi),$$

$$Y_2{}^0 = (\frac{1}{2})\sqrt{(\frac{5}{4\pi})}(3\cos^2\theta - 1) \qquad (1.2)$$

These expressions are complex; if we wish to have real wave functions, we can combine pairs of functions having the same $|m|$. This is possible for the free ion, because all functions ψ_m, $m = 0, \pm 1, \pm 2$ are degenerate. Having performed this we get a set of new functions

$$d_{xy} = (\frac{1}{i\sqrt{2}})(\psi_2 - \psi_{-2}) = R(r)\sqrt{(\frac{15}{4\pi})}\frac{xy}{r^2},$$

$$d_{xz} = -(\frac{1}{\sqrt{2}})(\psi_1 - \psi_{-1}) = R(r)\sqrt{(\frac{15}{4\pi})}\frac{xz}{r^2},$$

$$d_{yz} = (\frac{1}{i\sqrt{2}})(\psi_1 + \psi_{-1}) = R(r)\sqrt{(\frac{15}{4\pi})}\frac{yz}{r^2},$$

$$d_{x^2-y^2} = (\frac{1}{\sqrt{2}})(\psi_2 + \psi_{-2}) = R(r)\sqrt{(\frac{15}{16\pi})}\frac{(x^2-y^2)}{r^2},$$

$$d_{z^2} = \psi_0 = R(r)\sqrt{(\frac{5}{16\pi})}\frac{(2z^2 - x^2 - y^2)}{r^2} \qquad (1.3).$$

called Cubic Harmonics. These functions are sketched in Fig(1.1) with the radial part R(r) omitted. The similarity of the functions d_{xy}, d_{xz}, d_{yz}, which may be defined by a common symbol t_{2g}, is seen at first sight; the remaining two, which may be denoted e_g, are also inter-related, although this is not so obvious. Once we have understood these properties of d electrons, we can now talk about the concept, known as the 'quenching of the orbital angular momentum' which is observed in the

first transition metal series where the crystal field effects (up to 5 eV) dominate the spin-orbit coupling (up to 1 eV), but not the Coulomb interactions (around 10 eV).

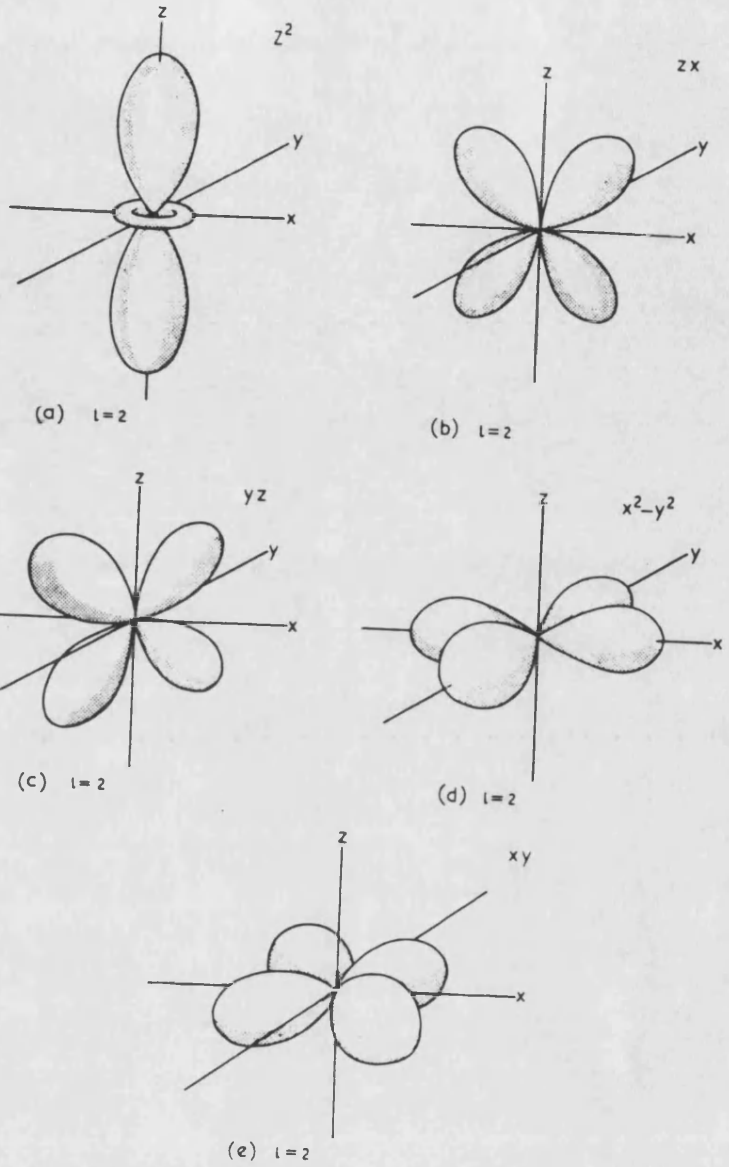

Fig 1.1 Orientations of 3d electrons

1-2 Quenching of the Orbital Angular Momentum

The first transition elements have an incomplete 3d shell and two 4s electrons. In a compound they lose their outer valence (4s) electrons (Here we should point out that the situation is not so simple, especially for a group of the d and f block elements, it is evident that these atoms have more than one shell containing electrons

of roughly equivalent energies, even though these shells generally have quite different shapes and spatial distributions. When we bring the atoms together in such a way that their outer orbitals interact and in the case of the d and f blocks that we should not consider the interaction of the valence s (or p) orbitals in isolation. For example, if the 4s orbitals in Cu(29) form the delocalised states in the metal, we should not be surprised if the 3d orbitals are also influential, for we know from the atomic states that these orbitals have somewhat similar energies). Thus, the 3d,electrons which are responsible for magnetism now become outermost electrons and they are subject to a strong crystal field due to neighbouring ions. Firstly we will discuss the role of the crystal field. For simplicity we assume the crystalline electrostatic potential to be of the following form:

$$V = Ax^2 + By^2 + Cz^2 \tag{1.4}$$

If the electron wave function is ψ, then we have

$$\Delta\epsilon = \int\int\int_{-\infty}^{\infty} \psi^* eV\psi dxdydz \tag{1.5}$$

as the interaction energy. For illustrative purpose, let us take the p state. Three wave functions corresponding to the degenerate p state are

$$\psi_A = xf(r) \quad \psi_B = yf(r) \quad and \quad \psi_C = zf(r) \tag{1.6}$$

Substituting these wave functions into Eq(1.5) we find

$$\begin{aligned} \Delta\epsilon_A &= AI_1 + (B+C)I_2 \\ \Delta\epsilon_B &= BI_1 + (C+A)I_2 \\ \Delta\epsilon_C &= CI_1 + (A+B)I_2 \end{aligned} \tag{1.7}$$

where $I_1 = e\int\int\int x^4|f(r)|dxdydz$ and $I_2 = e\int\int\int x^2y^2|f(r)|dxdydz$. It is obvious that the value I_1 is the same if x is replaced by y or z and the value I_2 is the same if xy is replaced by yz or zx.

From Eq(1.7) we see that the energies represented by $\Delta\epsilon_{A,B,C}$ will be different if A, B, and C are different. In other words, the 2L+1 levels which have the same energy (degenerate levels) in a free atom are split up in a crystalline field. When the energy split, that is, $\Delta\epsilon_A - \Delta\epsilon_C$ for example, is large, it will produce two important effects. Firstly, the spin-orbit coupling is broken up so that S and L will be separately quantised in the direction of the field. Secondly, the three components of orbital angular momentum L_x, L_y, and L_z are essentially quenched by the crystalline field. Here we will give a brief explanation of what is meant by quenching.

In a free atom, the 2J+1 levels which have the same energy in the absence of a magnetic field will have different energies in the presence of an applied field. Whenever there is an energy difference , there is a difference in population as demanded by the Boltzmann statistics. Without the field, the 2J+1 levels ranging from -J to +J are equally populated. The effect of magnetic field is to bring about a difference in energy and in turn a difference in population of the states corresponding to different J values. In the presence of a strong crystalline field, as discussed earlier, the S vector and the L vector are decoupled so we treat them separately. Since the spin is not coupled directly to the crystalline field, the S vector is not affected. However, so far as the orbital momentum is concerned, the effect of the crystalline field is to split the levels, the lowest of which then becomes a single ground state. For example: for L=1, one state, say ψ_C, becomes the ground state and the other

two states, say ψ_A and ψ_B, become excited states. From here it is not so difficult to show that the expectation values of L_z, L_x, and L_y are identically zero for ψ_C[4]. That means, even though the state ψ_C has a nonvanishing value of $L = 1$, the time average of the projection of the orbital momentum vector upon a specified axis is zero. Under such circumstances, the resultant magnetic moment J can be replaced by S. This is equivalent to saying that we have a non-magnetic orbital state or the orbital momentum is quenched. Although it is outside of our scope, we should remind ourselves that the spin quenching is also possible in a strong crystal field[5]. This situation is found e.g. in the $4d^n$ and $5d^n$ series, where covalency mixing plays a more important role (in this series the crystal field and spin-orbit effects become comparable with the Coulomb couplings). It is obvious from these examples that the purely ionic model becomes inadequate. However when we considered the rare earth metals the situation is different from the transition metals.

These metals have partially filled 4f shells which lie inside the $5s^2p^6$ shells. The magnetism comes from these shells, which are so far inside the atom that they are almost entirely unaffected by the crystal field. The crystal field for these materials are relatively small (up to 10^{-1} eV). The Coulomb interactions between the electrons within the central ion remain dominant, for these involve energies of 5 to 15 eV. The spin orbit coupling (0.3 to 5 eV) exercises a greater control over the orientations of L and S then those the crystal field. (On the other hand for the first transition series the crystal field effects(up to 10 eV) dominate the spin orbit coupling (up to 1 eV) but not the Coulomb interactions, so that the separate one electron momenta still couple together to give resultant L and S but their directions are strongly influenced by the crystal fields). So by comparing these two series of

metals one can easily say that the d electrons are not well localised in a crystal and they are different from the atomic orbitals. On the other hand the f electrons are very well localised in the crystal and the localised orbitals would be practically identical with the original atomic orbitals and the magnetism of this type of crystal would be based on magnetic moments of individual atoms. This is the direct consequence of the f shells which are surrounded by $5s^2p^6$ shells and they are not very strongly affected by crystal field.

So far we have discussed the origin of magnetism of atoms and free ions, and we compared the magnetism in transition metals and the rare earths. We saw that magnetism of atoms may be changed when the atoms are in a crystal (for example the first transition metal series) but sometimes it remains unchanged as in the case of rare earth series. After having this elementary knowledge we can give a very general way of classifying the materials.

All material can be classified into different magnetic groups in two ways. First of all a pure classification is possible, on the basis of some macroscopic characteristic of the substance (for instance, its susceptibility). The value of this quantity, or its observed dependence on different physical factors, makes possible a classification not based on the physical nature of either the atomic carriers of magnetism or interaction between these which determine the type of magnetic state. The second alternative is a physical classification, in which physical factors are taken into account as completely as possible, especially the nature of the atomic carriers of magnetism and the character of the interaction between them. We will not go into the details of this classification. Our concern is antiferromagnetic materials, which

have no net magnetic moment in an applied field, but the magnetic moments of individual atoms exhibit an ordered structure. The magnetic properties of given materials can be explained by analysing their spins. In attempting to explain the properties of spin, many different types of spin models have been introduced. We now briefly look at the physics behind these models.

1-3 The Exchange Interaction

In this section we will look at the questions of; why the spins of two electrons (or two ions if they have a net magnetic moment) sometimes want to be parallel and sometimes antiparallel to each other? What is the origin of the exchange interactions? and so on. Firstly we will discuss the origin of the exchange.

1-3-1 **Direct Exchange.** In order to understand this interaction we will consider a system of two electron which are localised about the same nucleus. Therefore this interaction is related to intraatomic exchange, which is distinct from interatomic exchange where the interacting electrons are localised about different nuclei. We turn briefly to the latter at the end of this section.

In the intraatomic case two situations can be distinguished: Either the electrons are in the same orbital, say $\psi_u(r)$ or they are in different orbitals on the same atom, say $\psi_u(r)$ and $\psi_v(r)$. There are also two other distinct alternatives: The directions of the electrons' spin are usually either parallel or antiparallel (these are called the triplet and singlet states, respectively).

There are actually two interactions taking place between these two electrons. The first is caused by the Coulomb force, which in this case leads to the mutual

repulsion of like charges. The second, which is a purely magnetic interaction, is from the Amperian force between the magnetic dipoles that each electron possesses by virtue of its spin. In the case of two electrons localised about the same nucleus, such as we are considering, the magnetic interaction between them is quite negligible compared with the electrostatic one.

Concerning this Coulomb energy, we find that because of the requirement of antisymmetry imposed by Pauli's principle (since electrons are fermions) a new term appears; since it has no classical counterpart, it presents conceptual difficulties, but it can be regarded as a correction or modification of the Coulomb term produced by the Pauli principle. It is known as the direct exchange interaction, and it is peculiar to systems consisting of identical fermions in such proximity that their spheres of influence overlap so that there is a coupling between them. Its magnitude depends in fact, upon the amount of overlap of the wave functions of the interacting particles, as well as upon the relative orientations of their spins.

Let us consider separately the two cases distinguished above in which the electrons are: (a) in the same orbital, and (b) in different orbitals on the same atom. We see that in case (a), the system can only exist in the singlet state-as dictated by Pauli's principle. In this case there can be no evidence of an exchange interaction here because no other distinguishable configurations are possible. However, in case (b) an energy difference appears between the singlet and the triplet configurations.

Let us look at case (a) first: when the two electrons are in the same orbital, we know from the Pauli principle that they must have antiparallel spins. In that

case the two-particle wave functions for the system can be written as

$$\phi_u(\mathbf{r},\sigma) = \psi_u(\mathbf{r})\chi_\alpha(\sigma)$$

$$\phi_v(\mathbf{r},\sigma) = \psi_u(\mathbf{r})\chi_\beta(\sigma) \tag{1.8}$$

Here $\psi_u(\mathbf{r})$ is the atomic orbital in which the two electrons are located. The ϕ_u and ϕ_v correspond to states of identical energy, say E_u, so that the total energy of the system with the Coulomb repulsion turned off is just $2E_u$. The total wave function is then can be written as

$$\psi_N = \frac{1}{\sqrt{2}} \begin{vmatrix} \phi_u(\mathbf{r}_1,\sigma_1) & \phi_v(\mathbf{r}_1,\sigma_1) \\ \phi_u(\mathbf{r}_2,\sigma_2) & \phi_v(\mathbf{r}_2,\sigma_2) \end{vmatrix} \tag{1.9}$$

which when written out in full becomes

$$\psi_N = \frac{1}{\sqrt{2}}\psi_u(\mathbf{r}_1)\psi_u(\mathbf{r}_2)[\chi_\alpha(\sigma_1)\chi_\beta(\sigma_2) - \chi_\alpha(\sigma_2)\chi_\beta(\sigma_1)] \tag{1.10}$$

If we now imagine the electrostatic force between the two electrons to be turned on, with the result that the system is perturbed slightly, the methods of first-order perturbation theory can be used to give an expression for the extra energy U produced in the system by this Coulomb repulsion between the electrons. In the usual quantum fashion, this expression for U turns out to be

$$U = \int\int \psi_N^* \frac{e^2}{r_{12}} \psi_N d\mathbf{r}_1 d\mathbf{r}_2 \tag{1.11}$$

where $\mathbf{r}_{12}$ is the separation between the electrons, and $d\mathbf{r}_1$, $d\mathbf{r}_2$ are the elemental volumes of configuration space. Substitution of Eq.(1.10) into Eq.(1.11) gives for U

$$\frac{1}{2}\sum_{\sigma_1,\sigma_2=\pm 1}[\chi_\alpha(\sigma_1)\chi_\beta(\sigma_2) - \chi_\alpha(\sigma_2)\chi_\beta(\sigma_1)]\int\int \psi_u^*(\mathbf{r}_1)\psi_u^*(\mathbf{r}_2)\frac{e^2}{r_{12}}\psi_u(\mathbf{r}_1)\psi_u(\mathbf{r}_2)d\mathbf{r}_1 d\mathbf{r}_2 \tag{1.12}$$

which is just

$$U = \int\int \psi_u^*(\mathbf{r}_1)\psi_u^*(\mathbf{r}_2)\frac{e^2}{r_{12}}\psi_u(\mathbf{r}_1)\psi_u(\mathbf{r}_2)d\mathbf{r}_1 d\mathbf{r}_2 \tag{1.13}$$

This makes use of the fact that the bracketed spin factor in Eq.(1.10) is unity when σ_1 and σ_2 have opposite signs, and zero otherwise. With the Coulomb repulsion turned on the total energy of the system is just $2E_u + U$.

Next let us look at the case (b): When the two electrons are located on different orbitals on the same atom, there is no restriction upon the electrons' spin alternatives; they can be either parallel or antiparallel. The result is that there are now four one-particle wave functions corresponding to the possible configurations which the electrons can adopt, that is $\psi_u(r)\chi_\alpha(\sigma)$, $\psi_u(r)\chi_\beta(\sigma)$, $\psi_v(r)\chi_\alpha(\sigma)$ and $\psi_v(r)\chi_\beta(\sigma)$. Correspondingly, four possible antisymmetrical total wave functions can be written down. If this quartet is denoted by ψ_I, ψ_{II}, and so forth, then the first possibility

$$\psi_I = \frac{1}{\sqrt{2}}\begin{vmatrix} \psi_u(\mathbf{r}_1)\chi_\alpha(\sigma_1) & \psi_v(\mathbf{r}_1)\chi_\beta(\sigma_1) \\ \psi_u(\mathbf{r}_2)\chi_\alpha(\sigma_2) & \psi_v(\mathbf{r}_2)\chi_\beta(\sigma_2) \end{vmatrix} \tag{1.14}$$

and the others are obtained by obvious permutations. Thus

$$\psi_{II} = \frac{1}{\sqrt{2}}\begin{vmatrix} \psi_u(\mathbf{r}_1)\chi_\beta(\sigma_1) & \psi_v(\mathbf{r}_1)\chi_\beta(\sigma_1) \\ \psi_u(\mathbf{r}_2)\chi_\beta(\sigma_2) & \psi_v(\mathbf{r}_2)\chi_\beta(\sigma_2) \end{vmatrix} \tag{1.15}$$

$$\psi_{III} = \frac{1}{\sqrt{2}}\begin{vmatrix} \psi_u(\mathbf{r}_1)\chi_\alpha(\sigma_1) & \psi_v(\mathbf{r}_1)\chi_\alpha(\sigma_1) \\ \psi_u(\mathbf{r}_2)\chi_\alpha(\sigma_2) & \psi_v(\mathbf{r}_2)\chi_\alpha(\sigma_2) \end{vmatrix} \tag{1.16}$$

and

$$\psi_{IV} = \frac{1}{\sqrt{2}}\begin{vmatrix} \psi_u(\mathbf{r}_1)\chi_\beta(\sigma_1) & \psi_v(\mathbf{r}_1)\chi_\alpha(\sigma_1) \\ \psi_u(\mathbf{r}_2)\chi_\beta(\sigma_2) & \psi_v(\mathbf{r}_2)\chi_\alpha(\sigma_2) \end{vmatrix} \tag{1.17}$$

With the electrostatic force between the electrons turned off these represent four possible states of the system, but they all have the same energy, which is $E_u + E_v$.

The real wave functions of the system can be formed by linear combination of these four starting functions. The best combinations to represent the system are ψ_{III}, ψ_{II}, $\frac{1}{\sqrt{2}}(\psi_I + \psi_{IV})$, and $\frac{1}{\sqrt{2}}(\psi_I - \psi_{IV})$.

Each of these four combinations are antisymmetric under a general transformation of both spin and positional coordinates as of course it has to be to satisfy the Pauli principle.

When the Coulomb repulsion is switched on, we can see that there is an energy change between these states which is

$$\begin{aligned} &\int\int \psi_u^*(\mathbf{r}_1)\psi_v^*(\mathbf{r}_2)\frac{e^2}{r_{12}}\psi_u(\mathbf{r}_1)\psi_v(\mathbf{r}_2)d\mathbf{r}_1 d\mathbf{r}_2 \\ \pm &\int\int \psi_u^*(\mathbf{r}_1)\psi_v^*(\mathbf{r}_2)\frac{e^2}{r_{12}}\psi_u(\mathbf{r}_2)\psi_v(\mathbf{r}_1)d\mathbf{r}_1 d\mathbf{r}_2 \end{aligned} \tag{1.18}$$

and has, therefore, two values.

The first term in this expression is just the Coulomb energy U. The second term is known as the exchange integral and is conventionally represented by J. The total energy of the system is then $E_u + E_v + U \pm J$. The lower energy state, obtained by taking the negative sign with J, corresponds to the case when the electrons' spin are parallel. It is triply degenerate. The state of higher energy, given by taking the positive sign with J, corresponds to the case when the electrons' spin are opposed. Therefore the triplet has always lower energy then the singlet. This is just the origin of Hund's rule which says that the ground state of an atom has maximum multiplicity.

It is better to regard the integral J as a correction to the Coulomb energy U resulting from a coupling between spins of contiguous electrons. Nowadays it is

called the exchange coupling. To look further at this viewpoint, which regards J as a correction to U, consider what happens as the two electrons approach very close to each other so that $(\mathbf{r}_2 - \mathbf{r}_1) \rightarrow 0$. As this happens each of wavefunctions ψ_{III}, ψ_{II}, and $\frac{1}{\sqrt{2}}(\psi_I + \psi_{IV})$ which corresponds to triplet state, tend to zero since their common orbital factor is zero when $\mathbf{r}_1 = \mathbf{r}_2$. (This contrast with the singlet state $\frac{1}{\sqrt{2}}(\psi_I - \psi_{IV})$ which does not tend to zero in such circumstances). Obviously this means that no two electrons of like spin may occupy the same position in space. This can be made even more clear by imagining one electron to pass the other in space so that $\mathbf{r}_2 - \mathbf{r}_1$ goes through zero and becomes negative. $|\psi(\mathbf{r}_1, \mathbf{r}_2)|^2$ is proportional to the probability of finding one electron at $\mathbf{r}_1$ and the other at $\mathbf{r}_2$. Its form will be having a sharp minimum of zero at $\mathbf{r}_1 = \mathbf{r}_2$. So two electrons of like spin can not occupy the same energy state, which is the consequence of the Pauli principle. The singlet state on the other hand is the opposite of the triplet state. The probability function has a sharp maximum at $\mathbf{r}_1 = \mathbf{r}_2$. So the triplet pays less Coulomb.

To summarise we can say that when the electrostatic interaction between two electrons localised about the same nucleus is switched on, an extra energy term is added to the system due to the mutual repulsion between the electrons. Its value is U+J if the electrons' spin are antiparallel and U-J if they are parallel. It is important to realise that the arguments relate entirely to the exchange interaction appearing between two electrons localised about the same nucleus. The orbitals $\psi_u(\mathbf{r})$ and $\psi_v(\mathbf{r})$ corresponding to different energy states-but associated with the same nucleus-are automatically orthogonal. We found above that the energy of the triplet state lies below that of the singlet one. It can be shown that this is a direct consequence of the orthogonality of the electrons' wave functions. When

the electrons are localised about separate nuclei, as in the hydrogen molecule, for example, the non-orthogonality plays a vital role[6].

1-3-2 The Formalism of Exchange. It is now known that, the exchange is related to the electrons' spin. What we now want is to express the energy $U \pm J$ in terms of spins. Pauli showed that the spin is a vector quantity. In accordance with this, we shall let the two electrons under consideration have the vector spin operator $\mathbf{s}_1$ and $\mathbf{s}_2$. The electrostatic energy between two electrons is $U \pm J$. If we wish to introduce a factor containing $\mathbf{s}_1.\mathbf{s}_2$ to replace the spin-dependent part $\pm J$, we must modify it. Various textbooks show how to modify this[7].. We will use the conventional way of this representation, which is

$$U - \frac{1}{2}J[1 + \frac{4\mathbf{s}_1.\mathbf{s}_2}{\hbar^2}] \tag{1.19}$$

This expression can be extended to a system containing more than two electrons. In this case the exchange term can be written as

$$-\frac{1}{2}\sum_{i<j=1}^{N} J_{ij}[1 + \frac{4\mathbf{s}_i.\mathbf{s}_j}{\hbar^2}] \tag{1.20}$$

in which the spin-dependent term is just

$$-\frac{2}{\hbar^2}\sum J_{ij}(\mathbf{s}_i.\mathbf{s}_j) \tag{1.21}$$

This expression is known as the Dirac Hamiltonian, and its origin is between individual pairs of electrons. A simplification of the Dirac Hamiltonian results from the fact that the couplings between the unpaired electrons in the same ion are strong. They are positive and give each ion, in the ground state, the maximum spin moment consistent with the Pauli exclusion principle.

So far all the formalism leads to a parallel alignment of electrons spins. When does the antiparallel alignment occur? This alignment occurs as a result of standard kinetic exchange[8]. The energy gain per electron is of order t^2U^{-1}, where t is hopping term and U is the Coulomb repulsion of two electrons.

The simple illustration of this exchange is as follows: Let us take two lattice sites with two electrons and find out the ground state if

a) S^z=1 (Triplet)

b) S^z=0 (Singlet)

Let us consider the case a) first. Due to the Pauli exclusion principle there is no hopping of electrons (t=0 initially). Then the ground state energy is $E = 2x0 = 0$, as in Fig(1.2a)

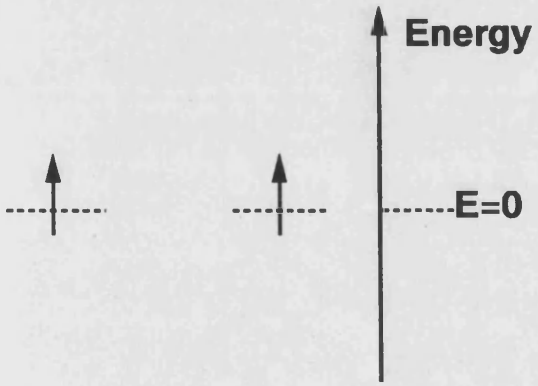

Fig. 1.2a Triplet alignment

Now let us take the case b). If the Coulomb repulsion (U=∞) is infinite, then the ground state is $E = 0$ as in Fig(1.2b).

If the potential energy tends to ∞ but $U < \infty$, then the second order per-

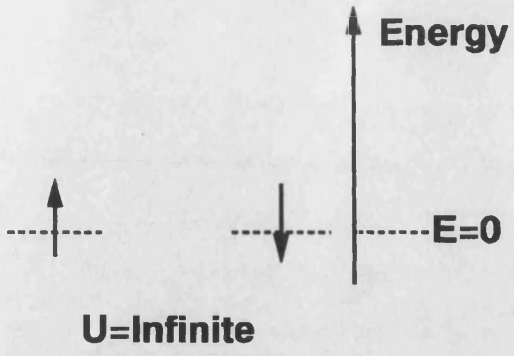

Fig. 1.2b Singlet with U=∞

turbation gives

$$\Delta E = -\frac{(matrix \quad elements)^2}{E_{ex} - E_0} = -\frac{t^2}{U}$$

as in Fig(1.2c). This is the situation when the singlet ordering is favourable as in the case of γ-Mn transition metal.

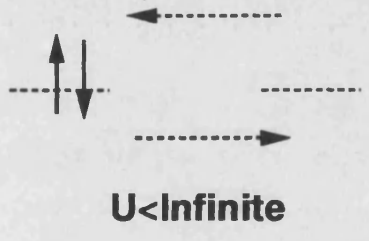

Fig. 1.2c Singlet alignment

Frequently, however, the context is rather the interaction between pairs of ions in which each constituent has a resultant spin. This case can still be worked within the above framework except that it is now concerned with a coupling between the resultant of all the electron spins in the ion. Suppose there are two ions labeled A and B, each having a number N of unpaired electron spins. Their total spin operators are $\mathbf{S}_A = \sum_A \mathbf{s}_i$ and $\mathbf{S}_B = \sum_B \mathbf{s}_j$, respectively, where i and j refer to the different atoms A and B. Assuming that pairs of electrons with one constituent on

each ion have the same exchange integral, say J_{AB}, then the expression (1.20) gives the exchange term for the pair of ions as

$$-\frac{1}{2}J_{AB}[N+\frac{4\sum_A \mathbf{s}_i.\sum_B \mathbf{s}_j}{\hbar^2}] \tag{1.22}$$

which is

$$-\frac{1}{2}J_{AB}[N+\frac{4\mathbf{S}_A.\mathbf{S}_B}{\hbar^2}] \tag{1.23}$$

This is the Heisenberg Hamiltonjan, and its spin-dependent term is evidently $-\frac{2}{\hbar^2}J_{AB}\mathbf{S}_A.\mathbf{S}_B$.

The preceding relates to an ion for which the individual spins of the electrons in a shell can be summed straightforwardly to give the total $\mathbf{S}(=\sum \mathbf{s}_i)$, and this implies that either the ion's total angular momentum is quenched or the spin-orbit coupling of the electrons in question is insignificant compared with their exchange interactions. The wide and often uncritical use of this Heisenberg Hamiltonian for ions is nevertheless, to be justified mainly by its success in accounting for a number of important phenomena and its simplicity. In this thesis we will use this Hamiltonian.

As we mentioned above, there are many exchange model, which were introduced in order to explain spin-spin interactions in materials. We now briefly look at these interactions

1-3-3 Other Types of Exchange Interactions

Type 1- **Direct Intraatomic Exchange Coupling.** Discovered by Heisenberg and Dirac, this is coupling between two electrons belonging to the same atom. As a result of the Pauli principle, electrons having spins parallel to some preferred

direction stay out of each others way to a greater extent then those having antiparallel ones. The Coulomb repulsion between electrons with parallel spins is, therefore, reduced in comparison with the antiparallel case.

Type 2- **Direct Interatomic Exchange Coupling.** Technically, whether the parallel or antiparallel spin alignment is energetically more favourable depends largely upon the degree of orthogonality of the wave functions describing the two interacting electrons. The truly orthogonal case occurs when the two electrons are in the same atom and always leads to the preference for parallel alignment as we already explained above. But as a degree of non-orthogonality is allowed into the problem, as in the case of electrons on different atoms for example, the end result depends more delicately upon the balance between certain terms. Calculation shows that in the majority of cases where the coupling between two electrons belonging to different atoms can be evaluated, the antiparallel alignment of their spins is preferred (the hydrogen molecule is the standard example[6]). This result is, of course, in direct contrast to the intraatomic case considered above.

A more physical view of the origin of this difference emerges from the realisation that, since in the molecular case the electrons are distributed around more than one ion core and are, therefore, inevitably more separated than in a comparable single-core case, their mutual interaction becomes relatively less important. In addition, since more than one nucleus is involved in this case, the relative importance of the interactions of the electrons with the ion cores is correspondingly increased. Both these influences tend to increase the importance of the interaction between the electrons and the ion cores. It is, therefore, perhaps not surprising that the

increase in the electrons' kinetic energy required by a rearrangement of the orbitals to give a parallel alignment of spins frequently outweighs the gain from the reduced Coulomb force between electrons. Consequently the antiparallel alignment is often found to be energetically favourable. This type of exchange coupling underlies the Heitler-London model of the hydrogen molecule and, hence, leads to the widely used concept of the covalent bond[6].

Type 3- **Indirect Interatomic Exchange Coupling.** The spins of two electrons localised on separate ions can be coupled over relatively large distance by means of an exchange coupling that acts between each localised spin and that of some intermediate electron. In this particular interaction this intermediary is a member of the itinerant class, so that the direct s-d exchange interaction is the basis of the whole mechanism since the itinerant and localised electrons have generally s and d shell atomic origins, respectively. It is an extension of the direct intraatomic coupling (Type 1) considered above. As Zener[9] pointed out, this Type 1 coupling was conceived to exist between the spins of two electrons localised in the same shell of an atom say the d shell. But it also exists between the spins of two electrons localised in different shells of the same atom say one from a d shell and one from an s shell. In the simple view of a metal the s electrons are itinerant, but Zener argued that the same Type 1 coupling will nonetheless exist between the total unbalanced spin of an ion (due to electrons in incomplete shells) and that of any nearby member of the itinerant class. However, the electron fluid has an important property: It is easily polarised by some local perturbation such as an excess charge or a local magnetic moment. Consequently, an ion possessing a net spin will be able in a metal to spin polarise the surrounding electron fluid by means of this direct s-d exchange

coupling. This region of spin polarised electrons can likewise couple to the spin of any other nearby ion, and thus a cooperative interaction results between the ionic spins in a metallic ferromagnet using the itinerant class as an intermediate medium. This is the indirect interatomic exchange coupling.

Type 4- **Interatomic Superexchange Coupling.** The superexchange was introduced when it became clear that in many nonmetalic solids there are strongly coupled spins localised on magnetic ions of a given species that are evidently very well separated from each other by ions of another species which is normally nonmagnetic. Examples of such compounds are MnSe, MnTe, or MnO. Anderson[10] has suggested that this interaction involves specifically an electron transfer from the normally nonmagnetic ion to a vacancy in a shell of the normally magnetic one. This would leave the previously nonmagnetic ion with an unbalanced spin, so that it would be paramagnetic and thus able to couple its spin with that of another nearby magnetic ion through the direct interatomic coupling (Type 2).

Type 5- **Direct s-d Exchange Coupling.** This interaction is known as the RKKY coupling[11]. In this model the electron fluid in the neighbourhood of the magnetic ion is imagined to be spin polarised with a parallel alignment to the ionic spin but with no particular refinement in the distribution of this polarisation about the ion. The RKKY result showed that this polarisation alternates in sign with increasing distance from the ion and they further showed that its amplitude decreases roughly as the cube of this distance. This oscillatory behaviour is the basis of the Friedel[12] oscillations.

Type-6 **Coupling Through s-d mixing.** These interactions are the concept

of resonant scattering. It can be said that an incident itinerant electron arriving in the ion's vicinity in opportune circumstances can be temporarily captured in pseudoatomic states around the ion. These are formed from the mixing (or hybridisation) of the outer orbitals of the ion with the delocalised orbitals containing the itinerant electrons. Any vacancies in the ion's inner shell give a net spin to the ion that couples by means of exchange with that of the incident electron, thus making the whole mechanism spin dependent.

Type 7- **Direct Itinerant Exchange.** We now turn to an exchange that is distinguished from the rest by the fact that no localised electrons are involved. It is the direct exchange coupling that occurs between itinerant electrons in a metal and that generally is called direct itinerant exchange. It occurred to early works looking for an explanation of ferromagnetism in pure metals[13] that just as the Type-1 effective coupling exists between the spin of electrons within an atom, so there should be an analogous coupling between spins of contiguous itinerant electrons in a metal. This would tend to give a parallel alignment to all the spins of the itinerant electrons and so make the electron fluid ferromagnetic. But they realised that such alignment could only be achieved at the expense of an increased kinetic energy for the system. It was argued, however that in a system of low itinerant electron concentration the exchange interaction is dominant and leads to ferromagnetic alignment of the spins.

As we mentioned above, we will use the Heisenberg model throughout this study. This model Hamiltonian puts one spin on each site of a lattice and has the spins interacting with a vector interaction. Although it is outside the scope of this study, the reader is reminded that this Hamiltonian has two limiting cases known

as the Ising model and the XY model. The coupling constant in one direction, say z, is taken to be different from those in the other directions. The Ising model has $J_x = J_y = 0$, whereas the XY model has $J_z = 0$[14]. The Heisenberg model itself is very difficult to handle, especially for the antiferromagnetic case. If we restrict our attention to the classical limit, which is the large spin limit of $S \to \infty$, the Quantum mechanics goes away and the problem is much simplified.

The reasons for taking the Classical limit of the Heisenberg model can be listed as follows. Firstly, this limit is easier to handle. Secondly, it explains much of the physical behaviour observed in some real materials. Thirdly, the materials we will consider have magnetic moments of about 2-3μ_B which is quite big compared with spin-half. All these reasons indicate that it is sometimes useful to take the Classical limit of this Hamiltonian use it to explain some of the observed properties of some real materials. We will now restrict our attention to those materials which we can most accurately describe using the Classical limit of the Heisenberg Hamiltonian. We should point out here that there are some other approaches to the same problem[39]. They are simply doing the band structure calculations. In other words they are using the itinerant model of electrons. Since the d electrons are not well localised this approach is not unacceptable. Crockford et all[39] for example calculated the magnetic moments of γ-Mn for three spin arrangements and found that the magnetic moment of Mn atom is close to experimental value. In addition to this they calculated the magnetic energy of these states and found that the energies of different phases are nearly degenerate. This result is in a good agreement with the classical Heisenberg prediction. This implies that itinerant electron effects do not significantly lift the degeneracy in γ-Mn. Moreover, Samson, Heine et all, and

Chana et al[40] found that itinerant electron model is usable for some materials(they call them as weak magnets) whereas for some other materials the Heisenberg model can describe the magnetism(they call these materials as strong magnets). However their calculations were about the disordered magnets. In other words they were interested in above the critical temperature. On the other hand, we are interested in mainly at the zero temperature where the magnetic moments are exist. So their calculations are not relevant to what we are doing. We are mainly interested about the fluctuations of spins. If we had used the itinerant model we would obtain some information about the fluctuations of the magnetic moments but this fluctuations would be the fluctuations of the magnitude of the spins which is not allowed in our model. In addition to all this, there is evidence[Endoh 19] for γ-Mn that the itinerant electrons do not play an important role. Thus by using the classical limit of the Heisenberg model at least we can have an indication about the observed behaviour in some real materials. First of all we will talk about the materials, which are mainly transition metal alloys, and the experiments themselves.

Transition metal alloys based on γ-Mn show very interesting behaviour. Manganese quenched into a face centre cubic structure exhibits type-I antiferromagnetism. This is a sequence oı ferromagnetic x-y layers which alternate in spin direction along the z-axis,as in Fig(1.3). The z-axis becomes inequivalent to the other Cartesian directions and the magnetism induces a huge tetragonal distortion of approximately six per cent parallel to the z-axis[15]. Neutrón scattering[16] shows that the spins align parallel to the z-axis where they are held in place by spin-orbit coupling. As we already mentioned the structure of γ-Mn is face centre cubic. Antiferromagnetism in f.c.c lattice is frustrated, with only a fraction of near-

est neighbours being allowed to be antiparallel. Now it is time that we should talk about frustrated antiferromagnets.

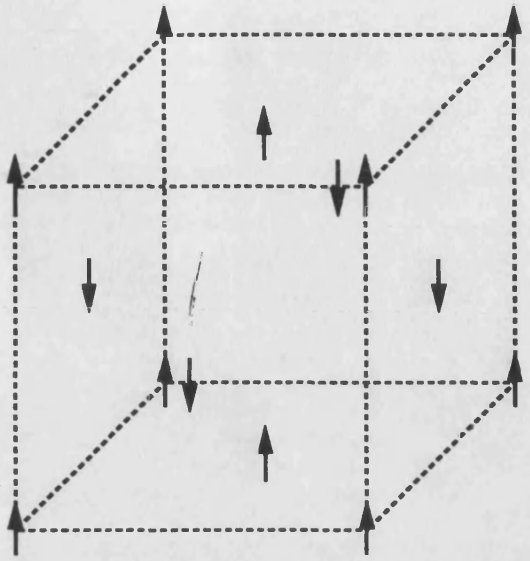

Fig. 1.3 Collinear spin Arrangement on the f.c.c

Geometrically frustrated lattices provide some of the most sophisticated and interesting types of antiferromagnet. The fundamental cause is that the frustration forces some of the bonds to gain less than their optimum energy. There is usually a variety of ways in which this loss can be spread amongst the different bonds, often leading to ground state degeneracy to leading order. This degeneracy is usually lifted on a smaller energy scale than that promoting the magnetism, and this then leads to the possibility of 'phase transitions' between different magnetic ground states caused by fairly small changes in the magnetic interactions. In particular, alloying a frustrated antiferromagnet can lead to such a phase transition at quite modest doping. The alloying is the main thing in our model. The frustrated antiferromagnetism can be appreciated in a simple example. In Fig(1.3) we are taking the triangular lattice as an example. For an antiferromagnetic triangular lattice the sum of the three spins

$(\mathbf{S}_1 + \mathbf{S}_2 + \mathbf{S}_3 = 0)$ must give zero spin. If we make two of the three spins, as shown in Fig(1.3), antiparallel to each other the third spin can not be made antiparallel to the first two spins. This is the simple picture of frustration. Since the f.c.c lattice is a collection of triangular lattice planes, the frustration can be appreciated in the f.c.c lattice as well.

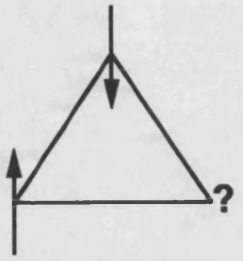

Fig. 1.4 Simple Picture of Frustration in the Triangular lattice

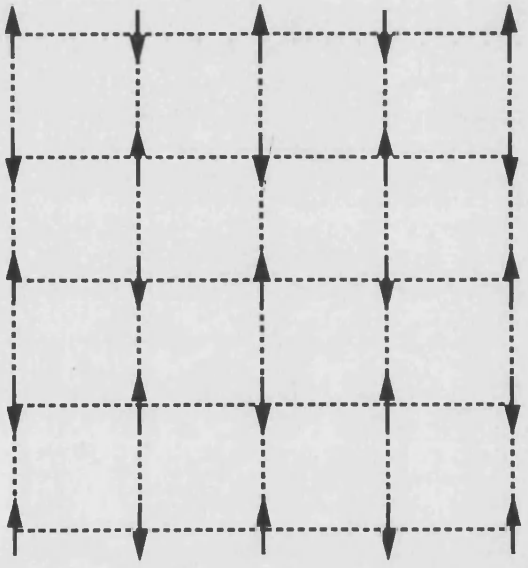

Fig. 1.5 Projection of Type-I ordering onto a square lattice

Some of the magnetic structures of f.c.c lattice can be projected onto two dimension without changing the direction of magnetic moments. For example, it is easy to appreciate that Type-I ordering (Fig(1.3)) can be projected onto an x-y plane

yielding a square lattice with $J_1 = 2J_2$, since one-third of the nearest neighbours become next nearest neighbours in this projection. Here J_1 and J_2 are nearest and next nearest neighbour couplings respectively. This projection is pictured in Fig(1.5). Double Spin Density Wave (DSDW, Fig(1.6)) can be projected onto a square lattice as well as in Fig(1.7). This is not the only way to project the f.c.c lattice onto two dimension. For example if it is projected onto the (1,1,1) direction it will lead to a triangular lattice with $J_1 = J_2$. We have given a brief introduction to the projections of f.c.c , because there are some real materials that can be projected onto two dimensions without changing the nature of the materials. If this is the case then we may attempt to understand those materials by using these two dimensional pictures instead of using more complicated three dimension. Firstly we will introduce some of real materials for which we can use the Classical Heisenberg model most accurately.

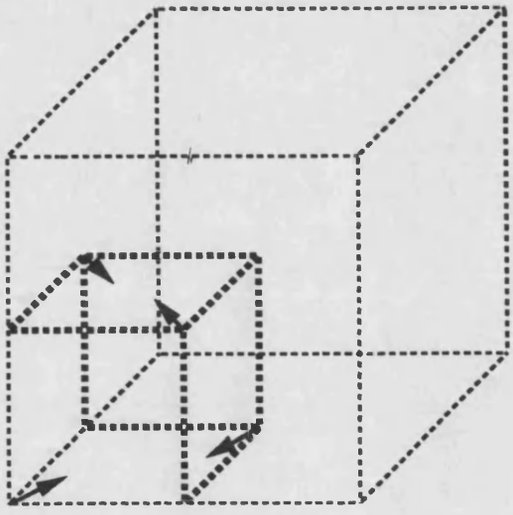

Fig. 1.6 DSDW ordering of f.c.c lattice

When another transition metal is doped into the manganese there are quite

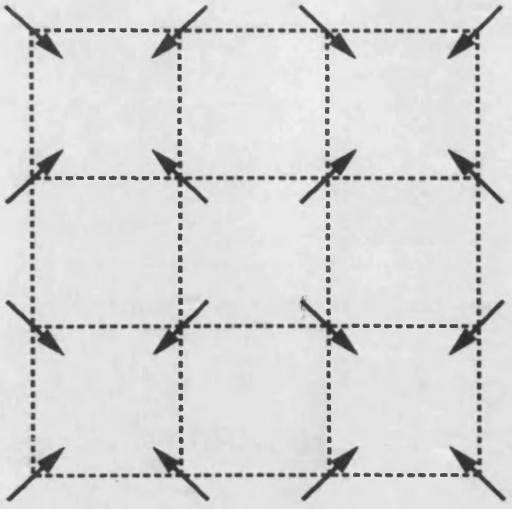

Fig. 1.7 Projection of DSDW onto a square lattice

dramatic changes in behaviour. Fe[17], Ir[18], Ni[19], and Cu[20] all substantially reduce the tetragonal distortion and for Fe, Ir, and Ni there is evidence of a cubic phase which is stabilised at doping concentrations of approximately a quarter.

Although the model we have established works for any frustrated antiferromagnetic system we will consider three such materials where the phenomenon has been observed by experiments. In other words we are taking three specific materials for which we can explain the magnetic phase transition by our model.

The first experiment we will consider is MnNi alloys. $Mn_{1-x}Ni_x$ alloys shows a sequence of structural as well as magnetic phase transition as a function of Ni concentration[20]. The phase diagram of this alloy is shown in Fig(6.1) of chapter six. Diffuse neutron scattering experiments show that the moment on the nickel site is small[21]. The nickel atoms behave more like paramagnetic impurities. The experiments showed that the alloy is face centre tetragonal (is called the t_2 phase) with $\frac{c}{a} < 1$ in the low doping regime (between 0-13% of doping) then it becomes

orthorhombic when the doping concentration is between 13%-18%. There is a second tetragonal structure (this phase is sometimes called the t_1 phase) with $\frac{c}{a} > 1$ when the doping is about 18%-20%. And finally the alloy becomes cubic by 25% doping. According to neutron diffraction experiments by Uchishiba[22] the spin direction in the t_2 phase with $\frac{c}{a} > 1$ is along the c-axis, while that in the t_1 phase with $\frac{c}{a} < 1$ is orthogonal to c-axis. In both cases the nearest neighbour pair of Mn atoms has antiparallel spins. It is assumed that the same situation holds good in the case of the orthorhombic phase, so that ferromagnetic layers are always perpendicular to the spin direction which is parallel to the shortest axis[22]. Careful studies of order in the alloys shows a tendency for the atoms to order in a Cu_3Au structure[23]. Another experiment suggests that Ni atoms anti-cluster[24], which means that there is a low probability of finding nearest neighbour impurities and an increased probability of finding next nearest neighbour impurities(this is a further evidence that there is a tendency to Cu_3Au structure because of this anti-clustering). The best, one can get from the anti-clustering is the Cu_3Au structure that one of the sublattices will be occupied by Ni atoms. For this alloy we will look at the question of how the system might transform from one phase to another. Firstly it is worth pointing out here that the first two phases of MnNi have two dimensional correspondence. The projection of the first phase (it is generally called t_2 phase) into the x-y plane leads to the collinear ordering of the square lattice, whereas the projection of the second phase (which is called t_1 phase) leads to the non-collinear arrangement (We will see the square lattice in more detail in the next Chapter). This means that we can explain the phase transition of MnNi in two dimensions. We will explain this transition by using the idea of spin reorientation with spins rotating away from the

quantisation axis after Ni addition. As we already explained, the experiments say that there is a sequence of magnetic phase transition in MnNi alloys. At the end of the day we will learn that by alloying, the non-collinear phase may be stabilised. Studying the magnetic Diffuse scattering for particular clusters, we will learn that the scattering peaks corresponds to the non-collinear arrangement of spins if the clusters have a single impurity. We will conclude in Chapter Six for this alloys that the alloying may cause a phase transition if

a) the Ni atoms anti-clusters

b) the number of such clusters are about the percolation threshold.

The Mn_3Pt alloy has been much studied because of its first-order phase transition between two ordered antiferromagnetic phases at around 365°K[25]. It shows quite different behaviour compared with MnNi alloys, involving a transfer of magnetic scattering between symmetrically unrelated Bragg spots. In face-centre-cubic nomenclature, the Bragg spots shift from being type-I to type-III, although the particular phases involved are quite unrelated to their face-centre-cubic counterparts. This phase transition occurs for the stochiometric alloy as a function of temperature, but a brief look at the phase diagram[26], shows that the transition is strongly affected by alloying. The alloy crystallises in the Cu_3Au structure with moments of about $3\mu_B$ sitting on the Mn atoms. The Pt atoms have a much smaller moment that they behave more like paramagnetic impurities. The initial problem of magnetic structure determination has proved non-trivial, with the original proposal[27] being recently challenged by Long[28]. In the new description the phase transition involves a reorientation of the spins between two phases which have identical angles between all the nearest neighbour spins, and are only different at next-nearest-neighbours.

One phase has three possible orientations for the spins, much akin to the triangular lattice phase, while the new phase is predicted to have twelve different possible spin orientations, which has led to the name 'hedgehog' phase being proposed. In chapter six we will predict this change of phase observed with alloying, giving further evidence that the proposed 'hedgehog' phase is correct.

The final experiment of our concern is MnCu alloys. This alloy is different from the first two in the sense that the phase transition has not been observed. In this alloy the clustering of Cu atoms is observed[29]. Although the tetragonal distortion is reduced as Cu is introduced the antiferromagnetic moment decays and vanishes before the cubic phase is obtained[14]. For this alloy large single crystals with modest, viz about 10% concentration of impurities have been studied with diffuse scattering[30]. The results are spectacular: Clustering of Cu atoms occurs very strongly over a fairly long length-scale and associated with this clustering is a much longer-length antiferromagnetic impurity associated with the original magnetic symmetry but perpendicular to the original direction. The scattering peak occurs exactly on the original Bragg spot. This is the experimental result that is very difficult to understand it. The reason for this is that the scattering peak is at the original Bragg spot. The peak at the origin says that all the Mn atoms rotate together. But why they should rotate together? One may think that this is because Cu atoms have perpendicular magnetic moment to the original direction. This may be the reason for this rotation. It can be argued that why the Cu atoms carry perpendicular magnetic moment? If they carry any magnetic moment, then the interaction would be some sort of exchange interactions as explained earlier. It was pointed out that if there is an exchange interaction, then the perpendicular Cu atoms

are unlikely. As can be picked up from these lines of arguments, indeed MnCu is hard to understand. We will see in Chapter Six that the peak at the origin may be explained by using the idea of clustering of Cu atoms and non-collinear arrangement of spins when the Cu atoms are introduced.

These three materials will be explained by our model, although, the model works for any frustrated antiferromagnetic systems. But the model required a little bit of modification. For example, if we try to explain the magnetic phase transition of γ-FeMn alloys, we must add a bigger magnetic moment into the system instead of adding paramagnetic impurities as in the case of MnNi, MnCu, Mn_3Pt. It is obvious that the model can be modified for specific materials. However, as we said above, three materials will be main interest for us in this thesis.

After giving a brief description of experimental studies, now we can introduce the main study step by step as follows: In Chapter Two we take the Classical limit of the Heisenberg model and find out the ground state ordering of spins for the two most common two dimensional Bravais lattices: the square and the triangular lattices. Taking the periodicity of the lattice into account we find a corresponding problem which is the structure factor. This structure factor plays the dominant topological role in our analysis. All the information about the lattice, its connectivity and whether or not it is frustrated is stored in this structure factor. As we will see, the minimum of the structure factor corresponds to the minimum of the Heisenberg Hamiltonian. So instead of finding the ground state energy of the Heisenberg Hamiltonian we simply find the the minimum of the structure factor. For bipartite lattices (for example the square lattice with only the first nearest neighbour

interactions) there is only one k point which leaves the structure factor minimum. This corresponds to an unfrustrated antiferromagnetic ordering. However for the non-bipartite lattices there is more than one k point which leaves the structure factor minimum. We will point out that more than one k points leads to non-unique solutions.

As a first example we considered the square lattice. As we will see later, if we include the second nearest neighbour interactions into account, we would find two different ground state orderings named as the collinear and the non-collinear phases. The collinear phase is the simplest ordering and is stable when $x' < 0.5$ ($x = \frac{J_2}{J_1}$) whereas the non-collinear phase is stable when $x > 0.5$. It is obvious that at $x = 0.5$ there is a phase transition between these two orderings. On the other hand, for the triangular lattice there are three ground state orderings depending on the x value. Each of the different ordering region has a stability. Again there is a phase transition between different antiferromagnetic orderings as a function of x. We will conclude in that Chapter that these two Bravais lattices have three dimensional correspondence, means that the spin ordering of these lattices are related to the real materials.

Once we have realised the existence of different orderings, then we may attempt to understand the phase transition between different orderings. We know that this phase transition can be obtained as a function of x. But our aim is different: we are expecting that this phase transition occurs as a function of impurity concentration. That is why in Chapter Three we will try to stabilise the non-collinear phase by alloying. In order to do this we simply consider a cluster of collinear arrangement of spins when it is degenerate with the non-collinear phase, and remove some of the

spins and find out which ordering is stable after these impurities. The calculation shows that after the impurities there is an x_c critical point that, in the interval $x_c < x < 0.5$ (where 0.5 is the degeneracy point), the non-collinear arrangement has lower energy then the collinear one. This result suggests that the impurities (or more precisely alloying) may cause a first order antiferromagnetic phase transition. This result itself is not enough to say that the impurities cause a first order AF-AF phase transition. It may or may not cause a phase transition. One thing is certain that the impurities changes the boundaries of the collinear phase. This phase used to be stable when $x < 0.5$, but now it is stable when $x < x_c$. In order to talk about a phase transition we must go to magnetic diffuse scattering calculations which give information about the non-collinear arrangements of spins.

In Chapter Four we study magnetic diffuse scattering. This scattering gives the information about the non-collinear arrangement of spins. We will study this scattering in small clusters involving paramagnetic impurities and we will see that the fluctuations of the spins from the quantisation direction after alloying, cause a long range ordering of non-collinear spins. These fluctuations give a sharp diffuse scattering peak. Once we obtain this sharp peak, then we may be able to say that there is a long range ordering of non-collinear arrangement. Although, the results from Chapter Three and Chapter Four are the first indications of a magnetic phase transition between two ordered states, they are not enough to say that alloying causes a magnetic phase transition. The reason for this is, the considered clusters are so small that they are not comparable with the whole crystal. The required picture of the magnetic phase transition is that, many such clusters must be created such that they interact with each other and percolate through the entire crystal.

Once we have created infinitely many clusters then we may be able to talk about a phase transition between two ordered antiferromagnetic states.

In Chapter Five we develop a linearised theory for the classical Heisenberg model which allows us to approximately solve for the local distortion of spins around an impurity in a non-collinear antiferromagnet. Provided that the ratio of disturbed to undisturbed bonds is small, the theory should be applicable. The theory is particularly useful when alloying lifts the degeneracy which is often found in non-collinear magnets. We will use this theory for γ-Mn alloys in general, and Mn_3Pt in particular.

In Chapter Six we give three examples for which alloying causes a first order phase transition. The first example is MnNi alloy. Experimentally MnNi alloys shows a wealth of phase transition as a function of Ni concentration[19]. In order to explain this phase transition theoretically, we simply take the projection of the f.c.c lattice into a two dimensional square lattice. Applying the results for the square lattice to this projection one can easily understand this phase transition. In addition to this we will use the results of linearised theory as well. We will conclude for this alloys that the both methods can be used in order to explain the phase transition.

The second example is the Mn_3Pt alloys. This alloy shows a first order phase transition at around 365°K[25]. In order to explain this transition theoretically we will use two different arrangement of spins and apply the results of the Chapter Five. We will see that the results we get from our theory is in agreement with experiments.

The final example is MnCu alloys. This alloy is completely different from first two. By using our model, we can predict the magnetic diffuse scattering and explain

the special behaviour observed in MnCu[30] as arising from the local clustering of Copper impurities.

And finally in Chapter Seven we conclude.

Chapter Two

Phase Transitions Between Magnetic States

In this chapter we will try to explain the existence of different magnetic states. The magnetic properties of given materials can be explained by analyzing their spins. In attempting to explain the properties of spins, many different types of spin models have been introduced as we mentioned in Chapter One. For simplicity we will consider the Heisenberg model here.

2-1 The Heisenberg model and its classical limit

Heisenberg proposed in 1928 that[31] if the magnetic electrons were deseribed by localised orbitals, then the resultant spins on the neighbouring atoms would align either parallel or antiparallel depending on the sign of the exchange integral J. Since we are dealing with antiferromagnetic systems, this model Hamiltonian is perhaps the simplest spin model with a localised spin on each lattice site interacting with its nearest neighbours via an antiferromagnetic coupling:

$$H = \sum_{i,j} J_{ij} \mathbf{S}_i . \mathbf{S}_j \tag{2.1}$$

where $\mathbf{S}_i$ and $\mathbf{S}_j$ are the resultant spins of neighbouring atoms, which are quantum mechanical operators satisfying the commutation relations ($\hbar = 1$)

$$[\mathbf{S}_i^{\alpha}, \mathbf{S}_j^{\beta}] = \sum_{\gamma} i\epsilon_{\alpha\beta\gamma}\delta_{ij}\mathbf{S}_i^{\gamma} \tag{2.2}.$$

The superscripts α, β, γ refer to space coordinates.

In a given system, the dominant Coulombic interactions between charges tend to exhibit a balance, at the same time these charges tend to exhibit a fixed total

spin subject to the Pauli exclusion principle. This spin would usually be maximum, according to Hund's third rule. The total spin constraint is

$$\mathbf{S}_i.\mathbf{S}_i = S(S+1) \tag{2.3}$$

and applies to each atom independently. If the given system is isolated, then the energy would be minimum. i.e the system is stable or the energy is a constant. In order to obtain the ground state energy, the Hamiltonian must be minimised. However, minimising the Hamiltonian subject to the constraint (2.3) yields a complicated quantum mechanical problem which is very difficult to solve, even approximately. It is now clear that the problem is very difficult. Does this mean that we are unable to understand the system? The answer is simply no! The relationship between classical physics and quantum physics has been well known for a long time. Classical physics is a limiting case of quantum physics, where infinitely many particles are considered. This means that quantum physics can be transferred to classical physics, if infinitely many particles act together. This idea may be brought to the Heisenberg model case. All the spins involved in the Hamiltonian Eq(2.1), may be considered as very large spins i.e $S \longmapsto \infty$. In this limit, the quantum mechanical Heisenberg Hamiltonian becomes a classical Hamiltonian and all three spin components commute with the Hamiltonian and simultaneously with each other. If we normalise the spins by $\hat{\mathbf{S}}_i = S^{-1}\mathbf{S}_i$ then the commutation relation becomes

$$[\hat{\mathbf{S}}_i^{\alpha}, \hat{\mathbf{S}}_j^{\beta}] = \frac{1}{S}\sum_{\gamma} i\epsilon_{\alpha\beta\gamma}\delta_{ij}\hat{\mathbf{S}}_i^{\gamma} \tag{2.4}$$

which is zero in the classical limit. Thus the spin can be taken as an ordinary three dimensional vector in this limit. According to commutation relations, the spins may be chosen as ordinary c-numbers. The remainder of the problem is simply to find

the relative direction in which each of the spins point in order that the Hamiltonian

$$H = S^2 \sum_{ij} J_{ij} \hat{\mathbf{S}}_i . \hat{\mathbf{S}}_j \qquad (2.1a)$$

is minimised. This classical limit allows us to treat the spins as vectors of fixed length, and the constraint becomes:

$$\mathbf{S}_i . \mathbf{S}_j = S^2 \qquad (2.3a).$$

We are interested in a Bravais lattice of spins, and the periodicity of such a lattice can be taken into account by using Bloch's Theorem. The Bloch's Transform of the spin is defined to be:

$$\mathbf{S}_\mathbf{k} = \frac{1}{\sqrt{N}} \sum_i \exp(i.\mathbf{k}.\mathbf{R}_i)\mathbf{S}_i \qquad (2.5)$$

with the inverse transformation

$$\mathbf{S}_i = \frac{1}{\sqrt{N}} \sum_\mathbf{k} \exp(-i\mathbf{k}.\mathbf{R}_i)\mathbf{S}_\mathbf{k} \qquad (2.6)$$

where N is the number of atoms in the lattice, $\mathbf{R}_i$ denoting their positions. (We have assumed one atom per unit cell). Noting that $\mathbf{S}_{-k}=\mathbf{S}_k^*$, where $\mathbf{S}_k^*$ represents the complex conjugate of the spin, the Hamiltonian becomes:

$$H = \sum_n J_n Z_n \sum_\mathbf{k} \gamma_{\mathbf{k}_n} \mathbf{S}_\mathbf{k} . \mathbf{S}_{-\mathbf{k}} = \sum_n J_n Z_n \sum_\mathbf{k} \gamma_{kn} |\mathbf{S}_\mathbf{k}|^2 \qquad (2.7)$$

in terms of the interaction parameters J_n, the coordination numbers Z_n, and the structure factor,

$$\gamma_{kn} = \frac{1}{Z_n N} \sum_{ij} \exp[i\mathbf{k}.(\mathbf{R}_i - \mathbf{R}_j)] \qquad (2.8)$$

runs over all pairs of neighbours denoted by ij. n denotes any particular shell of neighbours. The structure factor is itself normalised in the interval $-1 \leq \gamma_k \leq 1$ with $\gamma_0 = 1$.

As we will see in the next section, the structure factor plays the dominant topological role in our analysis.

It is now clear that the Hamiltonian is greatly simplified in reciprocal space. In real space each spin interacts with its nearest neighbour, whereas in reciprocal space the components only interact with themselves.

As well as the Hamiltonian, the constraint can be rewritten in reciprocal space as:

$$\sum_{\mathbf{k},\mathbf{k}',\mathbf{G}} \delta_{\mathbf{k}+\mathbf{k}'+\mathbf{q}-\mathbf{G}} \mathbf{S}_{\mathbf{k}} . \mathbf{S}_{\mathbf{k}'} = S^2 N \sum_{\mathbf{G}} \delta_{\mathbf{q}-\mathbf{G}} \tag{2.11}$$

where **G** denotes a reciprocal lattice vector and **q** is any vector. For **q**=0, this constraint becomes:

$$\frac{1}{N} \sum_{\mathbf{k}} \mathbf{S}_{\mathbf{k}} \mathbf{S}_{\mathbf{k}}^{*} = S^2 \tag{2.12}$$

which yields a normalisation for the sum of moduli. We have used the fact that $\mathbf{S}_{\mathbf{k}} = \mathbf{S}_{-\mathbf{k}}^{*}$. Constraint (2.11) is zero when $q \neq 0$ which are the remaining constraints. These constraints do not play a role in single collinear antiferromagnetism, but for our more exotic non-collinear arrangements we will find that the constraints are the major factor in determining the spin orientations.

So far we have been dealing with the Heisenberg model. We started with a Hamiltonian in real space subject to a simple constraint. Infinitely many pairs in real space brings a very difficult problem. In order to simplify this problem we transferred the Hamiltonian into reciprocal space. This time the constraints are a real mess! Consequently the classical limit of the Heisenberg Hamiltonian for any

particular shell is

$$H = JZ \sum_{\mathbf{k}} |\mathbf{S}_{\mathbf{k}}|^2 \gamma_{\mathbf{k}} \tag{2.13}$$

The ground state spin configuration will only involve Fourier components which minimise the structure factor:

$$H = JNS^2 \gamma_{k_{min}} \tag{2.14}$$

Although the structure factor is bounded by −1, it only achieves this value in systems which are not antiferromagnetically frustrated. In these bipartite systems, the structure factor is generally minimised by a unique k value which gives a non-degenerate ground state, with only a choice of quantisation direction for the moment axis necessary. For frustrated systems more than one point in reciprocal space minimises the structure factor; the classical ground state has a non trivial degeneracy.

Because of the lattice symmetries, the structure factor has the same value for all k points which are related by the point group. We have firstly looked at the correlation between spins orientation and the structure factor. Since the structure factor contains all information about the considered lattice, we will build the required tie between the spins ordering and the structure factor first.

2-2 The Structure Factor and Topological Frustration

The structure factor, Eq(2.8), contains the essential information about the considered lattice topology, including its connectivity and whether or not it is frustrated is stored in this structure factor. Since we have restricted attention to Bravais lattices, the contribution of each site is the same. Hence, the structure factor can

be rewritten as:

$$\gamma_k = \frac{1}{ZN}\sum_i \sum_{\Delta_j} \exp(i\mathbf{k}\mathbf{R}_i - (\mathbf{R}_i + \Delta_j)) = \frac{1}{Z}\sum_{\Delta_j} \exp i\mathbf{k}.\Delta_j \qquad (2.16)$$

where we simply replaced the nearest neighbour lattice vector $\mathbf{R}_j$ of $\mathbf{R}_i$ by $\mathbf{R}_j = \mathbf{R}_i + \Delta_j$ with Δ_j being the Z primitive vectors connecting nearest neighbours. The inversion symmetry ensures that the structure factor is real, and can be expressed as $\frac{Z}{2}$ cos term:

$$\gamma_k = \frac{2}{Z}\sum_{\Delta_j}{}' \cos \mathbf{k}\Delta_j \qquad (2.17)$$

where $\sum'$ indicates that we include only one vector of each pair. One can easily verify that the maximum value of γ_k is achieved for $\mathbf{k} = 0$ were all $\cos \mathbf{k}.\Delta_j = 1$. The remaining question is whether the minimum value -1 also obtained. The answer is positive for bipartite lattice and negative for a non-bipartite lattices: One can achieve this result in the following manner.

A bipartite lattice can be divided into two sublattices A and B. Choosing a two-point basis which consist of one site from A and neighbouring site from B, the original Brillouin zone is halved. The new reciprocal lattice vectors $\mathbf{Q}$ which are situated in the corners of the old Brillouin zone are the desired wave vectors which yield the minimum -1 of the structure factor, since they have the property that:

$$\exp i\mathbf{Q}.\mathbf{R}_i = 1 \quad if \quad \mathbf{R}_i \quad \epsilon A \quad and \quad \exp i\mathbf{Q}\mathbf{R}_i = -1 \quad if \quad \mathbf{R}_i \quad \epsilon B \qquad (2.18).$$

The choice makes each nearest neighbour contribution $\exp -i\mathbf{Q}(\mathbf{R}_i - \mathbf{R}_j) = -1$ and therefore we obtain $\gamma_{\mathbf{k}} = -1$.

As we mentioned above, the $\mathbf{Q}$ points which satisfies $\gamma_{\mathbf{k}} = -1$ are situated on the corner of first Brillioun zone, which are a sum of half shortest reciprocal lattice vectors.

In order to prove that let us define a basis $\mathbf{x}_1$, $\mathbf{x}_2$, $\mathbf{x}_3$ out of nearest neighbours. Assuming $\exp(i\mathbf{Q}.\mathbf{x}_i) = -1$ brings

$$\mathbf{Q}.\mathbf{x}_i = (2n_i + 1)\pi. \tag{2.19}$$

One can define the reciprocal vectors as

$$G_1 = 2\pi \frac{\mathbf{x}_2 \wedge \mathbf{x}_3}{\mathbf{x}_1.[\mathbf{x}_2 \wedge \mathbf{x}_3]} \quad etc \tag{2.20}.$$

In terms of Bravais lattice vectors. From eq(2.19) one can find that

$$\mathbf{Q} = \sum_i (n_i + \frac{1}{2})G_i = \frac{1}{2}\sum_i G_i + reciprocal \quad lattice \tag{2.21}$$

so

$$\mathbf{Q} = \frac{1}{2}[G_1 + G_2 + G_3] \tag{2.22a}$$

in three dimension and

$$\mathbf{Q} = \frac{1}{2}[G_1 + G_2] \tag{2.22b}$$

in two dimension. For our two dimensional bipartite lattice example it is obvious that

$$\mathbf{Q} = \frac{1}{2}[G_1 + G_2] = (\pm\pi, \pm\pi) \tag{2.23}.$$

It is quite obvious that using the primitive lattice vectors for the bipartite lattice one can obtain $\gamma_{\mathbf{k}} = -1$.

The situation is not the same for non-bipartite lattice. For this case there are three lattice points $\mathbf{R}_1$, $\mathbf{R}_2$, $\mathbf{R}_3$, so that any pair of these three are nearest neighbours. Let us call the corresponding primitive vectors which connect the three sites:

$$\mathbf{R}_1 - \mathbf{R}_2 = \delta_1, \quad \mathbf{R}_2 - \mathbf{R}_3 = \delta_2 \quad and \quad \mathbf{R}_3 - \mathbf{R}_1 = \delta_3 \tag{2.24}$$

If we want $\gamma_{\mathbf{k}} = -1$ then there must be a $\mathbf{k}$ with

$$\cos \mathbf{k}\delta_1 = \cos \mathbf{k}\delta_2 = \cos \mathbf{k}\delta_3 = -1 \tag{2.25}$$

This however implies that

$$\mathbf{k}\delta_1 = (2n_1 + 1)\pi \tag{2.26a}$$

$$\mathbf{k}\delta_2 = (2n_2 + 1)\pi \tag{2.26b}$$

$$\mathbf{k}\delta_3 = (2n_3 + 1)\pi \tag{2.26c}$$

where the n_i are arbitrary integers. Adding up the three equations above one obtains

$$\mathbf{k}(\mathbf{R}_1 - \mathbf{R}_2 + \mathbf{R}_2 - \mathbf{R}_3 + \mathbf{R}_3 - \mathbf{R}_1) = (2[n_1 + n_2 + n_3] + 3)\pi = 0 \tag{2.27}$$

which can obviously not be true.

Since non-bipartite lattices cannot be split into two sublattices in the sense of a bipartite lattice, it is obvious that it is impossible to achieve -1 for them. From the above discussion, we can define what we mean by topological frustration and how we can measure it:

Any lattice which is not bipartite is frustrated. The manifestation of topological frustration is the fact that the structure factor γ_k does not reach its theoretical minimum of -1. One can find the lower bound of the structure factor for these non-bipartite lattices. For example the lower bound of γ_k for the triangular lattice is[32]

$$\gamma_k \geq -\frac{1}{2} \tag{2.28}.$$

The importance of the structure factor and the frustration can be easily understood in two simple examples in two dimensions in the following section:

2-2-1Two Examples

In order to understand the differences between bipartite and frustrated lattice we will calculate the structure factor for the two most common Bravais lattices in two dimensions.

2-2-1a The Square Lattice

One can choose the two primitive lattice vectors as $\mathbf{a}_1 = (1,0)$, $\mathbf{a}_2 = (0,1)$ in the x-y plane as shown in Fig(2.1).

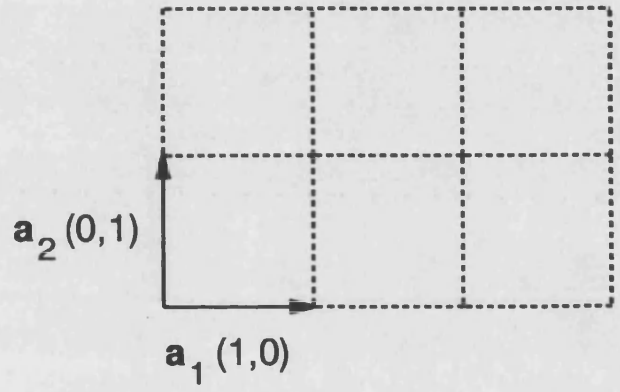

Fig. 2.1 Primitive lattice vectors of the Square Lattice

The coordination number is $z = 4$ and 4 lattice vectors connecting one lattice site to its nearest neighbours are $\pm\mathbf{a}_1$, $\pm\mathbf{a}_2$. One therefore obtains:

$$\gamma_{\mathbf{k}} = \frac{1}{4}(\exp ik_x + \exp -ik_x + \exp ik_y + \exp -ik_y) = \frac{1}{2}(\cos k_x + \cos k_y) \qquad (2.29)$$

Then it can be easily seen that $\gamma_{\mathbf{k}=0} = 1$ and $\gamma_{\mathbf{k}=\mathbf{Q}} = -1$, where

$$\mathbf{Q} = (\pm\pi, \pm\pi) \qquad (2.30)$$

is the wave vector of any corner of the first Brillouin zone. Thus $\gamma_{\mathbf{k}}$ takes any value in the interval [-1,1] which is shown in Fig(2.2).

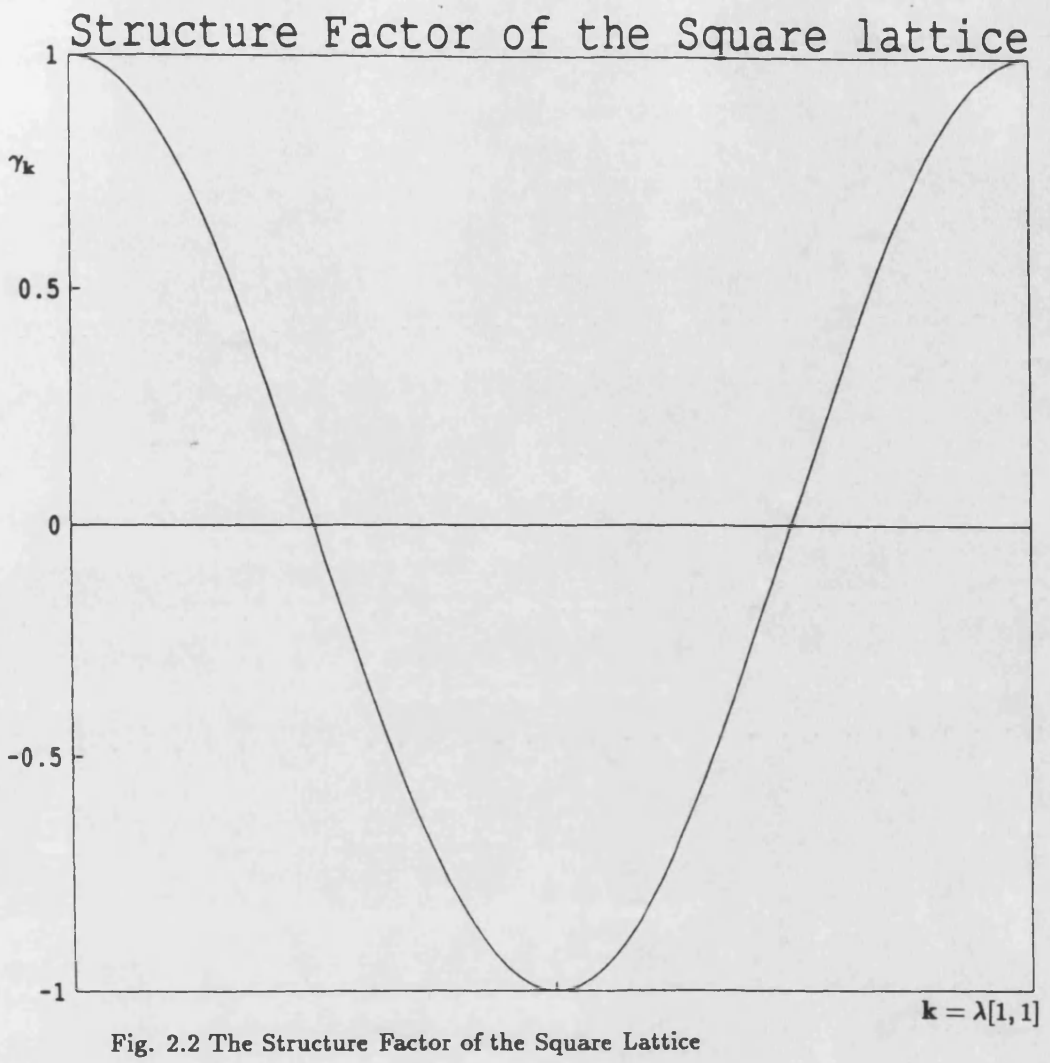

Fig. 2.2 The Structure Factor of the Square Lattice

2-2-1b **The Triangular Lattice**

The natural choice of the primitive lattice vectors is as $\mathbf{a}_1 = (1, 0)$ and $\mathbf{a}_2 = (\frac{1}{2}, \frac{\sqrt{3}}{2})$ as in Fig(2.3). Now we have $z = 6$. Then 6 lattice vectors connecting one lattice site to its nearest neighbours are $\pm\mathbf{a}_1$ $\pm\mathbf{a}_2$, and $\pm(\mathbf{a}_1 - \mathbf{a}_2)$. We therefore obtain:

$$\gamma_{\mathbf{k}} = \frac{1}{3}(\cos \mathbf{k}.\mathbf{a}_1 + \cos \mathbf{k}.\mathbf{a}_2 + \cos \mathbf{k}.(\mathbf{a}_1 - \mathbf{a}_2)) \tag{2.31}$$

$$= \frac{1}{3}(2\cos^2 \frac{k_x}{2} + 2\cos \frac{k_x}{2} \cos \frac{\sqrt{3}k_y}{2} - 1) \tag{2.32}$$

$$= \frac{1}{3}[2(\cos\frac{k_x}{2} + \frac{1}{2}\cos\frac{\sqrt{3}k_y}{2})^2 - (1 + \frac{1}{2}\cos^2\frac{\sqrt{3}k_y}{2})] \qquad (2.33)$$

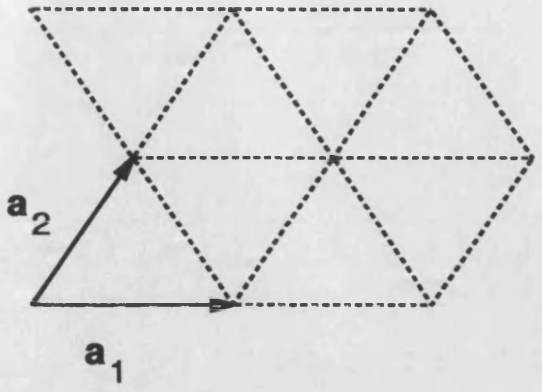

Fig. 2.3 Primitive Lattice vectors of the Triangular lattice

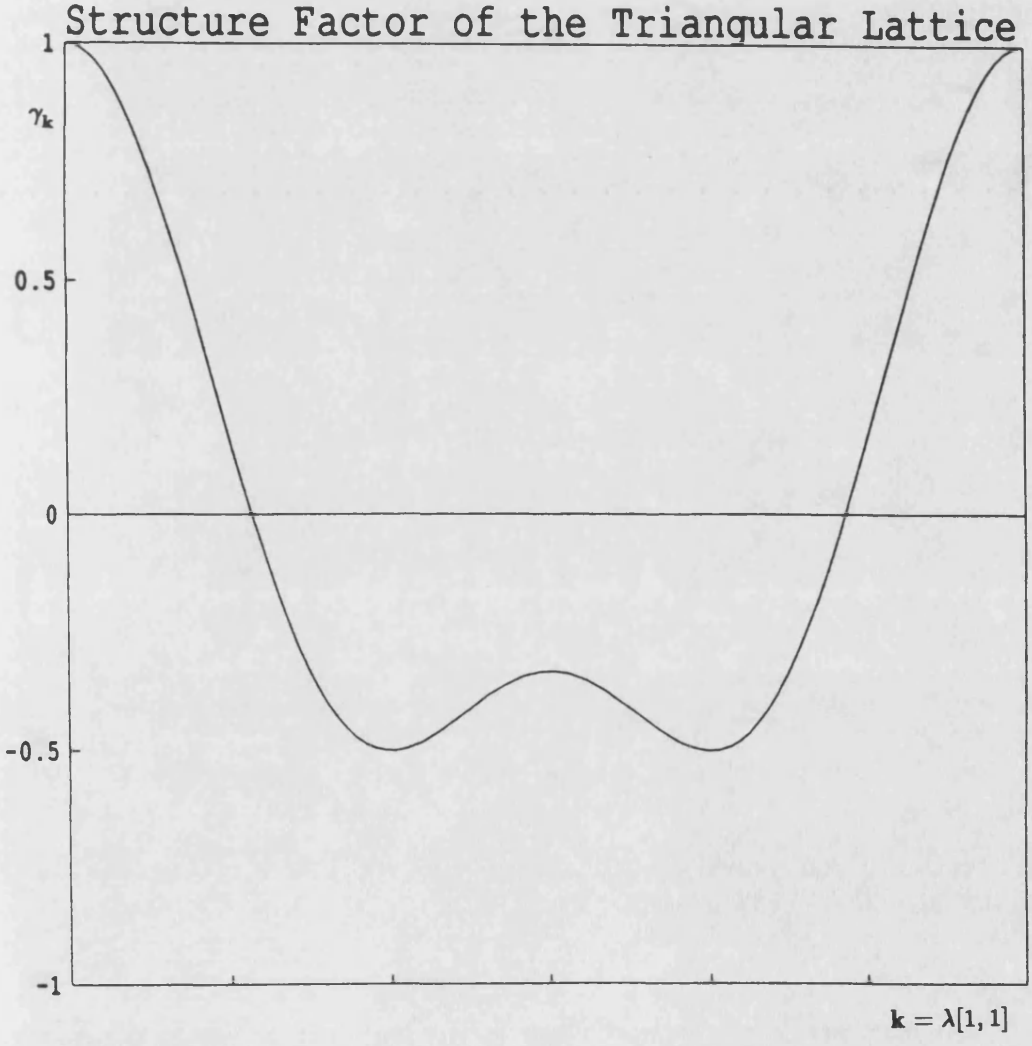

Fig 2.4 Structure factor of the Triangular Lattice

This expression has maxima $\gamma_{max} = 1$ for $\mathbf{k} = 0$ and has two minima $\gamma_{min} = -\frac{1}{2}$ for $\mathbf{k} = \mathbf{Q}_i$, where $\mathbf{Q}_1 = 2\pi(\frac{1}{3}, \frac{1}{\sqrt{3}})$, and $\mathbf{Q}_2 = 4\pi(\frac{1}{3}, 0)$. $\gamma_{\mathbf{k}} > -1$ is a property of frustrated lattices. The plot of $\gamma_{\mathbf{k}}$ is shown in Fig(2.4).

In this subsection we have calculated the structure factor for two lattices: bipartite and non-bipartite. We will also show that the structure factor is important for finding the spin arrangement of any given lattice. In the following section we will find this arrangement for the square and the triangular lattices using the minima of the structure factor.

The problem which must be solved here is simply to find some special $\mathbf{k}$ points which lead to a minimum energy for the considered system. In ferromagnets one finds $\mathbf{k}_s = 0$ which is unique. On the other hand in antiferromagnets on a bipartite lattice one can also find a unique $\mathbf{k}_s \neq 0$ which maps onto itself under the point group operation. As we will see later, this unique $\mathbf{k}_s$ gives a unique non-zero Fourier component of spin which specifies the magnetism. This component produces a unique direction to which all spins in the system are parallel. However, the lattices we are interested in have non-unique $\mathbf{k}_s$ points. These systems have a corresponding degeneracy and have frustrated spins.

When we discuss the frustration it would be useful to define a quantity which gives a measurement of frustration. One may define this quantity as:

$$\kappa = \frac{H_{AFG}}{H_{FG}} \tag{2.34}$$

subscripts AFG and FG denotes antiferromagnetic and ferromagnetic ground states respectively. If only the nearest neighbour interactions are considered the two Hamil-

tonians become:

$$H_{AFG} = -JN_{AP}S^2 + JN_PS^2 \tag{2.35}$$

and

$$H_{FG} = -JN_BS^2 \tag{2.36}$$

where N_B, N_{AP}, and N_P refer to the total, antiparallel, and parallel number of bonds respectively. Using

$$N_{AP} + N_P = N_B \tag{2.37}$$

Eq(2.34) can be rewritten as

$$\kappa = 1 - \frac{2N_P}{N_B} \tag{2.38}.$$

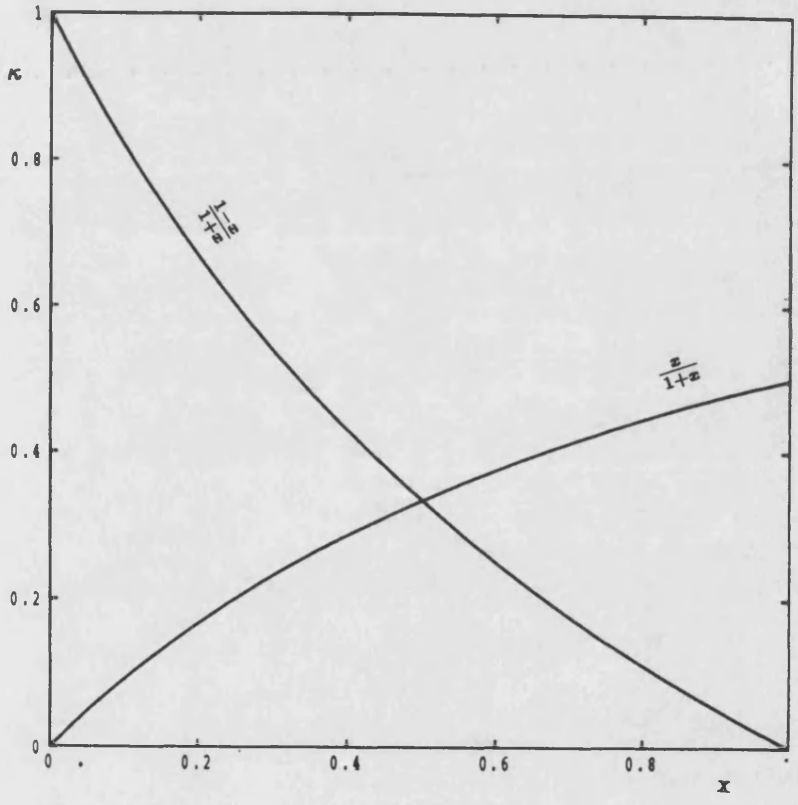

Fig 2.5 κ Function of the square lattice

Now the κ function is just a ratio of bonds, it is independent of energies. Here it can be easily seen that the maximum value of κ is 1. $\kappa = 1$ means that $N_P = 0$

and the system is unfrustrated. If κ decreases the system becomes frustrated. It should be pointed out here that the κ is positive definite. Thus a determination of κ gives an idea about the frustration. For example, for the collinear arrangement Neel state on the square lattice (as we will see later in this chapter the square lattice has two different spin arrangement named as the collinear an the non-collinear) the κ function is $\kappa = 1$. Because $N_P = 0$ for this case, and it tells us that the system is unfrustrated. It is not very difficult to drive the κ for f.c.c. If we take the Type-I arrangement as an example then $\kappa = \frac{1}{3}$ which is smaller than 1 and it is frustrated as we already knew. A plot of κ function for the square and the triangular lattices are shown in Fig(2.5) and Fig(2.6) respectively. Once we have defined this quantity, we can find the spin arrangements and different magnetic states on these lattices.

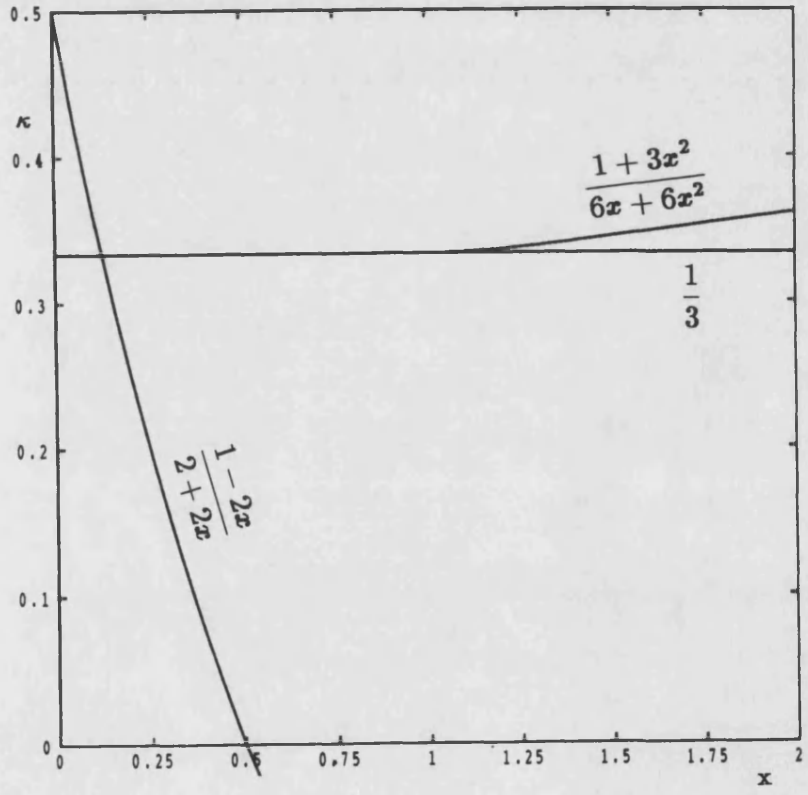

Fig 2.6 κ Function of the Triangular Lattice

2-3 Spin Arrangements and Different Magnetic States

As we explained in Chapter One, the f.c.c lattice can be projected onto two dimension leading to either a square or a triangular lattice depending on how the projection takes place. So if we find the spin arrangement of these two lattices, then we can explain some of the spin structure of f.c.c lattice. When we work with these two dimensional lattices, we must include the second nearest neighbour interactions into the interaction Hamiltonian, because in the projection of f.c.c some of the nearest neighbours become next nearest neighbours. This means that, although the second nearest neighbours are irrelevant for f.c.c, they must be taken into account for either square or triangular lattice, since they are not really next nearest neighbours. Firstly we will try the square lattice.

2-3a. Spin Arrangement of the Square Lattice:

In order to find the spin arrangement for any given lattice, one must find the number of k points which minimise the structure factor and correspondingly the Hamiltonian. The structure factor for the square lattice may be calculated as:

$$\gamma_{\mathbf{k}} = \frac{1}{2}(\cos k_x + \cos k_y) + x \cos k_x \cos k_y \qquad (2.39)$$

where $x = \frac{J_2}{J_1}$. The first term in this equation is the same as Eq(2.8), and the second term is due to second nearest neighbours interactions. This structure factor is different from the Eq(2.8). Here the second nearest neighbour interactions are taken into account as well. As we said above, before finding the spin arrangements, we must find the number of k points which minimise the structure factor. When

the structure factor is minimised it gives three turning points:

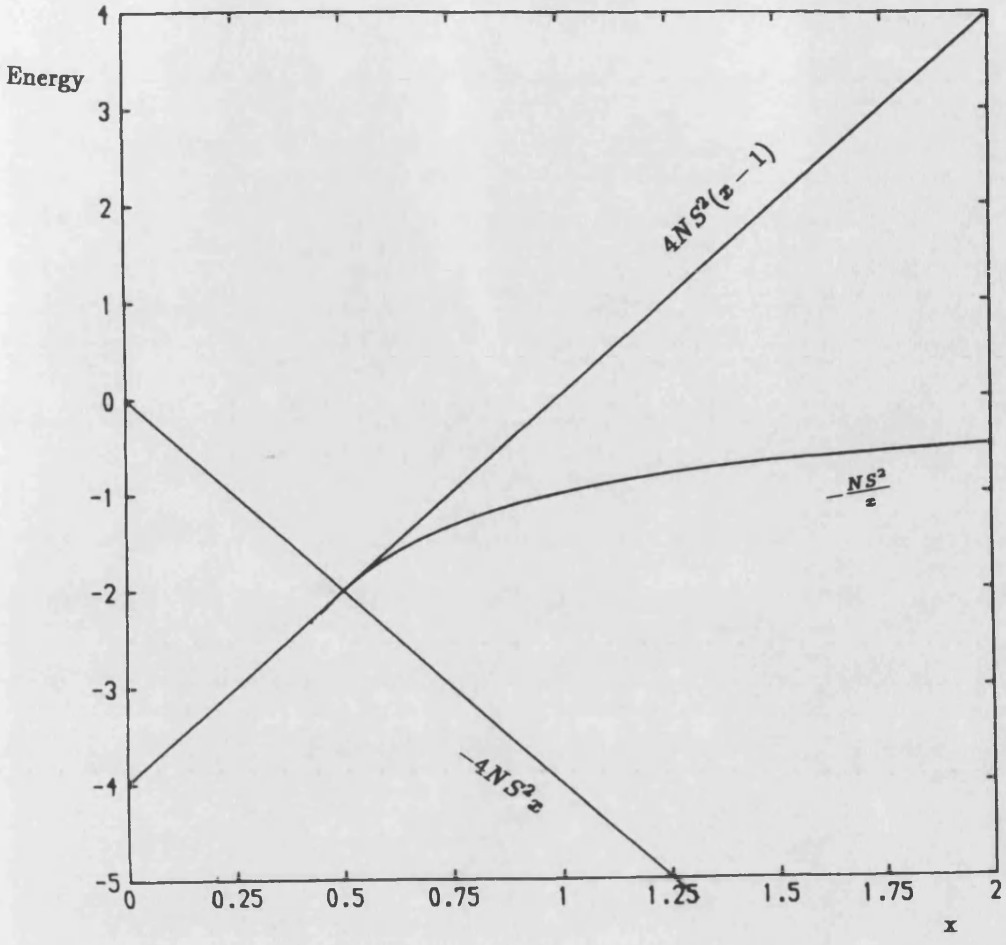

Fig2.7 The energies of three phases of the Square Lattice

1)- $\cos k_x = \cos k_y = -1$

and

$$H = NS^2 4(J_2 - J_1) \tag{2.40}$$

In this case the κ function becomes as $\kappa = \frac{1-x}{1+x}$.

2)-$\cos k_x = -\cos k_y = \pm 1$

and

$$H = -4J_2 NS^2 \tag{2.41}.$$

The κ function is $\kappa = \frac{x}{1+x}$.

3)-$\cos k_x = \frac{-J_1}{2J_2}$ and $\cos k_y = \frac{-J_1}{2J_2}$

and

$$H = NS^2(-\frac{J_1^2}{J_2}) \tag{2.42}$$

In order to determine which of the spin configurations is the ground state, a plot of energy versus $\frac{J_2}{J_1}(= x)$ is constructed, and this is shown in Fig(2.7). It can be seen that for $J_1 > 2J_2$ phase 1 is stable whereas for $J_1 < 2J_2$ phase 2 is stable, the phase we have labeled 3 is never the ground state.

The spin arrangement corresponding to 1 is the unique unfrustrated Neel antiferromagnet. The non-zero spin component is at the corner of the first Brillouin zone pictured in Fig(2.8).

Substituting the unique k value in Eq(2.15), the real space spin ordering is obtained as

$$\mathbf{S}_i = \hat{\mathbf{e}} S \exp(-\frac{\pi}{a}(1,1).R_i) \tag{2.43}$$

where we have taken $\mathbf{S}_k = S\sqrt{N}\hat{\mathbf{e}}$, and $\hat{\mathbf{e}}$ is a unit vector for some arbitrary direction. Using the term $R_i = a(n,m)$ for a translation vector one would obtain

$$\mathbf{S} = S\hat{\mathbf{e}} \exp(-i\pi(n+m)) \tag{2.44}$$

which gives two possible spin direction depending on the sum of the integers n and m:

a- when $n+m$ is even,

$$\mathbf{S} = S\hat{\mathbf{e}} = S_+ \tag{2.45}$$

b- When $n+m$ is odd,

$$\mathbf{S} = -S\hat{\mathbf{e}} = S_- \tag{2.46}$$

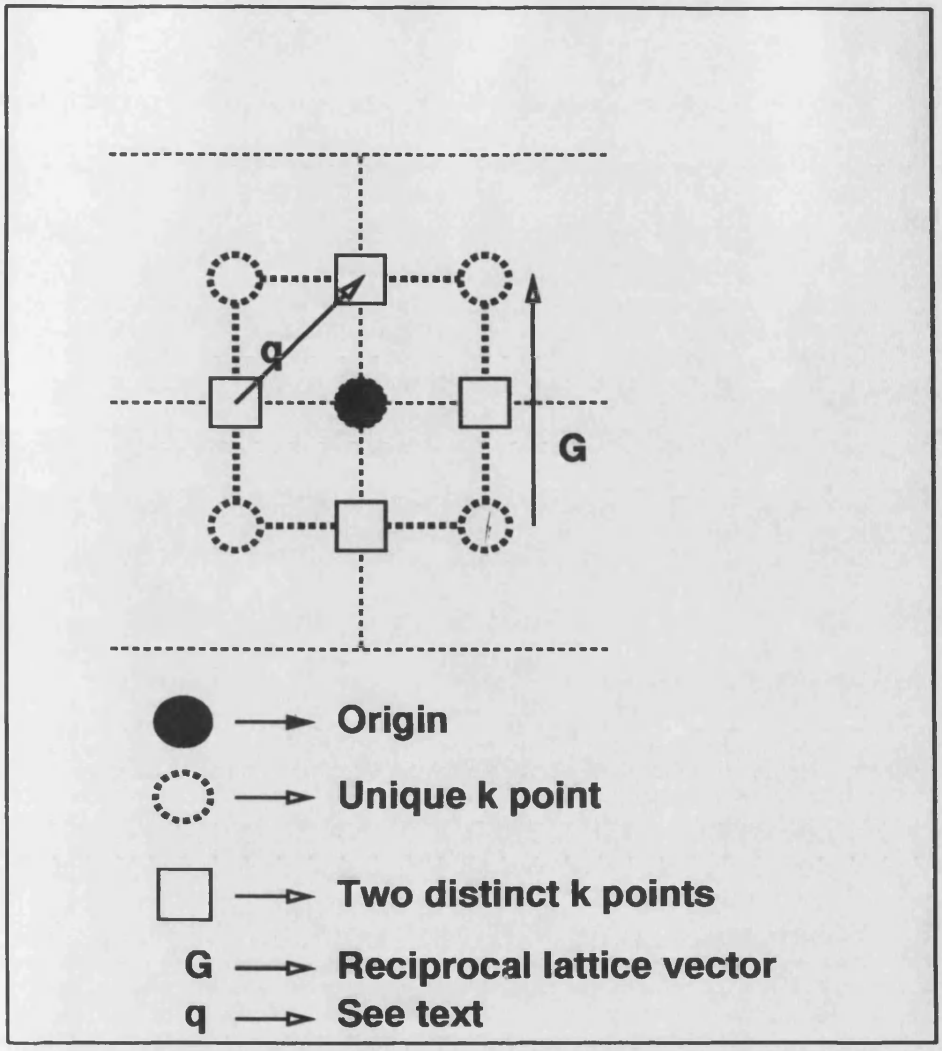

Fig. 2.8 k points which minimise the structure factor for Square lattice

which leads to all nearest neighbours being antiparallel to each other and is named as the collinear magnetic state as in Fig(2.9).

The spin arrangement corresponding to 2 is a frustrated antiferromagnetic arrangement. There are two points which minimise the structure factor. These points corresponds to $\mathbf{Q}_1 = \frac{\pi}{a}(1,0)$ and $\mathbf{Q}_2 = \frac{\pi}{a}(0,1)$ as shown in Fig(2.8). In this case the constraints of the Hamiltonian are not as simple as previously. Since there is a vector $\mathbf{q} = \mathbf{Q}_1 - \mathbf{Q}_2 = \frac{\pi}{a}(1,1)$ which maps one point onto the other is not a

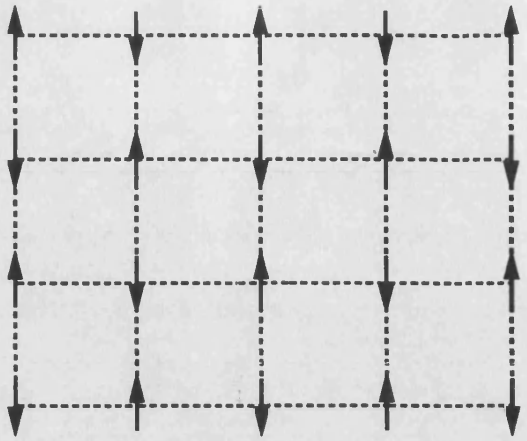

Fig. 2.9 Collinear Spin arrangement of the Square Lattice

reciprocal lattice vector the constraint (Eq (2.11)) becomes:

$$\mathbf{S}_{\mathbf{Q}_1}.\mathbf{S}_{\mathbf{Q}_2} = 0$$

i.e. the spins are orthogonal and real. Also choosing $\mathbf{q} = 0$ in the constraint gives:

$$|\mathbf{S}_{\mathbf{Q}_1}|^2 + |\mathbf{S}_{\mathbf{Q}_2}|^2 = NS^2$$

Using the constraints and transforming back to real space gives the general solution:

$$\mathbf{S}_i = S[\cos\theta\hat{\mathbf{e}}_1 \exp i\mathbf{Q}_1.\mathbf{R}_i + \sin\theta\hat{\mathbf{e}}_2 \exp i\mathbf{Q}_2.\mathbf{R}_i] \qquad (2.47)$$

where the two original directions $\hat{\mathbf{e}}_1$ and $\hat{\mathbf{e}}_2$ are orthogonal but otherwise are chosen arbitrarily. The θ degree of freedom describes a continuous degeneracy. A general θ ($\theta \neq 0$ or $\theta \neq \frac{\pi}{2}$) gives a non-collinear magnetic state as shown in Fig(2.10).

2-3b Spin Arrangement of The Triangular Lattice:

As we did on the square lattice case, firstly we must find some $\mathbf{k}$ points which minimise the structure factor. The structure factor for the triangular lattice is($x = \frac{J_2}{J_1}$):

$$\gamma_{\mathbf{k}} = 2J_1[2c_1{}^2 + 2c_1c_2 - 1] + 2xJ_1[2c_2{}^2 + 2c_2(4c_1{}^3 - 3c_1) - 1] \qquad (2.48)$$

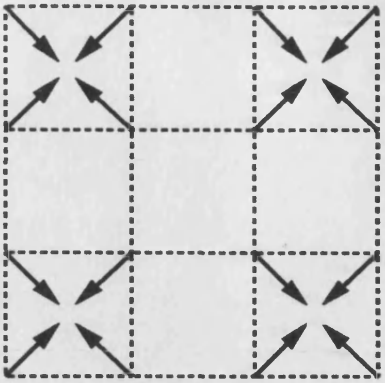

Fig. 2.10 Non-collinear Spin arrangement of the Square Lattice

in terms of cosines:

$$c_1 = \cos\frac{ak_x}{2}, c_2 = \cos\frac{\sqrt{3}ak_y}{2} \tag{2.49}$$

which may be chosen as independent variables. One can find the **k** points by minimising this structure factor. It gives four turning points:

1)

$$c_1 = -\frac{1}{2}, c_2 = 1 \tag{2.50.a}$$

or

$$c_1 = \frac{1}{2}, c_2 = -1 \tag{2.50.b}$$

with the energy:

$$H = NS^2(-3J_1 + 6J_2) \tag{2.51}$$

and

$$\kappa = \frac{(1-2x)}{2(1+x)}. \tag{2.52}$$

This state is stable(Fig(2.11)) when $J_2 < \frac{J_1}{8}$. There are two distinct Fourier components at $\mathbf{Q}_1 = \frac{2\pi}{a}(\frac{1}{3}, \frac{1}{\sqrt{3}})$ and $\mathbf{Q}_2 = \frac{4\pi}{3a}(1,0)$ pictured in Fig(2.12) which map onto

each other under inversion symmetry.

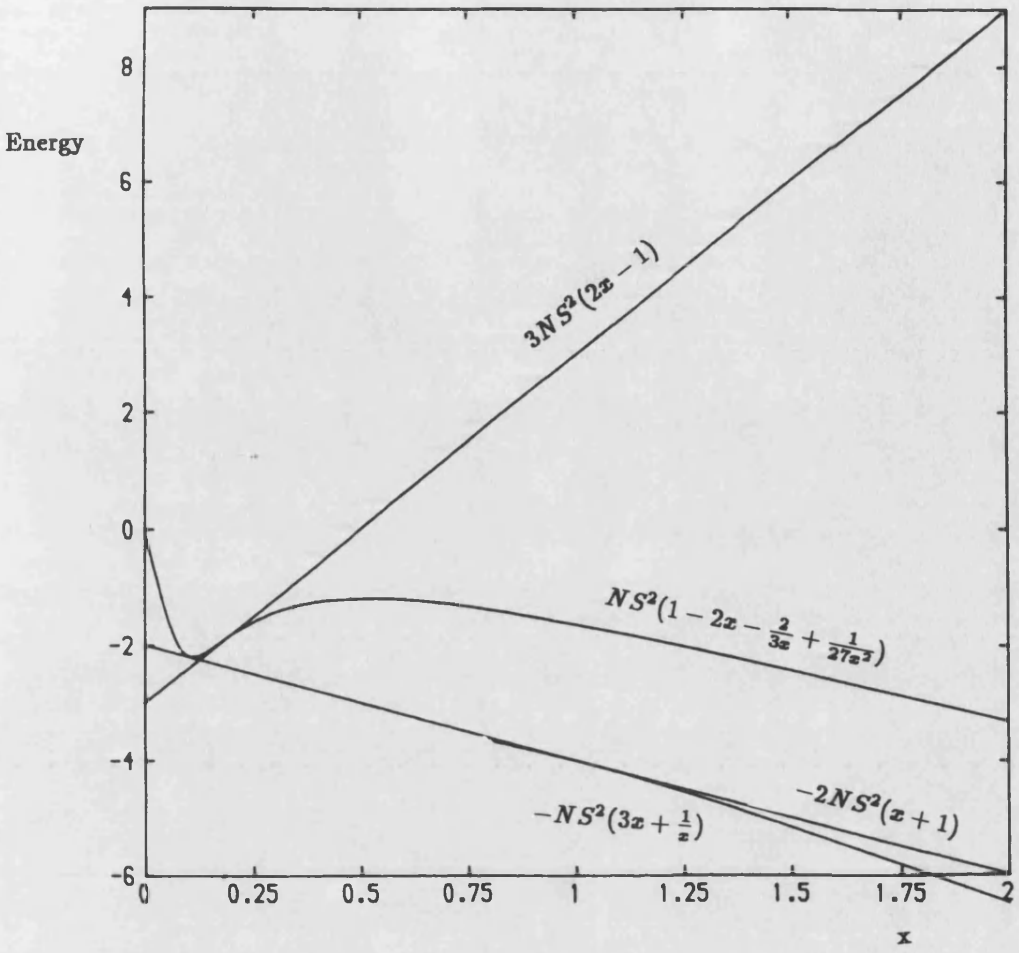

Fig 2.11 Energies of four phases of the Triangular Lattice

The constraint(2.11) yields:

$$2|\mathbf{S}_+|^2 = N; \mathbf{S}_+.\mathbf{S}_+ = 0 \tag{2.53}$$

which leads to the solution

$$\mathbf{S}_+ = \sqrt{\frac{N}{2}} \exp(i\phi)[\mathbf{S}_1 - i\sigma\mathbf{S}_2]; \sigma = \pm 1 \tag{2.54}$$

and

$$\mathbf{S}_i = S[\hat{\mathbf{e}}_1 \cos(\phi + Q_1 R_i) + \sigma\hat{\mathbf{e}}_2 \sin(\phi + Q_1 R_i)] \tag{2.55}$$

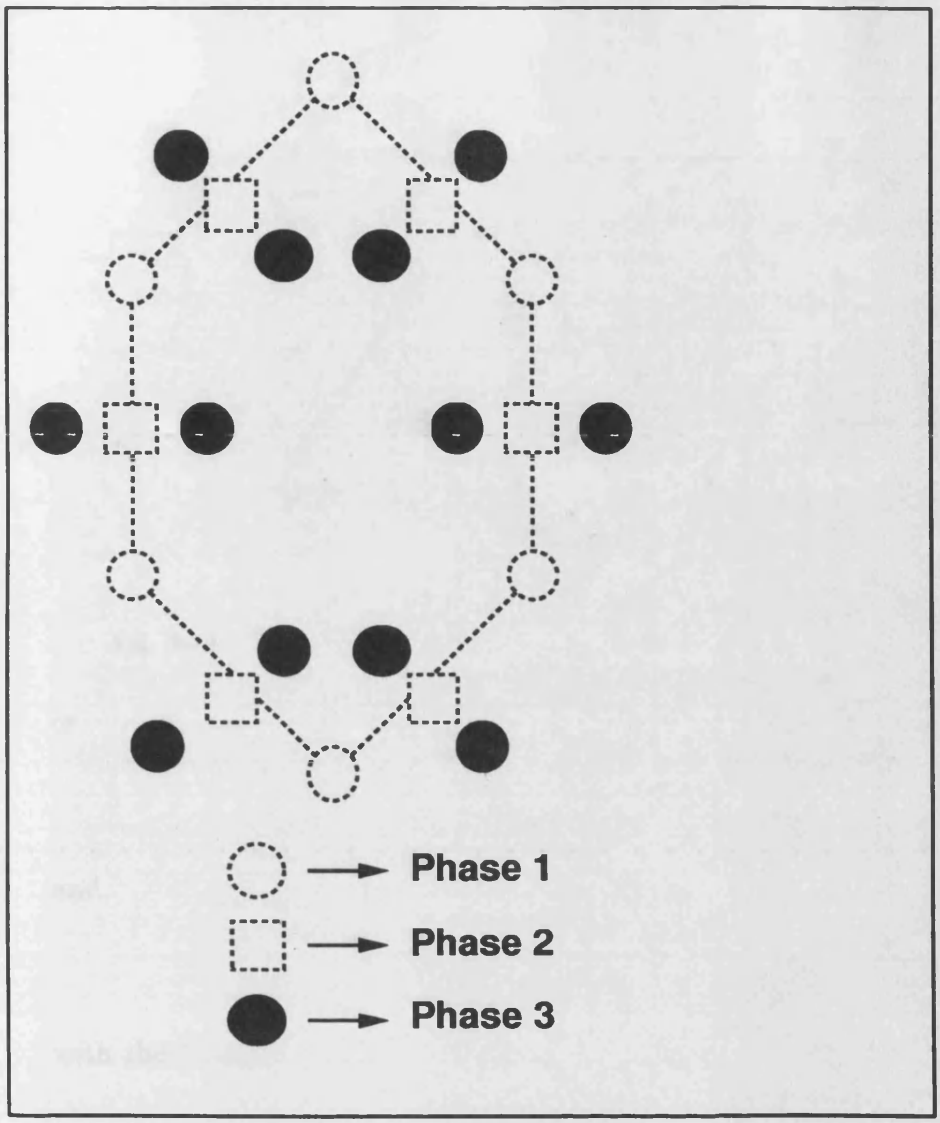

Fig. 2.12 k points which minimise the structure factor for the triangular lattice

for two arbitrary orthogonal directions $\hat{\mathbf{e}}_1$ and $\hat{\mathbf{e}}_2$; the quantisation direction freedom. The angle ϕ corresponds to a simple rotation of the spin axes, but the variable $\sigma = \pm 1$ corresponds to a topological degeneracy, pictured in Fig(2.13). This is the first example of a ground state which is necessarily non-collinear.

2)

$$c_1 = 1, c_2 = -1 \qquad (2.56.a)$$

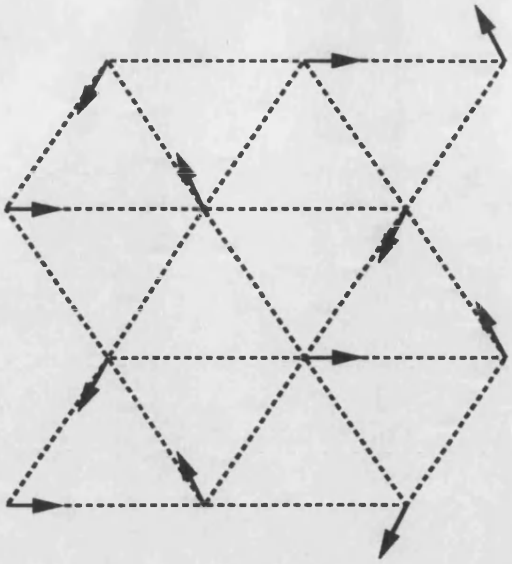

Fig. 2.13 Spin arrangement of Triangular lattice:Phase 1

or

$$c_1 = -1, c_2 = 1 \tag{2.56.b}$$

and

$$c_1 = c_2 = 0 \tag{2.56.c}$$

with the Hamiltonian

$$H = NS^2[-2J_1 - 2J_2] \tag{2.57}$$

and

$$\kappa = \frac{1}{3} \tag{2.58}$$

which is stable for $\frac{J_1}{8} < J_2 < J_1$. There are three distinct Fourier components at $\mathbf{Q} = \frac{\pi}{a}(0, \frac{2}{\sqrt{3}})$, $\mathbf{Q}_1 = -\frac{\pi}{a}(1, \frac{1}{\sqrt{3}})$, and $\mathbf{Q}_2 = \frac{\pi}{a}(1, -\frac{1}{\sqrt{3}})$ as shown in Fig(2.12) which map onto each other under the inversion symmetry. So the corresponding Fourier components are real. The constraint(2.11) yields:

$$\mathbf{S}_i.\mathbf{S}_j = \delta_{ij}|S_i|^2; \sum_{i=1} |S_i|^2 = N \tag{2.59}$$

which leads to the solution:

$$\mathbf{S}_i = S[\hat{\mathbf{e}}_1 \sin\theta\cos\phi\exp(iQR_i) + \hat{\mathbf{e}}_2 \sin\theta\sin\phi\exp(iQ_1R_i) + \hat{\mathbf{e}}_3 \cos\theta\exp(iQ_2R_i)] \quad (2.60)$$

for the three arbitrary orthogonal directions as shown in Fig(2.14).

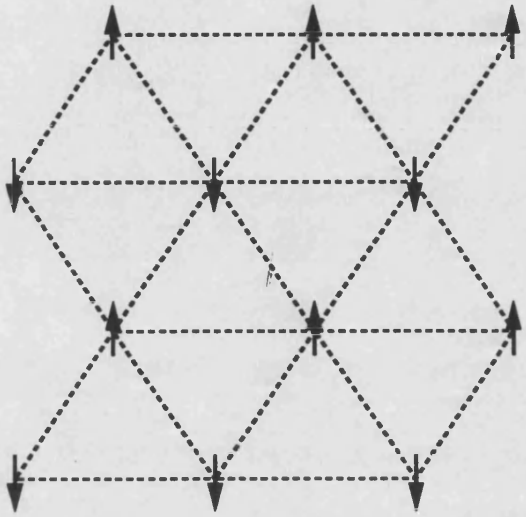

Fig. 2.14 Spin arrangement of the Triangular lattice:Phase 2

3)

$$c_1 = 1, c_2 = -\frac{1}{2} - \frac{J_1}{2J_2} \quad (2.61.a)$$

$$c_1 = -1, c_2 = \frac{1}{2} + \frac{J_1}{2J_2} \quad (2.61.b)$$

$$c_1 = c_2 = \pm\sqrt{\frac{J_2 - J_1}{4J_2}} \quad (2.61.c)$$

with the Hamiltonian

$$H = NS^2[-3J_2 - \frac{J_1^2}{J_2}] \quad (2.62)$$

and

$$\kappa = \frac{(1+3x^2)}{6x(1+x)} \quad (2.63)$$

which is stable for $J_1 < J_2$. This state has six distinct Fourier components, but now the positions of these points varies as the ratio $\frac{J_2}{J_1}$ is varied from $1 \rightarrow \infty$.These six points are pictured in Fig (2.12), where it is obvious that these points split if $\frac{J_2}{J_1}$ is varied. The six components are labeled $\mathbf{S}_1^{\pm}$, $\mathbf{S}_2^{\pm}$, $\mathbf{S}_3^{\pm}$, where $\mathbf{S}_i^{\pm}$ are continuously connected to the points $\pm\mathbf{Q}_i$. The inversion symmetry maps $\mathbf{S}_i^{+}$ onto $\mathbf{S}_i^{-}$. The constraints(9) yield:

$$\mathbf{S}_i^{+}.\mathbf{S}_j^{+} = 0, \mathbf{S}_i^{+}(\mathbf{S}_j^{+})^* = \delta_{ij}|\mathbf{S}_i^{+}|^2, \sum_i |\mathbf{S}_i^{+}|^2 = \frac{N}{2} \tag{2.64}$$

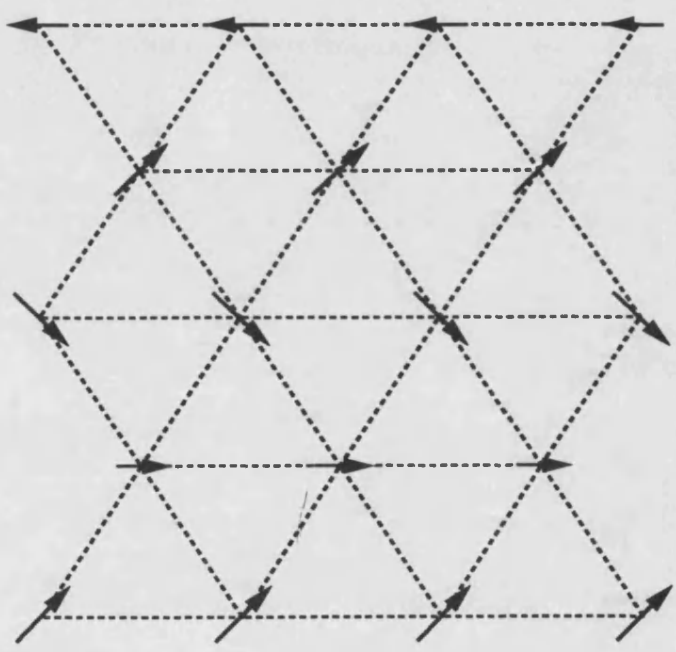

Fig. 2.15 Spin arrangement of the Triangular Lattice:Phase 3

This tells us that the inversion symmetry maps $\mathbf{S}_i^{+}$ onto $\mathbf{S}_i^{-}$ and so $\mathbf{S}_i^{-} = (\mathbf{S}_i^{+})^*$. When we think about these constraints more carefully, we can realise that each i requires two spin dimensions orthogonal to all other components. In three spin dimension only one component can be non-zero at one time. The spin arrangement

from one such component is:

$$\mathbf{S}_i = S[\hat{\mathbf{e}}_1 \cos(\phi + Q_3 R_i) + \hat{\mathbf{e}}_2 \cos(\phi + Q_3 R_i)] \tag{2.65}$$

as shown in Fig(2.15).

4)

$$c_2 = 1, c_1 = \frac{1}{2} - \frac{J_1}{6J_2} \tag{2.66.a}$$

$$c_2 = -1, c_1 = \frac{J_1}{6J_2} - \frac{1}{2} \tag{2.66.b}$$

$$c_2 = \pm \frac{J_1}{6J_2} \sqrt{(3 - \frac{J_1}{3J_2})} \tag{2.66.c}$$

and

$$H = NS^2[J_1 - 2J_2 - \frac{2{J_1}^2}{3J_2} + \frac{{J_1}^3}{27{J_2}^2}] \tag{2.67}$$

which is not stable anywhere.

2-4 Discussion:

In this chapter we have found the spin arrangement of two common lattices using the classical limit of the Heisenberg model. Instead of using the Heisenberg Hamiltonian we have used the structure factor which is the only variable in this Hamiltonian. For the square lattice the minimum of the structure factor leads to two types of magnetic states known as collinear and non-collinear states which are stable when $x < 0.5$ and $x > 0.5$ respectively ($x = \frac{J_2}{J_1}$). On the other hand, the triangular lattice has frustrated spin arrangements in three different magnetic states, all having different stability regions. in the first view one might say that this calculation has no relationship with the real materials. This is not true at all. In order to understand this point let us consider MnNi alloys. As we already mentioned in Chapter One the spin arrangements of this alloy has a two dimensional correspondence. If we take the projection of the spin arrangement of MnNi into the x-y plane, we would obtain a square lattice with $x = \frac{1}{2}$, which says that in this projection the nearest neighbour strength becomes twice as big as the second nearest neighbour strength. This is not the only way to project the MnNi system onto a two dimensional system. Another projection can be made along the (1,1,1) direction which gives a triangular lattice. In this projection half of the nearest neighbours in f.c.c becomes the second nearest neighbours so the ratio of $\frac{J_2}{J_1}$ (second nearest neighbours strength/first nearest neighbours strength) would be 1 i.e. $x = 1$. The x value is $\frac{1}{2}$ and 1 for these projection respectively. As we already explained these points corresponds to the phase transition points, since $x = \frac{1}{2}$ is the point that two phases of the square lattice are degenerate and the same is true for the case of the triangular lattice. Thus we can easily say that the calculations we have performed

so far can easily be transfered to the real materials. In other words if we find out the spin arrangements of the square and the triangular lattices, we would know the spin arrangements of some real materials as well (although we have taken MnNi alloys as an example, one can consider other Mn-alloys as well).

Theoretically, a phase transition between these magnetic states is possible, for example a change in temperature causes a change in x (the ratio of two coupling constants). When this x value is changed, the system may change its present phase if the required x value is obtained. For instead, in order to have a magnetic phase transition from collinear to non-collinear on the square lattice the x value must be changed from $x < 0.5$ to $x > 0.5$. The idea is the same for the triangular lattice. The question we want to tackle is a bit different: Although it is a phase transition between many magnetic states, we do not want to vary the temperature. Without varying the temperature how can we then observe a phase transition? There is an experimental way known as alloying. As we shall see in the next chapter, alloying causes a magnetic phase transition theoretically too...

Chapter Three

Impurities and their role in changing the boundaries of transition

In the previous chapter, it is proved that for the Heisenberg Hamiltonian either on a triangular lattice or on a square lattice there are more than one different type of antiferromagnetic ground state as a function of x ($x = \frac{J_2}{J_1}$). When x is varied the magnetic structure changes from one ordering to another one. This is the evidence of a first order magnetic phase transition when x is varied from one region to another one. The aim of this chapter is to find an explanation for this first order magnetic phase transition by alloying. Before going into further detail we shall review the boundaries of different magnetic states for triangular and square lattices.

3-1 Boundaries of different magnetic states

In chapter two we found the antiferromagnetic spin structures for the square and the triangular lattices. There it was mentioned that different magnetic states are stable in different regions. The square lattice has two distinct magnetic states named as collinear and non-collinear states. The collinear state with all nearest neighbours antiparallel to each other is the simplest one. This state is stable in the region $0 < x < 0.5$. On the other hand the collinear phase with rows of up and rows of down is degenerate with the non-collinear phase and stable in the region $x > 0.5$. Whereas for the triangular lattice the number of regions are three all leading to different magnetic structures. It will be seen in the following subsection that these boundaries are changeable by impurities. First of all we will look at the effect of impurities in the collinear states of the square lattice. As we mentioned above there

are two collinear states and we will name them the simple collinear state where all nearest neighbours are antiparallel and degenerate collinear state where spins are rows of up and rows of down. Firstly we will take the simple case.

3-2 The Effect of impurities in The Simple Collinear State

When the whole crystal is considered, analysing the effect of impurities become very complicated in real space. There are infinitely many atoms with magnetic moments interacting with each other, so any attempt to solve this problem generally fails. However, in order to understand the effect of impurities one can simplify the problem such that the effect of an impurity can be brought to a small cluster. The idea is firstly to understand the effect of impurities in a small cluster. Of course one cluster in a given crystal is far away from leading to a phase transition. In order to have a possible phase transition the number of such clusters must be around a percolation threshold such that they percolate through the entire crystal. This is the most satisfying picture of how the phase transition might occurs.

3-2-1 The Idea of a Cluster Calculation

As has been mentioned above, the effect of impurities in a crystal is very complicated to deduce. Because there are infinitely many atoms and the interactions among them are almost always impossible to take into account. However one can simplify the problem by some approximation. For example the effect of an impurity atom can be considered as a short range effect such that a certain number of atoms are influenced by the impurity atom. This certain number of atoms may occupy a small cluster in the whole crystal. Then by increasing the impurity concentration one can create many such clusters in the entire crystal. If the number of these

clusters is big enough let us say around the percolation threshold that they can start to percolate through the entire crystal. Once this situation is obtained then one may talk about the idea of a phase transition. But first of all we must know the effect of an impurity in such a cluster.

3-2-2 Single impurity in a Chosen Cluster.

The aim of this section is to analyse the effect of paramagnetic impurities in a chosen cluster. As we have seen in the previous chapter, the Heisenberg model predicts two different magnetic states for the square lattice: The collinear phase and the non-collinear phase. The non-collinear phase can be thought of as a superposition of the degenerate collinear phases as we mentioned in chapter one. Our goal is to find a theoretical explanation for a first order magnetic phase transition between different magnetic states. The antiferromagnetic square lattice can be divided into two sublattices A and B as in Fig(3.1). The nearest neighbours of A atoms are B atoms and vice versa.

Let us assume that one of the A atoms is replaced by a paramagnetic atom. The atoms in the A sublattice lose a parallel next nearest neighbour and the B atoms lose an antiparallel neighbour. From the A lattice point of view, the A moments have an increased field maintaining their original direction. But magnetic moments in the B sublattice lose an antiparallel neighbour which alters the balance between the parallel and antiparallel forces, weakening the field holding the moment in place. So the atoms on the B sublattice feel a weaker field than the A atoms. Since the magnetic moments are normalised, the only possibility looks like a rotation away from the quantisation axis in order to compensate this weaker field. We will assume

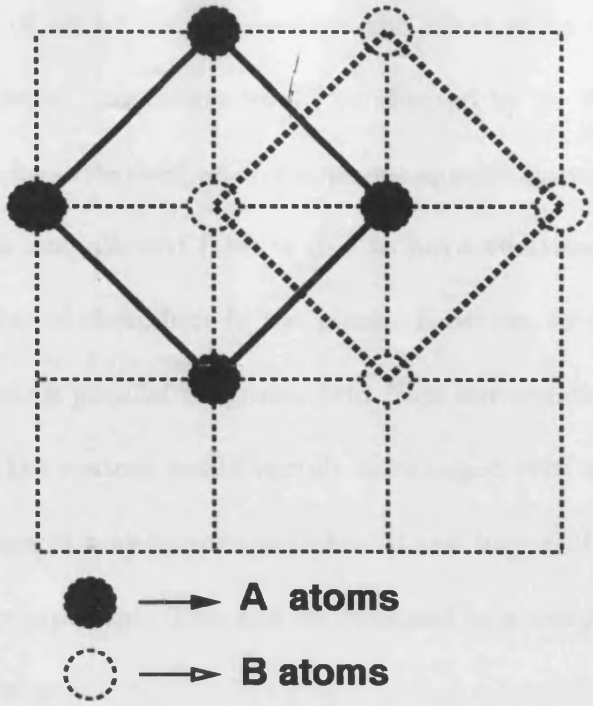

Fig. 3.1 Two Sublattices of Antiferromagnetic Square Lattice

that the impurity concentration is low such that the impurities can be isolated from each other. So the easiest way to start the analysis is a single impurity in a small cluster of the collinear phase (Fig(3.2)) when it is degenerate with the non-collinear one.

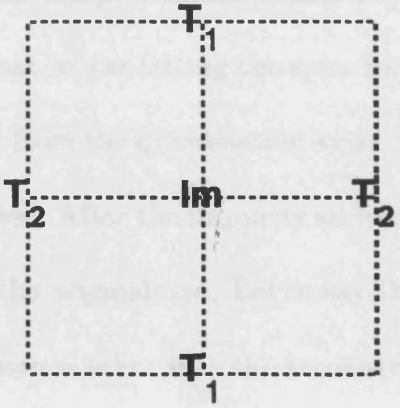

Fig. 3.2 Small Cluster of the Collinear Phase with one impurity

First of all let us assume that the effect of an impurity is short-range and only four nearest neighbours would be affected by it. Which means that these four spins would be disturbed after the paramagnetic impurity. Because the change in magnitude is not allowed (this is due to normalisation), the only possibility looks like a rotation of these four in the plane. However, in an antiferromagnetic system each spin feels a parallel magnetic field from surrounding atoms, which means that the spins in the system would remain unchanged even after the impurity. Although this is the case, it may happen or indeed it can happen that the spins can trap a perpendicular component. This can be obtained in a simple manner: the Hamiltonian of the system is

$$H = \frac{1}{2}\sum_{ij} J_{ij}\mathbf{S}_i.\mathbf{S}_j + \frac{1}{2}\sum_i (S^2 - \mathbf{S}_i.\mathbf{S}_i)\lambda_i$$

the minimum condition is satisfied if

$$\frac{\delta H}{\delta \mathbf{S}_1} = \sum_j J_{ij}\mathbf{S}_j - \lambda_i \mathbf{S}_i = 0$$

So $\mathbf{S}_i = \frac{1}{\lambda_i}\sum_j J_{ij}\mathbf{S}_j$ and $\mathbf{S}_i^{\perp} = \frac{1}{\lambda_i}\sum_j J_{ij}\mathbf{S}_j^{\perp}$, parallel and perpendicular components do not couple. So $\mathbf{S}_i^{\perp}$ must self-trap. Once the spins around the impurity have an extra perpendicular component this causes a spontaneous symmetry breaking. This is the main idea that we are letting the spins have an extra perpendicular component (or rotating away from the quantisation axis). This rotation changes the interaction energy of the cluster. After the impurity addition the interaction Hamiltonian would be different from the original one. Let us say this would be $H_1(T)$. Here T indicates that the Hamiltonian is taken into the account when the spins are rotated away from the quantisation axis. Now we will look at the energy gain by this rotation of spins after the impurity addition. In other words we want to look at the energy difference

of $H_1(T) - H_0'$. Where the H_0' is the Hamiltonian of the considered cluster with an impurity, but the remaining spins are exactly the same as before the impurity addition (they are not rotated). Taking a small cluster Fig(3.2) one can find how much energy can be gained by a paramagnetic impurity. This comes from the energy differences

$$\Delta H = H_1(T) - H_0' \qquad (3.1).$$

This energy varies as a function of ($x = \frac{J_2}{J_1}$). As we will see in the following subsection that there is an x_c critical point, which mainly controls this energy differences.

3-2-3 The Critical point and its Importance

As it is mentioned above the energy differences due to the impurity, varies as a function of ($x = \frac{J_2}{J_1}$). However there is an x_c critical point below which the energy difference is zero, whereas above it this energy varies. The main part of the problem here is to find this critical point. Once we have found this point then we may be able to talk about the stability of either phase. Before discussing this stabilising in more detail, we should look at how we can calculate this critical point. Let us turn back to our cluster calculation again (Fig(3.2)). As has been mentioned above, an impurity causes a spontaneous symmetry breaking, which leads to spins in the system reorienting themselves. An impurity in a small cluster (Fig(3.2)) changes the Heisenberg Hamiltonian. Let us assume that the effect of the impurity is short range, and only four spins would have an extra perpendicular component. Then we can easily find the energy differences and the critical point from equation(3.1): For our chosen small cluster with a single impurity the energy difference is

$$\Delta H = (6J_1 - 4J_2)(\mathbf{T}_1 + \mathbf{T}_2 + 2\mathbf{S}).\mathbf{S} + 4J_2(\mathbf{T}_1.\mathbf{T}_2 - S^2) \qquad (3.2)$$

where $\mathbf{T}_1$ and $\mathbf{T}_2$ are four spins affected by the impurity in the system. The normalisation of spins forces us to represent the affected spins as:

$$\mathbf{T}_1 = \mathbf{S}\cos\theta + \mathbf{S}'\sin\theta \qquad (3.3.a)$$

$$\mathbf{T}_2 = \mathbf{S}\cos\theta - \mathbf{S}'\sin\theta \qquad (3.3.b)$$

subject to $\mathbf{S}.\mathbf{S}' = 0$ and $\mathbf{T}_1.\mathbf{T}_1 = \mathbf{T}_2.\mathbf{T}_2 = S^2$. Then the energy differences becomes

$$\frac{\Delta H}{J_1 S^2} + constant = 12\cos\theta - 8x\cos\theta + 4x\cos 2\theta \qquad (3.4).$$

The remaining task is to calculate this energy in the ground state orientation. This tells us that the condition

$$\cos\theta = \frac{1}{2} - \frac{3}{4x} \qquad (3.5)$$

must hold in the ground state. We know that $\cos\theta$ is bounded below by -1 and above by +1. In order to get $\cos\theta$ in this interval x must be

$$x \geq \frac{1}{2} \qquad (3.6).$$

This value of x does not help us at all. Even $x = \frac{1}{2}$ corresponds to degenerate magnetic states where collinear and non-collinear states have the same energy which indicates that the degeneracy can not be removed by this impurity. If we had found $x_c < \frac{1}{2}$ we would have easily said that the non-collinear phase is stabilised. But it should be born in mind that the effect of impurity is considered as short range. Let us assume that it has a bit longer range such that eight spins are effected as shown in Fig(3.3).

Now the differences of two Hamiltonians becomes:

$$\begin{aligned}\delta H = {} & 2J_1\mathbf{T}_1\mathbf{R}_1 + 2J_1\mathbf{T}_2\mathbf{R}_2 - 4J_1\mathbf{T}_1\mathbf{S} - 4J_1\mathbf{T}_2\mathbf{S} + 4J_2\mathbf{T}_1\mathbf{T}_2 + 4J_2\mathbf{T}_1\mathbf{S} \\ & + 4J_2\mathbf{T}_2\mathbf{S} - 6J_1\mathbf{R}_1\mathbf{S} - 6J_1\mathbf{R}_2\mathbf{S} + 8J_2\mathbf{R}_1\mathbf{S} + 8J_2\mathbf{R}_2\mathbf{S} + 24J_1S^2 - 28J_2S^2\end{aligned} \qquad (3.7)$$

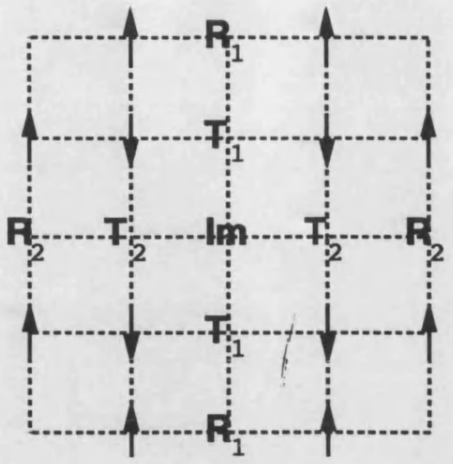

Fig. **3.3** One impurity in a Small Cluster with eight spins effected

Here the **T** spins are the same form as in the first example and the **R** spins are:

$$\mathbf{R}_1 = -\mathbf{S}\cos\phi - \mathbf{S}'\sin\phi \qquad (3.8.a)$$

and

$$\mathbf{R}_2 = -\mathbf{S}\cos\phi + \mathbf{S}'\sin\phi \qquad (3.8.b)$$

then the Hamiltonian becomes as:

$$\frac{\delta H}{J_1 S^2} = -8\cos\theta - 4\cos(\theta-\phi) - 12\cos\phi + 4x\cos 2\theta + 8x\cos\theta + 16x\cos\phi + const \quad (3.9).$$

This equation can be solved by direct calculation. However our interest is to solve it on the boundary of two magnetic phases where they are energetically degenerate. Supposing a small angle rotation for spins one can obtain a matrix equation as:

$$\delta H = (\theta \quad \phi)\begin{bmatrix} 6(1-2x) & -2 \\ -2 & 8(1-x) \end{bmatrix}\begin{pmatrix}\theta \\ \phi\end{pmatrix} \qquad (3.10)$$

which contains Eq(3.5) as well. From either Eq(3.9) or Eq(3.10) one can find the critical point as $x_c = 0.42725$. Below the critical point the collinear phase is stable, whereas above it the non-collinear phase has lower energy. From eigenvalues of

Eq(3.10) one can easily see that the θ values are bigger then the ϕ values. This indicate that if we walk away from impurity, the effect of it decreases. This tells us that the rotation of spins depends on the distance from the impurity. In other words the nearer spins to the impurity would be more effected and the rotation would be more appreciated, however the away spins would be less affected and the rotation would be negligible. As a result of this one may say that a single impurity can not cause a phase transition in a crystal.

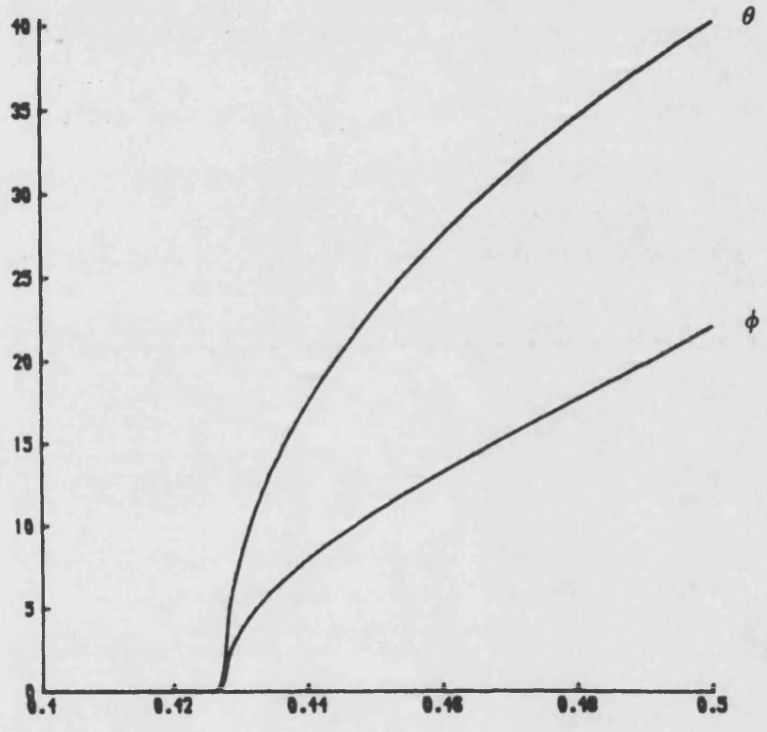

Fig 3.4 Variation of θ and ϕ values in the interval $0.42725 < x < 0.5$

It has quite short range effect and it dies outside of a small cluster. We should point out here that the change on θ and ϕ is in the region $0.42725 < x < 0.5$ (the phase we considered here is the collinear phase) because below the critical point there is no change of spins. When we examine the θ and ϕ values we can see that in the interval $0.42725 < x < 0.5$ the θ values are nearly twice as big as ϕ values

as depicted in Fig(3.4). These two calculations suggest that increasing the size of cluster changes the critical point. As is already known, for a cluster, which was studied with four affected spins, gave an x_c critical point which was bigger then the previously studied one. However, bigger clusters change the critical point quite slowly. As is mentioned above there is a certain limit of the cluster that, bigger clusters do not change the critical point. That is why we argued that the effect of an impurity is quite short range. Up to now all we have done is to chose a small cluster of a collinear phase and look for the effect of an impurity when this phase is degenerate with the non-collinear one. It is known from chapter two that this phase is stable between $0 < x < 0.5$. But the cluster calculation with an impurity showed that it is not stable when $x_c < x < 0.5$ as it was before. A probable interpretation of this is that the impurity stabilises the non-collinear phase in this particular cluster. It does not mean that there is a phase transition (first order) in the entire crystal. Because there is only one cluster in a huge crystal. It may be possible to talk about a first order AF-AF phase transition if infinitely many clusters exist in the entire crystal such that the clusters interact with each other in some sense. As the concentration of impurities is increased the impurities will start to interact and to align in order to optimise the Heisenberg contributions. We may consider the non-collinear impurities as randomly distributed weakly interacting objects. Impurities within a certain range will align and droplets of coherently connected impurities will form. Long-range phase coherence occurs when one of these droplets percolates through the entire system. This is a more satisfying picture for how a phase transition might occur.

In order to see the phase transition one must go to experiments. As we will

see in chapter four, magnetic diffuse scattering studies gives the information about this phase transition. At the moment we can only say that it may happen above the critical point, which is our main interest at the time being. We know that below it no one can talk about a possible phase transition because there the collinear phase always wins. All attention so far was about this critical point. For these two examples there was only one impurity. One can tackle the problem in another way asking how the critical point would be affected if there were more impurities in a chosen cluster? And how it changes if the cluster size is increased? We will answer these questions with examples in the following section.

3-2-4 The Variation of the Critical Point

In this section we will pay attention to the variation of the critical point in two cases: As a function of cluster size and as a function of impurity concentration. The former one is partly answered in the previous section. There two examples were studied. The first one which is rather a small cluster did not remove the degeneracy. It gave the critical point as the degeneracy point whereas the second one which is slightly bigger cluster changed the critical point and it stabilised the non-collinear phase in the cluster. As we explained previously the effect of the impurity dies out if we increase the cluster size such that after a certain limit the outsider spins would not effect the critical point. (In other words after a certain limit of the cluster size the outsider spins will be irrelevant to the critical point. But as we will see in the chapter four they are relevant for the diffuse scattering studies.) However we have not found this limit yet. We will find this limit in two cases: a) By simply increasing the cluster size and b) By increasing the impurity concentrations. For both cases

we will find the exact value of the critical point by using the Green's Functions technique.

3-2-4a Increasing the Cluster Size

We have already calculated the critical point for two clusters. Now we simply increase the size of the cluster and find out the critical point. The third cluster we will study, has 49 spins with the impurity as in Fig(3.5). In order to find the critical point we will use the same method as we previously used.

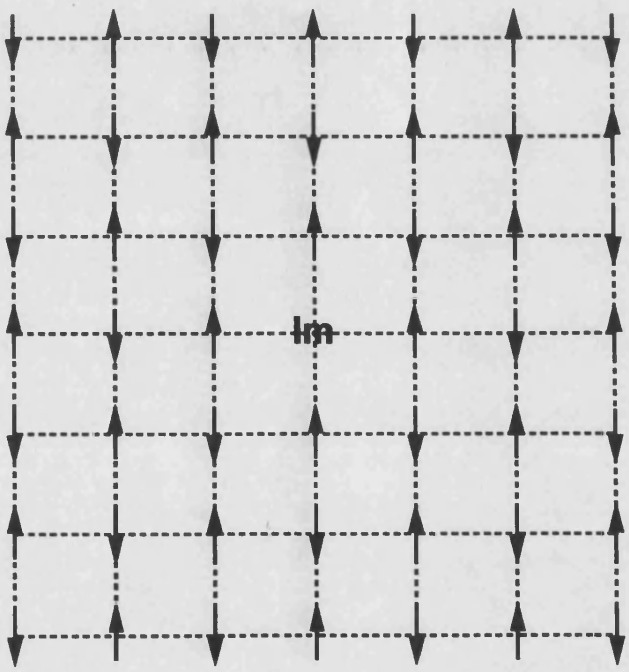

Fig. 3.5 49 spins in a Cluster

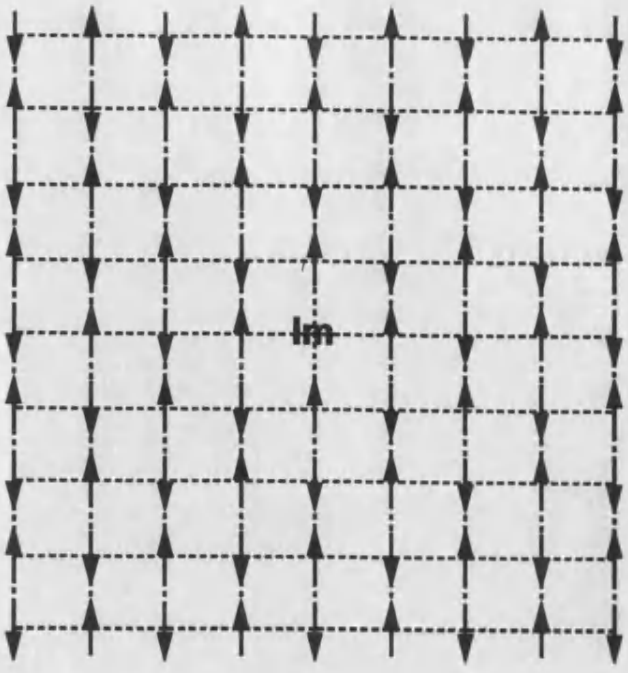

Fig. **3.6** 81 spins in a Cluster

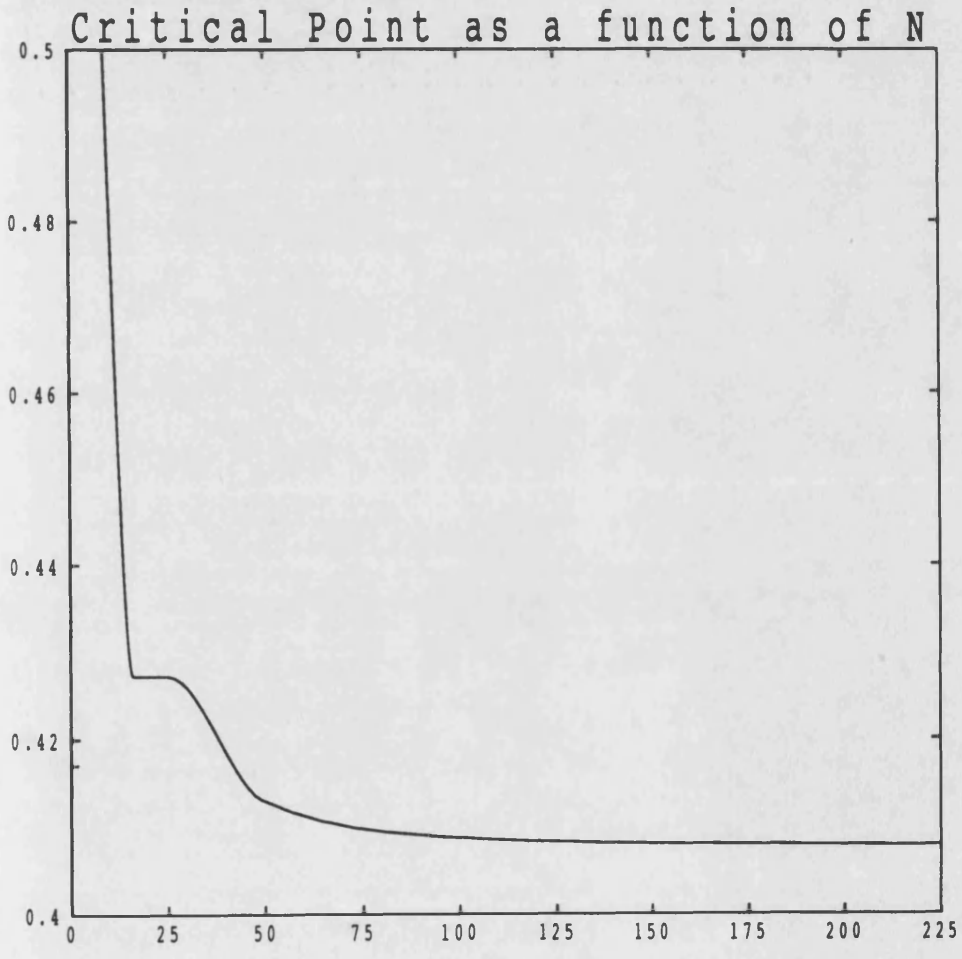

Fig 3.7 Critical point as a Function of Cluster size

This time the dimension of the characteristic matrix becomes slightly bigger. One can easily find from the secular determinant that the critical point is $x_c = 0.4131$, which is lower than the first two ones. When we take bigger clusters as in Fig(3.6) having 81 spins, the matrix we must work with becomes as a 25x25 matrix. Using a numerical method one can find that the critical point as $x_c = 0.4094$. We will find the critical point for three more clusters. For the first one the critical point is $x_c = 0.40833$, where 121 spins are effected. For the second one the critical point is $x_c = 0.40798$ involving 169 spins. Finally for the last one the critical point is $x_c = 0.40785$ having 225 spins. This sequence of calculations shows that the critical point is decreasing with increasing the size of the cluster as in Fig(3.7). In order to find the exact value of the critical point we must go to reciprocal space where the Green's functions come into account.

The Exact Value of the Critical point by Green's Functions.

In real space (for the square lattice) we dealt with the effect of an impurity and calculated the critical point, which is a measure of the stability region of the considered magnetic state. What we known is that the presence of an impurity disturbs the ground state Hamiltonian and gives an extra Hamiltonian due to the loss of some of the bonds around it. This perturbative Hamiltonian leads us to the use of the Green's Functions in order to find the exact critical value in the following way:

The Green's function is simply

$$G(Z) = [Z - H]^{-1} \qquad (G.1)$$

where H is the Hamiltonian matrix. This quantity is easiest to understand in the

basis for which H is diagonal, for which we find

$$G(Z)_{nn'} = \frac{\delta_{nn'}}{Z - E_n} \qquad (G.2).$$

The unitary matrix which diagonalises H is just the eigenvectors

$$U_{in} = a_i^n \qquad (G.3)$$

where

$$\sum_j H_{ij} a_j^n = E_n a_i^n \qquad (G.4).$$

So in the original basis the Green's function is

$$G(Z)_{ij} = \sum_n \frac{a_i^n a_j^{n*}}{Z - E_n} \qquad (G.5)$$

and the Green's function contains all the energies and eigenvector information. For example the energies can be found from $det[Z - H] = 0$. Once we have found the energies then we can easily find the eigenvectors from $\lim_{Z \to E_n}(Z - E_n)G(Z)$ which gives the wavefunctions. We can solve this problem for periodic systems by taking into account the finite number of degrees of freedom of the sublattices. In other words the Bloch's theorem can be used in order to reduce an infinite dimensional problem to a solvable finite problem.

Green's function's real use is in impurity problems. If the Hamiltonian involves a local disturbance, then the local Green's function at the disturbance contains all the information controlling the longer range consequences of the disturbance.

Now suppose that there is a local disturbance and that the Hamiltonian is

$$H = H_0 + H_1$$

with H_1 is local and H_0 is periodic. In reciprocal space H_0 is diagonal but H_1 is long-range, whereas in real space H_1 is local but H_0 is everywhere that is why the problem is so difficult. However, we can deal with this problem in some circumstances. From the definition

$$G^0(Z) = [Z - H_0]^{-1}$$

and

$$G(Z) = [Z - H_0 - H_1]^{-1}$$

$$= G^0(Z)[1 - H_1 G^0(Z)]^{-1}$$

$$= G^0(Z) + G^0(Z)H_1[1 - G^0(Z)H_1]^{-1}G^0(Z) \qquad (G.6)$$

where we can define the local change in the potential as

$$\Sigma(Z) = H_1[1 - G^0(Z)H_1]^{-1}$$

$$= [1 - H_1 G^0(Z)]^{-1}H_1 \qquad (G.7)$$

$\Sigma(Z)$ is the reason we can solve this problem because it is finite but has all the relevant information about H. When there is a pole away from the poles of $G^0(Z)$ from Eq(G.6) it is obvious that the only relevant bit is this local $\Sigma(Z)$ since H_1 is local. We may give a quite general definition of 'local' to mean that H_1 has only a finite number of non-zero eigenvalues. The key is to note that $\Sigma(Z)$ can be found exactly in the restricted subspace for which H_1 is finite. In this subspace, $\sum_j H_{1ij}b_j^m = f^m b_i^m$ and

$$\Sigma(Z)_{mm'} = f^m[f^m\delta_{mm'} - f^m G^0(Z)_{mm'}f^{m'}]^{-1}f^{m'} \qquad (3.11a)$$

$$= [\delta_{mm'}f^{m-1} - G^0(Z)_{mm'}]^{-1}$$

where

$$G^0(Z)_{mm'} = \sum_{ij} b_i^{m*} G^0(Z)_{ij} b_j^{m'}.$$

Note that these are only relevant components in $G^0(Z)$ for finding $\Sigma(Z)$(Here we have used that if $\sum_j H_{1ij} b_j^* = 0$, then $\sum_j \Sigma(Z)_{ij} b_j^* = 0$ provided that $[1 - H_1 G^0(Z)]^{-1}$ in Eq(G.7) is not divergent). This is quite general, but if we have a pole which is not a pole of $G^0(Z)$, then we also have

$$\lim_{Z \to E_n} (Z - E_n) G(Z)_{ij} = a_i^n a_j^{n*}$$

$$= \sum_{ij'} G^0(E_n)_{ii'} \lim_{Z \to E_n} (Z - E_n) \Sigma(Z)_{i'j'} G^0(E_n)_{j'j}$$

and so the wavefunction a_i^n is controlled by $G^0(E_n)_{ii'}$ and $\Sigma(Z)_{ij}$ near $Z = E_n$. If we restrict attention to the subspace where H_1 is finite, then H_1 is invertible and

$$\Sigma(Z)_{\alpha\beta} = [H_1^{-1} - G^0(Z)]^{-1}_{\alpha\beta} \qquad (3.11b).$$

Poles will show up as solutions to

$$\sum_\beta H_{1\alpha\beta}^{-1} U_\beta^n = \sum_\beta G^0(Z)_{\alpha\beta} U_\beta^n \qquad (3.12)$$

and then

$$\Sigma(Z)_{\alpha\beta} = \Sigma^R(Z)_{\alpha\beta} + \sum_n \frac{U_\alpha^n U_\beta^{n*}}{Z - E_n}.$$

The first term is the regular term and the second term is the divergent bit where we are mainly interested. From this we immediately deduce that

$$a_i^n = \sum_j G^0(E_n)_{ij} U_j^n \qquad (3.13)$$

Therefore we need only solve

$$\sum_\beta H_{1\alpha\beta}^{-1} U_\beta^n = \sum_\beta G^0(E_n)_{\alpha\beta} U_\beta^n \qquad (3.14)$$

for E_n and U^n_β, we can deduce the wavefunction from Eq(3.13). Let us apply this to an example. From the real space calculations we found that around an impurity the most effected spins are as shown in Fig(3.G1). For this cluster we need to know the local disturbance H_1 first. This is not the same as Eq(3.1). It is rather $H_1(\mathrm{T}) - H_0'$. Using the small angle rotation of the spins from the quantisation axis, we can rewrite the perturbed Hamiltonian as

$$H_1(T) = -\frac{1}{2}\sum_{<0j>}(\theta_0 - \theta_j)^2 + \frac{x}{2}\sum_{[0j]}(\theta_0 - \theta_j)^2 \tag{3.15}$$

where $< 0j >$ and [0j] runs over first and second nearest neighbours respectively and θ_is are small rotations of the spins away from the quantisation axis. What we need now is to find the matrix element of $[H_1]_{ij}$ which can be represented by $[H_1]_{ij} =< \theta_i|H_1|\theta_j >$. This is an NxN matrix whose elements are zero except those 9x9 submatrix centred at the origin (here we are taking only first and second nearest neighbours into account, so those eight spins would feel a change in potential around the impurity. The other spins would feel simply the distortion of these eight spins). This submatrix is

$$H_1 = \begin{bmatrix} 2x-2 & \frac{1}{2} & \frac{1}{2} & \frac{1}{2} & \frac{1}{2} & -\frac{x}{2} & -\frac{x}{2} & -\frac{x}{2} & -\frac{x}{2} \\ \frac{1}{2} & -\frac{1}{2} & 0 & 0 & 0 & 0 & 0 & 0 & 0 \\ \frac{1}{2} & 0 & -\frac{1}{2} & 0 & 0 & 0 & 0 & 0 & 0 \\ \frac{1}{2} & 0 & 0 & -\frac{1}{2} & 0 & 0 & 0 & 0 & 0 \\ \frac{1}{2} & 0 & 0 & 0 & -\frac{1}{2} & 0 & 0 & 0 & 0 \\ -\frac{x}{2} & 0 & 0 & 0 & 0 & \frac{x}{2} & 0 & 0 & 0 \\ -\frac{x}{2} & 0 & 0 & 0 & 0 & 0 & \frac{x}{2} & 0 & 0 \\ -\frac{x}{2} & 0 & 0 & 0 & 0 & 0 & 0 & \frac{x}{2} & 0 \\ -\frac{x}{2} & 0 & 0 & 0 & 0 & 0 & 0 & 0 & \frac{x}{2} \end{bmatrix} \tag{3.16}.$$

On the other hand the matrix elements of G are

$$G_{ij}(E) =< i|\frac{1}{E - H_0}|j > \tag{3.17}.$$

If these states (i and j) are expanded in terms of eigenfunctions of H_0, the matrix

elements become:

$$G_{ij} = \frac{1}{N}\sum_{k} \frac{\exp i\mathbf{k}(\mathbf{R}_i - \mathbf{R}_j)}{E - E_0(k)} \tag{3.18}$$

Notice that G_{ij} depends only on $(\mathbf{R}_i - \mathbf{R}_j)$. Thus there are only six different matrix elements of G in this part of our problem. Using these elements, our 9x9 Green's function operator can be expressed as

$$G = \begin{pmatrix} G_0 & G_1 & G_1 & G_1 & G_1 & G_2 & G_2 & G_2 & G_2 \\ G_1 & G_0 & G_2 & G_3 & G_2 & G_1 & G_4 & G_4 & G_1 \\ G_1 & G_2 & G_0 & G_2 & G_3 & G_1 & G_1 & G_4 & G_4 \\ G_1 & G_3 & G_2 & G_0 & G_2 & G_4 & G_1 & G_1 & G_4 \\ G_1 & G_2 & G_3 & G_2 & G_0 & G_4 & G_4 & G_1 & G_1 \\ G_2 & G_1 & G_1 & G_4 & G_4 & G_0 & G_3 & G_5 & G_3 \\ G_2 & G_4 & G_1 & G_1 & G_4 & G_3 & G_0 & G_3 & G_5 \\ G_2 & G_4 & G_4 & G_1 & G_1 & G_5 & G_3 & G_0 & G_3 \\ G_2 & G_1 & G_4 & G_4 & G_1 & G_3 & G_5 & G_3 & G_0 \end{pmatrix} \tag{3.19}$$

where

$$G_0 = \frac{1}{N}\sum_{k} \frac{1}{E - E_k} \tag{3.20}$$

$$G_1 = \frac{1}{N}\sum_{k} \frac{\frac{1}{2}(c_1 + c_2)}{E - E_k} \tag{3.21}$$

$$G_2 = \frac{1}{N}\sum_{k} \frac{c_1 c_2}{E - E_k} \tag{3.22}$$

$$G_3 = \frac{1}{N}\sum_{k} \frac{{c_1}^2 + {c_2}^2 - 1}{E - E_k} \tag{3.23}$$

can be calculated from equation(3.18)(we have not defined G_4 and G_5 here because as we will see later, they are not relevant for our problem). Here we have used $c_1 = \cos k_x$ and $c_2 = \cos k_y$. If we substitute these matrices into Eq(3.14) we would have a 9x9 matrix equation. It seems that we are dealing with a 9x9 matrix equation. However, this is not the case, in fact we are not dealing with a 9x9 matrix. This problem is reducible by using the symmetry operations. A symmetry operation is a matrix that carries the system onto itself. This means that

$$gGg^{-1} = G, \quad gH_1g^{-1} = H_1 \tag{3.24}$$

where g is a symmetry operation. From Eq(3.12) we can write

$$U^n = H_1 G^0(E_n) U^n$$

$$gU^n = gH_1 g^{-1} gG^0(E_n) g^{-1} gU^n$$

$$= H_1 G^0(E_n) gU^n \qquad (3.25).$$

this means that $\forall$ symmetries g, gU^n is also a solution. Now let us define a group G whose elements are point group symmetries of our chosen finite cluster such as

$$G = \{g: \quad point \quad group \quad symmetries\} \qquad (3.26)$$

Examples of the elements of a such group are rotation(r), inversion(i), reflection through an axis(g_α), and so on. If this group has an 'Abelian' subgroup(which means that there is a number of symmetry operations that they commute) such as $G' = \{g'\}$, we can choose the solution to diagonalise the group G. For our particular cluster $\{1, r, r^2 = i, r^3\}$ make an 'Abelian' group(here 1 is identity, r is 90° rotation, and i is inversion operations). For an illustration we will write down the explicit form of r which is

$$r = \begin{bmatrix} 1 & 0 & 0 & 0 & 0 & 0 & 0 & 0 & 0 \\ 0 & 0 & 0 & 0 & 1 & 0 & 0 & 0 & 0 \\ 0 & 1 & 0 & 0 & 0 & 0 & 0 & 0 & 0 \\ 0 & 0 & 1 & 0 & 0 & 0 & 0 & 0 & 0 \\ 0 & 0 & 0 & 1 & 0 & 0 & 0 & 0 & 0 \\ 0 & 0 & 0 & 0 & 0 & 0 & 0 & 0 & 1 \\ 0 & 0 & 0 & 0 & 0 & 1 & 0 & 0 & 0 \\ 0 & 0 & 0 & 0 & 0 & 0 & 1 & 0 & 0 \\ 0 & 0 & 0 & 0 & 0 & 0 & 0 & 1 & 0 \end{bmatrix} \qquad (G.8)$$

and its eigenvectors are

$$(1 \quad 0 \quad 0 \quad 0 \quad 0 \quad 0 \quad 0 \quad 0 \quad 0) \qquad (G.9)$$

$$(0 \quad 1 \quad 1 \quad 1 \quad 1 \quad 0 \quad 0 \quad 0 \quad 0) \qquad (G.10)$$

$$(0 \quad 0 \quad 0 \quad 0 \quad 0 \quad 1 \quad 1 \quad 1 \quad 1) \qquad (G.11)$$

$$(0 \quad 1 \quad -1 \quad 1 \quad -1 \quad 0 \quad 0 \quad 0 \quad 0) \qquad (G.12)$$

$$(0 \quad 0 \quad 0 \quad 0 \quad 0 \quad 1 \quad -1 \quad 1 \quad -1) \qquad (G.13)$$

$$(0 \quad 1 \quad i \quad -1 \quad -i \quad 0 \quad 0 \quad 0 \quad 0) \qquad (G.14)$$

$$(0 \quad 0 \quad 0 \quad 0 \quad 0 \quad 1 \quad i \quad -1 \quad -i) \qquad (G.15)$$

$$(0 \quad 1 \quad -i \quad -1 \quad i \quad 0 \quad 0 \quad 0 \quad 0) \qquad (G.16)$$

$$(0 \quad 0 \quad 0 \quad 0 \quad 0 \quad 1 \quad -i \quad -1 \quad i) \qquad (G.17)$$

We have looked at all the solutions and found out that the best energy solution is Eq(G.12), the others are not the ground state energy solutions. It means that we can choose this wavefunction as our wavefunction(since it diagonalise G). Once we have decided which wavefunction must be used then we can attempt to find the critical point.

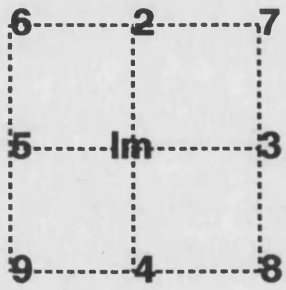

Fig. 3.G1 The arrangement of distortion of spins in a small cluster

We are looking for zero energy solutions. It means that we need only $E_0(k)$ in equation(3.18). In order to find $E_0(k)$ we must use the explicit form of H_0 in terms of θ values. Which is

$$H_0 = -\frac{1}{2}4N + \frac{1}{4}\sum_{<ij>}(\theta_i - \theta_j)^2 + \frac{x}{2}4N - \frac{x}{4}\sum_{[ij]}(\theta_i - \theta_j)^2 \qquad (3.27).$$

This Hamiltonian can be transfered into k space by using the Fourier transform of θ's as

$$\sum_i \theta_i^2 = \frac{1}{N}\sum_{ikk'} \exp -i\mathbf{R}_i(\mathbf{k}+\mathbf{k}')\theta_k\theta_{k'} \tag{3.28}$$

$$\sum_i \theta_i^2 = \sum_k \theta_k\theta_{-k} \tag{3.29}$$

and

$$\sum_{<ij>} \theta_i\theta_j = \frac{1}{N}\sum_{kk'<ij>} \exp(-i\mathbf{k}\mathbf{R}_i - i\mathbf{k}'\mathbf{R}_j)\theta_k\theta_{k'} \tag{3.30}$$

$$\sum_{<ij>} \theta_i\theta_j = \sum_k \theta_k\theta_{-k}\gamma_k \tag{3.31}$$

where

$$\gamma_k = \frac{1}{Z}\sum_{<ij>} \exp(i\mathbf{k}(\mathbf{R}_i - \mathbf{R}_j)) \tag{3.32}$$

where Z is the coordination number. Then the H_0 is

$$H_0 = -2N(1-x) + 2(1-x)\sum_k |\theta_k|^2 - \frac{1}{2}\sum_k |\theta_k|^2(\gamma_{k_1} - x\gamma_{k_2}) \tag{3.33}$$

which is

$$H_0 = -2N(1-x) + \sum_k |\theta_k|^2[2 - 2x - c_1 - c_2 + 2xc_1c_2] \tag{3.34}$$

Then the Green's function is

$$G_{kk'}{}^0 = \frac{\delta_{kk'}}{E - E_k} = \frac{\delta_{kk'}}{E - 2[1 - x - \frac{c_1+c_2}{2} + xc_1c_2]} \tag{3.35}.$$

We are looking for zero energy solutions i.e E=0. Using the wave function it is easy to write a matrix equation as

$$H_1G^0\phi = a\begin{bmatrix} 0 \\ -\frac{1}{2}(G_0 + G_3 - 2G_2) \\ \frac{1}{2}(G_0 + G_3 - 2G_2) \\ -\frac{1}{2}(G_0 + G_3 - 2G_2) \\ \frac{1}{2}(G_0 + G_3 - 2G_2) \\ 0 \\ 0 \\ 0 \\ 0 \end{bmatrix} \tag{3.37}$$

where G_0, G_2, and G_3 are as defined from equation(3.20) to Eq(3.23). If we substitute H_1G^0 into equation(3.11b) we would obtain

$$(1 - H_1G^0)\phi = [1 + \frac{1}{2}(G_0 + G_3 - 2G_2)]\phi = 0 \tag{3.38}$$

Since the cluster is antisymmetric under 90° rotation then we need to calculate only

$$f(E) = 1 + \frac{1}{2}(G_0 + G_3 - 2G_2) = 0 \tag{3.39}$$

in order to find the critical point, which gives $x_c = 0.407760$. This value of x_c is lower then the previously found one. This is the exact value of x_c for an impurity in the collinear phase. Now one can say that in the interval $0.407760 < x < 0.5$ the non-collinear phase may be stabilised. So it may be possible to remove degeneracy and observe a first order AF-AF phase transition in the previously calculated interval. This is the consequence of an impurity in the chosen cluster. We should point out here that the point group symmetry is now different from the ground state which is antisymmetric under 90° rotation. Now we want to move on to many impurities in a chosen cluster and look for the variation of x_c critical point as a function of impurity concentration.

3-2-4b Increasing The Impurity Concentration

In the previous section we have seen the variation of the critical point and its exact value. The exact value of it is found by using the Green's function. Now we want to look at how the critical point varies as a function of impurity concentration. The way to look at it is the same as what we did for single impurity calculation. Here again a small cluster is going to be chosen freely and the effect of impurities will be analysed. The impurities are randomly distributed objects. So we can not decide

about the position of impurities, the material itself decides where the impurities should go in the crystal. We discuss this point in more detail when we consider the experiments (MnNi and MnCu case). Thus it is expected that two clusters with the same size may give different critical point if the positions of impurities are different. We will discuss this point after the calculations. First of all let us choose a cluster(Fig(3.8)) with two impurities and find out the critical point.

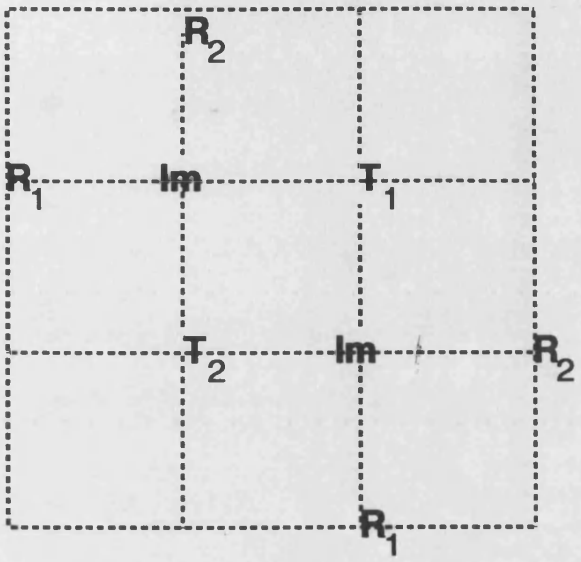

$$T_1 = S_1 \cos\theta - S_2 \sin\theta$$
$$T_2 = S_1 \cos\theta + S_2 \sin\theta$$
$$R_1 = S_1 \cos\phi - S_2 \sin\phi$$
$$R_2 = S_1 \cos\phi + S_2 \sin\phi$$
$$S_1 : S_2 = 0$$

Fig. 3.8 Two Impurities in a small Cluster

In order to find this point, again we will look the energy differences as we did for the single impurity case. The energy difference for this new cluster is

$$\delta H = -4\cos\theta - 12\cos\phi + x(\cos 2\theta + 4\cos(\theta - \phi) + 2\cos\theta + 8\cos\phi) \qquad (3.40).$$

The small angle approximation leads to a matrix equation as:

$$\delta H + constant = (\theta \quad \phi)\begin{pmatrix} 2-5x & 2x \\ 2x & 6-10x \end{pmatrix}\begin{pmatrix} \theta \\ \phi \end{pmatrix} \qquad (3.41)$$

The secular determinant of square matrix gives the critical point as $x_c = 0.357709$. This is the point above which the spins want to rotate themselves perpendicular

to the original direction. When we look at the change of spins we can easily see that below the critical point the spin remain unchanged however above it the spins rotate. The change on θ and ϕ is shown in Fig(3.9) where it is obvious that the T

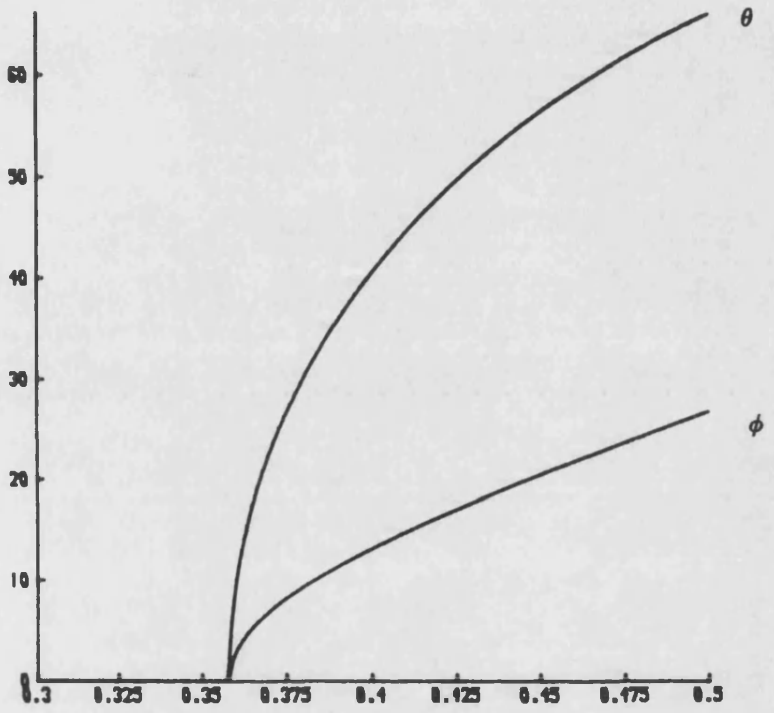

Fig 3.9 The variation of θ and ϕ values

spins rotate more then the R spins. This rotation is above the critical point. One can compare this result with the single impurity case. Before comparing it, we should remind that the number of affected spins are only eight. In other words the cluster size is very small. So we firstly should increase the cluster size gradually and find out the critical point as close as possible to the exact value of it which comes from the Green's functions calculations. When we increase the size of the cluster

the

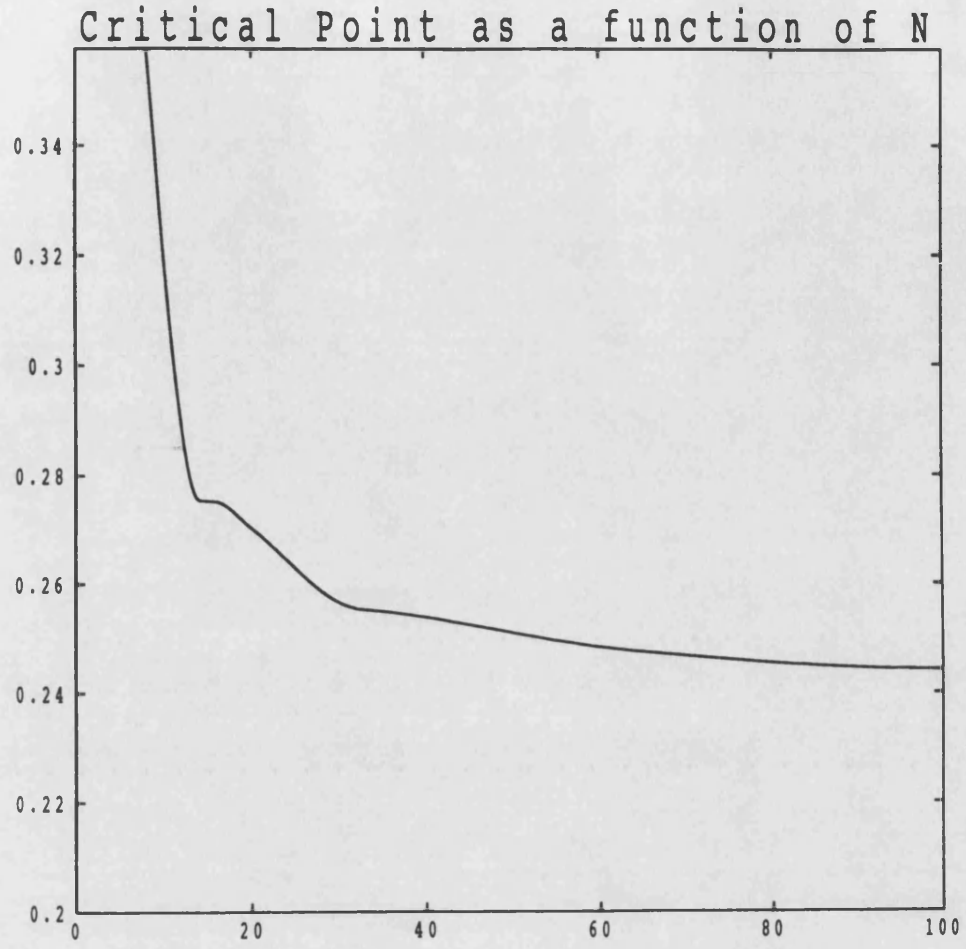

Fig 3.10 Critical point as a Function of cluster size: 2 impurities

variation of x_c would be as plotted in Fig(3.10). To find out whether or not the critical point converges to a certain value, we should continue increasing the cluster size, and find out the critical point for the considered clusters. We are pretty much sure that the critical point must approach a certain limit (This is because as can be seen in Fig 3.9 the θ values are bigger then the ϕ values i.e spins outside the cluster will rotate less then the spins inside the cluster. This means that after a certain size of cluster, the outside spins will prefer to stay as they were before the impurity was added). We have not found this limit because the number of spins involved becomes very large if we continue to increase the size of the cluster. We can find

the exact value of the critical point in reciprocal space by using Green's functions. The calculation is straightforward because the ideas are the same as for the single impurity case. Now there are two impurities. So we would not repeat the calculations here. The result would be sufficient enough because tackling to two impurities case in terms of Green's functions is no more than the extension of one impurity case. It should be pointed out here that the Green's function calculations is slightly different from the single impurity case. From Fig(3.G2) it is clear that the symmetry of this cluster is different from the single impurity case. It is antisymmetric under 180° rotation. One can define two symmetry operations as

$$g_1 U = U \quad and \quad g_2 U = -U$$

where g_1 and g_2 are reflection operations along two perpendicular directions as shown in Fig(3.G2). These two operators are commute(the 'Abelian group is g_1, g_2, and $g_1 g_2 = inversion$), so one can choose the wavefunction as

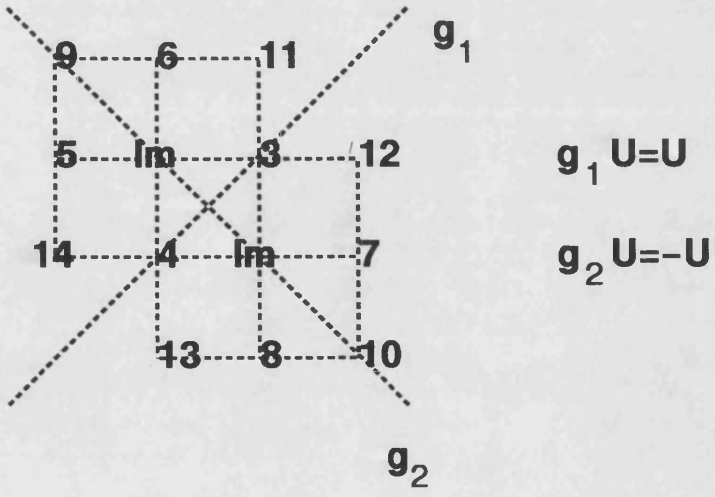

Fig. **3.G2** Symmetry of two impurities cluster

$$\phi = \begin{bmatrix} 0 \\ 0 \\ a \\ -a \\ -b \\ b \\ b \\ -b \\ 0 \\ 0 \\ c \\ c \\ -c \\ -c \end{bmatrix}$$

which is the best energy solution(we have looked at the other eigenvectors as well, but they are not the ground energy solutions). So one can easily verify that

$$G^0(Z)\phi = \begin{bmatrix} 0 \\ 0 \\ \alpha = a(G_0 - G_2) + 2b(G_2 - G_3) + 2c(G_1 - G_4) \\ -\alpha \\ -\beta = a(G_3 - G_2) - b(G_0 - G_2 - G_7 + G_5) + c(G_6 - G_1) \\ \beta \\ \beta \\ -\beta \\ 0 \\ 0 \\ \gamma = a(G_1 - G_4) + b(G_1 - G_6) + c(G_0 + G_2 - G_7 - G_5) \\ \gamma \\ -\gamma \\ -\gamma \end{bmatrix}$$

where $G_0 ... G_7$ can be calculated from Eq(3.18). Using the local disturbance H_1 one can reduce the problem to a 2x2 determinant problem. From this determinant one can find the critical point as $x_c = 0.237413$. In addition to this critical point the Green's functions calculations shows that there is another point which corresponds to a stable energy state. This point is $x_c^e = 0.4117075$ which is slightly bigger than the critical point of a single impurity. In other words Green's functions say that there are two solutions to this problem. One of them is reasonable, which is the lower one and corresponds to the ground state ordering. The problem is the second

one. We know that there are two impurities, each of them can be considered as an independent one impurity cluster. In other words two single impurity clusters created now. These two clusters interact with each other and make bonding and antibonding combination. We believe that the small x_c corresponds to the bonding contribution whereas the second one is due to the antibonding of these two clusters. However it can easily be said that the critical point is now smaller. As we expect the concentrations of impurity changes the critical point. Before moving on to a different cluster it might be useful to play with the position of impurities and find out the critical point. When we choose the impurities as nearest neighbours to each other as in Fig(3.11), the critical point would be $x_c = 0.410254$, which indicates that the relative positions of impurities are important.

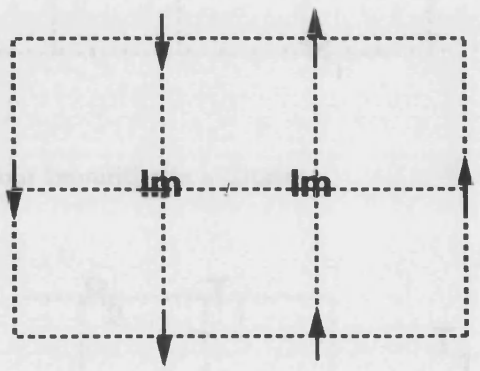

Fig. 3.11 Two nearest neighbour impurities in a cluster

When we want to find the critical point we must be aware of this. For any given lattice we can put the impurities wherever we want. But in the real material we are not allowed to do this. Because the structure of the alloy itself decides to do this positioning. For example in MnCu the two nearest neighbours of Cu atoms are favourable whereas in MnNi they are not. So when we are studying the critical point

we must know which material is going to be chosen. Then we can decide where the impurities might go. Now we may go to another stage which is four impurities in a chosen cluster as in Fig(3.12a).

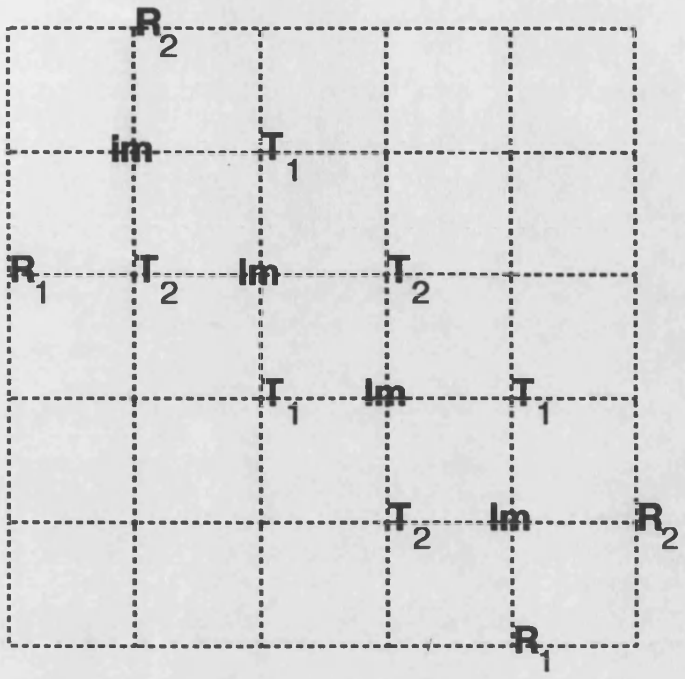

$$T_1 = S_1 \cos\theta + S_2 \sin\theta$$
$$T_2 = S_1 \cos\theta - S_2 \sin\theta$$
$$R_1 = S_1 \cos\phi + S_2 \sin\phi$$
$$R_2 = S_1 \cos\phi - S_2 \sin\phi$$

$$S_1 \cdot S_2 = 0$$

Fig. **3.12a** Four Impurities in a Cluster

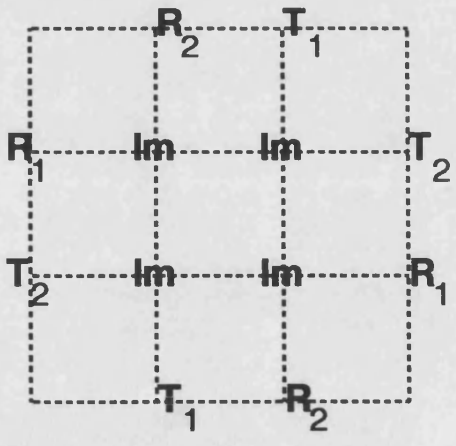

$$T_1 = S_1 \cos\theta - S_2 \sin\theta$$
$$T_2 = S_1 \cos\theta + S_2 \sin\theta$$
$$R_1 = -S_1 \cos\phi + S_2 \sin\phi$$
$$R_2 = -S_1 \cos\phi - S_2 \sin\phi$$

Fig. **3.12b** Four Impurities in a Cluster different positions of impurities

Again the goal is to find the critical point. First of all the energy differences

are required. It is

$$\delta H + const = (\theta \quad \phi)\begin{pmatrix} 4-12x & 4x \\ 4x & 12-20x \end{pmatrix}\begin{pmatrix} \theta \\ \phi \end{pmatrix} \tag{3.42}$$

The secular determinant gives $x_c = 0.311017$. Now we can compare this result with a single impurity and double impurities. It is obvious that the critical point becomes smaller if the impurity concentration is increased. Again one can find the exact critical point by using the Green's functions as $x_c = 0.167874$. We found three critical points for three different clusters. We saw that the critical point decreases with increasing the number of impurities, if the positions of impurities are carefully chosen so that one can obtain the best results from it. We should make this point more clear. Let us take the four impurities case in a cluster. We have already said that for Fig(3.12a) the critical point $x_c = 0.167874$. However, if we consider another possibility of four impurities as in Fig(3.12b) the critical point becomes $x_c = 0.412915$. This indicates that the position of impurities are important but unfortunately we can not decide where the impurities should go. This is controlled by the materials themselves. For example in MnNi alloys the Ni atoms anti-cluster means that the probability of finding two nearest neighbour impurities is very small, whereas for MnCu alloys the Cu atoms cluster and the probability of two nearest neighbour impurities is quite big. It is obvious that materials decide themselves where the impurities might go. Although we do not know where to put impurities, we can explain the interaction of impurities. As we pointed out for the case of two impurities, we found two critical points. We mentioned that the existence of two critical points can be interpreted as two impurities play bonding and anti-bonding contribution. This idea can be generalised for three and four impurities cases. As we naively expect there must be many critical points as a result of this bonding and

anti-bonding business. We believe that the smallest one, which corresponds to the ground state ordering is due to the bonding contributions and bigger ones ,which correspond to low-lying excitations, due to mixing of bonding and antibonding.

All these interactions we have been talking about are the case of if the impurities are next nearest neighbours to each other. In other words if they are in the same sublattice that they give the best result. We know from Fig(3.11) (this is a two impurities cluster) that if the impurities are nearest neighbours to each other the result is not very good. This interaction of impurities can be understood when we realise that the collinear phase is a combination of two sublattices as we explained earlier. If the impurities are in the same sublattice (for example if they are next nearest neighbours to each other) the spins in the another sublattice would feel uncomfortable since they lose some of antiparallel spins. In order to cancel this uncomfortable situation locally they would rotate and the result obtained from this situation is the best result we can obtain. However, if the impurities are in different sublattices (for example if they are nearest neighbours to each other) the obtained result is not as good as the former case. Let us take two impurities cluster as an example(Fig(3.11a)). As can be seen in this picture, the A atoms are unhappy since they are losing one of their good neighbour. Same is true for B atoms. However, two of A atoms and two of B atoms are quite comfortable since they are losing one of their bad next nearest neighbour. The only possibility looks like A_3 and B_3 are uncomfortable. So these two atoms may rotate in order to cancel this slight unhappiness. When we compare this situation with the single impurity case we can easily say that the single impurity does better than two impurities(if the impurities are in different sublattices) since for the single impurity case, at least four spins (nearest

neighbours to impurity) would be effected, but as we already explained, only two spins are unhappy and they may rotate.

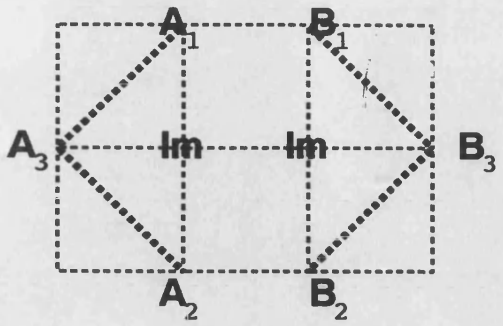

Fig. 3.11a Two impurities in different sublattices

However if the impurities are away from each other it does not make too much differences being on the same sublattice or different sublattices. The result is pretty much the same for two cases. This is because bonding and antibonding contribution to the local distortion in the presence of impurities. We should point out here that the same argument does not work for the improved collinear state. For this state if the impurities are on the same line, the result we can obtain is much better than if the impurities are opposite lines. This is the way how the impurities interact with each other.

By adding more impurities, we are increasing the local crystal field which is responsible for spin rotations. The big local crystal field causes more spins to rotate. If all the spins are rotated such that all of them have two perpendicular component the state can not remain collinear. It should be reminded that the last two calculations are in small clusters, it is not concerning the entire crystal. So it is still early to talk about a phase transition. The phase transition occurs if many such

clusters are created such that they interact with each other and percolate through the entire crystal. So far our calculations are for the simplest collinear phase. There is another collinear phase which is degenerate with the non-collinear one. We want to study the impurities in this collinear phase now. But there is a little problem here because it is degenerate with the non-collinear phase and we should worry about how to stabilise this state. Firstly we call this state an improved collinear state in order to indicate that this phase is different from the collinear phase we have been considering so far and we will not think about stabilising the state at the time being. We simply look at the critical point if the impurity is present.

3-3 The Critical Point in the Improved Collinear State

Now we are in a position that we can perform the cluster calculations and find out the critical point as we did for the simplest collinear state. We will start our calculations with a small cluster and zero anisotropy then we will increase the anisotropy and the size of the cluster. Let us chose a small cluster first(Fig(3.13)).

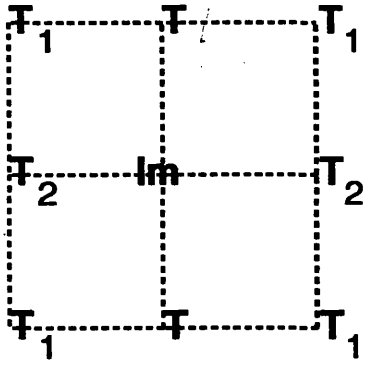

Fig. 3.13 One impurity in the degenerate Collinear phase: a Small Cluster

The energy differences for the cluster is

$$\delta H = -2TS + 4TT_1 + 4xTT_2 - 4xTS + 4T_1T_2 + 12xT_1S - 2T_2S + 4xT_2S \qquad (3.43)$$

Fig. 3.14 25 spins of degenerate collinear state with an impurity

where

$$T = S\cos\theta + S'\sin\theta \tag{3.44}$$

$$T_1 = S\cos\theta_1 - S'\sin\theta_1 \tag{3.45.a}$$

$$T_2 = -S\cos\theta_2 + S'\sin\theta_2 \tag{3.45.b}$$

when we substitute these T's into Eq(3.42) we would obtain

$$\begin{aligned}\delta H = &-2\cos\theta + 4x\cos(\theta-\theta_1) - 4x\cos(\theta-\theta_2) - 4x\cos\theta \\ &-4\cos(\theta_1-\theta_2) - 12x\cos\theta_1 + 2\cos\theta_2 - 4x\cos\theta_2\end{aligned} \tag{3.46}$$

Using the small angle approximation one can obtain x_c critical point from the secular determinant as $x_c = 0.5528$. We know that this phase was stable when $x > 0.5$ before the impurity addition now it is stable when $x > 0.5528$. One thing is certain that in the interval $0.5 < x < 0.5528$ this phase is not stable. What is happening in that interval then? We do not want to answer this question now. Firstly we want to increase the size of the cluster and find out x_c critical point. Let us take a bigger cluster (Fig(3.14)).

In order to find the critical point we follow the same method as previously performed. Again using the small angle approximation one can find the critical point as $x_c = 0.628684$. Obviously the non-stability region is increased. The increasing on x_c is quite large. The question now is whether or not x_c is converging to a certain value. As we know from the simplest collinear case the x_c is converging and we found it as $x_c = 0.40776$ by using the Green's function method. Before using the Green's functions for this case we want to continue to increase the size of the cluster and look at the change on x_c. Now we will consider a big cluster (Fig(3.15)).

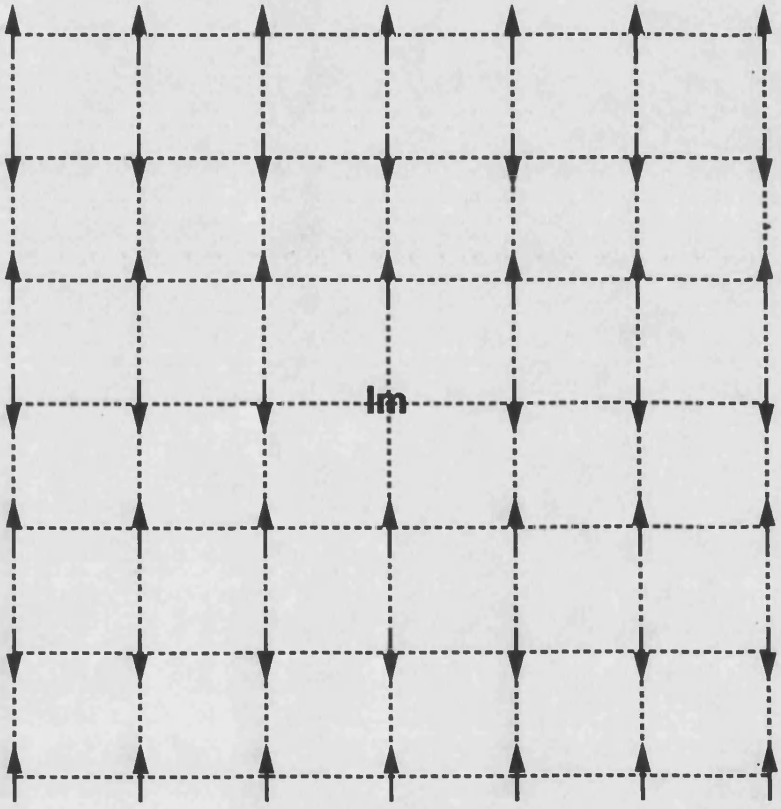

Fig. 3.15 49 spins in degenerate collinear phase with an impurity

Using the same method one can find the critical point as $x_c = 0.677906$. It is obvious from these three results that x_c is increasing. As we shall see later on,

the Green's function calculation of x_c says that the critical point is divergent. It means that one impurity changes the present phase to another one. However this is not the case. Because in real materials one impurity does not effect the system. This may means that we chose the wrong phase. The wrong chosen thing is not the phase at all. What we missed was some kind of extra interactions. There must be other interactions which prevents this sudden phase transition. The model we have been tackling is the classical Heisenberg model:

$$H = \sum_{ij} S_i S_j + x \sum_{[ij]} S_i S_j \tag{3.47}$$

where S_i are classical spins of magnitude S and x is the ratio of bond strengths between next nearest neighbours, denoted by [ij], and nearest neighbours, denoted by ij. In order to prevent this sudden phase transition by an impurity, we will include much smaller contributions corresponding to spin-orbit coupling, crystal field interactions, and other effects[31]:

$$H_1 = -\frac{y}{4} \sum_{ij} [\mathbf{S}_i \mathbf{S}_j]^2 - \frac{z}{2} \sum_i [(S_i^x)^4 + (S_i^y)^4 + (S_i^z)^4] \tag{3.48}.$$

The first term is isotropic and prefers states with collinear (although not necessarily antiparallel) spins, while the second term attempts to align the spins parallel to the Cartesian directions. Obviously, this fourth order contribution is non-linear in its own right, and therefore further complicates the optimisation under constraints problem. The choice $y > 0$ and $z > 0$ ensures that if the Heisenberg model allows a collinear ground state, then that solution will be stabilised by the additional smaller contribution. Once the collinear state is stabilised we can perform the cluster calculations and look at the variation of the critical point.

3-3-1Cluster Calculation

It is proved previously that the improved collinear state can be stabilised by much smaller contributions. Now we want to find the critical point which is the main criteria to the phase transition. First of all we will fix those smaller terms and find out the critical point as a function of the cluster size. Basically we will choose a small cluster with an impurity and find out the critical point then increase the size of the cluster while the small terms are fixed. We have done this calculation for various y and z terms. The plot of the critical point versus $\frac{1}{N}$.(where N is the number of spins in the cluster) shows that the critical point approaches the boundary point(Fig(3.16)). These calculations are real space calculations and far away from the exact value.

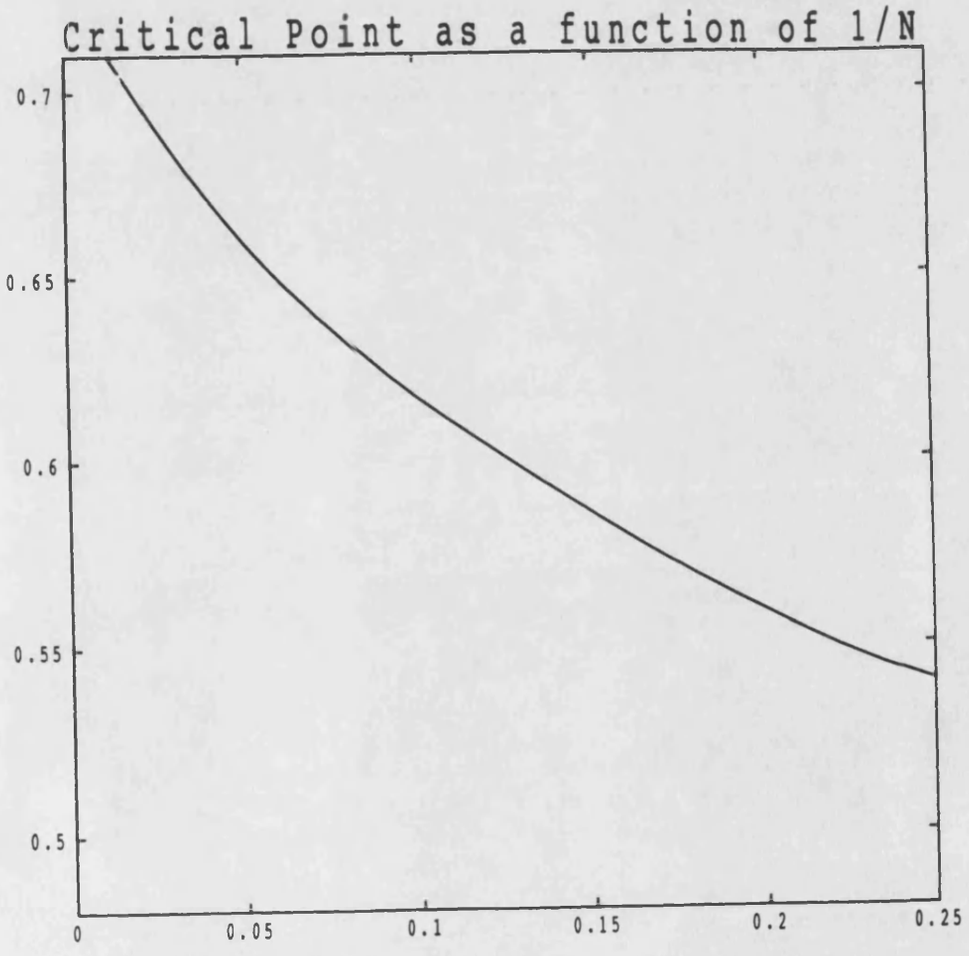

Fig 3.16 Critical point as a Function of 1/N

In order to find the exact critical point again we must use the Green's functions technique which is linearising the problem. In order to find the critical point we must solve

$$det|1 - H_1 G| = 0 \tag{3.49}$$

where

$$-H_1 = \begin{pmatrix} 2x+2y & -\frac{1}{2}-\frac{y}{2} & -\frac{1}{2}-\frac{y}{2} & \frac{1}{2}-\frac{y}{2} & \frac{1}{2}-\frac{y}{2} & -\frac{x}{2} & -\frac{x}{2} & -\frac{x}{2} & -\frac{x}{2} \\ -\frac{1}{2}-\frac{y}{2} & \frac{1}{2}+\frac{y}{2} & 0 & 0 & 0 & 0 & 0 & 0 & 0 \\ -\frac{1}{2}-\frac{y}{2} & 0 & \frac{1}{2}+\frac{y}{2} & 0 & 0 & 0 & 0 & 0 & 0 \\ \frac{1}{2}-\frac{y}{2} & 0 & 0 & \frac{y}{2}-\frac{1}{2} & 0 & 0 & 0 & 0 & 0 \\ \frac{1}{2}-\frac{y}{2} & 0 & 0 & 0 & \frac{y}{2}-\frac{1}{2} & 0 & 0 & 0 & 0 \\ -\frac{x}{2} & 0 & 0 & 0 & 0 & \frac{x}{2} & 0 & 0 & 0 \\ -\frac{x}{2} & 0 & 0 & 0 & 0 & 0 & \frac{x}{2} & 0 & 0 \\ -\frac{x}{2} & 0 & 0 & 0 & 0 & 0 & 0 & \frac{x}{2} & 0 \\ -\frac{x}{2} & 0 & 0 & 0 & 0 & 0 & 0 & 0 & \frac{x}{2} \end{pmatrix} \tag{3.50}$$

and

$$G = \begin{pmatrix} G_0 & G_1 & G_1 & G_2 & G_2 & G_3 & G_3 & G_3 & G_3 \\ G_1 & G_0 & G_4 & G_3 & G_3 & G_2 & G_5 & G_5 & G_2 \\ G_1 & G_4 & G_0 & G_3 & G_3 & G_5 & G_2 & G_2 & G_5 \\ G_2 & G_3 & G_3 & G_0 & G_6 & G_1 & G_1 & G_7 & G_7 \\ G_2 & G_3 & G_3 & G_6 & G_0 & G_7 & G_7 & G_1 & G_1 \\ G_3 & G_2 & G_5 & G_1 & G_7 & G_0 & G_4 & G_8 & G_6 \\ G_3 & G_5 & G_2 & G_1 & G_7 & G_4 & G_0 & G_6 & G_8 \\ G_3 & G_5 & G_2 & G_7 & G_1 & G_8 & G_6 & G_0 & G_4 \\ G_3 & G_2 & G_5 & G_7 & G_1 & G_6 & G_8 & G_4 & G_0 \end{pmatrix} \tag{3.51}$$

in terms of

$$G_0 = \frac{1}{E - E_K} \tag{3.52.a}$$

$$G_1 = \frac{\cos k_y}{E - E_k} \tag{3.52.b}$$

$$G_2 = \frac{\cos k_x}{E - E_k} \tag{3.52.c}$$

$$G_3 = \frac{\cos k_x \cos k_y}{E - E_k} \tag{3.52.d}$$

$$G_4 = \frac{2\cos^2 k_y - 1}{E - E_k} \tag{3.52.e}$$

$$G_5 = \frac{2\cos k_x (2\cos^2 k_y - 1)}{E - E_k} \tag{3.52.f}$$

$$G_6 = \frac{2\cos^2 k_x - 1}{E - E_k} \tag{3.52.g}$$

$$G_7 = \frac{\cos k_y(\cos^2 k_x - 1)}{E - E_k} \tag{3.52.h}$$

$$G_8 = \frac{(\cos^2 k_x - 1)(\cos^2 k_y - 1)}{E - E_k} \tag{3.52.i}$$

and

$$E_k = 2z + 2x(1 - \cos k_x \cos k_y) + y(2 - \cos k_x - \cos k_y) + (\cos k_x - \cos k_y) \tag{3.53}$$

Using the symmetry properties of the wave function the problem can be reduced to a 3x3 problem as

$$\begin{vmatrix} \frac{1}{y+1} + G_1 & G_2 & G_3 \\ G_2 & \frac{1}{y-1} + G_4 & G_5 \\ G_3 & G_5 & \frac{1}{2x} + G_6 \end{vmatrix} \tag{3.54}$$

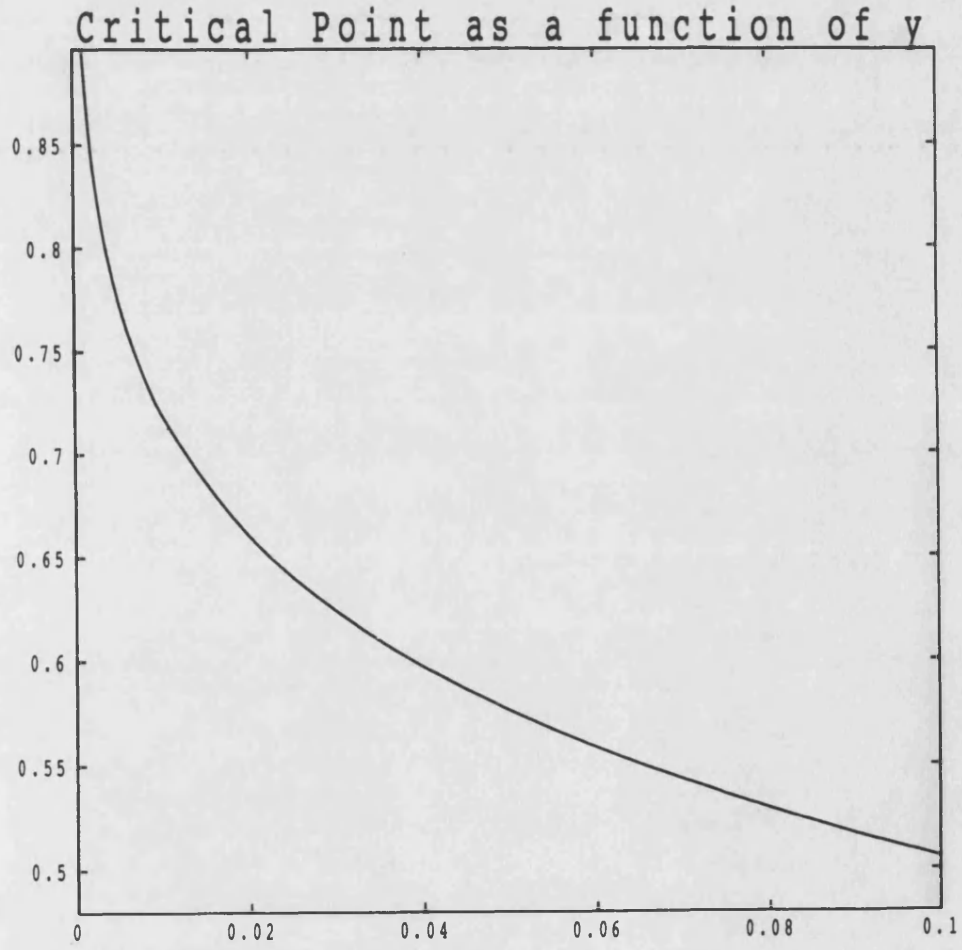

Fig 3.17 The Critical point as a function of y

We did two calculations: in the first calculation we set $z = 0.$ and varied the y term.

By setting $z = 0$, we obtained a $2x2$ determinant as

$$\begin{vmatrix} \frac{1}{y+1} + (G_1 - G_3) & (G_2 - G_5) \\ (G_2 - G_3) & \frac{1}{y-1} + (G_4 - G_5) \end{vmatrix} \tag{3.54a}$$

For $z = 0$ we calculated the critical point from this determinant. As we can see in Fig(3.17) the critical point approaches to the boundary point. When $y = 0.12$ the critical point become smaller then 0.5 which is not usable for us. In the second calculation we set $y = 0$ and varied the z term. As can be seen in Fig(3.18) this time it goes below the boundary point when $z = 0.12$. These two

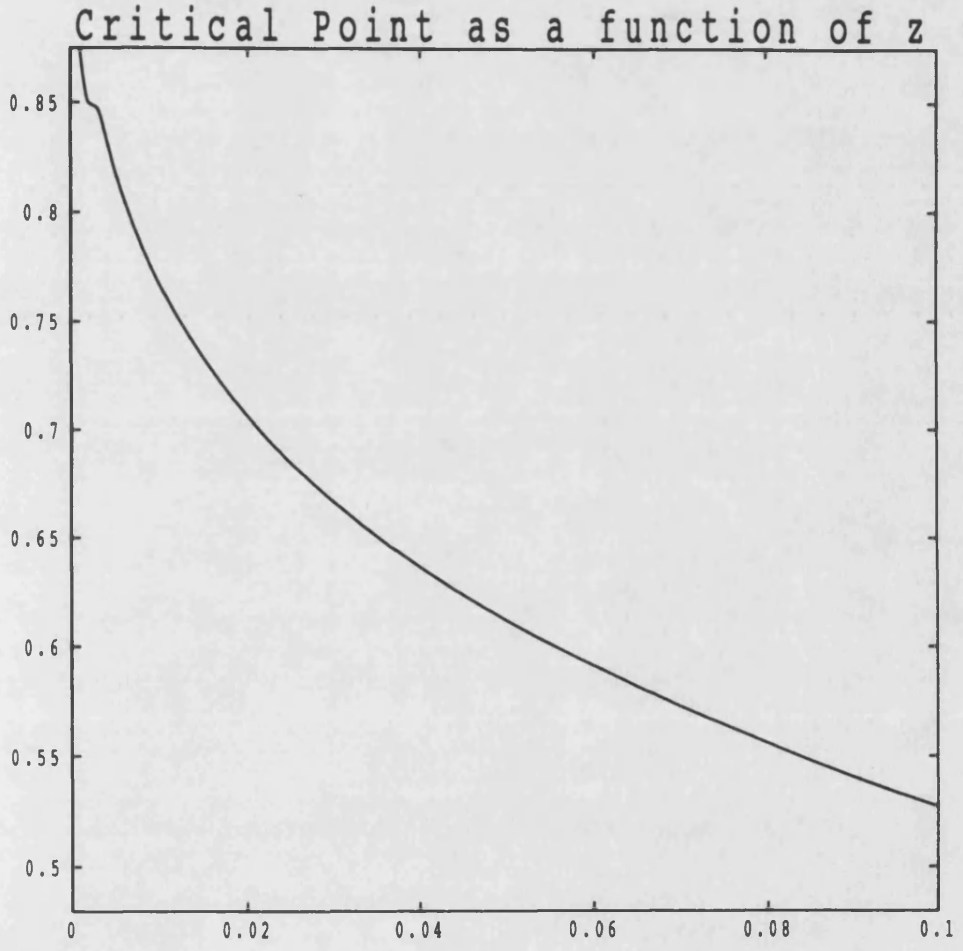

Fig 3.18 Critical point as a function of z

calculations are exact and can be compared with the results for the cluster calculations. When we perform the cluster calculations we did not know the exact result. What we saw there that the critical point is increasing with the cluster size. Now

we know that the critical point is divergent. It has a certain value and below that value the collinear state is not stable any more. So one might think that the non-collinear state is stable there. Hereafter one can repeat many impurity calculations by simply choosing more then one impurities in the cluster. We will not repeat the same calculations again. However the variation of the critical point is shown from Fig(3.19a) to Fig(3.19c) for different clusters.

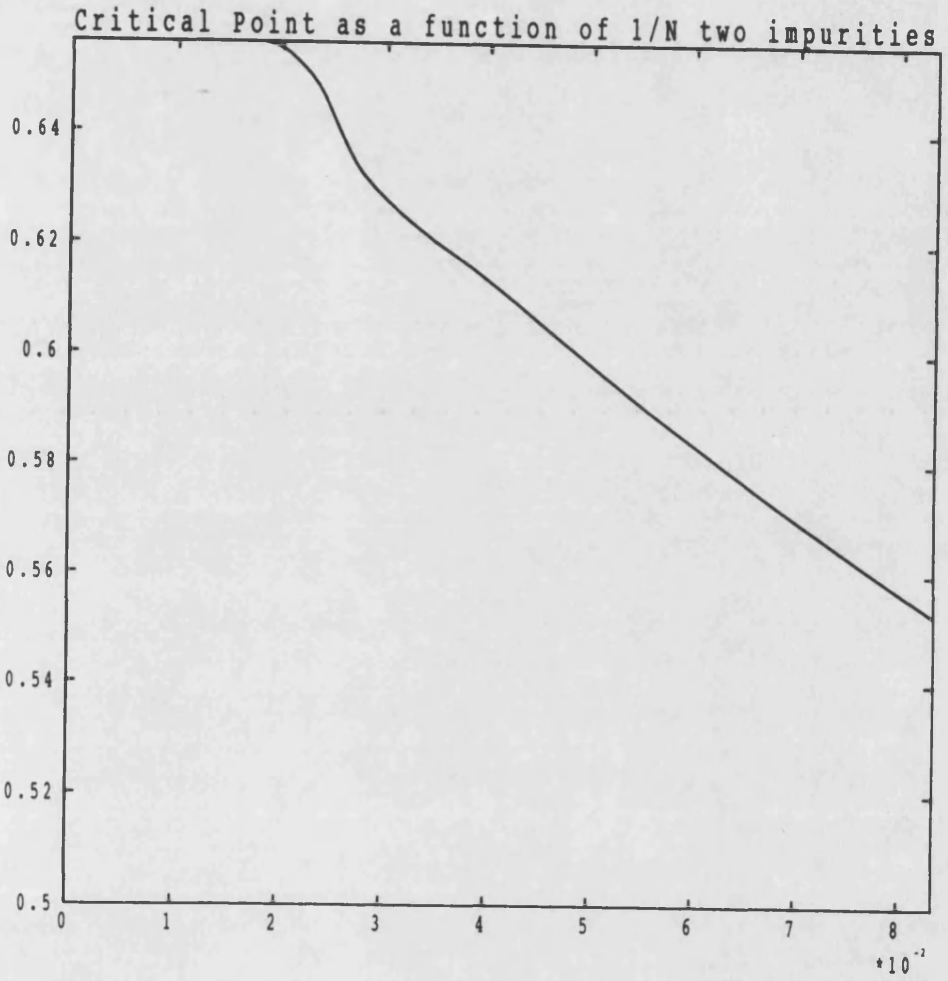

Fig 3.19a Critical point as a Function of 1/N; 2 impurities

In Fig(3.19a) we took a cluster with two impurities(the arrangement of impurities is shown in Fig(3.19a1)). In order to get rid of divergancy we added just a bit y term into the Heisenberg Hamiltonian (y=0.001). As it can be seen in this picture the critical point increases with increasing the cluster size, as we predicted before.

Obviously the critical point has a certain value, but we have not calculated it. However, it can be calculated by the Green function calculations.

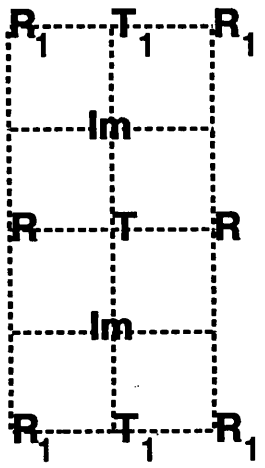

$$T = S_1 \cos\theta + S_2 \sin\theta$$

$$T_1 = S_1 \cos\phi - S_2 \sin\phi$$

$$R = S_1 \cos\psi - S_2 \sin\psi$$

$$R_1 = S_1 \cos\varphi + S_2 \sin\varphi$$

Fig. 3.19a1 Position of two impurities in a cluster

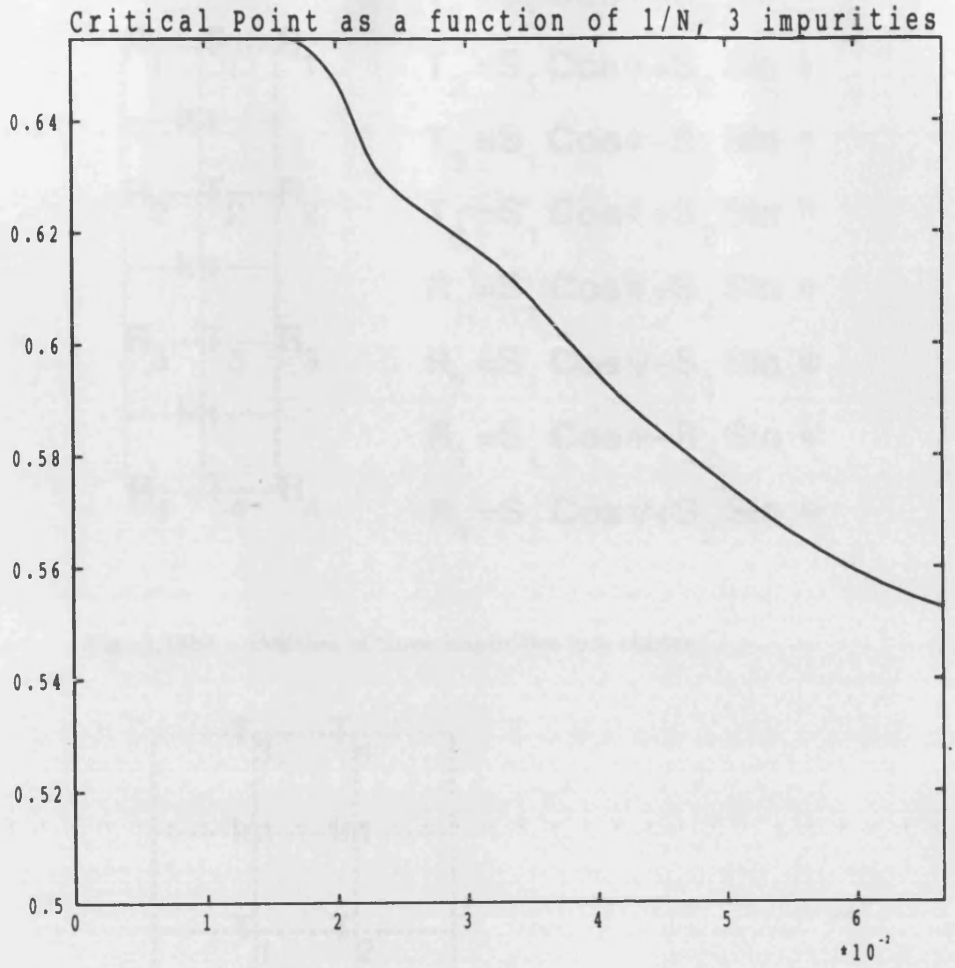

Fig 3.19b Critical point as a function of 1/N: 3 impurities

In Fig(3.19b) we have considered three impurities in a cluster(position of impurities is shown in Fig(3.19b1)). Again the critical point is increasing with increasing the cluster size. Little bit of y term (y=0.001) ensures that the critical point is not divergent. We have not calculated the exact value of the critical point, however, it can be found by the technique we have used for the single impurity problem.

In Fig(3.19c) we plotted x_c against 1/N in the presence of four impurities(position of impurities is shown in Fig(3.19c1.ps)). It is obvious that x_c is increasing with the cluster size. y term (y=0.001) is included to the Heisenberg Hamiltonian

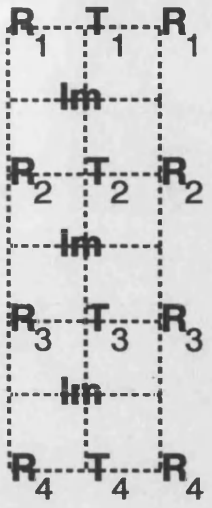

$$T_1 = S_1 \cos\theta - S_2 \sin\theta$$
$$T_2 = S_1 \cos\phi + S_2 \sin\phi$$
$$T_3 = S_1 \cos\phi - S_2 \sin\phi$$
$$T_4 = S_1 \cos\theta + S_2 \sin\theta$$
$$R_1 = S_1 \cos\varphi + S_2 \sin\varphi$$
$$R_2 = S_1 \cos\psi - S_2 \sin\psi$$
$$R_3 = S_1 \cos\varphi - S_2 \sin\varphi$$
$$R_4 = S_1 \cos\psi + S_2 \sin\psi$$

Fig. **3.19b1** Position of three impurities in a cluster

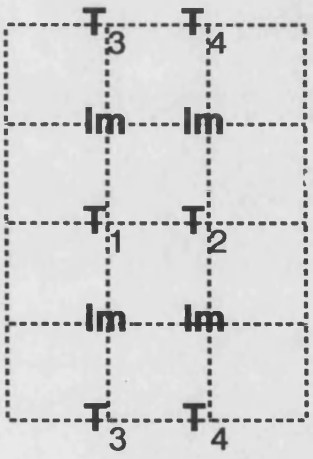

Fig. **3.19c1** Position of four impurities in a cluster

to make sure that the critical point is not divergent. The exact value of it again can be calculated by using the Green's function method.

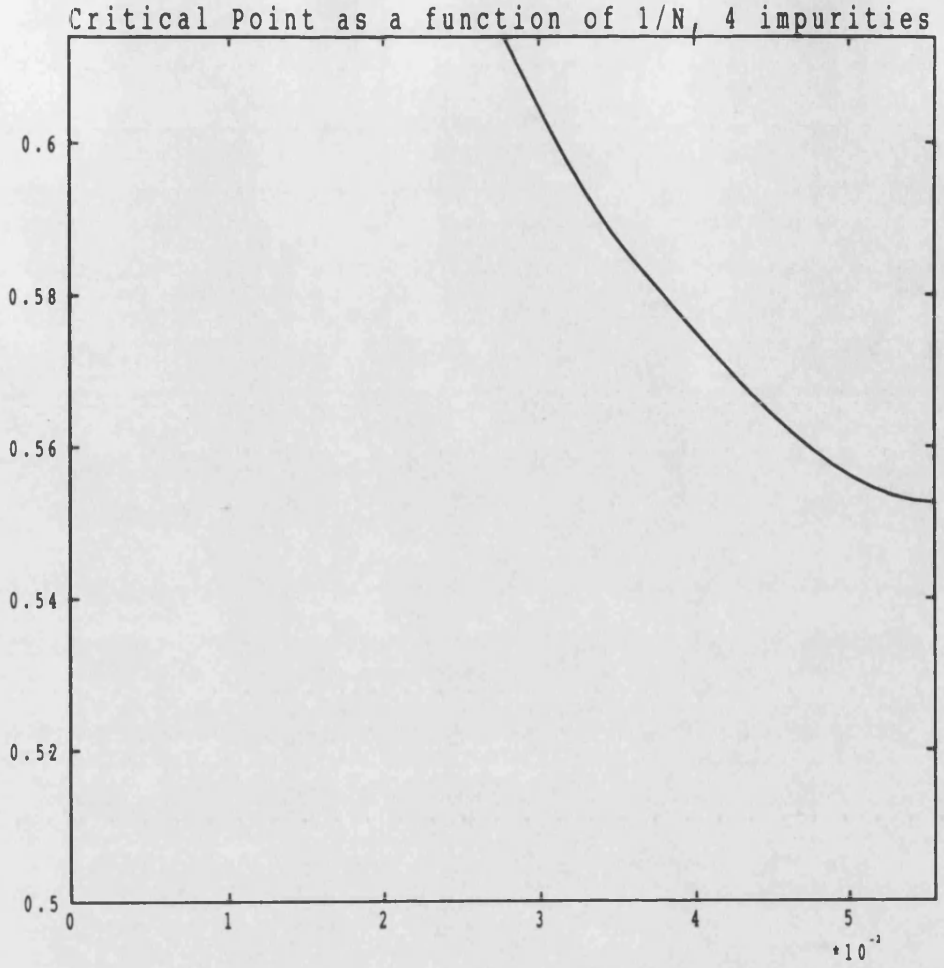

Fig 3.19c Critical point as a function of 1/N; 4 impurities

3-4 Discussion:

In this chapter we mainly investigated the effect of impurities in two collinear states named as simple and improved collinear states. In the simple collinear case we observed that after an impurity the state is stable below a critical point which is less than the boundary point. There is a region $x_c < x < 0.5$ that the structure is not the collinear state. There the non-collinear state has lower energy. It is known from the previous chapter that without the impurity both states (collinear and non-collinear) have the same energy at the boundary point which is $x = 0.5$. But the impurity changed the boundary point. Now these two state are degenerate at the critical point. This means that if we add an impurity at the degeneracy point we can remove the degeneracy and stabilise the non-collinear state. In the second case we add extra terms into the Hamiltonian in order to stabilise the improved collinear state which has the same energy as the non-collinear state. Without these extra terms (spin-orbit and crystal field) we saw that an impurity completely change the present state which is not the case for real materials. With these extra interactions we calculated the critical point. Again we observed that there is a region that the non-collinear state has lower energy. So one may say that the degeneracy can be removed by impurity additions. If it is so then impurities can cause a magnetic phase transition. It is still early to talk about a magnetic phase transition. In order to observe a magnetic phase transition we must go to experiments which are magnetic diffuse scattering studies. As we will see in chapter four, the impurities cause a magnetic phase transition in agreement with experiments. At the moment we can say that impurities changes the boundaries of the states and may cause a first order magnetic phase transition if the required amount of clusters were created such that

the interaction among the clusters percolate through the entire crystal. In other words if the amount of created clusters are about the percolation threshold. This is the most satisfying picture of how a phase transition might occurs. However, as we said above, we still need to go magnetic diffuse scattering experiments in order to make sure that the phase transition occurs by alloying. This is the topic of the next chapter.

Chapter Four

Magnetic Diffuse Scattering as a Probe

In the previous chapter it was pointed out that paramagnetic impurities may cause a first order magnetic phase transition. Because the impurities trap a local non-collinear arrangement as found previously. This phase transition can not be easily observed. There is an experimental technique known as magnetic diffuse scattering which gives information about fluctuation of magnetic moments. In order to understand whether or not impurities (in a light doping regime) do cause a first order magnetic phase transition one must analyze these scattering events. This is not a straight forward analysis. It is really a complicated problem. The origin of this scattering is neutron. In order to have a basic understanding of this scattering, we should give a brief introduction about the usage of neutrons in condensed matter physics.

Usage of Neutrons in Condensed Matter.

The usefulness of thermal neutrons arises from basic properties of the neutron. The theory of x-ray scattering is similar to the theory of neutron scattering in some sense. Both theories are important in the study of condensed matter. But we should develop neutron scattering in order to have some more information. The reason that the neutrons give more information than x-ray scattering can be summarised as follows.

Firstly the de Broglie wavelength of thermal neutrons is about the same order of interatomic distances in condensed matter. Thus, interference effects occur which

yield information on the structure of the scattering system.

Secondly the penetration depth of neutron in matter is extremely long, largely because they are uncharged. Neutron scattering is therefore well suited to the study of bulk properties, and surface scattering effects can usually be neglected in the interpretation of data. Since a neutron is uncharged, it can penetrate deeply into the target and it comes close to the nucleus. Neutrons are thus scattered by nuclear forces, and for certain nuclides the scattering is large. An important example is light hydrogen which is virtually transparent to x-rays (this is because the x-ray scattering is proportional to atomic number Z and a hydrogen atom has only one electron) but which scatters neutrons strongly.

Thirdly, the energy of thermal neutrons is of the same order as that of many excitations in condensed matter. So when the neutron is inelasticly scattered by the creation or annihilation of an excitation, the change in the energy of the neutron is a large fraction of its initial energy. Thus measurement of the neutron energies provides accurate information on the energies of the excitations, for example phonons. Thus the neutron scattering can be used for measuring phonon dispersion.

Fourthly, the neutron has a magnetic moment, which means that neutrons interact with the unpaired electrons in magnetic atoms. Elastic scattering from this interaction gives information on the arrangement of electron spins. Inelastic magnetic scattering on the other hand gives the energies of magnetic excitations (magnons).

It is convenient to develop the theories of nuclear and magnetic scattering separately. Firstly we will derive a general expression for the neutron cross-section.

Then we will consider the nuclear scattering and develop it for the magnetic case.

4-1 Neutron Scattering Cross Section

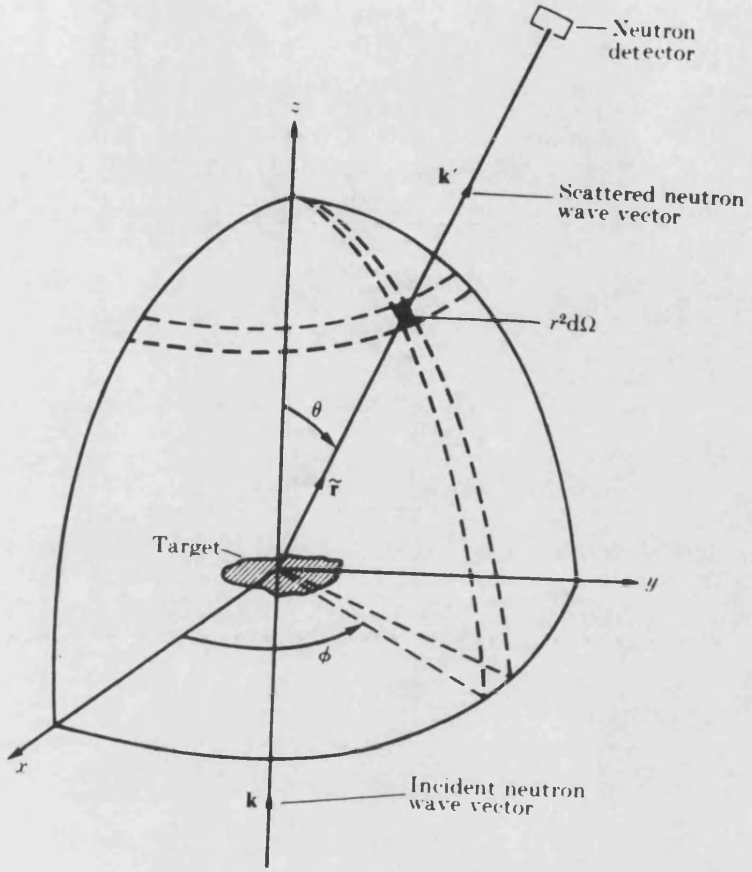

Fig 4.1 The Geometry of the Scattering

The geometry of the scattering experiment is shown in Fig(4.1). A neutron specified by the wave vector $\mathbf{k}$ is scattered into a state with wave vector $\mathbf{k}'$, the transfer of momentum to the target sample is $\hbar\boldsymbol{\kappa}$ where the scattering vector $\boldsymbol{\kappa} = \mathbf{k} - \mathbf{k}'$. The basic quantity that is measured is the partial differential cross-section which gives the fraction of neutrons of incident energy E scattered into an element of solid angle $d\Omega$ with an energy between E' and $E' + dE'$, the cross-section is described by

$$\frac{d^2\sigma}{d\Omega dE'} \tag{4.1}$$

We begin by obtaining an expression for the differential cross-section for the elastic scattering (no energy loses). Then we will generalise it to the inelastic case.

The incident neutron has the state $\psi_{\mathbf{k}}$ and the scattered neutron has the state $\psi_{\mathbf{k}'}$. The direction of propagation of the scattered neutron with respect to the incident neutron is defined by the polar angle θ and the azimuthal angle ϕ. If the flux of incident neutrons defined as the number per unit area per unit time, is N, then the number scattered per unit time into the element of solid angle $d\Omega = \sin\theta d\theta d\phi$ is

$$N(\frac{d\sigma}{d\Omega})d\Omega \tag{4.2}$$

where $\frac{d\sigma}{d\Omega}$ is the differential cross-section.

If the target sample has no excitations or the energy of low lying excitation is very big compared with energies of neutrons then clearly the scattering is elastic. To calculate the differential cross-section for this case we need to know the probability of a transition from the plane wave state k to plane wave state k' both having the same energy. This probability is given by Fermi's Golden rule as

$$W_{\mathbf{k}\rightarrow\mathbf{k}'} = \frac{2\pi}{\hbar}|\int d\mathbf{r}\psi_{\mathbf{k}'}{}^{*}\hat{V}\psi_{\mathbf{k}}|^{2}\rho_{\mathbf{k}'}(E') \tag{4.3}$$

where $\hat{V}$ is the interaction potential that causes the transition, in our case the interaction between the incident neutron and the target sample, and $\rho_{\mathbf{k}'}(E')$ is the density of final scattering states per unit energy range. To evaluate the latter we must first decide upon the normalisation of our wave functions. For a large box of volume L^3 the states $\psi_{\mathbf{k}}$ and $\psi_{\mathbf{k}'}$ are, respectively,

$$\psi_{\mathbf{k}} = \frac{1}{L^{\frac{3}{2}}}\exp(i\mathbf{k}.\mathbf{r})$$

and

$$\psi_{\mathbf{k}'} = \frac{1}{L^{\frac{3}{2}}} \exp(i\mathbf{k}'.\mathbf{r})$$

It follows that our density of final state is[34]

$$\rho_{\mathbf{k}'}(E) = (\frac{L}{2\pi})^3 \frac{d\mathbf{k}'}{dE}.$$

Clearly,

$$d\mathbf{k}' = k'^2 d\Omega dk'$$

and

$$dE' = dE = \frac{\hbar^2 k}{m} dk,$$

so that

$$\rho_{\mathbf{k}'}(E) = (\frac{L}{2\pi})^3 \frac{mk}{\hbar^2} d\Omega \tag{4.4}$$

To obtain the cross-section we have to determine the incident flux of neutrons. This is

$$\phi(\mathbf{k}) = \frac{velocity \quad of \quad incident \quad neutrons}{L^3} = \frac{\hbar k}{mL^3} \tag{4.5}$$

then

$$d\sigma = W_{\mathbf{k}\to\mathbf{k}'} = L^6 (\frac{m}{2\pi\hbar^2})^2 | \int d\mathbf{r} \psi_{\mathbf{k}'}{}^* \hat{V} \psi_{\mathbf{k}} |^2 d\Omega \tag{4.6}$$

if we call

$$(\frac{m}{2\pi h^2}) \int d\mathbf{r} \exp(-i\mathbf{k}'.\mathbf{r}) \hat{V} \exp(i\mathbf{k}.\mathbf{r}) = < \mathbf{k}' | \hat{V} | \mathbf{k} > \tag{4.7}$$

we have

$$\frac{d\sigma}{d\Omega} = | < \mathbf{k}' | \hat{V} | \mathbf{k} > |^2 \tag{4.8.a}$$

$$= |f(\kappa)|^2 \tag{4.8.b}$$

where $f(\kappa)$ is called the scattering amplitude.

We turn now to the calculation of the partial differential cross-section that includes inelastic events. For such events the neutron energy is changed. This energy

$$\hbar w = \frac{\hbar^2}{2m}(k^2 - k'^2) \tag{4.9}$$

is finite. The change in the neutron energy can be considered as the response of the target sample through a rearrangement of its various states.

A state of the target is labeled by the index λ. In most cases this will have to be a composite label in order to specify a state completely. The corresponding eigenvector is $|\lambda>$, so that the initial state of the system and the incident neutron can be described as

$$|\mathbf{k}>|\lambda>=|\mathbf{k}\lambda> \tag{4.10}$$

The states $|\lambda>$ form a complete set. The energy associated with the target state described by $|\lambda>$ is denoted by E_λ. If the response of the target sample to the neutron interaction is to change from the state $|\lambda>$ to the state $|\lambda'>$, then the conservation of energy requires that

$$\hbar w = E_{\lambda'} - E_\lambda \tag{4.11}$$

then the cross-section becomes

$$(\frac{d\sigma}{d\Omega})_{\lambda'}^{\lambda} = \frac{k'}{k}|<\mathbf{k}'\lambda'|\hat{V}|\mathbf{k}\lambda>|^2 \tag{4.12}$$

where the factor $\frac{k'}{k}$ arises from the density of final neutron states divided by the incident neutron flux.

The partial differential cross-section can be obtained from this last equation by incorporating the energy conservation. Using the properties of δ function i.e

$$\int_{\infty}^{\infty} dE'\delta(E + E_\lambda - E' - E_{\lambda'}) = 1 \tag{4.13}$$

one can obtain the differential cross-section as

$$(\frac{d^2\sigma}{d\Omega dE'})^{\lambda}_{\lambda'} = \frac{k'}{k}| < \mathbf{k}'\lambda'|\hat{V}|\mathbf{k}\lambda > |^2\delta(\hbar w + E_\lambda - E_{\lambda'}) \tag{4.14}$$

We must now sum over the final state λ' as well as average over the initial states λ, using a probability factor p_λ. This factor might have the Boltzmann form

$$\frac{\exp(-\frac{E_\lambda}{k_B T})}{\sum_\lambda \exp(-\frac{E_\lambda}{k_B T})} \tag{4.15}$$

or some other form such as the Bose-Einstein form in the case of phonons. Thus

$$\frac{d^2\sigma}{d\Omega dE'} = \frac{k'}{k}\overline{\sum_{\lambda\lambda'} p_\lambda| < \mathbf{k}'\lambda'|\hat{V}|\mathbf{k}\lambda > |^2\delta(\hbar w + E_\lambda - E_{\lambda'})} \tag{4.16}$$

The horizontal bar in this equation stands for any relevant averages over and above those included in the probability p_λ. This expression is the first Born approximation to the cross-section. One consequence of the approximation is that the nuclear scattering amplitude depends on $\kappa = \mathbf{k} - \mathbf{k}'$.

When we derive the partial cross-section we have omitted the neutron spin. For a proper approach it must be included. However, for the special case when the interaction operator $\hat{V}$ is completely independent of neutron spin this omission is a good approximation. It is worth pointing out here that including the neutron spin brings an additional summation over p_σ for the spin probability to the differential cross-section.

For the time being we should remind that this is the cross-section that the experimentalists generally use. They simply measure the matrix element $| < \mathbf{k}'\lambda'|\hat{V}|\mathbf{k}\lambda > |^2$ for different purposes. In order to calculate this matrix element we must know the detailed form of the interaction operator $\hat{V}$. We will consider two

different cases and calculate this matrix element by using some approximate form for $\hat{V}$.

4-1-1 Nuclear Scattering

Although our main interest will be in magnetic scattering, we shall briefly consider the nuclear contribution. Let us begin by considering the nuclear scattering from a single fixed zero-spin nucleus located at **R**. In reality of course, the nuclei in a solid are not strictly located nor are they completely free. There is at the present no complete theory of the nucleon-nucleon interaction[33] but we know from experimental results that it has a very short range (of the order $1.5\text{x}10^{-13}cm$). Because this is much less then the wavelength of low-energy neutrons, and the nuclear radius is only about an order of magnitude greater, the neutron-nucleus scattering can contain only s-wave components[34]. In other words the scattering is isotropic, and can therefore be characterised by a single parameter b called the scattering length. b can be complex, and the real part may be either positive or negative depending on the energy of the incident neutron and the particular nucleus involved in the scattering. In general we can have different scattering lengths not only for each atomic type but also for each isotope.

The only form of $\hat{V}(\mathbf{r})$ which gives isotropic scattering in the Born approximation is a delta function.

Thus we set

$$\hat{V}(\mathbf{r}) = \frac{2\pi\hbar^2}{m} b\delta(\mathbf{r} - \mathbf{R}) \tag{4.17}$$

This potential is called as the Fermi pseudo-potential. Using this potential one can

easily calculate the cross-section from equation(4.7) by setting $\mathbf{R} = 0$

$$< \mathbf{k}'|\hat{V}|\mathbf{k} >= (\frac{m}{2\pi\hbar^2})\frac{2\pi h^2}{m}\int d\mathbf{r}\exp(-i\mathbf{k}'.\mathbf{r})\delta(\mathbf{r})\exp(i\mathbf{k}.\mathbf{r}) = b \qquad (4.18)$$

Then the cross-section would be

$$\frac{d\sigma}{d\Omega} = | < \mathbf{k}'|\hat{V}|\mathbf{k} > |^2 = b^2 \qquad (4.19)$$

which gives a total cross-section

$$\sigma = 4\pi|b|^2 \qquad (4.20)$$

We have taken the scattering length as a constant, independent of the neutron energy. This is valid at the low neutron energies which are used.

Now we will consider the scattering from many fixed nuclei situated at lattice sites $\mathbf{R}_n$. If we have a compound or if there are isotopes, the scattering amplitudes of the different nuclei may be different. In this case the total pseudopotential is

$$\hat{V}(\mathbf{r}) = \frac{2\pi\hbar^2}{m}\sum_n b_n\delta(\mathbf{r} - \mathbf{R}_n) \qquad (4.21)$$

now b_n describes the scattering length of the nth nucleus. Thus

$$< \mathbf{k}'|\hat{V}|\mathbf{k} >= \sum_n b_n \int d\mathbf{r}\exp(-i\mathbf{k}'\delta(\mathbf{r} - \mathbf{R}_n)\exp(i\mathbf{k}\mathbf{r}) \qquad (4.22)$$

$$= \sum_n b_n \exp(i\kappa\mathbf{R}_n) \qquad (4.22.a)$$

with $\kappa = \mathbf{k} - \mathbf{k}'$ and the cross-section becomes

$$\frac{d^2\sigma}{d\Omega dE} = \frac{k'}{k}\sum_{\lambda\sigma} p_\lambda p_\sigma \sum_{\lambda'\sigma'} | < \sigma'\lambda'|\sum_n b_n \exp(i\kappa\mathbf{R}_n)|\sigma\lambda > |^2\delta(energy) \qquad (4.23)$$

Since the nuclei are rigidly bound, $\exp(i\kappa \mathbf{R}_n)$ in the previous equation is not an operator. So it follows that the matrix element is proportional

$$< \lambda | \lambda' >= \delta_{\lambda,\lambda'} \tag{4.24}$$

which means that there is just one term in the sum over $\lambda' = \lambda$. The sum of p_λ is unity by definition. This last results imply that $E_\lambda = E'_\lambda$ and the scattering is therefore elastic. In view of these various results, the expression (4.23) for scattering by a rigid array of nuclei reduces to

$$\frac{d\sigma}{d\Omega} = \sum_\sigma p_\sigma \sum_{nn'} \exp(i\kappa(\mathbf{R}_n - \mathbf{R}_{n'})) < \sigma | {b_{n'}}^* b_n | \sigma > \tag{4.25}$$

since $\sum_\sigma p_\sigma$ is unity by definition, this equation becomes

$$= \sum_{nn'} \exp[i\kappa(\mathbf{R}_n - \mathbf{R}'_n)] < {b'_n}^* b_n > \tag{4.26}$$

In general b_n will depend on which isotope is at the site $\mathbf{R}_n$ and what nuclear spin is associated with the isotope. Clearly there is no correlation between values of $\mathrm{b}_{n'}$ and b_n for $n \neq n'$, i.e.

$$< {b'_n}^* b_n >=< {b'_n}^* >< b_n >= | < b > |^2 \quad if \quad n \neq n' \tag{4.27a}$$

But if $n = n'$,

$$< {b'_n}^* b_n >=< |b_n|^2 >=< |b|^2 > \tag{4.27b}$$

Therefore we can write

$$< {b'_n}^* b_n >= | < b > |^2 + \delta_{nn'}(< |b|^2 > - | < b > |^2) \tag{4.28}$$

This enables us to separate the cross-section into two parts

$$\frac{d\sigma}{d\Omega} = (\frac{d\sigma}{d\Omega})_{coh} + (\frac{d\sigma}{d\Omega})_{incoh} \tag{4.29}$$

where the coherent cross-section is

$$(\frac{d\sigma}{d\Omega})_{coh} = |<b>|^2 |\sum_n \exp(i\kappa.\mathbf{R}_n)|^2 \tag{4.30}$$

and the incoherent cross-section

$$(\frac{d\sigma}{d\Omega})_{incoh} = N[<|b|^2> - |<b>|^2] = N<|b - <b>|^2> \tag{4.31}$$

We see that only the mean scattering potential $< b >$ gives rise to interference effects and coherent scattering, while the incoherent scattering is proportional to the mean-square deviation $< |b - < b > |^2 >$. If the nucleus possesses a nonzero spin, then the nuclear scattering amplitude will depend upon the relative orientation of this spin with the neutron spin. Since these nuclear spins are disordered, they lead to a large incoherent scattering.

4-1-2 Bragg Scattering

The coherent elastic scattering from a rigid lattice is also referred to as Bragg scattering. This involves the quantity

$$\sum_n \exp(i\kappa.\mathbf{R}_n) \tag{4.32}$$

which contains N terms. We evaluate the lattice sum $\sum_n \exp(i\kappa \mathbf{R}_n)$ for a one dimensional crystal of lattice constant a and then write down the result for three dimensions. For a crystal of N atom with $R_n = na$ where n is an integer between 0 and N-1

$$\sum_{n=0}^{N-1} \exp i\kappa na = \frac{1 - \exp iN\kappa a}{1 - \exp i\kappa a} \tag{4.33}$$

and

$$|\sum_{n=0}^{N-1} \exp in\kappa a|^2 = \frac{1 - \cos N\kappa a}{1 - \cos \kappa a} = \frac{\sin^2 \frac{1}{2} N\kappa a}{\sin^2 \frac{1}{2}\kappa a} = \frac{2\pi N}{a}\delta(\kappa - \mathbf{G}) \tag{4.34}$$

So it can be shown that

$$|\sum_{n} \exp(i\kappa.\mathbf{R}_n)|^2 = \frac{(2\pi)^2 N}{V_0} \sum_{G} \delta(\kappa - \mathbf{G}) \tag{4.35}$$

where V_0 is the volume of the unit cell and **G** is a reciprocal lattice vector. This is an important result! The coherent or Bragg cross-section then becomes

$$(\frac{d\sigma}{d\Omega})_{coh} = < |b|^2 > \frac{(2\pi)^3 N}{V_0} \sum_{G} \delta(\kappa - \mathbf{G}) \tag{4.36}$$

If the lattice has more than one atom per unit cell, say m atoms at ρ_1, ρ_2, ... relative to some reference point in the unit cell, then

$$(\frac{d\sigma}{d\Omega})_{coh} = \frac{(2\pi)^3 N}{V_0} \sum_{\mathbf{G}} |F(\mathbf{G})|^2 \delta(\kappa - \mathbf{G}) \tag{4.37}$$

where

$$F(\mathbf{G}) = \sum_{i=1}^{m} < b_i > \exp(i\mathbf{G}.\rho_i) \tag{4.38}$$

is the unit cell structure factor.

The important point is that there is no coherent scattering unless

$$\kappa = \mathbf{k} - \mathbf{k}' = \mathbf{G} \tag{4.39}$$

By squaring this relation and making use of the fact that the magnitude of the reciprocal lattice vector in some direction hkl is equal to some multiple of 2π times the inverse spacing of the planes in that direction, d(hkl), we obtain the familiar Bragg law

$$\sin\theta = \frac{n\lambda}{2d(hkl)} \tag{4.40}$$

for the angle 2θ between the incident beam and the diffracted beam.

4-1-3 Magnetic Scattering

We now turn our attention to the interaction between the magnetic moment of the neutron and those of the crystal. We will consider a very simple model in which neutrons are scattered from a system of fixed spins by the magnetic interaction of their dipole moments with those of the spins.

The cross-section for the scattering of the neutron from an initial state $|i>$ to a final state $|f>$ is proportional to the modulus squared of the matrix element $<f|V|i>$, where V is the interaction potential between the neutron and the spin system. V is given by

$$V = -\mu_n.\mathbf{B} \tag{4.41}$$

where **B** is the magnetic field created by the dipole moments of the spins. The magnetic vector potential at **r** due to one such dipole at the origin is

$$\mathbf{A}(\mathbf{r}) = \frac{\mu_0}{4\pi}\frac{\mu \wedge \mathbf{r}}{r^3} \tag{4.42}$$

where μ is the magnetic dipole moment of the spin. If we have large numbers of dipoles with dipole moments μ_l at positions $\mathbf{r}_l$ then the total vector potential is

$$\mathbf{A}(\mathbf{r}) = \frac{\mu_0}{4\pi}\sum_l \frac{\mu_l \wedge (\mathbf{r}-\mathbf{r}_l)}{|r-r_l|^3} \tag{4.43}$$

To obtain the magnetic field we take the curl of this potential. We will find it expedient to make use of the vector identity

$$\frac{\mathbf{r}-\mathbf{r}_l}{|r-r_l|^3} = -\nabla(\frac{1}{|r-r_l|}) \tag{4.44}$$

to write the magnetic field in the form

$$\mathbf{B}(\mathbf{r}) = -\frac{\mu_0}{4\pi}\sum_l \nabla \wedge [\mu_l \wedge \nabla(\frac{1}{|r-r_l|})] \tag{4.45}$$

Assuming for the purposes of illustration that the scattering dipole moments are those of electrons, we can write the moments μ_l in the form

$$\mu_l = -\frac{e\hbar}{m_e}\mathbf{s}_l \tag{4.46}$$

where the spin s_l is a dimensionless variable. Similarly, the moment of the neutron can be written

$$\mu_n = \frac{g_n e\hbar}{m_n}\mathbf{s}_n \tag{4.47}$$

where $g_n = -1.91$. Then the interaction potential becomes

$$V(\mathbf{r}, \mathbf{s}_n) = -\frac{g_n \mu_0 e^2 h^2}{4\pi m_e m} \sum_l \mathbf{s}_n . \nabla \wedge [\mathbf{s}_l \wedge \nabla(\frac{1}{|\mathbf{r} - \mathbf{r}_l|})] \tag{4.48}$$

where $\mathbf{r}$ now represents the position vector of the neutron.

We write the initial state of the neutron as

$$|i> = V^{-\frac{1}{2}} \exp i\mathbf{k}_i.\mathbf{r}|s_n>_i \tag{4.49}$$

The i subscript here denotes the initial configuration. We have broken the neutron state into a spatial part, which we represent by a simple Schroedinger wavefunction, and a spin part. The factor of $V^{-\frac{1}{2}}$ ensures that the neutron wavefunction is normalised to one neutron per volume V. Similarly, we can write the final state of the neutron in the form

$$|f> = V^{\frac{-1}{2}} \exp i\mathbf{k}_f\mathbf{r}|s_n>_f \tag{4.50}$$

then the matrix element

$$<f|V|i> = \frac{1}{V} <s_n|_f \int d^3\mathbf{r} \exp -i\mathbf{k}_f\mathbf{r} V(\mathbf{r}, \mathbf{S}_n) \exp i\mathbf{k}_i\mathbf{r}|s_n>_i \tag{4.51}$$

We now substitute for $V(\mathbf{r}, \mathbf{s}_n)$ from equation(4.48) and use the identity

$$\int d^3\mathbf{r} \exp i\kappa.\mathbf{r}\nabla \wedge \mathbf{F} = -i \int d^3\mathbf{r} \exp i\kappa\mathbf{r}\kappa \wedge \mathbf{F} \tag{4.52}$$

Then

$$< f|V|i >= \frac{g_n\mu_0 e^2h^2}{4\pi m_e m V} < s_n|_f \int d^3\mathbf{r} \exp i\kappa\mathbf{r} \sum_l s_n\kappa \wedge (\mathbf{s}_l \wedge \kappa \frac{1}{|\mathbf{r} - \mathbf{r}_l|})s_n >_i \tag{4.53}$$

where $\kappa = \mathbf{k}_i - \mathbf{k}_f$ The integral over $\mathbf{r}$ can now be performed, and we get

$$< f|V|i >= \frac{g_n\mu_0 e^2h^2}{m_e m V} < s_n|_f \sum_l s_n \frac{\kappa \wedge (\mathbf{s}_l \wedge \kappa)}{\kappa^2} \exp i\kappa\mathbf{R}_l|s_n >_i \tag{4.54}$$

the vector quantity

$$\frac{\kappa \wedge (\mathbf{s}_l \wedge \kappa)}{\kappa^2} = \hat{\kappa} \wedge (\mathbf{s}_l \wedge \hat{\kappa}) \tag{4.55}$$

is the component of $\mathbf{s}_l$ in the plane perpendicular to $\hat{\kappa}$, which is the unit vector in the direction of κ. Using the identity

$$\sum_l \mathbf{s}_l \exp i\mathbf{k}.\mathbf{R}_l = N^{\frac{-1}{2}} \mathbf{s}_\mathbf{k} \tag{4.56}$$

one can write the matrix element as

$$< f|V|i >= \frac{g_n\mu_0 e^2h^2}{m_e m V} < s_n|_f \mathbf{s}_n \hat{\kappa} \wedge (\mathbf{s}_\mathbf{k} \wedge \hat{\kappa})|s_n >_i \tag{4.57}$$

The problem here is to evaluate $\hat{\kappa} \wedge (\mathbf{s}_\mathbf{k} \wedge \hat{\kappa})$. Once we have calculated this quantity then the cross-section may be approximated to

$$I(\mathbf{k})\alpha|\hat{\kappa} \wedge (\mathbf{s}_\mathbf{k} \wedge \hat{\kappa})|^2 \tag{4.58}$$

which is the perpendicular component of spin along $\hat{\kappa}$. This is the quantity that we need for evaluating the magnetic Bragg scattering. Now we want to consider the diffuse case where the spins fluctuate from their fixed values.

4-2 Magnetic Diffuse Scattering

In the previous section we evaluated the cross-section of neutrons scattering from fixed spins of crystal. Now we want to consider the scattering in the presence of impurities.

If there is any impurity in the system, then we can express the spins as

$$\mathbf{S}_R = \mathbf{S}_R{}^0 + \delta\mathbf{S}_R \tag{4.59}$$

where $\delta\mathbf{S}_R$ is spin fluctuation. Then one can calculate the Fourier transform of the spin as

$$\mathbf{S}_\mathbf{k} = \sum_i (\mathbf{S}_i{}^0 + \delta\mathbf{S}_{R_i}) \exp i\mathbf{k}.\mathbf{R}_i \tag{4.60}$$

Thus the magnetic scattering intensity

$$I(\mathbf{k}) \alpha |\hat{\kappa} \wedge (\mathbf{S}_\mathbf{k} \wedge \hat{\kappa})|^2 \tag{4.61}$$

can be written as

$$I(\mathbf{k}) \alpha |\hat{\kappa} \wedge [(\mathbf{S}_\mathbf{k}{}^0 + \delta\mathbf{S}_\mathbf{k}) \wedge \hat{\kappa}]|^2 \tag{4.62}$$

which is

$$I(k)_m + I(k)_{diff} \tag{4.63}$$

Here we have omitted terms like $\mathbf{S}_k^\perp \delta\mathbf{S}_k^\perp + \delta\mathbf{S}_k^\perp \mathbf{S}_k^\perp$. This is because the contribution from this term is small. This leads to a sum of two scattering. If we choose the propagating to be parallel to the spin direction, then the magnetic scattering intensity disappears. The only remaining thing is now diffuse, which is

$$I(k)_{diff} \alpha |\hat{\kappa} \wedge (\delta\mathbf{S}_\mathbf{k} \wedge \hat{\kappa})|^2 \tag{4.64}$$

This is the quantity that gives information about fluctuations. In the next section we will use this approximation in order to see any non-collinear spin arrangement in the square lattice.

4-3 Examples:

Firstly we will consider the collinear arrangement on the square lattice Fig(2.8). Using equation(4.58) one can work out the magnetic Bragg spots. We showed the Bragg spots of three phases in the square lattice from Fig(4.2a) to Fig(4.2c).

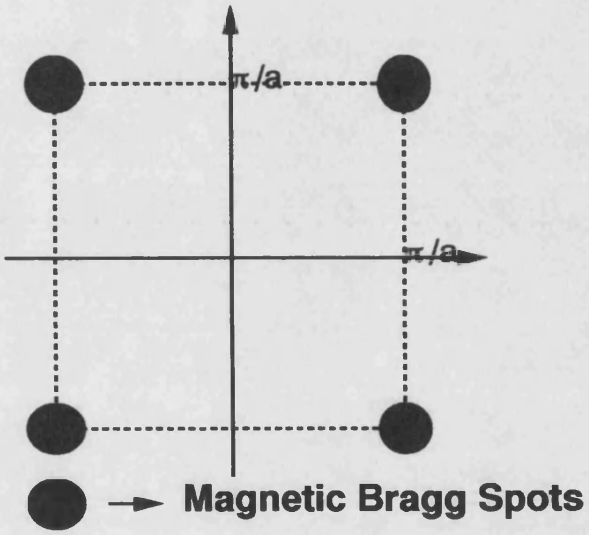

Fig. 4.2a Magnetic Bragg Spots Of the Collinear Phase

Fig(4.2a) is the Bragg spots of the simple collinear arrangement. Fig(4.2b) is the Bragg spots of the degenerate collinear arrangement and Fig(4.2c) shows the Bragg spots of the non-collinear arrangement in the first Brillioun zone.

The question is now whether or not the impurities cause a non-collinear

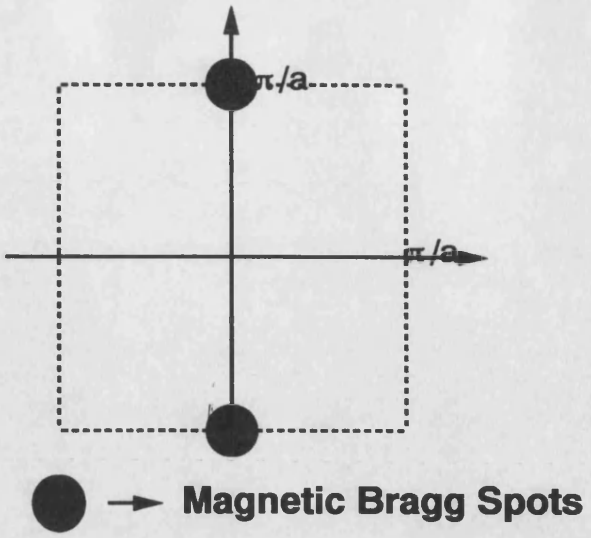

Fig. 4.2b Magnetic Bragg Spots of degenere collinear Phase

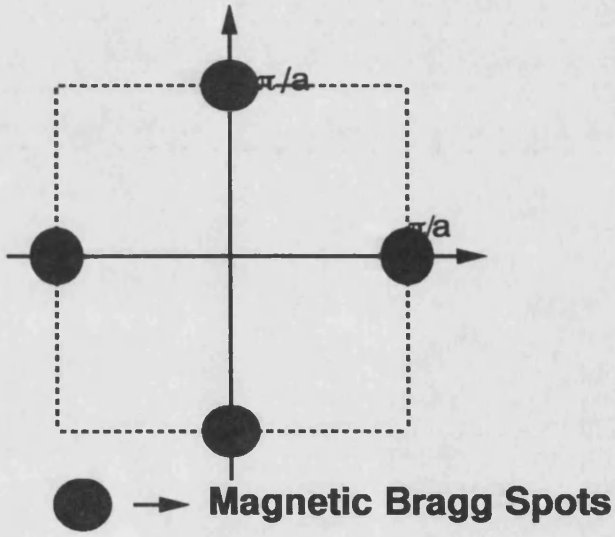

Fig. 4.2c Magnetic Bragg Spots of Non-collinear Phase

arrangement in the collinear phase? In order to find out this we will work with the diffuse scattering. Firstly we will consider a small cluster with an impurity Fig(3.2). In the presence of the impurity we can represent the spins as

$$\mathbf{S}_l = \mathbf{S}_l^{\,0} + \delta \mathbf{S}_{R_l} \tag{4.65}$$

We need $\delta \mathbf{S}_{\mathbf{k}}$ for calculating the diffuse magnetic scattering. This is

$$\delta \mathbf{S}_{\mathbf{k}} = \frac{1}{N} \sum_{R_l} \exp i\mathbf{k}\mathbf{R} \delta \mathbf{S}_{\mathbf{R}_l} \tag{4.66}$$

In this cluster we assume that only four spins would be effected after an impurity. So $\delta \mathbf{S}_{\mathbf{R}}$ are

$$\delta \mathbf{S}(R_0) = -S_0 \tag{4.67}$$

$$\delta \mathbf{S}(R_1) = (\mathbf{T}_1 - \mathbf{S}_1) \tag{4.68}$$

$$\delta \mathbf{S}(R_2) = (\mathbf{T}_2 - \mathbf{S}_2) \tag{4.69}$$

then the Fourier transform of $\delta \mathbf{S}(\mathbf{R})$ is

$$\begin{aligned} \delta \mathbf{S}_{\mathbf{k}} = -\mathbf{S}_0 \exp i\mathbf{k}\mathbf{R}_0 + (\mathbf{T}_1 - \mathbf{S}_1)(\exp i\mathbf{k}\mathbf{R}_1 + \exp -i\mathbf{k}\mathbf{R}_1) \\ +(\mathbf{T}_2 - \mathbf{S}_2)(\exp i\mathbf{k}\mathbf{R}_2 + \exp -i\mathbf{k}\mathbf{R}_2) \end{aligned} \tag{4.70}$$

Using the Bravais lattice vectors of the square lattice as shown in Fig(2.1), this equality becomes

$$\delta \mathbf{S}_{\mathbf{k}} = 2\cos k_x(\mathbf{T}_1 - \mathbf{S}_1) - \mathbf{S}_0 + 2\cos k_y(\mathbf{T}_2 - \mathbf{S}_2) \tag{4.71}$$

Using the equation(3.3a,3.3b) of chapter three for T spins we can rewrite this equation as

$$\delta \mathbf{S}_{\mathbf{k}} = \mathbf{S}_0[2\cos\theta(\cos k_x + \cos k_y) - 1] + \mathbf{S}_1[2(1 - \sin\theta)(\cos k_y - \cos k_x)] \tag{4.72}$$

In order to find the scattering peaks, we need $|\kappa \wedge [\delta \mathbf{S}_k \wedge \kappa]|^2$. This gives $|\delta \mathbf{S}_k - [\hat{\kappa}\delta \mathbf{S}_k]\hat{\kappa}|^2$, again we can ignore the second term and work with only

$$|\delta \mathbf{S}_{\mathbf{k}}|^2 = S^2[2\cos\theta(\cos k_x + \cos k_y) - 1]^2 + 4(1 - \sin\theta)^2(\cos k_x - \cos k_y)^2 \tag{4.73}$$

Here we have used $\mathbf{S}_0.\mathbf{S}_1 = 0$. This can be separated into two parts as

$$|\delta S_\perp|^2 = 4(1 - \sin\theta)^2(\cos k_x - \cos k_y)^2 \tag{4.74}$$

and

$$|S_{\|}|^2 = [2\cos\theta(\cos k_x + \cos k_y) - 1]^2 \tag{4.75}$$

The first equation gives the scattering peaks when $\cos k_x = -\cos k_y = 1$ or vice versa which is shown in Fig(4.3) by X.

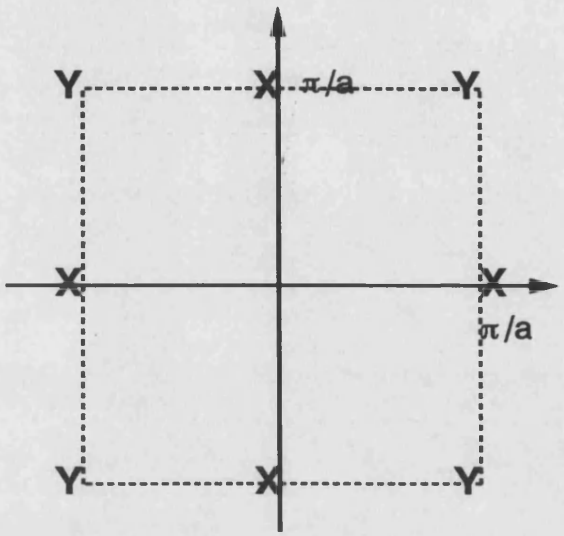

Fig. 4.3 Diffuse Scattering Peaks of Collinear Phase after an Impurity

However the second equation gives scattering peaks when $\cos k_x = \cos k_y = -1$, which is indicated by Y in Fig(4.3). It is obvious that the peaks at Y points corresponds to the Bragg spots of the collinear state. We know from chapter three that in the interval $x_c < x < \frac{1}{2}$ for the simple collinear phase the spins must be represented by two components after the impurity addition. In this interval these X peaks are observable. It is easy to see that the symmetry of the X peaks is the same as the symmetry of the non-collinear phase. Thus it may be concluded that the impurity trap a local non-collinear arrangement of spins. In addition to this we looked at the variation of $|\delta S_{\perp}|^2$ as a function of $\mathbf{k}$ and as a function of the cluster size. (We must point out here that, for all the finite size of cluster we are using $\delta\theta_{\mathbf{k}}$

instead of $\delta \mathbf{S}_{\mathbf{k}}$. This means that the origin of the first Brillouin zone is moved to $\mathbf{k}=(\pi,\pi)$, since $\delta \mathbf{S}_{\mathbf{k}} = \delta_{\mathbf{k}+\mathbf{q}}$). The plot of $|\delta S_{\perp}|^2$ in Fig(4.4) shows that there is a peak around $\mathbf{k} = \pm(\pi,0), \quad \pm(0,\pi)$

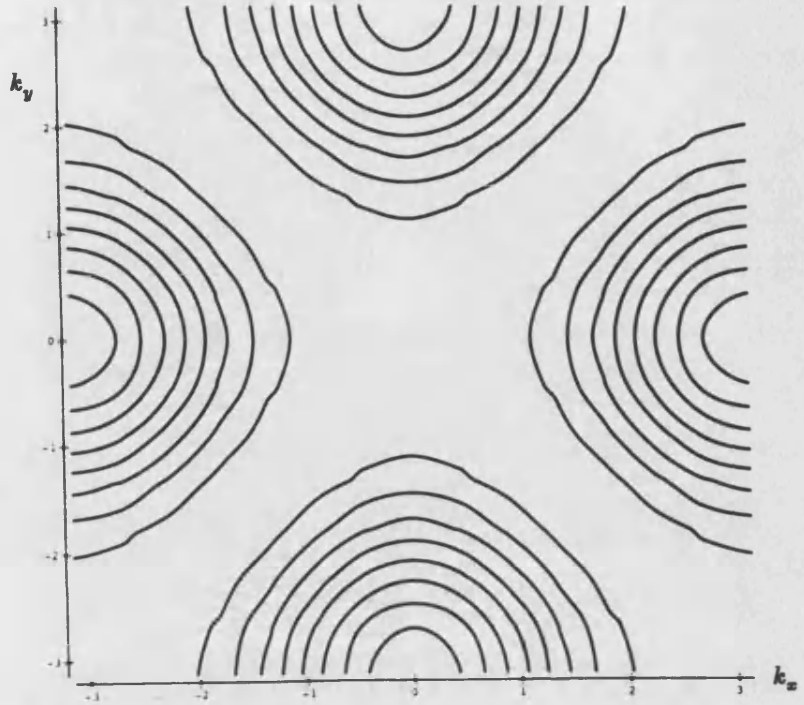

Fig 4.4 Magnetic Diffuse Scattering in a small Cluster

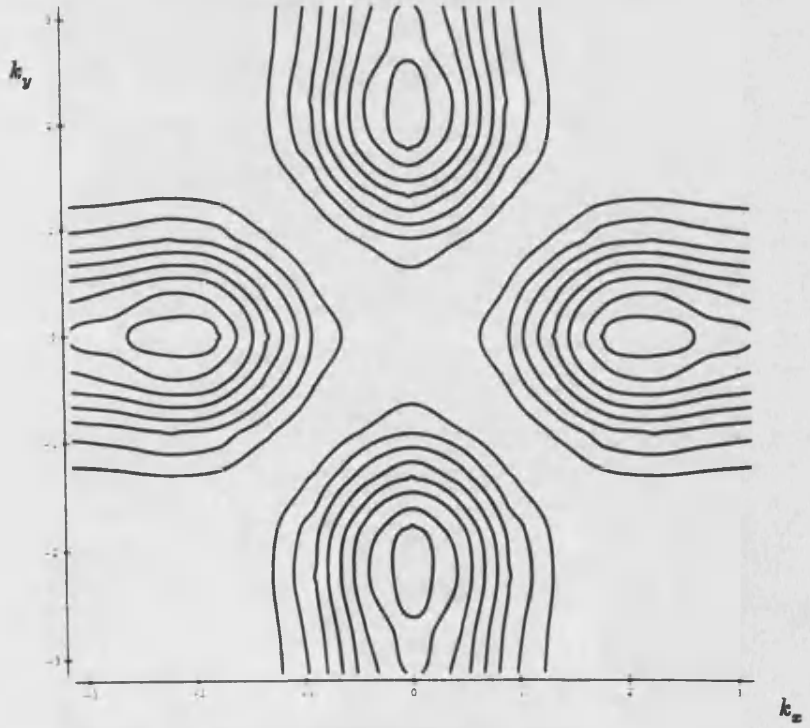

Fig 4.5a Magnetic Diffuse Scattering; 9 spins

We observed that this peak spreads out towards the origin by increasing the size

of the cluster as shown from Fig(4.5a) to Fig(4.5d). This results indicates that the scattering is converging towards the Green function calculations of the Scattering[35]

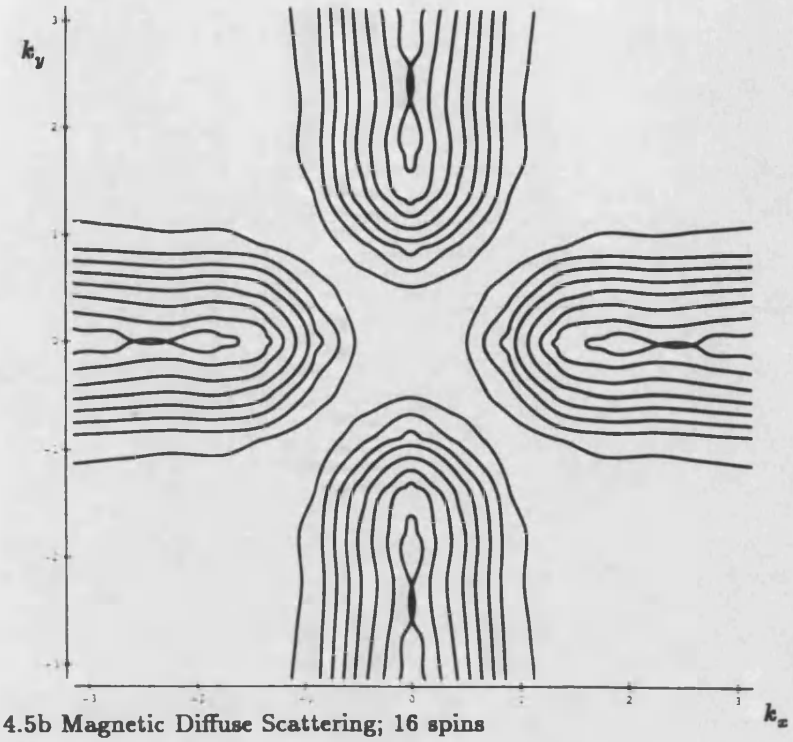

Fig 4.5b Magnetic Diffuse Scattering; 16 spins

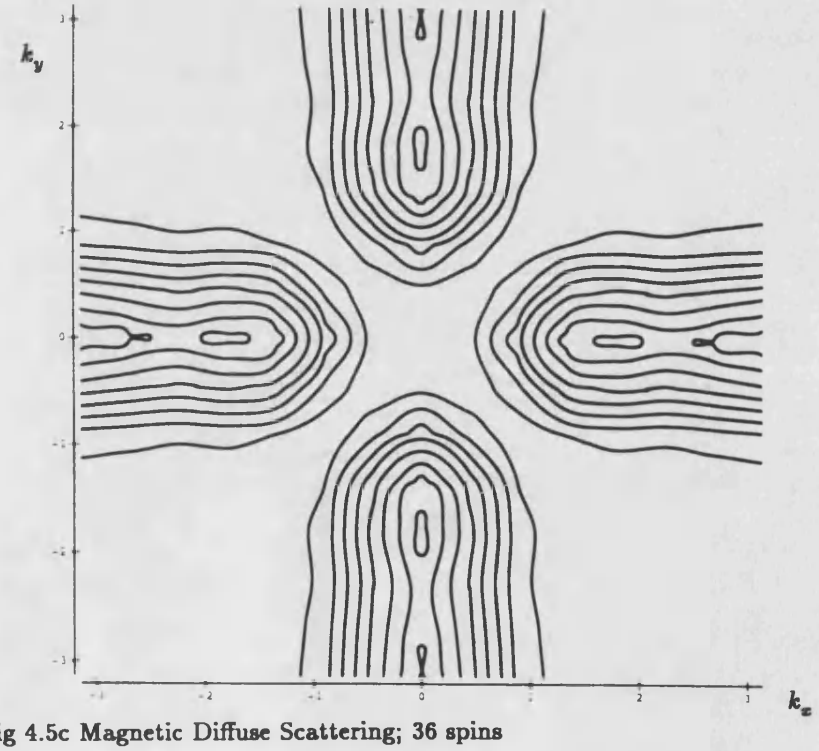

Fig 4.5c Magnetic Diffuse Scattering; 36 spins

which says that there is a long range correlation between the fluctuations. This results is something like the results observed in MnCu alloys[29]. It means that the

prediction of our model is not far away from the reality. If this long range correlation

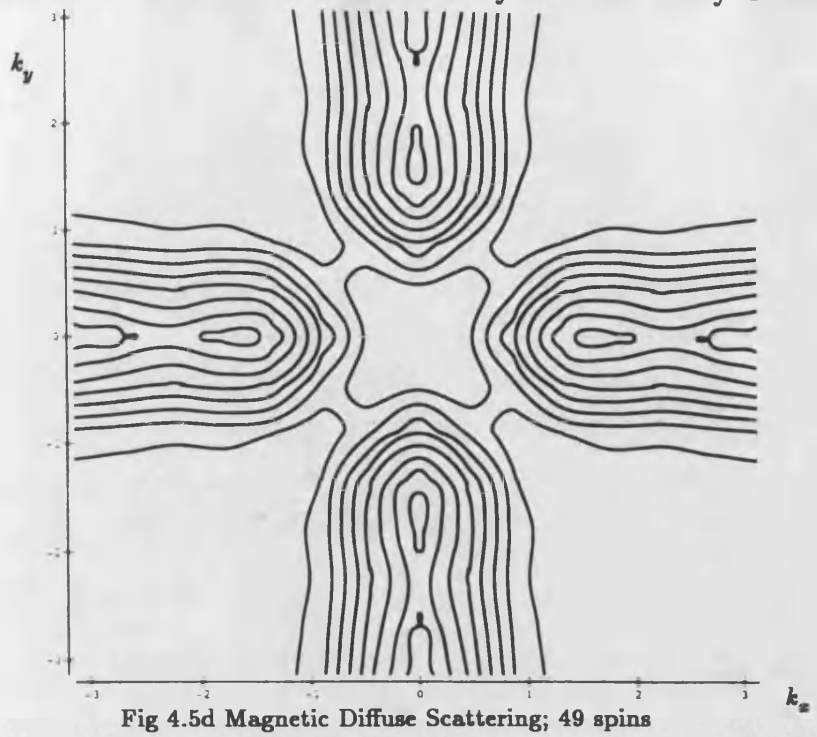

Fig 4.5d Magnetic Diffuse Scattering; 49 spins

occurs, it is probable that the system picks up another ordering. So the impurities may causes a first order antiferromagnetic phase transition if required amount of clusters are created such that the clusters interact with each other. This point will become more clear when we tackle more than one impurities in the chosen cluster.

In chapter three we saw that the critical point decreases with increasing impurity concentration. Now we want to look at more than one impurity cases. Firstly we will consider the two impurities case Fig(3.8). The critical point for this cluster is $x_c = 0.237413$. The aim here is to calculate $|\delta S_\perp|^2$ in order to find the diffuse scattering peaks. One can find $\delta S_\perp$ as

$$\delta S_\perp = 0.65i \sin(\frac{k_x}{2} + \frac{k_y}{2}) - 0.19i[\sin(\frac{3k_x}{2} - \frac{k_y}{2}) + \sin(\frac{3k_y}{2} - \frac{k_x}{2}] \qquad (4.76)$$

Where 0.65 and 0.19 are eigenfunctions of $\delta\phi_i$ which are calculated at the critical point. The contour plot of $|\delta S_\perp|^2$ in Fig(4.6) shows that we would get some scatter-

ing peak at around $\mathbf{k} = \pm(\pi, 0), \quad \pm(0, \pi)$. The symmetry of this peak is not related to

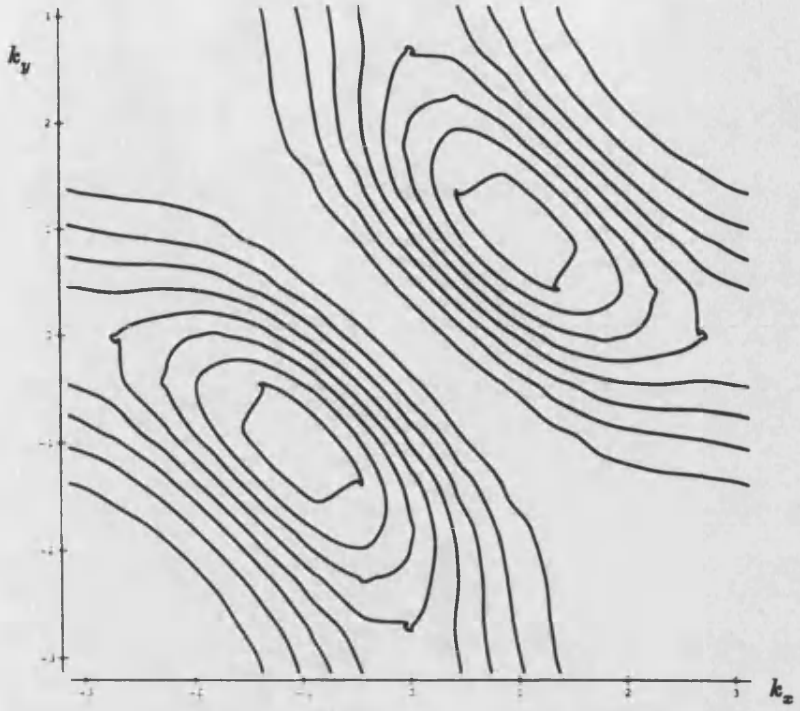

Fig 4.6 Magnetic Diffuse Scattering; 2 impurities, small cluster

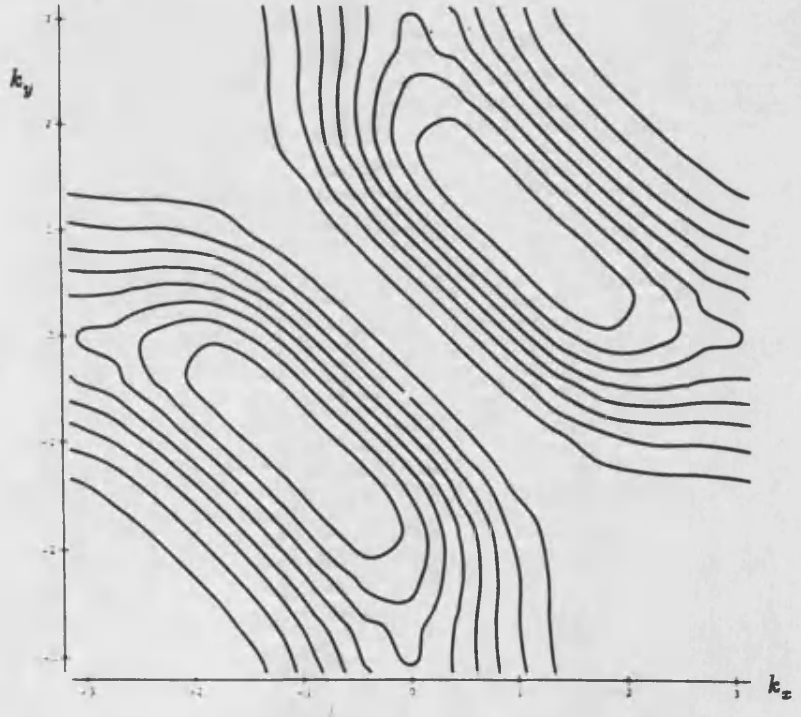

Fig 4.7a Magnetic Diffuse Scattering; 2 impurities, 18 spins

the symmetry of the collinear phase. It is related to the symmetry of the non-collinear one. So it may be possible to say that the impurities do cause a phase

transition from collinear to non-collinear. One can compare this plot with the single impurity case. The diffuse peaks occur exactly at the same places. In order to make this comparing complete we should observe the scattering peaks by increasing the size of the cluster as we did for the single impurity case. As can be seen from Fig(4.7a) to Fig(4.7d) as we increase the cluster size the scattering peak spreads out

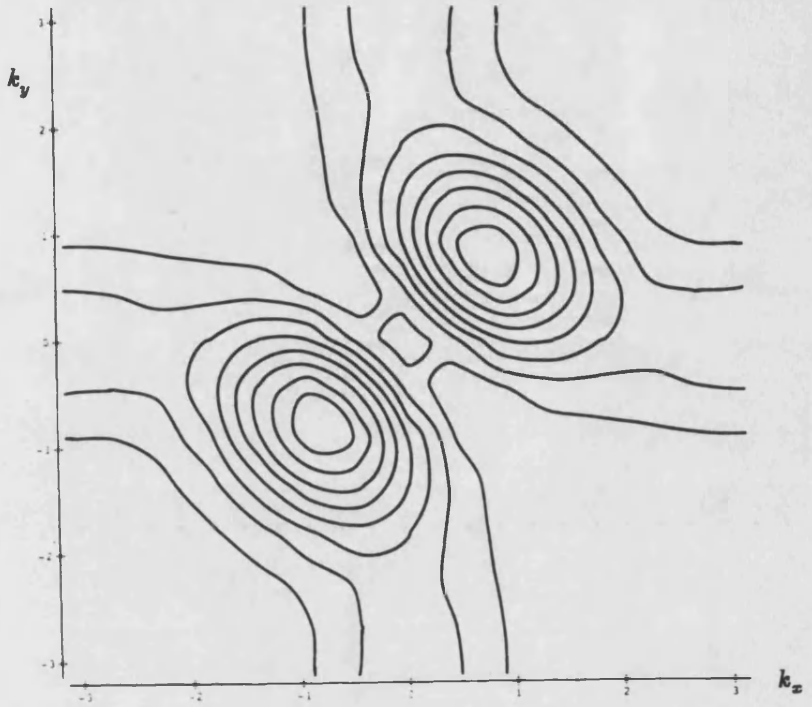

Fig 4.7b Magnetic Diffuse Scattering; 2 impurities 28 spins

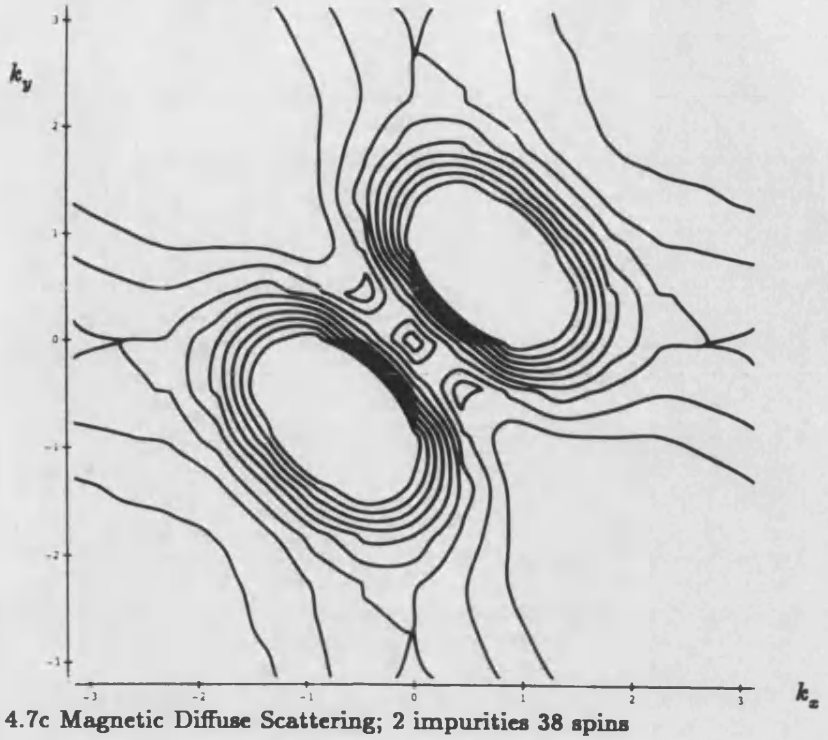

Fig 4.7c Magnetic Diffuse Scattering; 2 impurities 38 spins

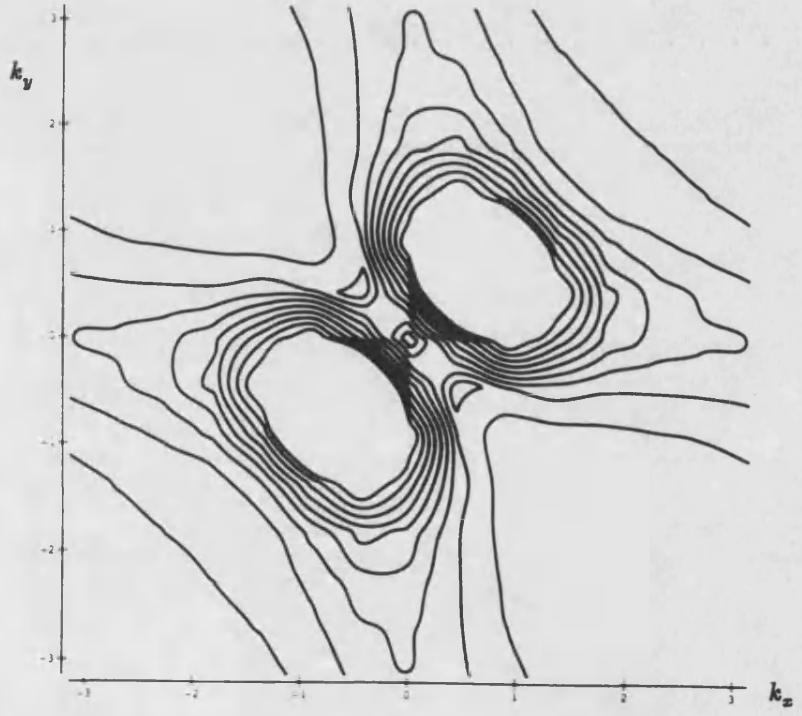

Fig 4.7d Magnetic Diffuse Scattering; 2 impurities 48 spins

towards the origin and it converges to the exact calculations by the Green's functions as can be seen in Fig(4.8). Again it is clear that at the exact critical point there is a long range correlation of the fluctuations. However, the magnetic diffuse scattering

shows that there is a huge peak around the origin(Fig(4.8)) which is at the same place as the Bragg spot of the collinear phase. As we will see in chapter Five, this cluster is more convenient to the clustering of impurities as in $MnCu_1$ alloys. In these alloys the diffuse scattering occurs at the original Bragg spot, indicating that the spins rotate together when Cu atoms introduced. Now we want to move on to three and four impurities in a cluster in order to complete the diffuse scattering in the simple collinear state in the presence of impurities.

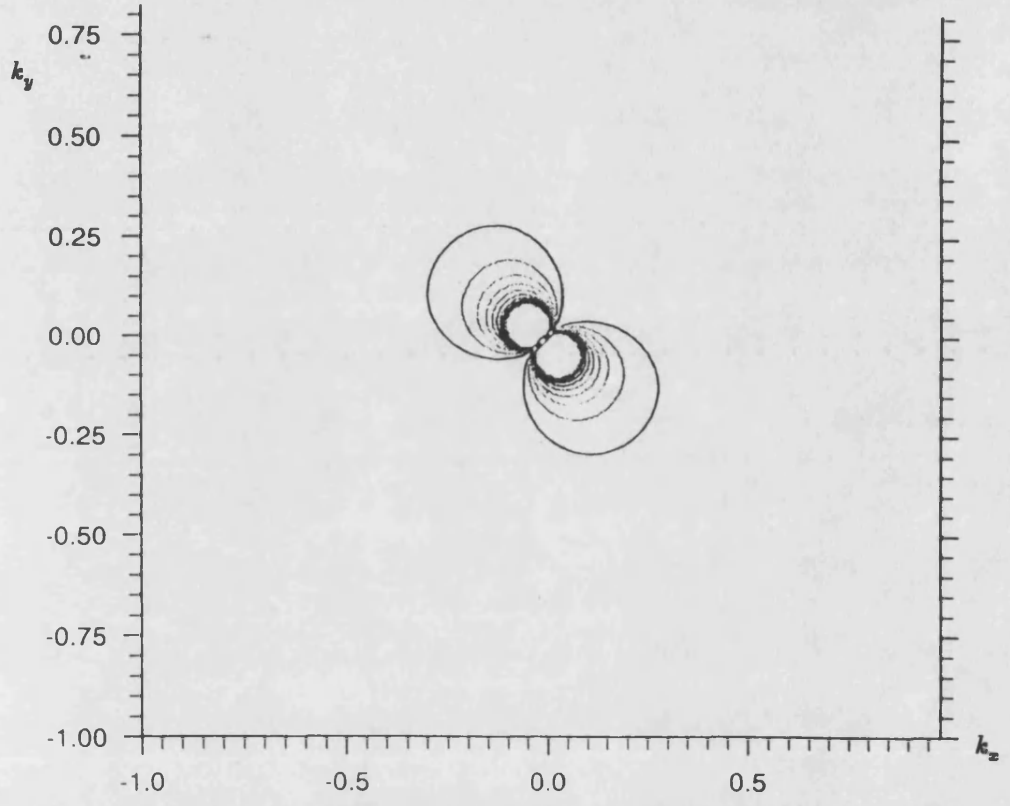

Fig 4.8 Magnetic Diffuse scattering at the exact critical point; 2 impurities

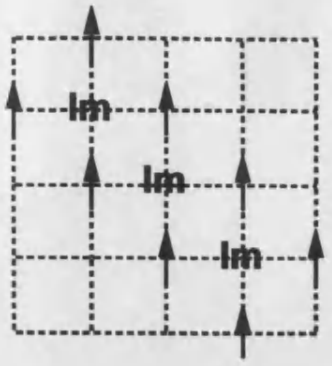

Fig. 4.9 Three Impurities in Collinear Phase

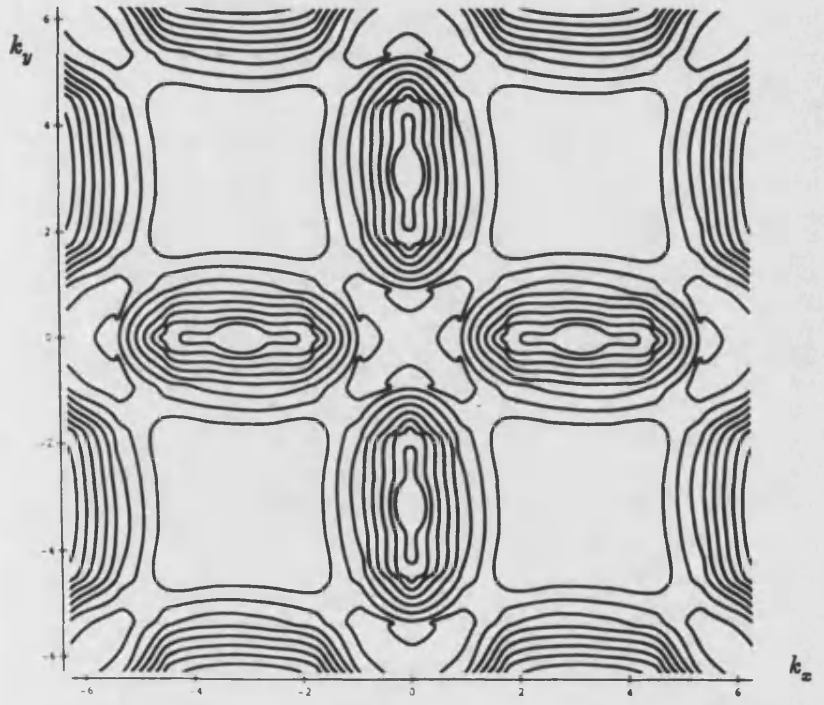

Fig 4.10 Magnetic Diffuse Scattering; 3 impurities, small cluster

For the three impurities in a cluster Fig(4.9) one can calculate $\delta S_\perp$ as

$$\delta S_\perp = 0.48(\cos k_x - \cos k_y) + 0.11[\cos(k_x + 2k_y) - \cos(2k_x + k_y)] \qquad (4.77)$$

where again 0.48 and 0.11 are the eigenfunctions as indicated in the previous example. In order to find the diffuse scattering again we must calculate $|\delta S_\perp|^2$. The contour plot is given in Fig(4.10). The diffuse peaks are at the same positions as for the single impurity case, here it should be reminded that the cluster is again a small

one. Again using the symmetry of the scattering pattern we can easily say that it is

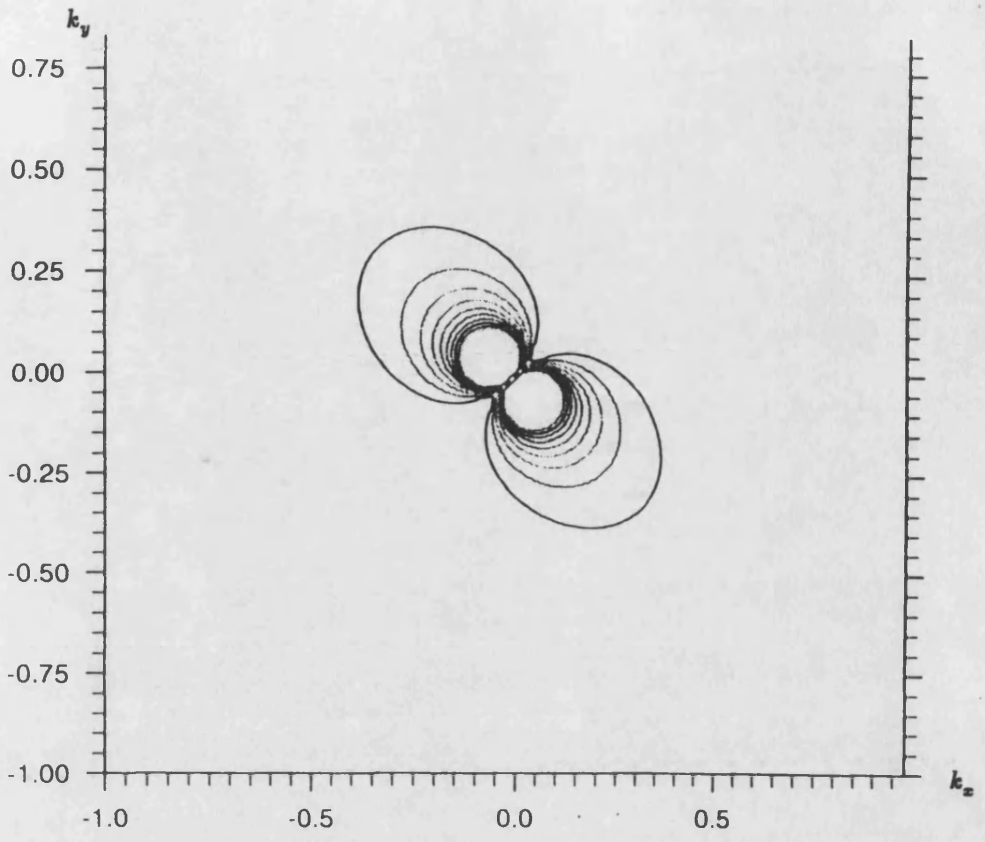

Fig 4.11 Magnetic Diffuse Scattering at the exact critical point;3 impurities

related to the non-collinear arrangement. Firstly we should look at the variation of these peaks by increasing the cluster size as we have done previously. We observe that the scattering pattern spreads out towards the origin by increasing the cluster size the same as last two example above and it is converging to the Green's function calculations as in Fig(4.11) As can be seen in this picture there is a diffuse peak at the origin as well as half way between the corners of first Brillioun zone. This cluster, like the previous two impurities cluster, is more relevant to MnCu alloys.

Finally in this section we will attempt to calculate the diffuse scattering with four impurities. As we have been doing previously, we should calculate the $\delta S_{\perp}$ once

more. Using Fig(3.12) one can calculate it as

$$\delta S_{\perp} = -0.47\sin(\frac{k_x}{2}+\frac{k_y}{2}) + 0.36\sin(\frac{3k_x}{2}-\frac{k_y}{2}) - 0.36\sin(\frac{k_x}{2}-\frac{3k_y}{2}) \\ -0.075\sin(\frac{5k_x}{2}-\frac{3k_y}{2}) + 0.075\sin(\frac{3k_x}{2}-\frac{5k_x}{2}) \tag{4.78}$$

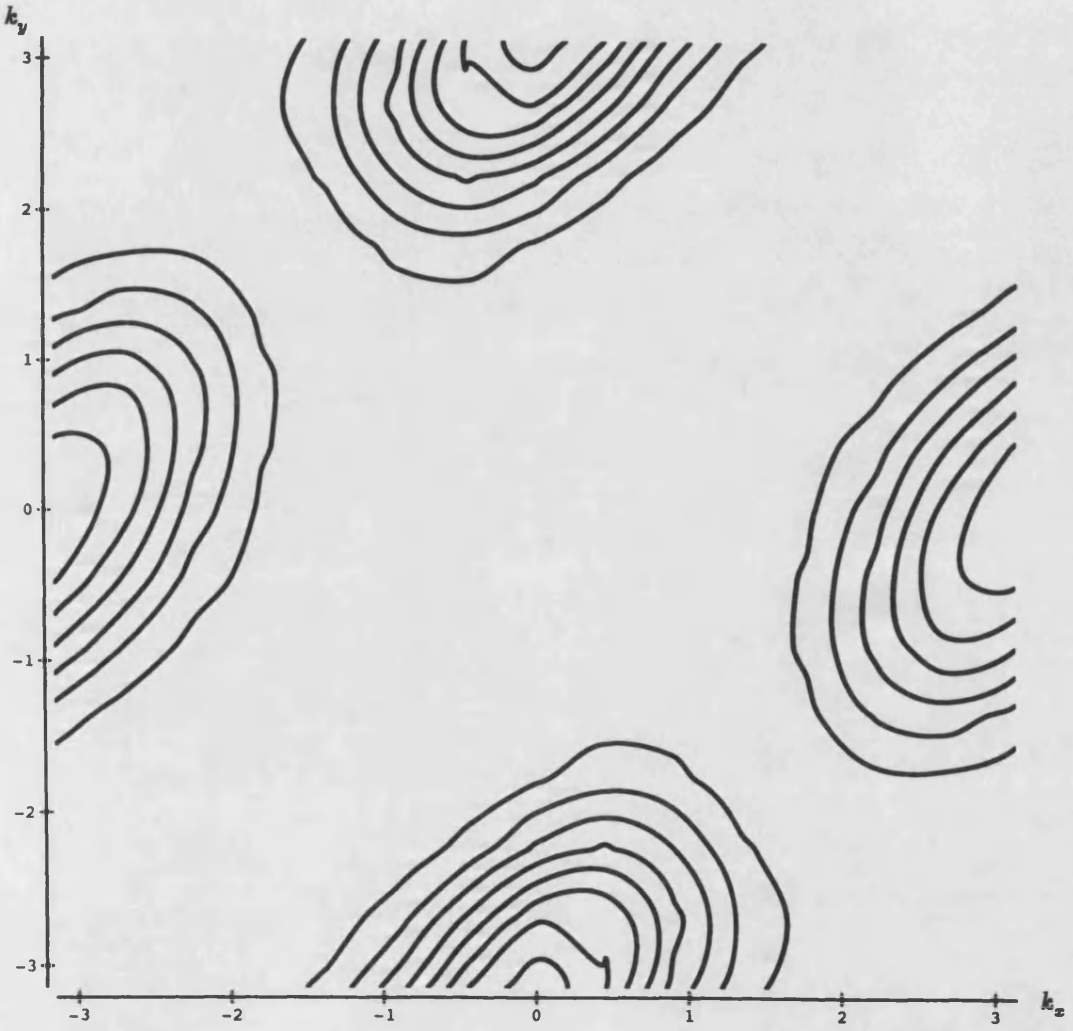

Fig 4.12 Magnetic Diffuse Scattering; 4 impurities, small cluster

In order to have the diffuse scattering we should calculate $|\delta S_{\perp}|^2$. The contour plot of it shows that the scattering pattern is similar to previously studied three example. The remaining task is once more look at the variation of this peaks by increasing

the cluster size. It can be seen from Fig(4.12) to Fig(4.13c) that the scattering

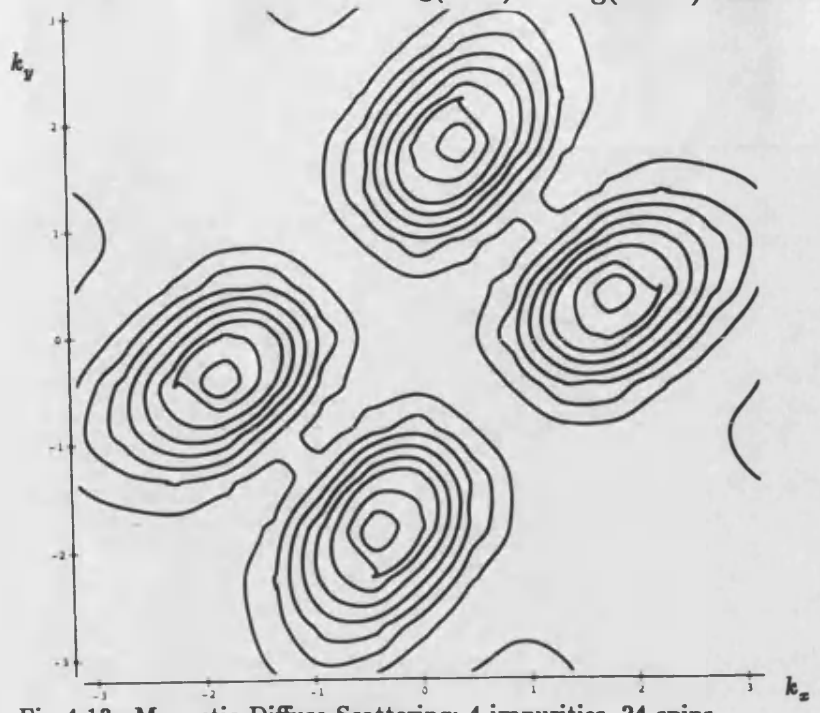

Fig 4.13a Magnetic Diffuse Scattering; 4 impurities, 24 spins

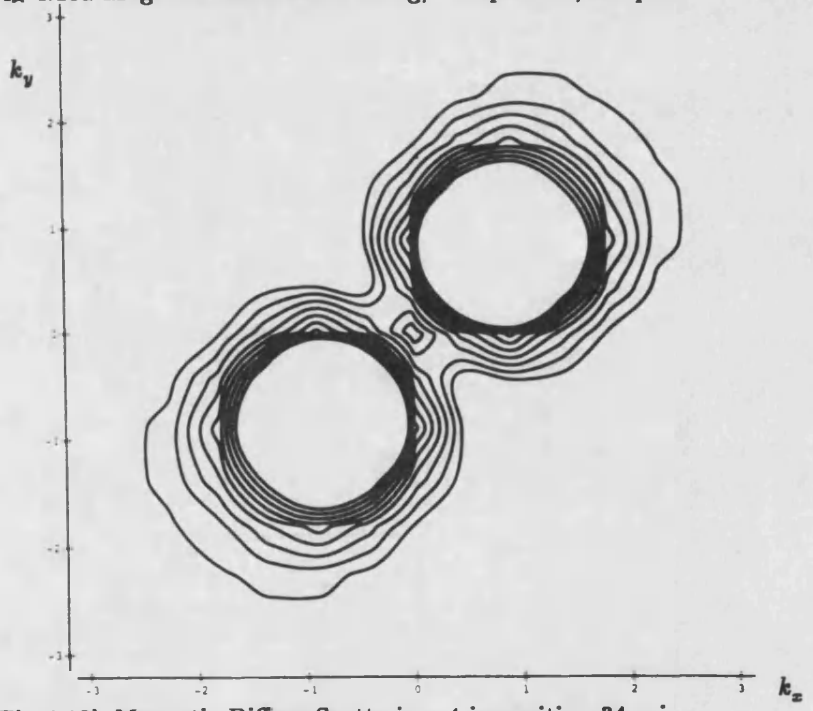

Fig 4.13b Magnetic Diffuse Scattering; 4 impurities, 34 spins

peak spreads out towards the origin by increasing the cluster size,and it is nicely converging to the exact calculation by the Green's function, as shown in Fig(4.14).

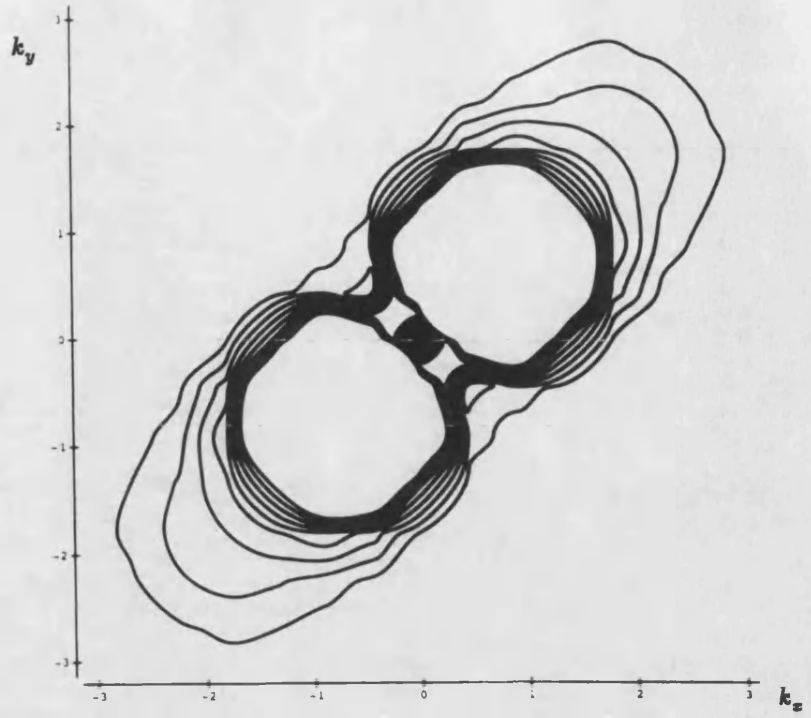

Fig 4.13c Magnetic Diffuse Scattering; 4 impurities, 44 spins

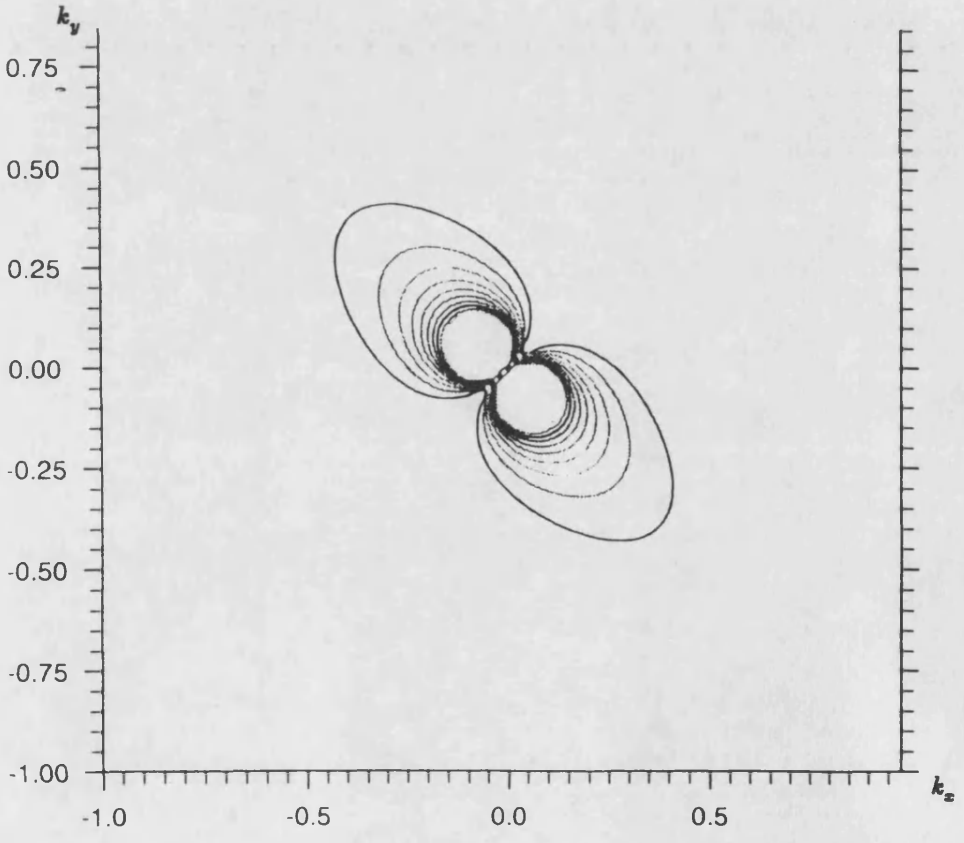

Fig 4.14 Magnetic Diffuse Scattering at the exact Critical point, 4 impurities

As we previously mentioned the symmetry of the scattering peak is not related to

the symmetry of the collinear phase. Fig(4.14) indicates that there is a diffuse peak at the origin as well as half way between the corners of first Brillioun zone. The peak at the origin is the Bragg spot of the collinear phase indicating that the spins should rotate together when the impurities are introduced. However the peaks at the half way between the corners of the Brillioun zone correspond to non-collinear arrangement. Which peak has bigger intensity is not of interest at the time being because we do not know where we must put the impurities yet. For example, if we consider the MnNi alloys, it is obvious that Ni atoms should stay away from each other as a result of anti-clustering. However in MnCu alloys, the Cu atoms stay close to each other due to the clustering.

For the time being it may be said that impurities removes the degeneracy and stabilise the non-collinear phase, hence causes a phase transition from collinear to non-collinear, which was our main aim. In the previous chapter we calculated the stability regions of the considered states in the presence of impurities and we said that these impurities may cause a first order AF-AF phase transition. Now it is clear from the diffuse scattering studies that in the presence of impurities we may obtain non-collinear arrangement of spins in a cluster. As we already pointed out, especially for the anti-clustering of impurities this transition is more probable. In order to complete our calculations we will study this scattering for the improved collinear state as well with and without extra interactions in the Hamiltonian (spin-orbit coupling, crystal field, etc).

The improved collinear phase, as we saw in chapter two, is degenerate with the non-collinear phase. In the previous chapter we have seen that the impurities

in this phase cause a sudden phase transition. In order to get rid of this sudden transition we said that some extra interactions must be included such as spin-orbit, crystal field etc. Once we have stabilised this phase by this extra interactions then we can try the diffuse scattering calculations in order to see whether or not there is a phase transition. Firstly we will try no extra interaction case. In order to do the diffuse scattering we will follow the same method as previously used. A sequence of cluster calculations show that the symmetry of the scattering pattern is related to the symmetry of the non-collinear phase as can be seen in Fig(4.15).

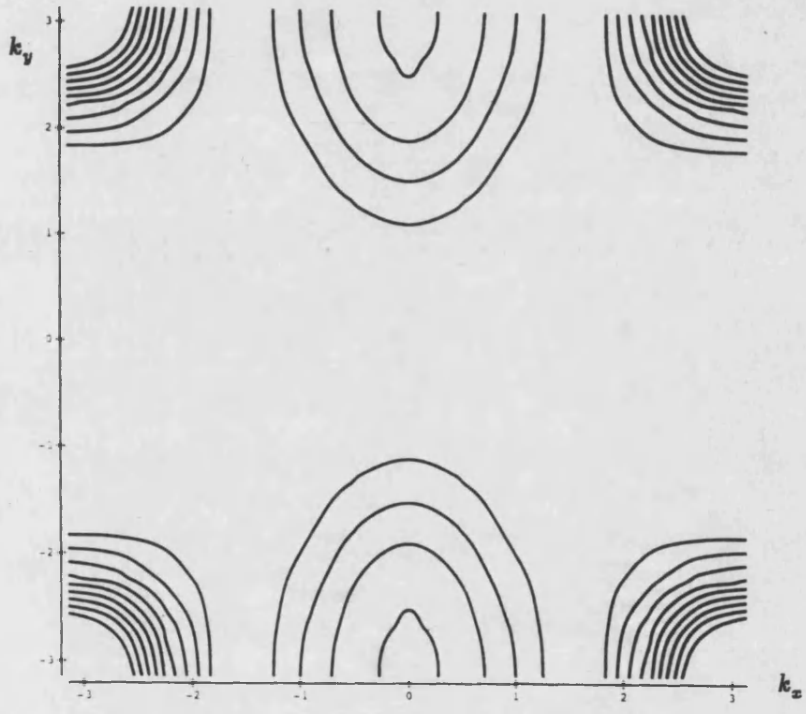

Fig 4.15 Magnetic Diffuse Scattering From improved Coll.State:1 impurity

In this picture the origin is at the $k = (\pi, 0)$. This is due to the fact that we have used $\delta\theta_k$ to calculate the diffuse scattering. But we know that $\delta \mathbf{S}_k \alpha \delta_{\mathbf{k+q}}$, that is why the origin is removed. The symmetry of the scattering peak indicates that the magnetic ordering is non-collinear. If there is a non-collinear arrangement then one may say that the impurities change the present phase which was the collinear phase.

The same calculation can be performed with more than one impurity. The result would be pretty much the same.We will not give the detailed calculations for this case. However the results as shown from Fig(4.16) to Fig(4.18) support

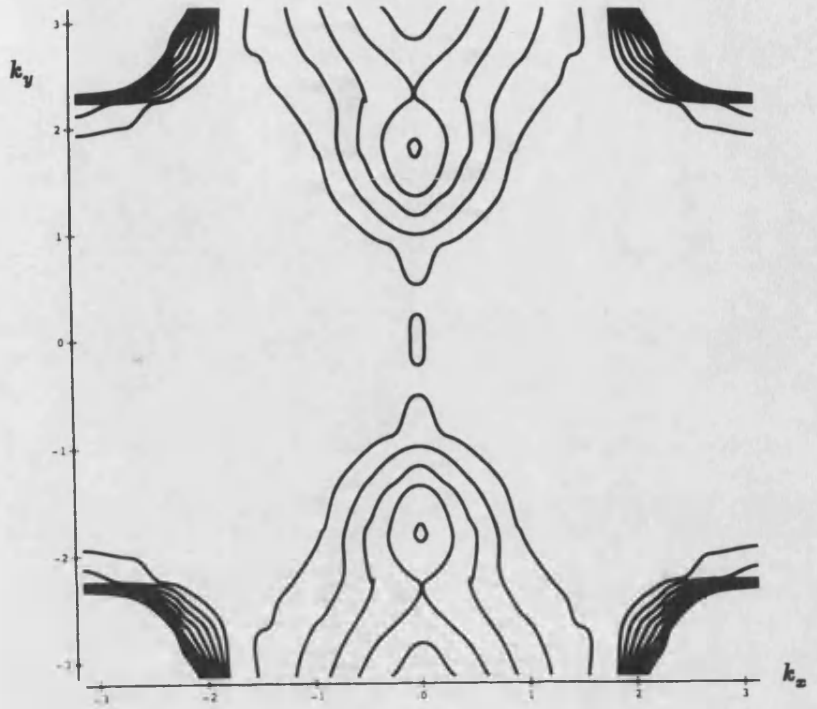

Fig 4.16 Magnetic Diffuse Scattering, Improved Coll. State:1 impurity, big cluster

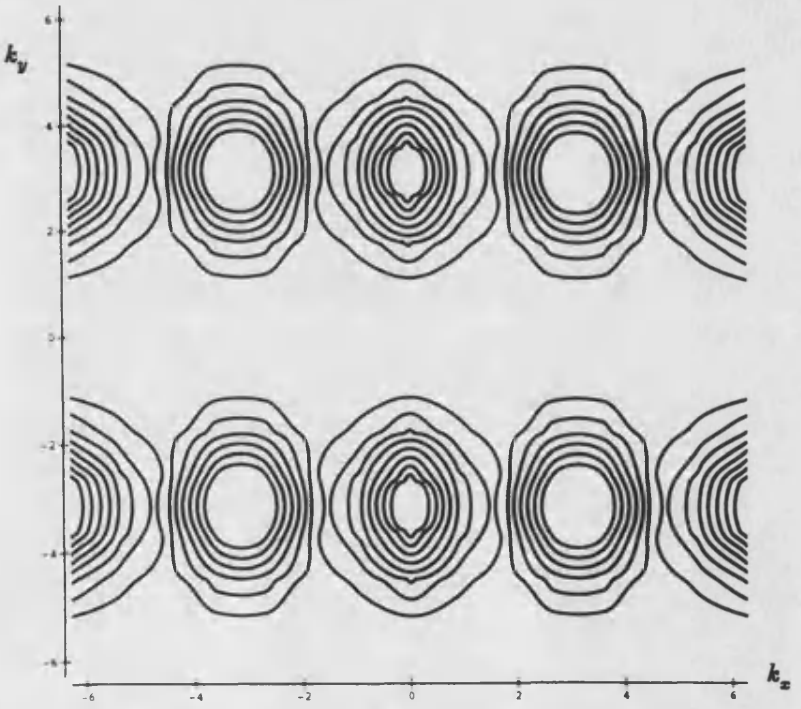

Fig 4.17 Magnetic Diffuse Scattering, improved Coll. State: 2 impurities

our prediction (in these pictures the origin is removed because of using θ values as

explained earlier). It says that impurities remove the degeneracy and stabilise the non-collinear arrangement. So there is a first order AF-AF phase transition in the presence of impurities in the considered cluster.

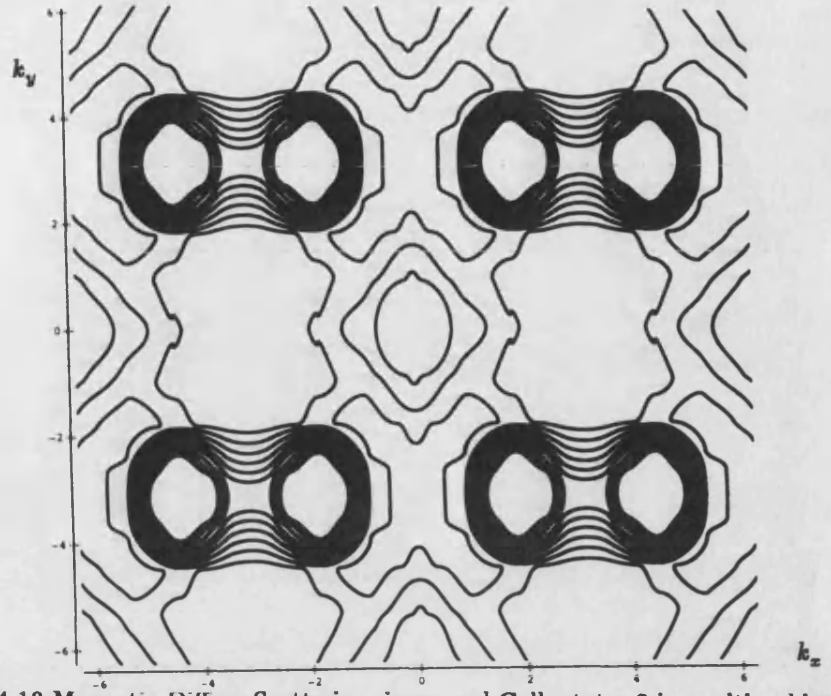

Fig 4.18 Magnetic Diffuse Scattering, improved Coll. state: 2 impurities, big cluster

4-4 Discussion:

In chapter three we saw that the boundaries of different arrangement can be changed by impurities, and we said that the impurities may cause a first order phase transition. In this chapter we studied the magnetic diffuse scattering after the impurity additions. We started with a small cluster of the simple collinear phase containing a single impurity. We saw that the symmetry of the diffuse scattering pattern is the same as the symmetry of the non-collinear phase. By increasing the cluster size we realise that the results converge to the exact results of the Green's function calculations which says that there may or may not be a long rang ordering of the non-collinear phase depending on clustering or anti-clustering of impurities.

If there is a long range order of the non-collinear phase then one may say that the impurities cause a phase transition. We realised that if the impurity concentration is increased the scattering pattern becomes visible even for small clusters. All these calculations suggest that the impurities may cause a first order antiferromagnetic phase transition. In chapter three we saw that there is a limit for the cluster size that, making the cluster bigger does not change the x_c critical point. However in this chapter we have proved that by increasing the cluster size the scattering pattern converge to the exact results. This tells us that for the diffuse scattering, every fluctuation takes part. The same calculations of the diffuse scattering has been done for the improved collinear state. The results says that the symmetry of the diffuse scattering pattern is not related to the symmetry of the collinear arrangement.

So far in this chapter we studied the diffuse scattering as we already said. The clusters we have considered are small clusters and they are negligible compared

with the crystal. Hence with a small cluster we can not talk about a phase transition because only a small number of spins become non-collinear in the presence of an impurity. If this is the case then how can we explain the phase transition in terms of alloying? Suppose that we have created many clusters in the crystal and these clusters talk to each other. In other words there is a correlation between clusters. When this happens then the long range order of non-collinear impurities may be achieved (we are assuming that all clusters are in phase. This is controlled by the temperature. If the temperature is low enough this ordering can be obtained). As a result of many clusters we can say that the impurities can cause a magnetic phase transition if the required amount of impurities (this amount must be around the percolation threshold that the clusters are about to percolate through the entire crystal) are doped into the system such that many clusters are created and they percolate through the entire crystal below a certain temperature (this temperature is the Neel temperature for an antiferromagnetic systems).

Using the results from Chapter Three and Chapter Four we can finally conclude that the alloying 'does' cause a magnetic phase transition from one ordering to another if the required amount of impurities are doped such that infinitely many clusters are created and they interact with each other.

Chapter Five

In this Chapter we develop a linearised theory for the classical Heisenberg model which allows us to approximately solve for the local distortion of spins around an impurity in a non-collinear antiferromagnet. Provided that the ratio of disturbed to undisturbed bonds is small, the theory should be applicable. The theory is particularly useful when alloying lifts the degeneracy which is often found in non-collinear magnets. We will see in the following Chapter that the theory is applicable to both MnNi and Mn_3Pt.

5-1 Introduction

Geometrically frustrated lattices provide some of the most sophisticated and interesting types of antiferromagnet. The fundamental cause is that the frustration forces some of the bonds to gain less than their optimum energy. There is usually a variety of ways in which this loss can be spread amongst the different bonds, often leading to ground state degenerate at leading order. This degeneracy is usually lifted on a smaller energy scale than that promoting the magnetism, and this in turn leads to the possibility of phase transitions between different magnetic ground states.

We will be dominantly concerned with lattices related to the face-centre-cubic lattice. γ-Manganese is the face-centre-cubic variety of manganese and Mn_3Pt orders into a Cu_3Au structure, which finds the atoms on a face-centre-cubic lattice with one of the four natural sublattices occupied by platinums. Both of these systems show a variety of antiferromagnetic phases; γ-Mn shows four experimentally[19], and Mn_3Pt has two[27]. Many different theoretical explanations have been presented for the cause of these phase transitions[23,26].

γ-Mn has type-I antiferromagnetism, which means that the magnetic Bragg spots appear half way between nuclear Bragg spots along either of the three cartesian directions. This type of magnetism can be described in terms of the collinear state for which we find alternating planes of up and down spins as we travel parallel to one of the three cartesian directions. This state finds precisely one third of the nearest neighbours parallel and hence frustrated. However, there is a large degeneracy to leading order, which can be described in terms of a superposition of the three possible collinear states. Equal amounts of all three possibilities shares the frustration equally between all bonds, and there are also phases for which there is a compromise, for example when we superimpose two collinear states. The magnetic Bragg intensity does not vary much in magnitude, although at a phase transition Bragg intensity would be shifted from one Bragg spot to another which is symmetrically related, as a second or third collinear component is introduced. It is important to realise that as more paramagnetic impurities are doped into the manganese, the ground state becomes more non-collinear. For almost pure manganese we have a collinear phase, which transforms eventually to the equal bond phase via a sequence of compromise phases[19].

Mn_3Pt shows quite different behaviour, involving a transfer of magnetic scattering between symmetrically unrelated Bragg spots. In face-centre-cubic nomenclature, the Bragg spots shift from being type-I to type-III, although the particular phases involved are quite unrelated to their face-centre-cubic counterparts. This phase transition occurs for the stochiometric alloy as a function of temperature, but a brief look at the phase diagram[25,26], shows that the transition is strongly affected by alloying. The initial problem of magnetic structure determination has

proved non-trivial, with the original proposal[25,27] being recently challenged by Long[28]. In the new description the phase transition involves a reorientation of the spins between two phases which have identical angles between all the nearest-neighbour spins, and are only different at next-nearest-neighbours. One phase has three possible orientations for the spins, much akin to the triangular lattice phase, while the new phase is predicted to have twelve different possible spin orientations, which has led to the name 'hedgehog' phase being proposed.

5-2 The linearised Heisenberg model

We are dealing with the most elementary description of magnetism, since the non-collinear nature of the states is significantly difficult to deal with: We work with the classical limit of the Heisenberg model. We use the representation:

$$H_0 = \frac{1}{2}\sum_{ij} J_{ij}\hat{\mathbf{S}}_i.\hat{\mathbf{S}}_j + \frac{1}{2}\sum_i \lambda_i \left[\hat{\mathbf{S}}_i.\hat{\mathbf{S}}_i - 1\right] \qquad (5.1a)$$

where the second term constitutes Lagrange multipliers which will be used to constrain the lengths of the spins to unity. This Hamiltonian can be minimised directly:

$$\frac{\partial H_0}{\partial \hat{\mathbf{S}}_i} = \sum_j J_{ij}\hat{\mathbf{S}}_j + \lambda_i\hat{\mathbf{S}}_i = \mathbf{0} \qquad (5.1b)$$

from which we can deduce a ground state solution, $\hat{\mathbf{S}}_i^0$ say, which has energy:

$$E_0 = -\frac{1}{2}\sum_i \lambda_i^0 \qquad (5.1c)$$

in terms of the Lagrange multipliers. In principle we would have liked to have solved this Hamiltonian for systems which involve periodic choices of coupling constants, J_{ij}, which have local disturbances, such as missing bonds corresponding to paramagnetic impurities. In practice this type of problem is prohibitively difficult in all but

the most elementary cases[35], and so in this Chapter we will discuss a linearisation scheme from which we can deduce the likely physics.

We include an infinitesimal interaction to some external field and solve the resulting problem perturbatively. We elect to couple our external field to several of the existing spins:

$$H_1 = \delta \sum_i \kappa_i \hat{\mathbf{T}}.\hat{\mathbf{S}}_i \tag{5.2a}$$

where δ is the infinitesimal coupling constant, κ_i measures the strengths with which the different spins feel the disturbance and $\hat{\mathbf{T}}$ is the orientation of the external field. In the presence of this 'source' term the ground state satisfies:

$$\frac{\partial H}{\partial \hat{\mathbf{S}}_i} = \sum_j J_{ij}\hat{\mathbf{S}}_j + \lambda_i \hat{\mathbf{S}}_i + \delta\kappa_i \hat{\mathbf{T}} = \mathbf{0} \tag{5.2b}$$

with energy:

$$E = \frac{\delta}{2}\sum_i \kappa_i \hat{\mathbf{T}}.\hat{\mathbf{S}}_i - \frac{1}{2}\sum_i \lambda_i \tag{5.2c}$$

This constitutes the problem that we will attempt to solve. It is useful to realise that we are dealing with a fairly general Hamiltonian which includes, as special cases, both a substitutional missing spin and an additional interstitial spin. To omit a spin we can orient $\hat{\mathbf{T}}$ antiparallel to the offending spin, couple it in precisely the same way as the existing spin, and then choose $\delta = 1$ to 'cancel' the existing spin out. In order to add a new interstitial spin, we can couple $\hat{\mathbf{T}}$ to the relevant neighbouring spins and then optimise the resulting solution over the orientation of $\hat{\mathbf{T}}$, effectively allowing the additional spin to choose its orientation.

Since we have been unable to solve our problem exactly, we have resorted to a perturbative expansion. We are intending to work with small distortions around

a known solution and so we reformulate the problem in terms of the change with respect to some reference solution: That of the original Hamiltonian H_0. We set:

$$\hat{\mathbf{S}}_i = \hat{\mathbf{S}}_i^0 + \delta\mathbf{S}_i \qquad \lambda_i = \lambda_i^0 + \delta\lambda_i \tag{5.3}$$

in terms of which the constraints become $2\hat{\mathbf{S}}_i^0.\delta\mathbf{S}_i + \delta\mathbf{S}_i.\delta\mathbf{S}_i = 0$. Inserting this assumption into the governing equations and using the constraints and known solution we obtain:

$$\lambda_i^0\delta\mathbf{S}_i + \sum_j J_{ij}\left[\delta\mathbf{S}_j - (\delta\mathbf{S}_j.\hat{\mathbf{S}}_i^0)\hat{\mathbf{S}}_i^0\right] + \delta\kappa_i\left[\hat{\mathbf{T}} - (\hat{\mathbf{T}}.\hat{\mathbf{S}}_i^0)\hat{\mathbf{S}}_i^0\right]$$

$$= -\delta\lambda_i\delta\mathbf{S}_i - \frac{1}{2}(\lambda_i^0 + \delta\lambda_i)\delta\mathbf{S}_i.\delta\mathbf{S}_i\hat{\mathbf{S}}_i^0 \tag{5.4a}$$

with energy:

$$\Delta E = \delta\sum_i \kappa_i\hat{\mathbf{T}}.\hat{\mathbf{S}}_i^0 + \frac{\delta}{2}\sum_i \kappa_i\hat{\mathbf{T}}.\delta\mathbf{S}_i - \frac{1}{4}\sum_i \delta\lambda_i\delta\mathbf{S}_i.\delta\mathbf{S}_i \tag{5.4b}$$

This result is exact and enables us to deduce the leading order perturbative correction directly: The right-hand side of (5.4a) can be neglected as can the final term in the energy (5.4b). Although we will not be concerned with the result here, if we wanted to proceed with the perturbation theory, we would also need the change in Lagrange multipliers:

$$\delta\lambda_i = -\sum_j J_{ij}\hat{\mathbf{S}}_i^0.\delta\mathbf{S}_j - \delta\kappa_i\hat{\mathbf{S}}_i^0.\hat{\mathbf{T}} + \frac{1}{2}(\lambda_i^0 + \delta\lambda_i)\delta\mathbf{S}_i.\delta\mathbf{S}_i \tag{5.4c}$$

to complete the theory.

One of the more interesting issues is that of how several impurities interact with each other. Unfortunately, in the present analysis there is no point in including

several impurities, because to the order in which we solve the problem different impurities do not interact. The analysis is effectively identical when there are several impurities; the only difference being an additional label on the vector, $\hat{\mathbf{T}}$, and coupling constant, κ, to label the impurity type. In this Chapter we will be concerned only with the leading order effect of which type of ground state a particular type of impurity prefers.

In order to proceed further we have been forced into linearising the problem. In practice, this amounts to allowing each spin the freedom to rotate through a small angle picking up an additional small component perpendicular to its original direction. To describe this freedom, we need to choose a local two-dimensional basis perpendicular to the original spin direction; one for each site. If we elect to use:

$$\hat{\mathbf{X}}_i = \frac{\hat{\mathbf{T}} - [\hat{\mathbf{T}}.\hat{\mathbf{S}}_i^0]\hat{\mathbf{S}}_i^0}{|\,\hat{\mathbf{S}}_i^0 \times \hat{\mathbf{T}}\,|} \tag{5.5a}$$

$$\hat{\mathbf{Y}}_i = \frac{\hat{\mathbf{S}}_i^0 \times \hat{\mathbf{T}}}{|\,\hat{\mathbf{S}}_i^0 \times \hat{\mathbf{T}}\,|} \tag{5.5b}$$

for atoms which are not originally parallel to $\hat{\mathbf{T}}$, and choose $\hat{\mathbf{X}}$ and $\hat{\mathbf{Y}}$ arbitrarily if $\hat{\mathbf{S}}_i^0$ is parallel to $\hat{\mathbf{T}}$, then in terms of:

$$\hat{\mathbf{T}}.\hat{\mathbf{S}}_i^0 = \cos\phi_i \qquad \phi_i \epsilon (0, \pi) \tag{5.5c}$$

and:

$$\delta\mathbf{S}_i = -\delta\left[x_i\hat{\mathbf{X}}_i + y_i\hat{\mathbf{Y}}_i\right] \tag{5.5d}$$

to leading order:

$$\lambda_i^0 x_i + \sum_j J_{ij}\left[\hat{\mathbf{X}}_i.\hat{\mathbf{X}}_j x_j + \hat{\mathbf{X}}_i.\hat{\mathbf{Y}}_j y_j\right] = \kappa_i \sin\phi_i \tag{5.6a}$$

$$\lambda_i^0 y_i + \sum_j J_{ij}\left[\hat{\mathbf{Y}}_i.\hat{\mathbf{Y}}_j y_j + \hat{\mathbf{Y}}_i.\hat{\mathbf{X}}_j x_j\right] = 0 \tag{5.6b}$$

$$\Delta E = \delta \sum_i \kappa_i \hat{\mathbf{T}}.\hat{\mathbf{S}}_i^0 - \frac{\delta^2}{2}\sum_i \kappa_i \sin\phi_i x_i \tag{5.6c}$$

where we now recognise a linear problem for finding x_i and y_i. The coupling between the different components depends strongly on the allowed local rotational freedom, and for our particular chosen representation we find:

$$\hat{\mathbf{X}}_i.\hat{\mathbf{X}}_j = \frac{1 - \cos^2\phi_i - \cos^2\phi_j + \cos\phi_i\cos\phi_j \hat{\mathbf{S}}_i^0.\hat{\mathbf{S}}_j^0}{\sin\phi_i \sin\phi_j} \tag{5.7a}$$

$$\hat{\mathbf{X}}_j.\hat{\mathbf{Y}}_i = \frac{\cos\phi_j \hat{\mathbf{T}}.[\hat{\mathbf{S}}_i^0 \times \hat{\mathbf{S}}_j^0]}{\sin\phi_i \sin\phi_j} \tag{5.7b}$$

$$\hat{\mathbf{Y}}_i.\hat{\mathbf{Y}}_j = \frac{\hat{\mathbf{S}}_i^0.\hat{\mathbf{S}}_j^0 - \cos\phi_i\cos\phi_j}{\sin\phi_i\sin\phi_j} \tag{5.7c}$$

The first observation we make is that for coplanar distortions (viz $\hat{\mathbf{T}}$ in the plane of a coplanar spin state), we have no need of the y_i because the fluctuations perpendicular to the plane do not couple to the fluctuations in the plane. Secondly, if the impurity spin, $\hat{\mathbf{T}}$, is orthogonal to a coplanar spin state, then all the $\cos\phi_i$ all vanish and so again we have no need of the y_i. We should point out that on a practical level this real-space formulation is not greatly useful, and we have only used it on finite clusters as an independent check for our analysis.

In the presence of the periodicity we can write these equations is k space as

$$(x,y)_{\mathbf{k}\alpha} = \sum_l e^{i\mathbf{k}.(\mathbf{R}_l + \mathbf{c}_\alpha)}(x,y)_{l\alpha} \tag{5.8a}$$

$$K_{\mathbf{k}\alpha} = \sum_l e^{i\mathbf{k}.(\mathbf{R}_l+\mathbf{c}_\alpha)}\kappa_{l\alpha}\sin\phi_\alpha \tag{5.8b}$$

$$\epsilon_{\mathbf{k}\alpha\alpha'} = \delta_{\alpha\alpha'}\lambda_\alpha^0 + \frac{1}{N}\sum_{ll'} e^{i\mathbf{k}.(\mathbf{R}_l+\mathbf{c}_\alpha-\mathbf{R}_{l'}+\mathbf{c}_{\alpha'})}J_{l\alpha l'\alpha'} \tag{5.8c}$$

we eventually derive:

$$\sum_{\alpha'} \hat{\mathbf{X}}_{\alpha}.\hat{\mathbf{X}}_{\alpha'}\epsilon_{\mathbf{k}\alpha\alpha'}x_{\mathbf{k}\alpha'} + \sum_{\alpha'} \hat{\mathbf{X}}_{\alpha}.\hat{\mathbf{Y}}_{\alpha'}\epsilon_{\mathbf{k}\alpha\alpha'}y_{\mathbf{k}\alpha'} = K_{\mathbf{k}\alpha} \qquad (5.9a)$$

$$\sum_{\alpha'} \hat{\mathbf{Y}}_{\alpha}.\hat{\mathbf{X}}_{\alpha'}\epsilon_{\mathbf{k}\alpha\alpha'}x_{\mathbf{k}\alpha'} + \sum_{\alpha'} \hat{\mathbf{Y}}_{\alpha}.\hat{\mathbf{Y}}_{\alpha'}\epsilon_{\mathbf{k}\alpha\alpha'}y_{\mathbf{k}\alpha'} = 0 \qquad (5.9b)$$

$$\Delta E = \delta E + \delta^2 E = \delta \sum_{i} \kappa_i \hat{\mathbf{T}}.\hat{\mathbf{S}}_i^0 - \frac{\delta^2}{2}\frac{1}{N}\sum_{\mathbf{k}\alpha} K_{\mathbf{k}\alpha}^{*} x_{\mathbf{k}\alpha} \qquad (5.9c)$$

for the induced spin distortion, $x_{\mathbf{k}\alpha}$ $y_{\mathbf{k}\alpha}$, and its energy, ΔE. We will calculate this energy for particular materials to understand which phase is stabilised by the impurity spin. In order to find out whether or not there is a phase transition we should study the magnetic diffuse scattering, as we already pointed out in Chapter Four. The diffuse scattering profiles from our impurities can be deduced from the local spin deformation $\delta \mathbf{S}_{\mathbf{k}}$, which is elementary to deduce:

$$\delta \mathbf{S}_{\mathbf{k}} = \delta \left[\hat{\mathbf{T}} - \sum_{\alpha} (x_{\mathbf{k}\alpha}\hat{\mathbf{X}}_{\alpha} + y_{\mathbf{k}\alpha}\hat{\mathbf{Y}}_{\alpha}) \right] \qquad (5.10)$$

We will restrict attention to the square-modulus of the spin density, $\mid \delta \mathbf{S}_{\mathbf{k}} \mid^2$. The remainder of the problem is to apply the theory to some particular materials.

The linear term in the energy is dominant if it exists. For the case of a missing spin, the orientation of the perturbation, $\hat{\mathbf{T}}$, is necessarily anti-parallel to one of the spins, $\hat{\mathbf{S}}_0^0$ say, and the coupling is via the original bonding, viz $K_i = J_{0i}$. We find that $\delta E = -\delta \sum_i J_{0i}\hat{\mathbf{S}}_0^0.\hat{\mathbf{S}}_i^0 = \delta\lambda_0^0$ and simply measures the loss in energy from the omitted spin. For the case of an additional spin, the vector $\hat{\mathbf{T}}$ represents the orientation of this additional spin and is free to rotate towards its preferred direction. The linear term then chooses this orientation so as to be antiparallel to the local field:

$$\mathbf{F} = \sum_{i} \kappa_i \hat{\mathbf{S}}_i^0 \qquad (5.11)$$

and yields a contribution to the energy from the additional spin coming from its interaction with this local field. The quadratic term in the energy comes from the polarisation of the surrounding spins by the local impurity and constitutes the effect that we are dominantly interested in.

It is quite common for the systems in which we are interested that an additional spin is placed at a local 'dead spot', viz a point for which the local field, **F**, vanishes. The reason for this is that the substitutional site is usually one of high symmetry, and if there are an equal number of bonds to all of the possible sublattices, then the local field will cancel in a pure antiferromagnet. For this situation it is the polarisability of the spin state which will select the preferred spin orientation for the moment impurity, and the impurity moment will be held in place much more weakly than usual.

5-3 Predictions for manganese alloys

In order to set the scene, we should first off study the simplest variants of our model in order to check the internal consistency and validity of our results. Several features are special to non-collinear ground states: If we have a collinear ground-state, then the omission of a spin has absolutely no polarisation effect on the spin configuration predicted by our perturbation theory. This result comes from the fact that the local perturbation is parallel to the affected spins and so is attempting to alter their length, which is not permitted by the spin constraints. For a finite perturbation it is possible for a perpendicular distortion to self-trap[38]. This behaviour is not permitted by our linearisation, which prohibits such a non-linear response. For an impurity addition, on the other hand, there is no polarisation

if there is a local field, F, for the same reason, but if the impurity spin is added at a 'dead spot' then there is a polarisation effect. The impurity spin orients itself perpendicular to the collinear spin direction and induces a short-range perpendicular distortion. At first sight one might have expected a long-range response to the impurity, because of the low-energy 'Goldstone modes', but because we are at a 'dead spot' there is no coupling to the underlying antiferromagnetism and the distortion necessarily decays. For non-collinear states there is almost always some form of polarisation coming from a local impurity, because usually not all of the affected spins are parallel to the impurity and so some of the neighbours can reorient and make use of the impurity.

Perhaps the simplest system to study is the square lattice Neel state. Due to collinearity, the only polarisation effects come from impurities added at 'dead spots' A spin sitting above a 'square', which couples uniformly to its four neighbours, yields a polarisation energy of: $\delta^2 E = -0.36338\delta^2\kappa^2/J$, where κ is the coupling constant. Since there are four bonds, for similar magnitude coupling constants the system only manages about 1/11 of the available bonding. This form might be anticipated from the fact that the competition is between one additional bond versus four original bonds (viz $\lambda_\alpha^0 = 4J$) and second order perturbation theory, although the magnitude is rather more difficult to guess. The scale of the effect is the same order as the antiferromagnetism, and so for the more interesting frustrated antiferromagnets the disorder can lift any underlying degeneracy and predict the ground state.

Probably the simplest non-collinear system to study is the triangular lattice with its 120° ground state. This particular system has only a discrete chiral de-

generacy and local defects are unable to effect a transition between the degenerate ground states. The example is instructive, however, because it suggests what we might expect from a general non-collinear spin state. If a particular spin is infinitesimally reduced in length, the nearest-neighbours are able to rotate to compensate, because the local field they feel is at 120° to their direction. Although the moments are highly coordinated, with $Z \stackrel{\Gamma}{=} 6$, the frustration in the lattice ensures that only half of the bonds can be achieved in the ground state and so the stabilising field is smaller than that of the square lattice, (viz $\lambda_\alpha^0 = 3J$). The natural site for an impurity lies above the plane, connecting to a triangle of moments below. Once again we are sitting at a 'dead spot', and so the additional moment is free to rotate. The impurity spin orients itself perpendicular to the coplanar spin configuration and induces a polarisation energy of: $\delta^2 E = -0.5\kappa^2/J$, more than that for the square lattice. Considering the fact that there are now fewer bonds, this is a large difference. This difference can be attributed to two effects; firstly, the local field holding the spins in place is smaller, and secondly, the larger intrinsic coordination plays a role in extending the polarisation further from the impurity. In other words, since we only need three neighbours to balance the local field and we have six to choose from, there is more opportunity for the deformation to spread. This argument is general and quite central to an interpretation of these phenomena. The distortion in a frustrated antiferromagnet is usually stronger and longer-range than in a non-frustrated magnet. When we consider the reduction of the magnitude of a spin, however, the characteristics are different. The infinitesimal reduction yields a linear loss of $\delta E = 3\delta J$ from the local field and a polarisation contribution of $\delta^2 E = -0.57608\delta^2 J$. This polarisation energy comes from a surprisingly small re-

gion with the distortion decaying very fast. Unlike the previous case, where the distortion was perpendicular to the plane of moments, now the distortion is in the plane of moments. The fact that all the spins are 120° to each other now means that there is a loss of a factor of two in transmitting the coupling between spins and we would now need all six of the spins to compensate the local stabilising field of three. Even worse, some of the spins are actually parallel to the imposed distortion and these spins find it more difficult to reorient, further reducing the polarisation spread. Impurities composed of omitted spins polarise subject to the frustration, but impurity moments added at 'dead spots' can sometimes polarise effectively in a less frustrated way.

In Chapter Six we will apply the theory to two particular materials: MnNi and Mn_3Pt alloys. We will see that the theory can predict the observed phase transitions in these alloys.

Chapter Six

Three Examples

In previous chapters we have established a theoretical model, which can explain the first order antiferromagnetic phase transition for the square lattice. In this chapter we will show that this model can explain the antiferromagnetic phase transition for the real materials. We will consider three examples.

6-1 MnNi Alloys

Transition metal alloys based on γ-Mn shows very interesting magnetic behaviour. Manganese quenched into a face centred cubic structure exhibits type-I antiferromagnetism. This is a sequence of ferromagnetic x-y layers which alternate in spin direction along the z axis. the z axis becomes inequivalent to the other Cartesian directions and the magnetism induces a huge tetragonal distortion.

When another transition metal is doped into the manganese there are quite dramatic changes in behaviour. Fe[17], Ir[18], Ni[19], and Cu[20] all substantially reduce the tetragonal distortion and for Fe, Ir and Ni there is evidence of a cubic phase which is stabilised by doping concentrations of approximately a quarter. In this particular study we will consider the case of MnNi.

Mn atoms have 2.0 μ_B magnetic moment in a face centred cubic lattice. $Mn_{1-x}Ni_x$ alloys shows a sequence of structural as well as magnetic phase transition as a function of Ni concentration[19]. The phase diagram of this alloy is shown in Fig(6.1). Diffuse neutron scattering experiments show that the moment on the nickel

site is small[23]. The nickel atoms behave more like paramagnetic impurities.

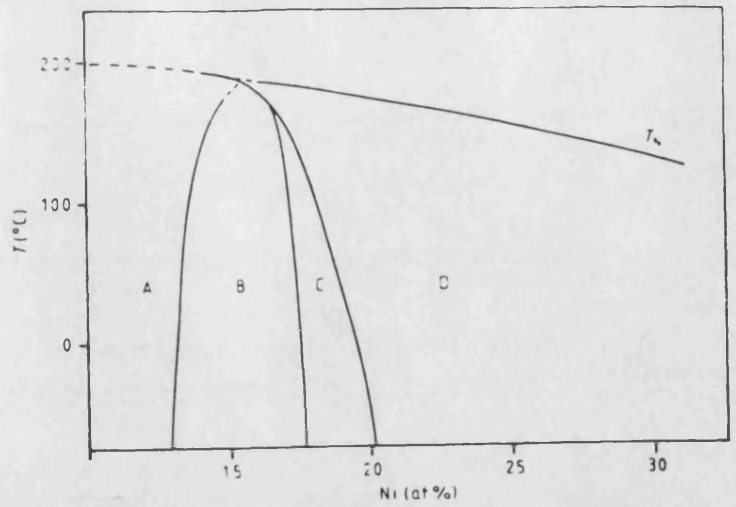

Fig 6.1 Experimental Phase diagram of MnNi alloys, after Honda et al(1976)

The experiments showed that the alloy is face centre tetragonal (it is called the t_2 phase) with $\frac{c}{a} < 1$ at the low doping regime (between 0-13% of doping) then it becomes orthorhombic when the doping concentration is between 13%-18%. There is a second tetragonal structure (this phase is sometimes called the t_1 phase) with $\frac{c}{a} > 1$ when the doping is about 18%-20%. And finally the alloy becomes cubic by 25% doping. According to neutron diffraction experiments by Uchishiba[22] the spin direction in the t_2 phase with $\frac{c}{a} > 1$ is along the c-axis, while that in the t_1 phase with $\frac{c}{a} < 1$ is orthogonal to c-axis (we have pictured these phase in Fig(6.2a) and Fig(6.2b) respectively).

In both cases the nearest neighbour pair of Mn atoms has antiparallel spins. It is assumed that the same situation holds good in the case of orthorhombic phase, so that ferromagnetic layers are always perpendicular to the spin direction which is parallel to the shortest axis[22]. Careful studies of order in the alloys shows a tendency for the atoms to order in a Cu_3Au structure[23]. Another experiment suggests that Ni atoms anti-cluster[24], which means that there is a low probability

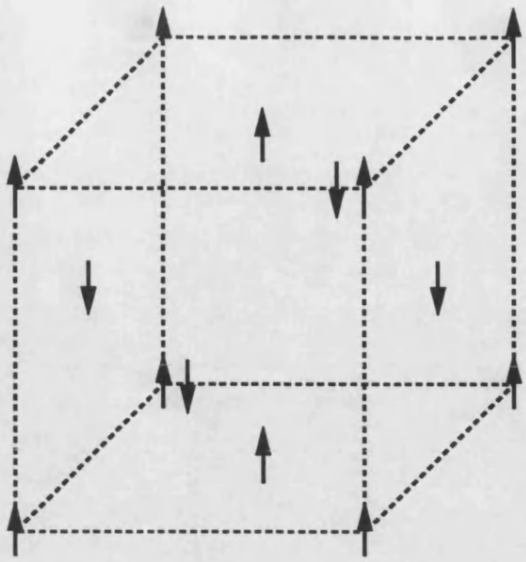

Fig. **6.2a** t_2 phase of MnNi alloys

of finding nearest neighbour impurities and an increased probability of finding next nearest neighbour impurities. For this alloy we will look at the question of how the system might transform from one phase to another.

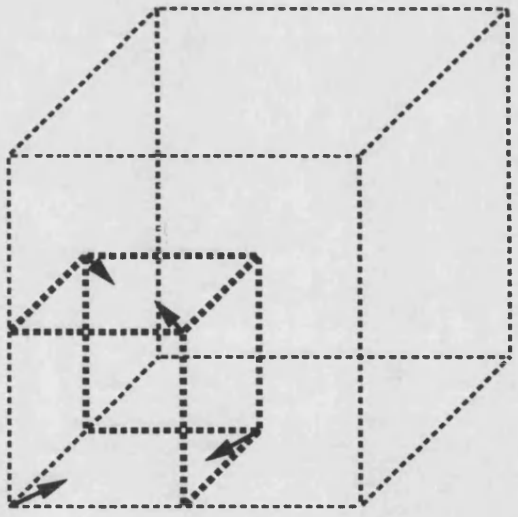

Fig. **6.2b** t_1 phase of MnNi alloys

The aim here is to explain the magnetic phase transition in a theoretical way. Firstly we will restrict attention to t_2 and t_1 phases in order to apply the

square lattice calculations to the alloys. Both phases can be projected onto the two dimensional square lattice without changing the orientation of spins. In this projection one would obtain $J_1 = 2J_2$ (where J_1 and J_2 are the first and second nearest neighbours exchange coupling respectively). As we pictured in Fig(6.3) the projection of t_2 gives the simple collinear phase in the square lattice and the projection of t_1 phase is the non-collinear arrangement as shown in Fig(6.4).

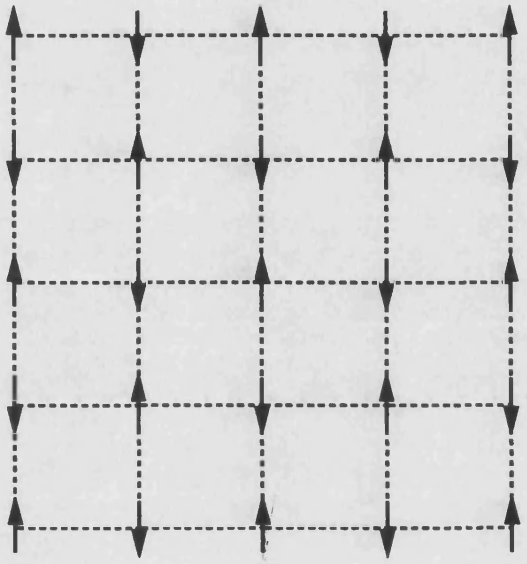

Fig. **6.3** The Projection of the t_2 Phase

In order to explain the phase transition from t_2 to t_1 in MnNi alloys we will restrict attention to the impurity concentration. But firstly we should review the square lattice.

6-1-1 The Square Lattice

In order to understand the spin spin interaction in the square lattice we will consider the Heisenberg model as we did in chapter two and chapter three. The

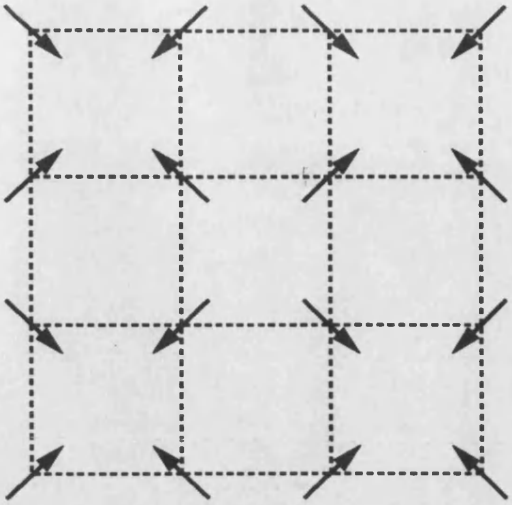

Fig. 6.4 The Projection of the t_1 Phase

Heisenberg Hamiltonian for a spin system is

$$H = \sum_{ij} J_{ij} \mathbf{S}_i . \mathbf{S}_j \tag{6.1}$$

This Hamiltonian predicts two different types of spin ordering for the ground state depending on the x value ($x = \frac{J_2}{J_1}$): Collinear (which is the projection of t_2 phase) and non-collinear (projection of t_1 phase) as proved in chapter two. The non-collinear phase can be interpreted as a linear superposition of collinear phases as shown in Fig(6.5).

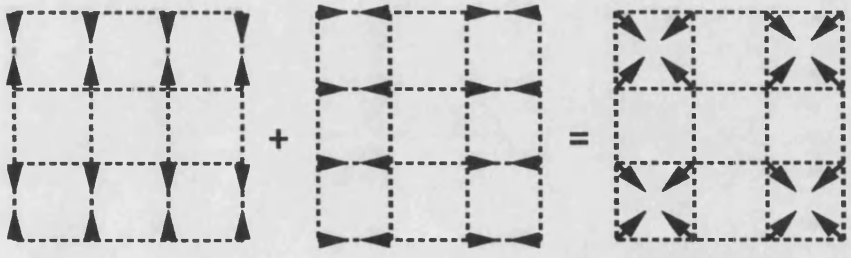

Fig. 6.5 Superposition of two collinear arrangement leads to non-collinear one

Using the periodicity of the lattice, one can rewrite the Hamiltonian in k

space as

$$\frac{H}{J_1 S^2} = \sum_k (\gamma_{k_1} + x\gamma_{k_2})|\hat{\mathbf{S}}_\mathbf{k}|^2 \tag{6.2}$$

where $x = \frac{J_2}{J_1}$, $\gamma_{k_1} = \frac{1}{2}(\cos k_x + \cos k_y)$ and $\gamma_{k_2} = \cos k_x \cos k_y$. In Chapter Two we have seen that the collinear and the non-collinear phases have,different stability regions as shown in Fig(2.7). After this review we can look at the effects of paramagnetic impurities in the square lattice.

6-1-2 The Impurity Calculations

In this section the effects of a paramagnetic impurity will be investigated in a small cluster in order to explain the possibility of a magnetic phase transition from t_2 to t_1 in MnNi alloys.

We will start with a small cluster of t_2 phase involving a paramagnetic impurity as shown in Fig(3.2). We are assuming that at least four spins would be affected after a paramagnetic impurity and they would have an extra perpendicular component. However in an antiferromagnetic system each spin feels a parallel magnetic from surrounding atoms. This means that the spins in the system would remain unchanged even after impurities. On the other hand an impurity causes a spontaneous symmetry breaking. This broken symmetry allows spins to have an extra perpendicular component

If we consider our small cluster (above) one can find how much energy can be gained by a paramagnetic impurity. This comes from the energy differences of

$$\Delta H = H_0 - H_1 \tag{6.3}$$

where H_1 and H_0 are the Heisenberg Hamiltonians for rotated and unrotated spins

in the chosen cluster respectively. This energy varies as a function of x($x = \frac{J_2}{J_1}$). However one can find a critical x_c point that below which the energy difference is zero. The critical point is $x_c = \frac{1}{2}$ for our chosen small cluster, but if the size of the cluster is increased the critical point is decreased. For example $x_c = \frac{1}{2} - \frac{1}{12}$ for a bigger cluster (Fig(3.3)). We saw in chapter three that the exact value of the critical point can be found by using the Green's functions as $x_c = 0.407760$ for a single impurity in the collinear state. As we mentioned in chapter two the collinear phase is stable when $x < 0.5$. But now we know after an impurity addition this phase is stable when $x < x_c$. The interval $x_c < x < 0.5$ is very important with respect to energy differences. In this interval the non-collinear arrangement has lower energy then the collinear one. So one may say that the arrangement is non-collinear in this interval. If this is the case the impurities stabilise the non-collinear phase and cause a first order phase transition.

Another interesting result comes from magnetic diffuse scattering studies. We saw in the previous chapter that the magnetic diffuse scattering studies show that after the impurity addition the symmetry of the scattering pattern is the same as the symmetry of the non-collinear phase. However the clusters we have considered are small clusters and they are very very small compared with the crystal. Hence with a small cluster we can not talk about a phase transition because only a small number of spins become non-collinear in the presence of an impurity. If this is the case then how can we explain the phase transition in terms of alloying? Suppose that we have created many clusters in the crystal and these clusters talk to each other. In other words there is a correlation between clusters. When this happens then the long range order of non-collinear impurities may be achieved (we are

assuming that all clusters are in phase. This is controlled by the temperature. If the temperature is low enough this ordering can be obtained). As a result of many clusters we can say that the impurities can cause a magnetic phase transition if the required amount of impurities are doped into the system such that many clusters are created and they percolate through the entire crystal below a certain temperature (this temperature is the Neel temperature for an antiferromagnetic systems). This result is in agreement with experiments[19]. Although the square lattice give some idea about the possibility of a first order phase transition, it is not enough to explain all the observed phases in MnNi alloys. In order to proceed further, we have forced to use the linearised Heisenberg Hamiltonian' as explained in Chapter Five. Now we will attempt to explain the observed phase transition by using this idea.

6-1-3 The predictions of the Linearised theory for MnNi

The classical Heisenberg model exhibits a host of degenerate ground states for the face-centre-cubic lattice, of which the most relevant three for us are depicted in Fig(6.6) and are called the SSDW, DSDW and TSDW states (standing for Single, Double and Treble Spin Density Waves). The most sensible explanation for the observed experimental phase diagram of γ-Mn_xNi_{1-x}[19] with nickel doping is that of a sequence of phase transitions between the SSDW state for undoped γ-manganese, through an intermediate DSDW state, finally reaching a cubic TSDW state at about a quarter doping. The dominant antiferromagnetic interaction is probably representable as nearest-neighbour Heisenberg-like and therefore the interaction which lifts the degeneracy is expected to have a smaller energy scale. Although many possible mechanisms for lifting this degeneracy have been proposed[36], we believe that

the role of the alloy disorder is central to an explanation for the phase diagram. The present model makes predictions for the amount of energy available to each of the different states from isolated impurities and thereby enables a comparison between the different states to be made.

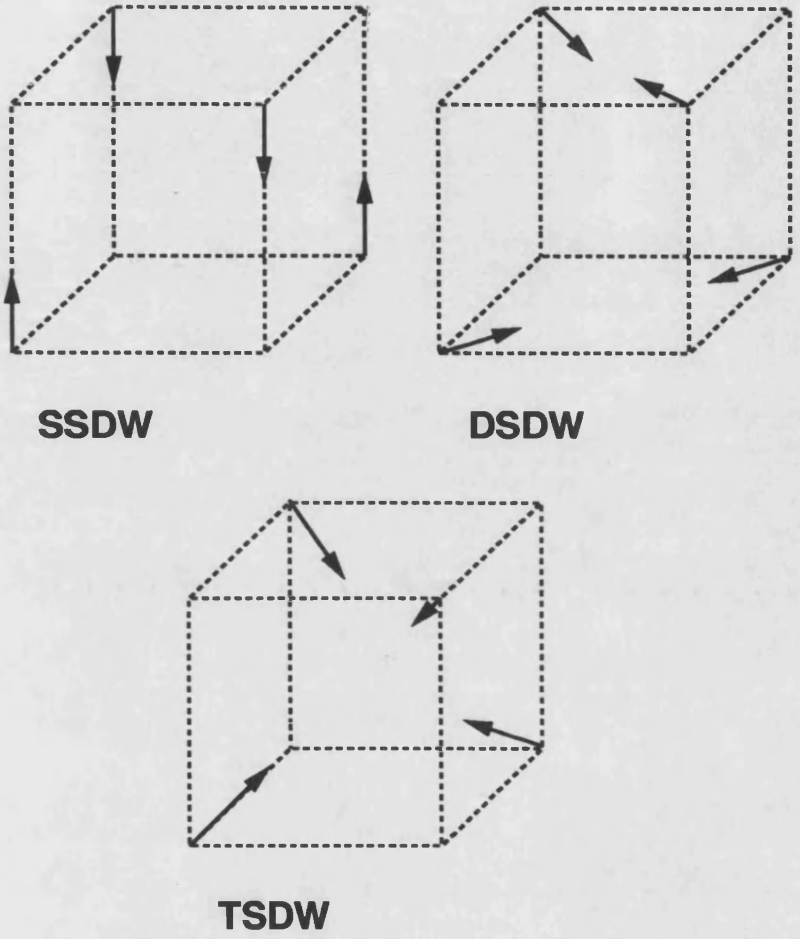

Fig. 6.6 Three Spin Orderings in γ-Mn

Before we move onto a comparison with the experiments, which involve the consideration of substitutional impurities, firstly we will consider the role of interstitial impurities. This is not as absurd as might at first be considered, if one remembers that adding a small quantity of interstitial carbon into the alloys alters the phase diagram considerably[37]. There are two natural sites to add an interstitial impu-

rity; firstly there is a tetrahedral site in the centre of a tetrahedron of manganese atoms and secondly there is an octohedral site with six nearest neighbours.

Tetrahedral interstitials lie at 'dead spots'. The additional spin tries to align itself orthogonal to as many existing spins as it can. For the case of the SSDW and DSDW there is a direction which is orthogonal to all the collinear or coplanar spins respectively, and impurities oriented in this direction yield a polarisation energy of: $\delta^2 E = -0.5\kappa^2/J$. For the TSDW state, however, all three spin dimensions are used in the ground state and there is no preferred direction for the impurity. Whatever the orientation of the impurity, the polarisation energy is: $\delta^2 E = -0.33333\kappa^2/J$ for the TSDW state. This type of impurity prefers a spin state employing a low number of spin dimensions. This basic result appears to be true for *all* 'dead spot'-impurities, which like to orient anti-parallel to existing spins and therefore prefer an unused spin direction.

Octohedral interstitials do not lie at 'dead spots', since they only neighbour three out of the four natural antiferromagnetic sublattices. The local field, $\mathbf{F} = -2\kappa\hat{\mathbf{S}}^0_\alpha$, for the spin to which the impurity is not a neighbour. The linear contribution does not break the degeneracy and yield a contribution of $-2\delta\kappa$ to each state, when the impurity is aligned parallel to the sublattice which it does not neighbour. The polarisation contribution does lift the degeneracy, however, and yields 0, $-0.36338\kappa^2/J$ and $-0.40126\kappa^2/J$ for the SSDW, DSDW and TSDW states respectively. The SSDW cannot benefit because it is collinear, and the TSDW is the best choice because it is the 'most' non-collinear state. It is possible (but unlikely) that octohedrally coordinated carbon impurities might explain the observed contraction

of the Mn-Ni phase diagram under the action of a small amount of doped carbon. Once again, this result appears quite general and robust: When additional moments are included at sites which feel a local field, the states which are preferred are those with the highest degree of non-collinearity.

Now we turn to the experimentally relevant case of substitutional doping. In these alloys it is generally believed that the nickel impurities do not carry moments and behave as paramagnetic impurities[36]. This leads us quite naturally to consider the predictions of our theory when a moment is infinitesimally reduced in magnitude. The linear contribution does not lift the degeneracy, yielding $\delta E = 4\delta J$ for each state. The polarisation does lift the degeneracy quite strongly, however, yielding 0, $-0.72676J$ and $-0.90905J$ for the SSDW, DSDW and TSDW respectively. The collinear SSDW can gain nothing but the other two form a strong polarisation cloud and recoup a sizable fraction of the lost bonding energy, viz about a quarter. This calculation gives a satisfactory explanation for the phase transitions in γ-manganese alloys. In the collinear phase the paramagnetic impurities can recoup none of their lost bonding energy, whereas in the non-collinear phases a contribution proportional to the impurity concentration times the original antiferromagnetic energy is regained. Since the energy scale which lifts the degeneracy is likely to be a small fraction of the antiferromagnetic energy scale, a doping level of a quarter to cause the phase transition seems perfectly reasonable. Remember that the undoped alloy suffers a distortion of around 6% [15] and therefore the energy scale which lifts the degeneracy cannot be a lot smaller than J. Indeed, the magneto-elastic components must be of order J.

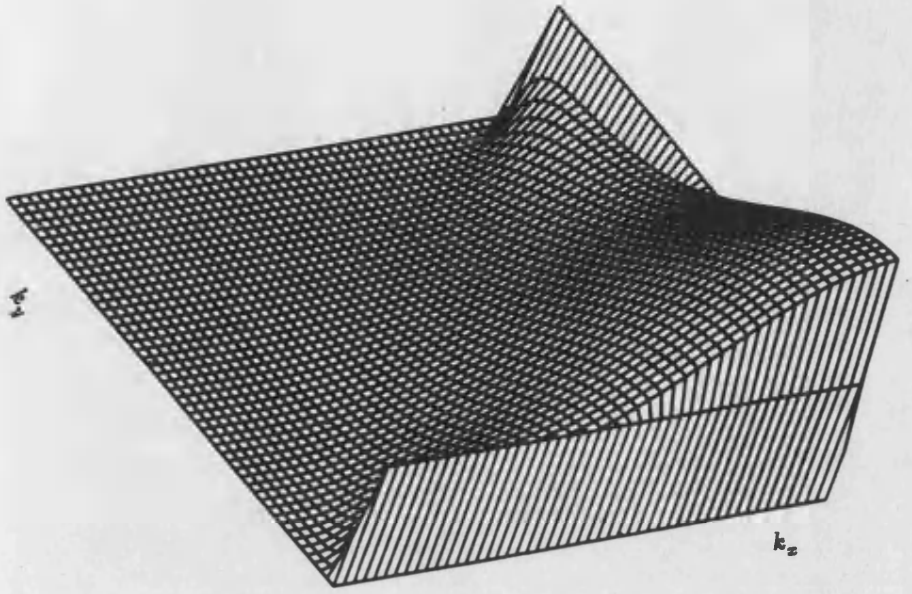

Fig 6.7 Diffuse Scattering of TSDW state

If we proceed to a more direct verification of the theory, then we arrive at some problems. The definitive experiment that analyses local spin configurations around alloy disorder is magnetic diffuse neutron scattering. The relevant experiments have been performed, and large peaks associated with non-collinear deformations around the alloy impurities have been observed[16]. The form of this scattering can be understood in terms of a minor reorientation of the surrounding shell of nearest neighbours. The present theory is for an isolated impurity, and the resulting distortion is much longer-range. However, one can try to understand whether there is still agreement with the diffuse scattering. It is elementary to deduce the reciprocal-space spin density from the local impurity and polarisation cloud, and if we ignore the perpendicular nature of the scattering which is sensible in

the highly non-collinear states, then we can associate the diffuse scattering with the square of the magnitude of the spin density. We plot this quantity for the TSDW state in Fig(6.7). Although there is obviously a large amount of scattering around the relevant Bragg spots, the form of this scattering is violently anisotropic and is dominantly found away from the line connecting the zone centre to the 'vanishing' magnetic Bragg spots[41]. Although this result is rather disappointing, the fact that the experiments were performed when the doping fraction is about a quarter implies that each manganese atom has several neighbouring impurities on average, and so it is not that surprising that the longer-range aspects of the diffuse scattering are poorly described.

6-1-4 Conclusion

The projection of t_2 and t_1 spin ordering for MnNi alloy corresponds to collinear and non-collinear spin ordering in the square lattice. It is experimentally known that the spin ordering changes from t_2 to t_1 as a function of Ni concentration.

The problem we have tackled here is to investigate theoretically the effects of paramagnetic impurities in the collinear phase of the square lattice (which is equivalent to t_2 phase) and looked for a possibility of non-collinear phase (t_1 phase).

We started with a paramagnetic impurity in a small cluster and found a critical point below which the system is unaffected by an impurity, but above which the spins may have an extra perpendicular component. Studying the magnetic diffuse scattering we realised that in fact the impurities lead to a long range order of non-collinear arrangement. This indicates that the paramagnetic impurities cause a first order antiferromagnetic phase transition which is in agreement with experiments. In

order to complete the explanation for MnNi, we have used the linearised Heisenberg Hamiltonian. The theory successfully predicts the expected phase diagrams as far as the energetics go, with the relevant degree of non-collinearity being either increased or decreased in agreement with the type of impurity found. The energy scale for which impurities break the degeneracy are always a small but significant fraction of the dominant antiferromagnetic coupling constant, and so we should usually expect alloying to cause phase transitions in frustrated systems with degeneracy. Alloying non-magnetic impurities into γ-Mn is expected to destabilise the collinear ground state in favour of the fully non-collinear TSDW state.

We will compare the predictions of the linearised theory for these alloys with the Mn_3Pt alloys in order to see that the theory is better for the second alloys at the end of following section.

6-2 Mn_3Pt Alloys

In this section we will consider Mn_3Pt alloys. Experimentally these alloys show a first order phase transition at around 365°K. The aim is the same as MnNi case, i.e explain this phase transition in a theoretical way.

The structure of Mn_3Pt is Cu_3Au-type. The atoms sit on an fcc lattice which is reduced to a simple cubic lattice with four atoms per unit cell as shown in Fig(6.8).

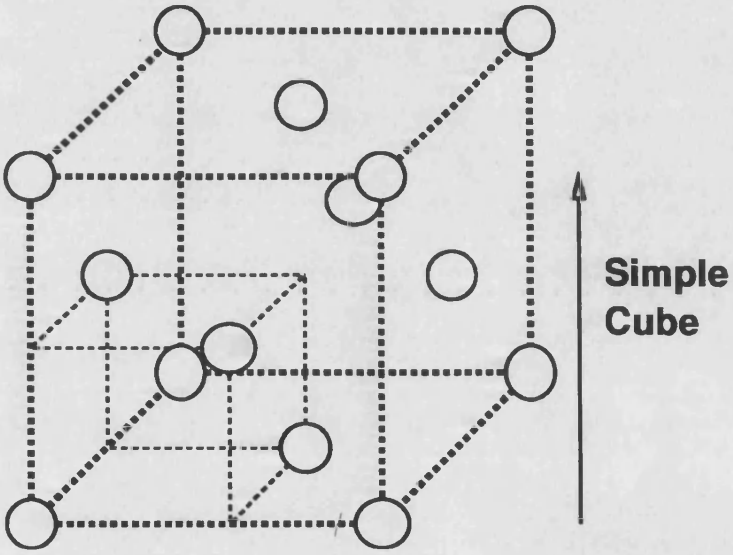

Fig. **6.8** Simple Cube with Four atom per unit cell

It is experimentally found that Mn atoms have $3\mu_B$ magnetic moments whereas Pt atoms have a very small magnetic moment that we can ignore.

This alloy is experimentally interesting because it shows a first order AF-AF phase transition at 365°K[25]. From Fig(6.9) to Fig(6.11) we show the expected Bragg spots for fcc and the two experimentally observed magnetic Bragg spots of Mn_3Pt in the two different phases.

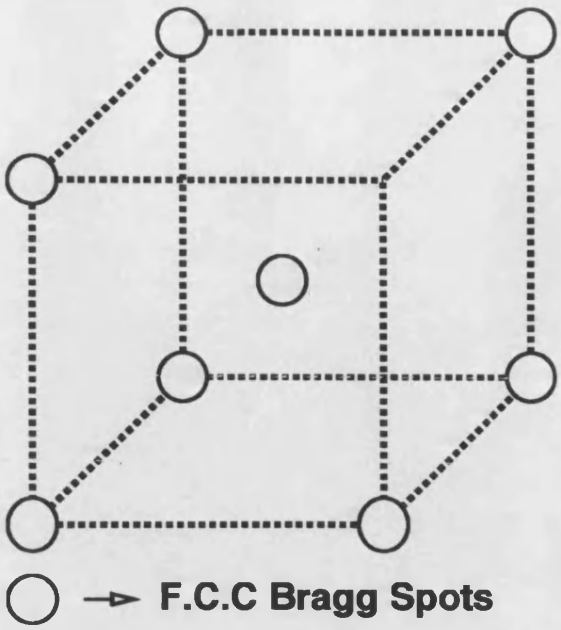

Fig. **6.9** Bragg Spots of the f.c.c Lattice

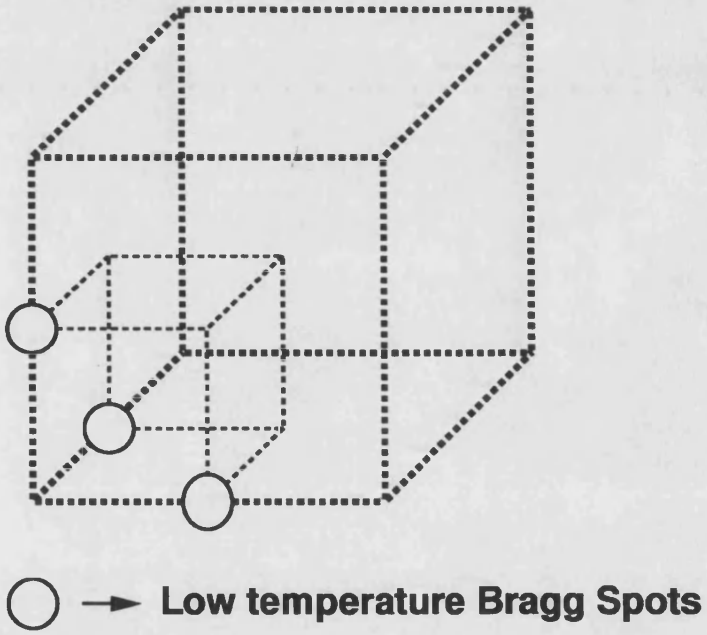

Fig. **6.10** Low temperature Magnetic Bragg spots of Mn_3Pt

There are two phases: the low temperature, and the high temperature. The low temperature phase has three spin directions, all nearest neighbour spins in the system being oriented at 120° to each other as depicted in Fig(6.12).

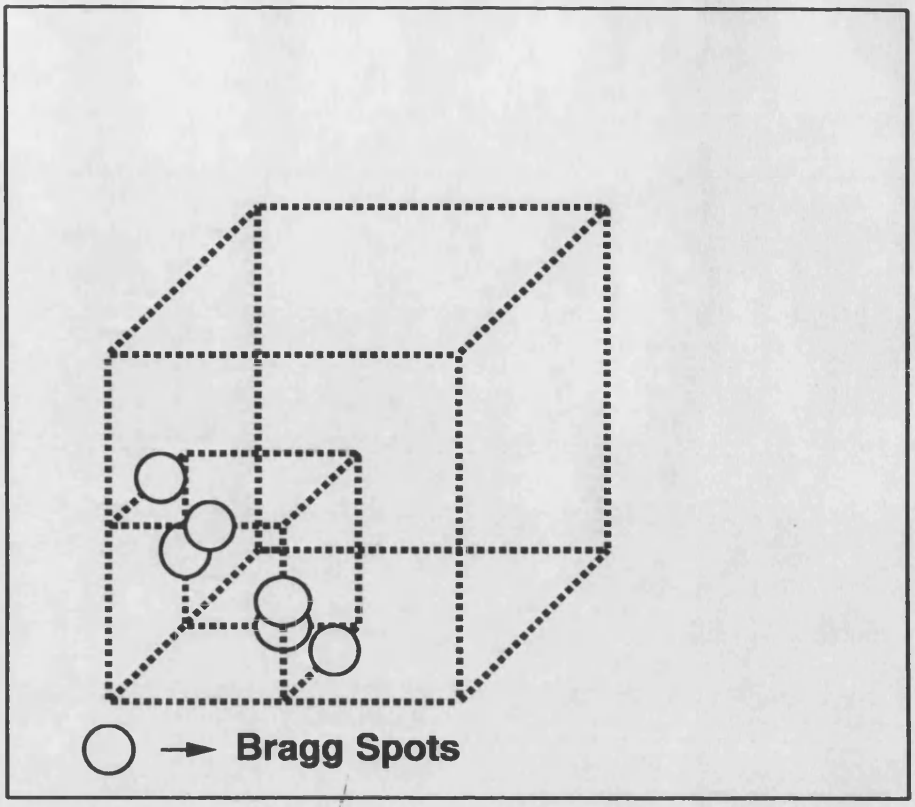

Fig. 6.11 High Temperature Magnetic Bragg Spots of Mn_3Pt

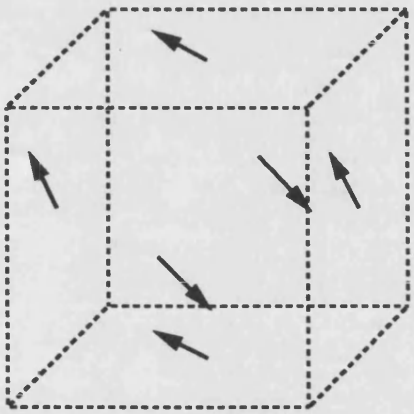

Fig. 6.12 Low Temperature Phase of Mn_3Pt

However the structure at high temperature is rather complicated[28]. The spins are pointing all over the place as in Fig(6.13).

Now we want to explain this phase transition in a theoretical way. In order

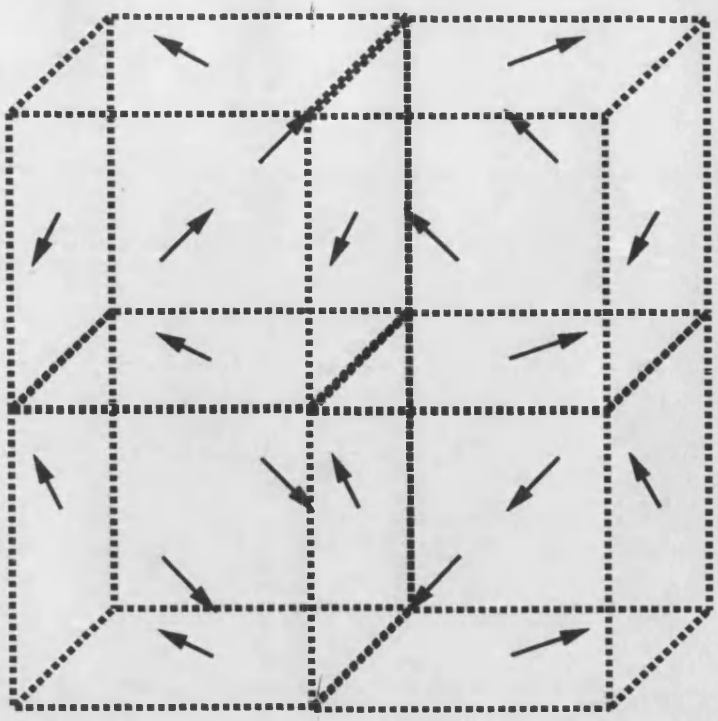

Fig. 6.13 High Temperature Phase of Mn_3Pt

to do this we will consider the Heisenberg model, which is

$$H = J \sum_{ij} \mathbf{S}_i . \mathbf{S}_j \tag{6.4}$$

where ij runs over nearest neighbours. For our case one can rewrite this Hamiltonian as

$$H = \frac{J}{4} \sum_{cubes} (\mathbf{S}_1 + \mathbf{S}_2 + \mathbf{S}_3)^2 \tag{6.5}$$

where the cubes in the sum is shown in Fig(6.14).

The three spins in the unit cell make a triangle. So this may lead to a 120° phase. Making all the unit cells identical, we can generate the low temperature phase. But we know that this is not the only ground state ordering. There are other orderings.

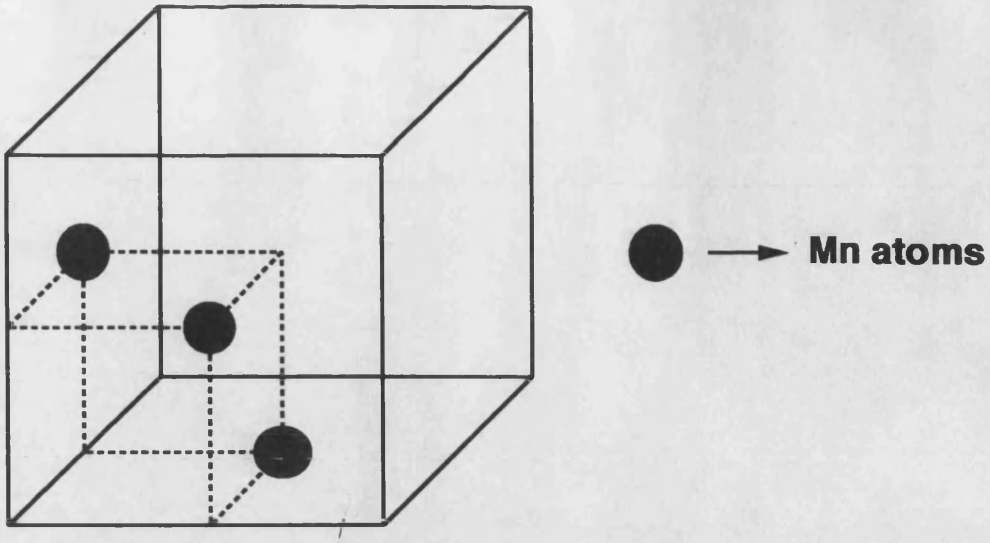

Fig. 6.14 The Cube in Equation 6.5

Before generating these ground state orderings we want to compare the degeneracy in Mn_3Pt with the Kagome Net, since our system magnetically consists of planes of Kagome Nets. The Mn atoms form a Kagome Net as shown in Fig(6.15) and show a very high degeneracy[33].

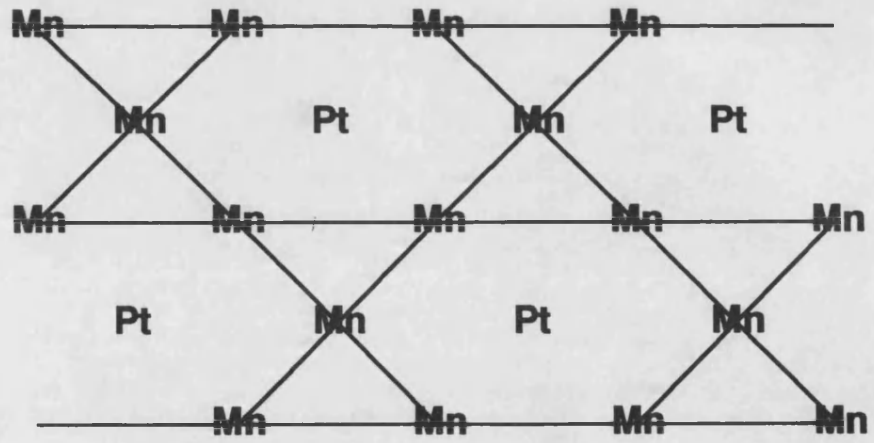

Fig. 6.15 Kagome Net

Our system is magnetically degenerate too, but it is not as bad as the Kagome Net.

When we work with the Heisenberg model it predicts that the magnetic Bragg spots should be on the dashed line of Fig(6.16), which indicates that the degeneracy is quite high.

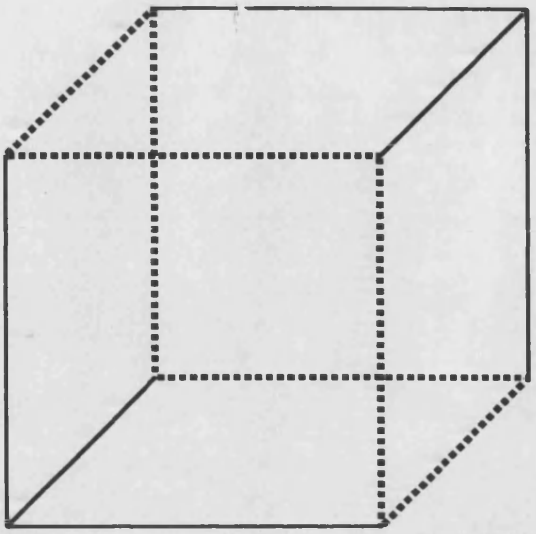

Fig. **6.16** Heisenberg Prediction of Magnetic Bragg Spots

Our task is not to worry about this degeneracy now. We know from experiments that two different ground state orderings is observed. We should now worry about generating this orderings by using our unit cell.

6-2-1 **Two Symmetry Operations**

Let us define two symmetry operations in order to generate two ground states orderings. The first symmetry operation is simply translation through three Cartesian axis. This symmetry operation translates the unit cell along the three perpendicular direction without changing the directions of spins in the unit cell as shown in Fig(6.17).

Translating the unit cell along three Cartesian axis produces the low temper-

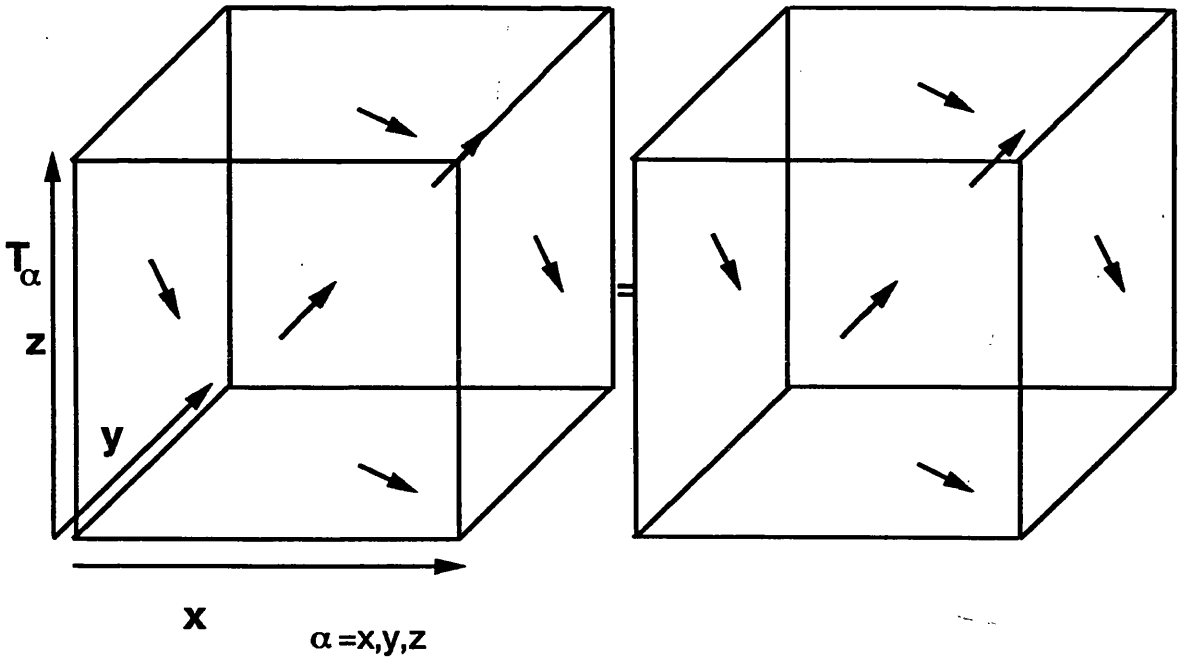

Fig. 6.17 Translation of a unit cell Through a Cartesian Direction

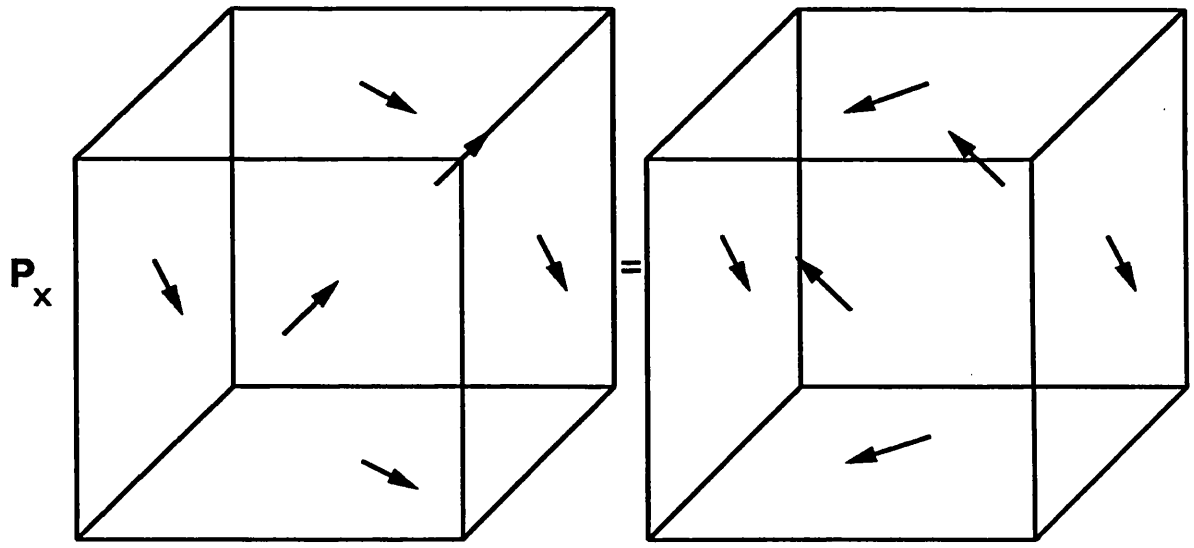

Fig. 6.18 Translation+Simultaneous Spin Reflection perpendicular to Translation axis

ature phase, which is quite easy to generate.

The second symmetry operation is Translation + Simultaneous Spin Reflection perpendicular to the translation axis. In Fig(6.18) we have shown one of these three symmetry operations.

It is obvious that using this symmetry operation one can produce 12 spin directions which is the high temperature phase. Thus one can generate two different ground states ordering by using these two simple symmetry operations.

So far in our Heisenberg model we have included only the first nearest neighbour interactions. The second nearest neighbour interactions were omitted at the first approach, but one can easily work out that these second nearest neighbours remove the degeneracy of the two ground state. There are two types of them: the first one is inside a unit cell. The first nearest neighbours force each second nearest neighbour in a unit cell to be parallel to its opposite next nearest neighbour as shown in Fig(6.19).

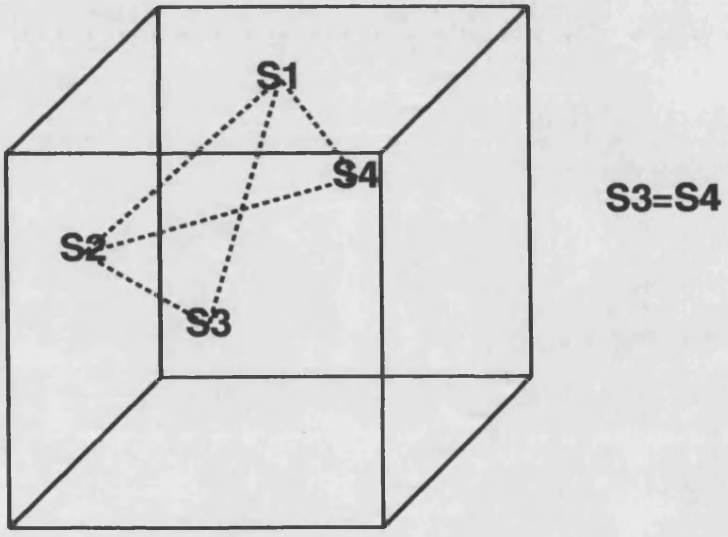

Fig. **6.19** Next nearest Neighbour interactions in a unit cell

As can be seen in this picture S_1, S_2 and S_3 are nearest neighbours to each other and they make a triangle. S_4 is also a nearest neighbour of S_1 and S_2. Since

the system is antiferromagnetic one can easily write down that

$$\mathbf{S}_1 + \mathbf{S}_2 + \mathbf{S}_3 = 0$$
$$\mathbf{S}_1 + \mathbf{S}_2 + \mathbf{S}_4 = 0 \qquad (6.6)$$

This proves that $\mathbf{S}_3 = \mathbf{S}_4$ which are next nearest neighbours to each other. Using the same manner it is not difficult to see that $\mathbf{S}_1 = \mathbf{S}_5$ and $\mathbf{S}_2 = \mathbf{S}_6$.

The second of these next nearest neighbour interactions is between two unit cells. In this case two next nearest Mn atoms have a common Pt atom as a nearest neighbour as shown in Fig(6.20).

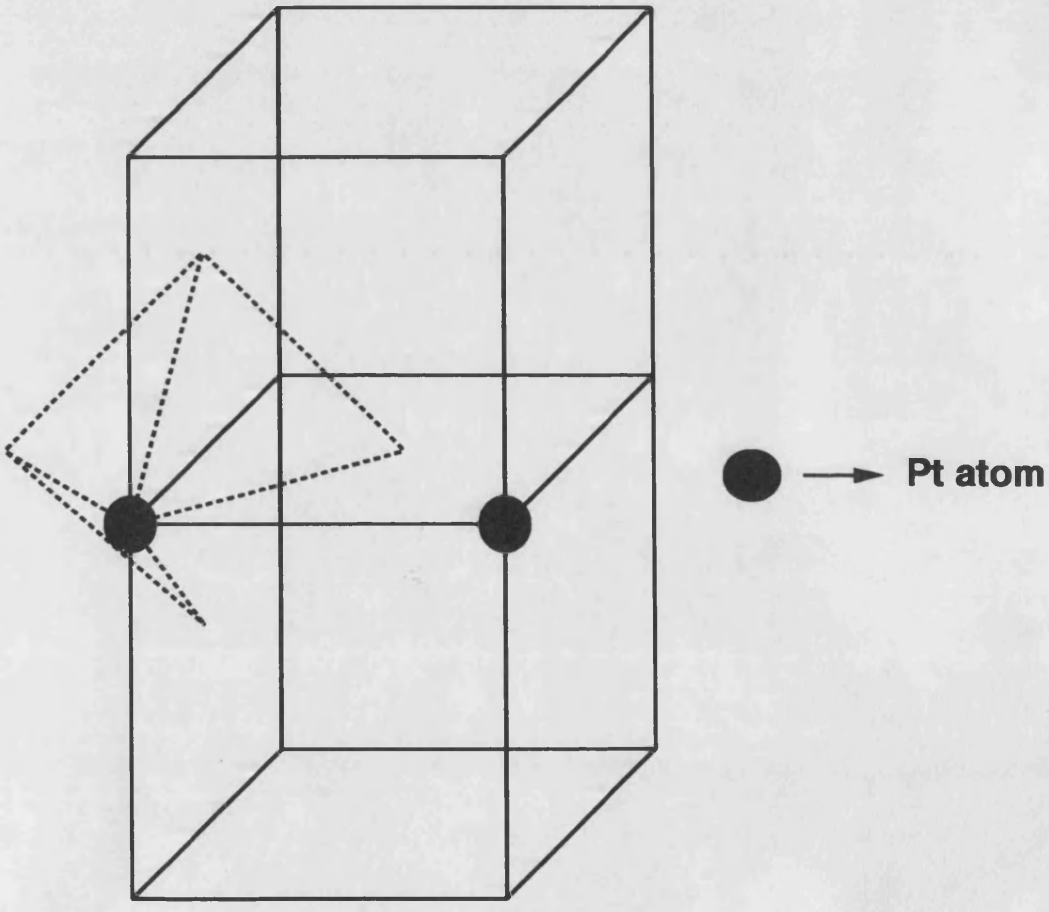

Fig. **6.20** Next Nearest Neighbour interactions between two unit cells

In this case one should include an extra interactions of spins into the Heisen-

berg Hamiltonian; namely

$$H = J_1 \sum_{ij} \mathbf{S}_i.\mathbf{S}_j + J_2 \sum_{[ij]} \mathbf{S}_i.\mathbf{S}_j \tag{6.7}$$

where the first term runs over the nearest neighbour, and the second term runs over the second nearest neighbours. This second term brings two alternatives to the spin direction. If $J_2 < 0$ the parallel alignment of these paired next nearest neighbours gives the maximum negative energy contribution to the Eq(6.7). In this case the sum of three nearest neighbours (they make a triangle) gives zero total spin and it is good for an antiferromagnetic system. So if $J_2 < 0$ then the parallel alignment of next nearest neighbour spins are favourable. This leads to the low temperature phase. However, if $J_2 > 0$, the maximum negative energy contribution to Eq(6.7) would come from the antiparallel alignment. In this case we would end up with $\mathbf{S}_1.\mathbf{S}_3 + \mathbf{S}_2.\mathbf{S}_4 = -2S^2$. On the other hand it is easy to prove that $\mathbf{S}_1.\mathbf{S}_3 + \mathbf{S}_2.\mathbf{S}_4 = \frac{1}{2}(\mathbf{S}_1 + \mathbf{S}_2 + \mathbf{S}_3 + \mathbf{S}_4)^2 \geq 0$. This tells us that the best we can do is to make them orthogonal to each other. So one can say that if $J_2 > 0$, the perpendicular alignment is favourable. This leads to the high temperature phase.

It is now obvious that by including the second nearest neighbour interactions into the Heisenberg Hamiltonian, we can remove the degeneracy. Experimentally we know that there are two ground state ordering depending on the temperature. The experimental phase diagram is shown in Fig(6.21).

One can predict from this phase diagram that the second nearest neighbour coupling varies as a function of temperature. That is why there are two different spin orientations depending on J_2. Our aim is to try to explain this transition in

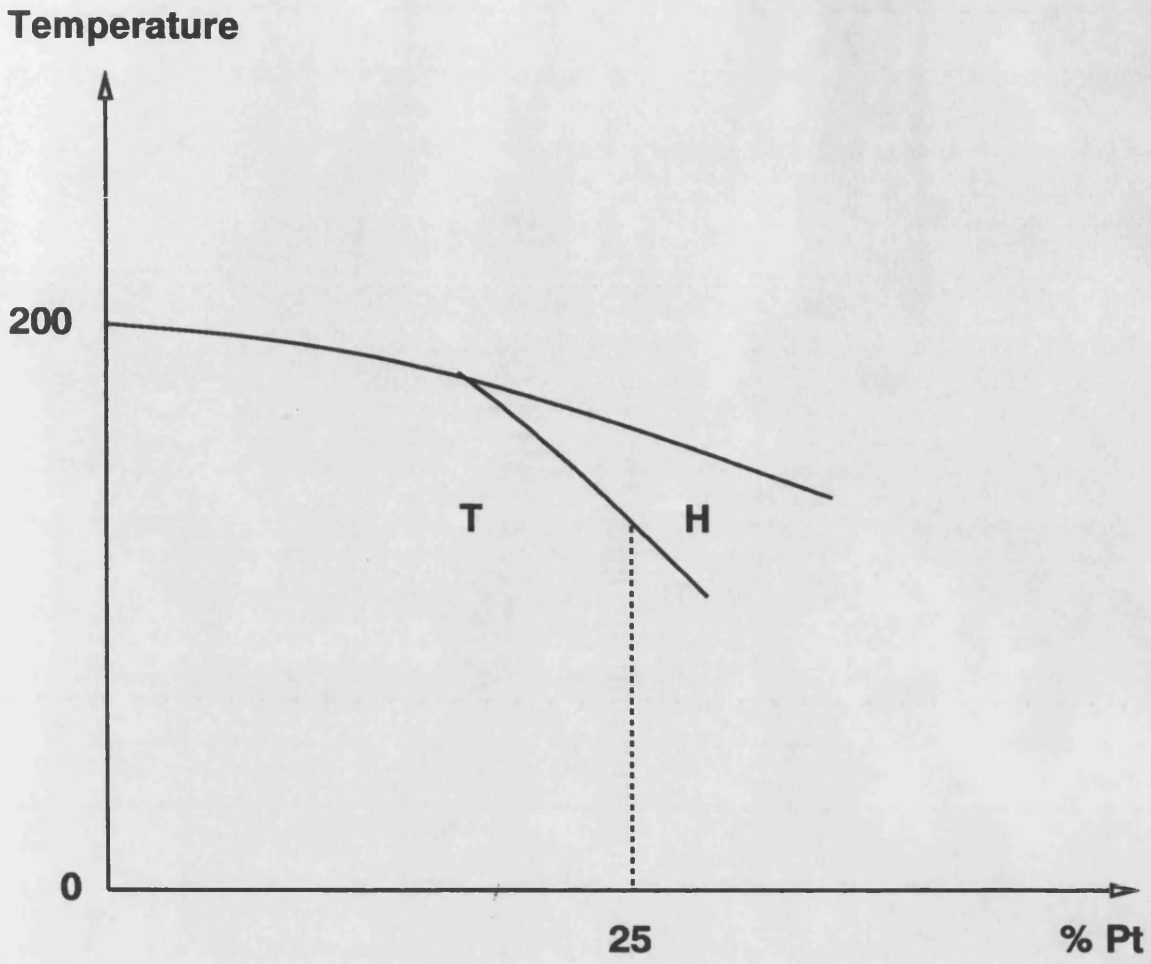

Fig. 6.21 Experimental Phase Diagram of Mn_3Pt

a theoretical way as we mentioned earlier. We will fix the temperature where the two phases are degenerate, in other words when $J_2 = 0$. Then we will replace either a single Pt with Mn or a single Mn with Pt and find out which ordering has lower energy. Then we might be able to predict which state would be stabilised by this replacement. The interactions are now among the first nearest neighbours ($J_2 = 0$). In Chapter Five we have developed a linearised theory especially for these alloys. Now we simply apply the prediction of this theory for Mn_3Pt.

6-2-2 Prediction of the Linearised theory for Mn_3Pt

Unlike the γ-manganese system, where the disorder is huge, Mn_3Pt is a well-ordered stochiometric alloy for which the experimentally induced compositional changes are small[25,27]. This material is therefore a much more suitable candidate for our theory. The experimental phase diagram indicates that there is a strong dependence of the phase boundary on the alloy concentration, with additional manganese stabilising the triangular phase and with additional platinum stabilising the hedgehog phase: The theory should predict this.

We will consider the substitution of a platinum atom by a manganese atom Fig(6.22). The bond lengths are equal and so the additional bonds will have a very similar strength to the underlying bonds. We will treat all bonds as being equal. There are twelve nearest-neighbour manganese atoms at each platinum site. For both phases we are adding at a 'dead spot', with one each of the twelve hedgehog spin orientations and an equal mixture of the three sublattices for the triangular phase. The polarisation contribution to the hedgehog phase is independent of the orientation of the impurity spin at: $-0.70823\delta^2 J$. For the coplanar triangular phase the polarisation depends strongly on the orientation of the impurity spin, ranging from $-0.61654\delta^2 J$ when the impurity is coplanar with the spin state to: $-0.95493\delta^2 J$ when the spin is perpendicular to the spin state. The prediction is straightforward, additional manganese should favour the triangular phase, with an energy saving of about $J/4$ per impurity. This is perfectly consistent with the experimental phase diagram. The physical explanation for the effect is identical to our previous examples, with the impurity at the 'dead spot' preferring the phase with

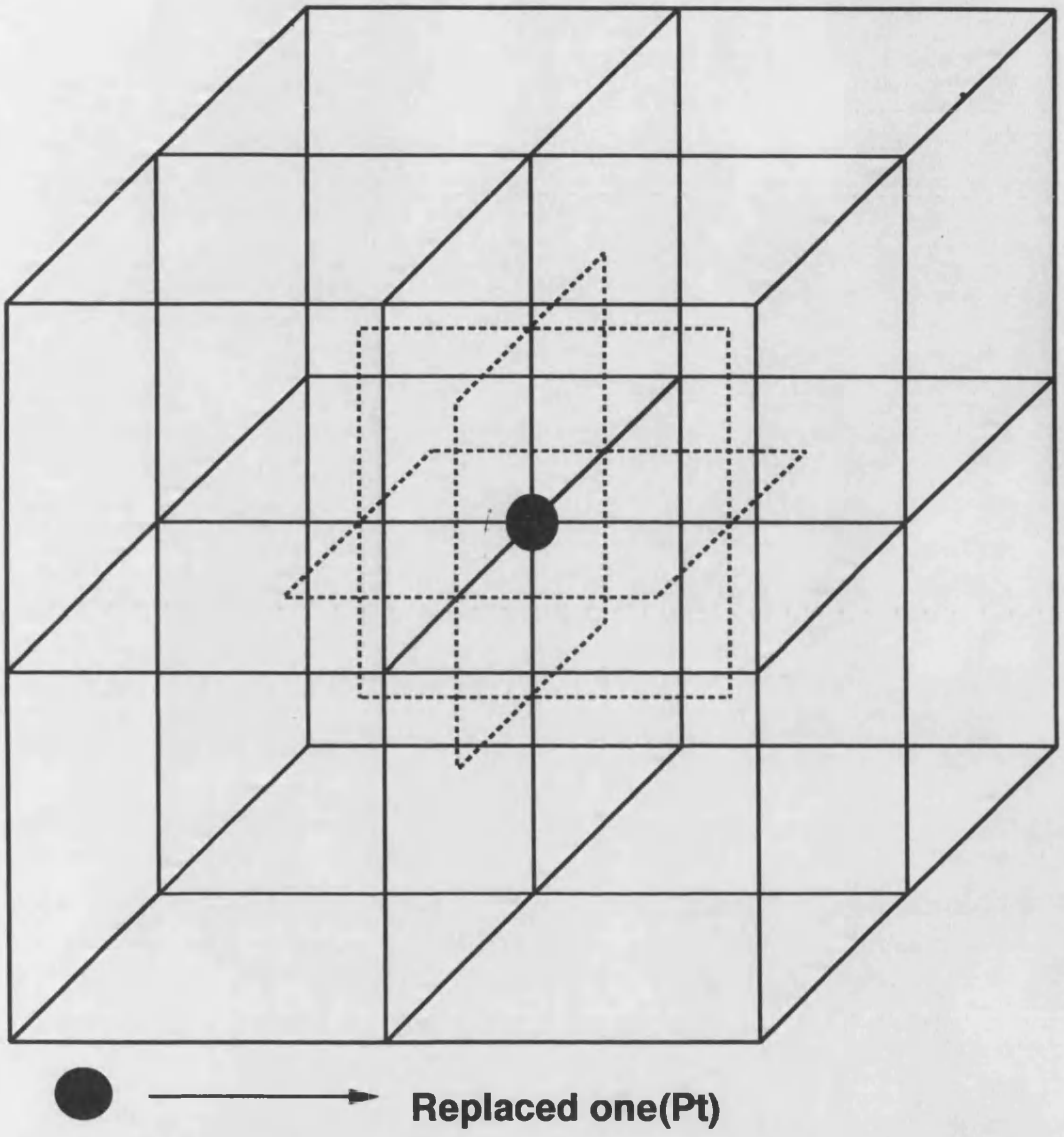

Fig. **6.22** Substitution of a Pt atom by a Mn atom

the spin-space dimension which is unused.

When we consider the diffuse scattering profile for this triangular impurity, we find scattering very similar to that found for the γ-manganese system, as depicted

in Fig(6.23). The scattering is peaked around the existing Bragg spots and indicates a susceptibility towards the TSDW state as doping is increased. This is as might be expected, since from the point of view of the local impurity, we may also consider this type of doping to be locally γ-manganese with more distant 'disorder' from the ordered platinum sites. In this picture the impurity reinstates the third dimension of the TSDW in place of eliminating it as was the case for the omission of a spin in the TSDW.

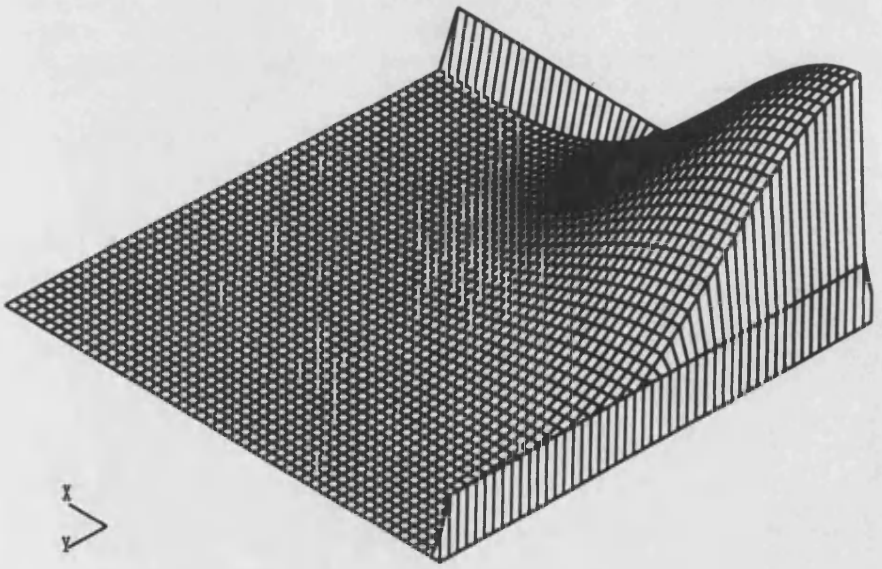

Fig 6.23 Diffuse Scattering of Mn_3Pt; Triangular Phase

The second type of impurity in this system is the substitution of a manganese atom by a platinum atom Fig(6.24). There is very little similarity to the γ-manganese system for this case. Each manganese atom has eight nearest-neighbour manganese atoms and four nearest-neighbour platinum atoms. Since all the neighbouring spin orientations are 120°, the first shell of neighbours polarise in an iden-

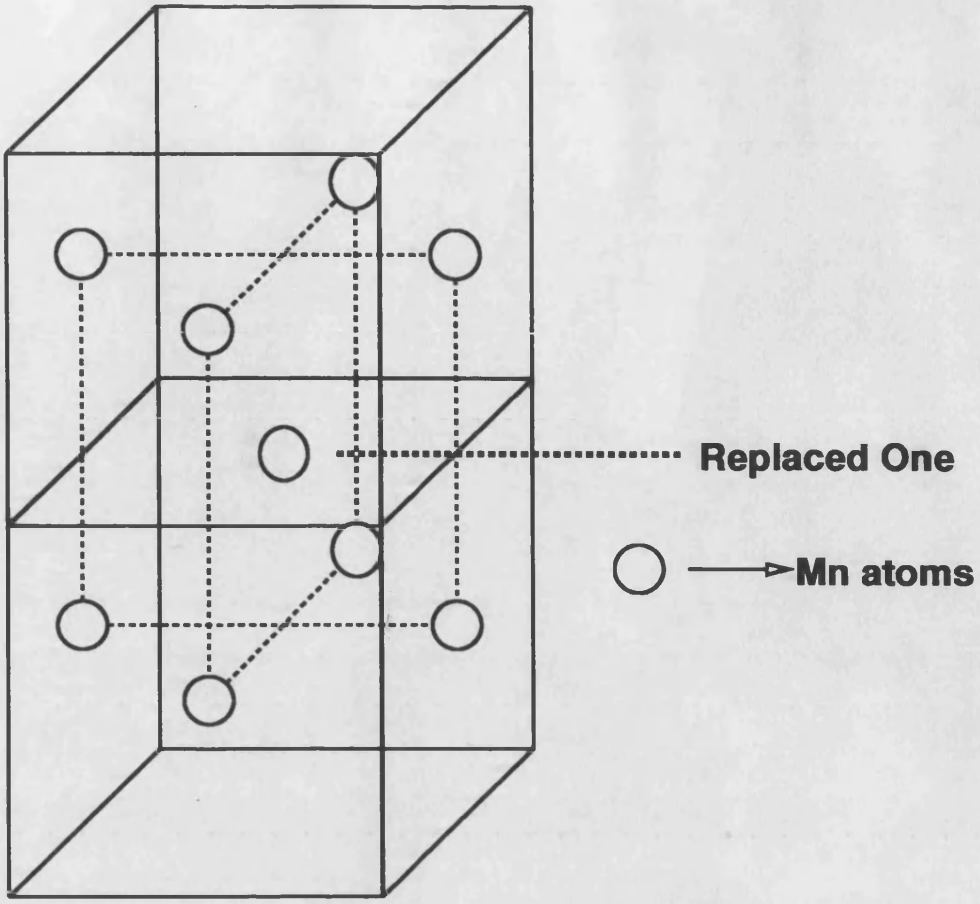

Fig. **6.24** Substitution of a Mn atom by a Pt atom

tical way when considered independently, it is only the manner in which the polarisation cloud extends to more distant neighbours which lifts the degeneracy. Since there are eight nearest-neighbours achieving 50% of the bonding, the linear term is $\delta E = \delta\lambda_\alpha^0 = 4J$. The degeneracy is lifted by the polarisation energy which is: $-0.66679\delta^2 J$ for the triangular phase and: $-0.75850\delta^2 J$ for the hedgehog phase. The experimental prediction is again clear, additional platinum atoms should stabilise the hedgehog phase. The energy saving per bond is much smaller than for the manganese substitution, being around $J/10$ per impurity. Since the polarisation only behaves differently at second nearest-neighbours, this difference is to be expected. The physical explanation for the stability fits well with our existing inter-

pretation, where omission of spins prefers more highly non-collinear phases because the polarisation can spread further, there being less parallel spins which are difficult to polarise and more options in terms of neighbours to use. The theory agrees with experiment, in the sense that the observed phase boundary points in the right direction, although we would predict a change in slope for the phase boundary at the stochiometric compound with the hedgehog phase dying out faster with manganese doping than the triangular phase does with platinum doping. There is no clear evidence for this prediction, since the experiments are rather unclear[25,27].

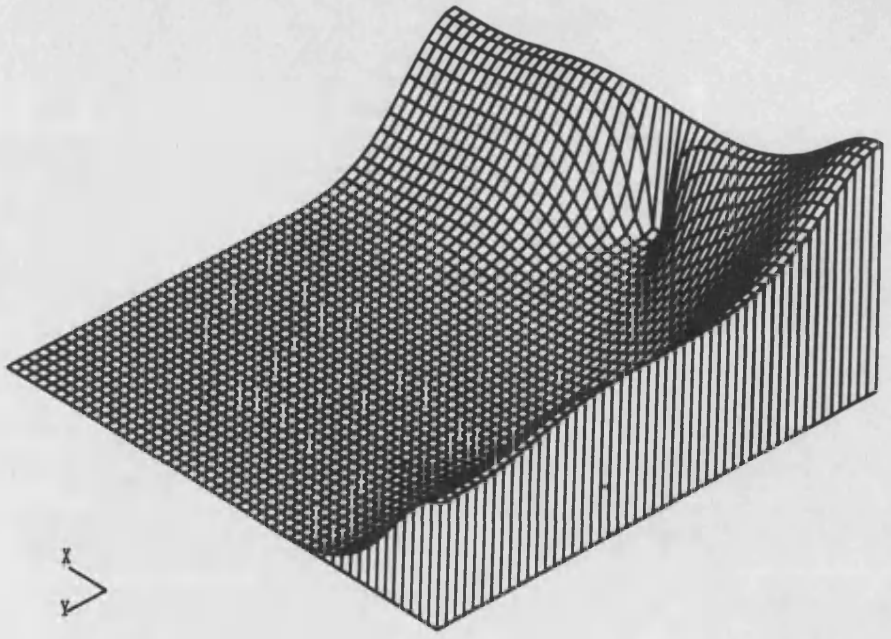

Fig 6.25 Diffuse Scattering; hedgehog phase

The diffuse scattering calculation for the impurity in the hedgehog phase yields the profile depicted in Fig(6.25). The scattering is again peaked at the type I antiferromagnetic Bragg spots, and there is a clear dip where the existing hedgehog Bragg spots sit.

6-2-3 Conclusion:

We have developed a linearised theory which approximately solves the Heisenberg model for the magnetic distortion around a local moment impurity in a non-collinear ground-state. We have looked at both total energies and induced spin densities. The theory can be applied to any non-collinear spin system. If the dominant magnetic interaction yields degenerate ground states, then this degeneracy will be lifted by weaker phenomena. Transitions between different states from a degenerate class can then be accomplished using alloying, which involves the dominant magnetic energy scale and might be expected to dominate the weaker effects which lift the degeneracy. All our calculations corroborate this basic hypothesis, with the energy scale from magnetic distortions being a sizable fraction of the original bond strengths.

We have recognised three basic impurity types: (1) The substitution of an existing magnetic atom by a paramagnetic impurity: (2) Either substitution or interstitial doping of a magnetic impurity at a local 'dead spot': (3) Either substitution or interstitial doping of a paramagnetic impurity at a site with a local field. For both (1) and (3), the doping prefers the member of the degeneracy class which has the highest degree of non-collinearity. The reason for this choice is that the polarisation cloud surrounding the impurity spreads out further and more effectively in a high dimensional spin state. As well as the obvious idea that there are less collinear spins which are difficult to polarise, there is also the idea of using rotations of different directions for different purposes, with polarisation along different paths ending up polarising in different directions, rather than cancelling out as usually happens in

coplanar states. For (2), however, we find an opposite result, with local 'dead spot' impurities preferring low-dimensional spin states. When optimising the distortion for this case, the impurity is free to take up any direction it might want. For a low dimensional spin state, it is best for the impurity to orient perpendicular to the spin state and then, since all the relative angles are 90° to the impurity field, there is no competition with the spin-magnitude constraint and the polarisability is maximum. For a three dimensional spin state there are always some spins with components parallel to the impurity spin which are less easy to polarise.

We have applied our theory to both γ-manganese alloys and Mn_3Pt. The theory successfully predicts the expected phase diagrams as far as the energetics go, with the the relevant degree of non-collinearity being either increased or decreased in agreement with the type of impurity found. The energy scale for which impurities break the degeneracy are always a small but significant fraction of the dominant antiferromagnetic coupling constant, and so we should usually expect alloying to cause phase transitions in frustrated systems with degeneracy.

Alloying non-magnetic impurities into γ-manganese is expected to destabilise the collinear ground-state in favour of the fully non-collinear TSDW state. Substition of manganese for platinum in Mn_3Pt is expected to stabilise the triangular phase and substitution of platinum for manganese is expected to stabilise the hedgehog phase.

As far as magnetic diffuse scattering is concerned, all the manganese alloys considered showed a preponderence of scattering at type I Bragg spots. This is not immediately obvious, because all the fundamental geometries considered have

ground state degeneracies which range over all the edges of the antiferromagnetic Brillouin zone which do not connect to the chemical Bragg spots. It would appear that the additional symmetry inherent to type I antiferromagnetism is favoured by paramagnetic impurities. The details of the scattering are controlled by the point-symmetry of the isolated defects that we have considered, and this symmetry will not be representative of a heavily doped system. The range of the diffuse scattering has always proved to be about a half of the Brillouin zone, and there has been no opportunity for dramatic effects.

The theory is restricted to isolated impurities, and it would be useful to extend the perturbation theory to cope with interactions between impurities, effects which will attempt to drive the phase transitions between different antiferromagnets.

6-3 MnCu Alloys

Experimentally for the case of $\gamma - Mn_{1-x}Cu_x$, large single crystal with modest, viz about 10%, concentration of impurities have been studied with diffuse scattering[36]. The results are spectacular: clustering of copper atoms occurs very strongly over a long length scale and associated with this clustering is a much-longer range antiferromagnetic impurity associated with the original magnetic symmetry, but perpendicular to the original quantisation direction as in Fig(6.26).

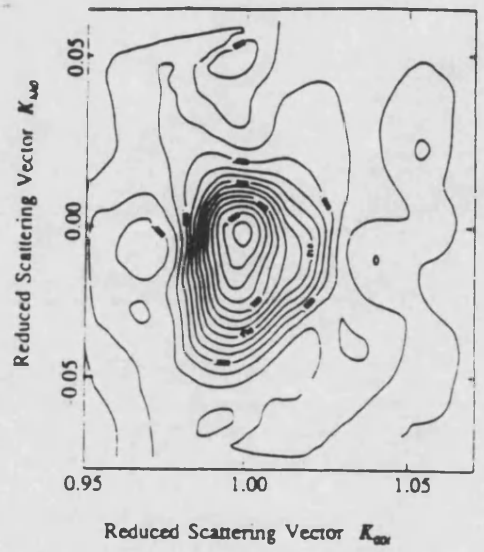

Fig 6.26 Experimental Magnetic Diffuse Scattering of MnCu

Firstly, the basic idea is that locally some of a secondary phase is trapped. This second phase is associated with scattering at new reciprocal space points which are related to the original by point group symmetries, whereas the observed scattering occurs at the original scattering centre. The scattering is miles away from where it would naively be expected. This scattering is very difficult to understand. Firstly the diffuse peak is at the original magnetic Bragg spot, suggesting that all spins are rotating together when Cu atoms are introduced. If this is the case, what does cause this rotation? One may think that the Cu atoms carry perpendicular moment, but

why they should carry perpendicular moment? We know from Chapter Three and Chapter Four that impurities trap a secondary phase. This is unlikely for MnCu alloys. The structure of MnCu is f.c.c and therefore it is totally different to the square lattice. In other words we can not explain this observed diffuse peak by using the square lattice calculations.

In order to understand this diffuse scattering in this system we elect to use the Heisenberg model, but we include a parameter, x, whose existence can be attributed to the tetragonal distortion:

$$H = \frac{J}{2} \sum_{<jj'>_-} \mathbf{S}_j.\mathbf{S}_{j'} + \frac{Jx}{2} \sum_{<jj'>_+} \mathbf{S}_j.\mathbf{S}_{j'} \tag{6.8}$$

where we assume that there is a unique collinear ground state, the first summation includes all anti-parallel bonds and the second summation includes all parallel bonds. The magnetic state which is stable finds alternating planes of 'up' and 'down' moments as we travel parallel to the z-axis as in Fig(1.2) The z-axis becomes inequivalent to the other Cartesian directions and the magnetism induces a huge tetragonal distortion. This tetragonal distortion is controlled by our parameter x which should be less then unity. Experimentally, additional copper reduces the size of the tetragonal distortion[5], and so we ought to consider the consequences of increasing x in our model.

We are interested in non-collinear distortion. We will restrict attention to planer rotations, allowing each spin to be described by an angle, ϕ_j say. In order to obtain a linear problem one must restrict attention to the moment at which an impurity becomes stable and the distortion is infinitesimal, we can effectively linearise the problem. We can then let $\Phi \rightarrow \Phi_0 + \phi$ where ϕ is the infinitesimal

change, and then

$$H \rightarrow -\frac{JS^2}{2}N(Z_- - xZ_+) + \frac{JS^2}{4}\sum_{<jj'>_-}(\phi_j - \phi_{j'})^2 - \frac{JS^2x}{4}\sum_{<jj'>_+}(\phi_j - \phi_{j'})^2 \quad (6.9)$$

where Z_- and Z_+ are the coordination numbers of antiparallel and parallel neighbours respectively ($Z_- = 8$ and $Z_+ = 4$ for face-centred-cubic). For the pure system we have translational symmetry and so we can transform to reciprocal space:

$$H = -\frac{JS^2}{2}N(Z_- - Z_+x) + \frac{JS^2}{2}\sum_k |\phi_k|^2[Z_-(1-\gamma_{k_-}) - xZ_+(1-\gamma_{k_+})] \quad (6.10)$$

where $\gamma_{k_\pm}$ are the relevant normalised structure factors (for face-center cubic, $\gamma_{k_-} = c_3\frac{(c_1+c_2)}{2}$ and $\gamma_{k_+} = c_1c_2$ in terms of $c_i = \cos(ak_i)$). We now clearly recognise a linear problem with an associated dispersion;

$$\epsilon_k = \frac{JS^2}{2}[Z_-(1-\gamma k_-) - xZ_+(1-\gamma_{k_+})] \quad (6.11)$$

from which we can define Green's function, allowing us to solve problems with local impurities present.

We now move on to impurity calculations. The impurity potential is just

$$H_{imp} = JS^2N_{imp}(Z_- - Z_+x) - \frac{JS^2}{2}\sum_{<j_{imp}j>_-}(\phi_{j_{imp}} - \phi_j)^2 + \frac{JS^2x}{2}\sum_{<j_{imp}j>_+}(\phi_{j_{imp}} - \phi_j)^2 \quad (6.12)$$

where N_{imp} is the number of impurities and j_{imp} denote their positions. It is straightforward to construct reciprocal space Green's function from our dispersion, then to transform them to real space, combine them with the impurity potential and thence find the Green's function for the system with the impurities included.

We must isolate the bound state at zero energy by choosing x to be the specific value at which a bound state first become stable, x_c say. We can quite

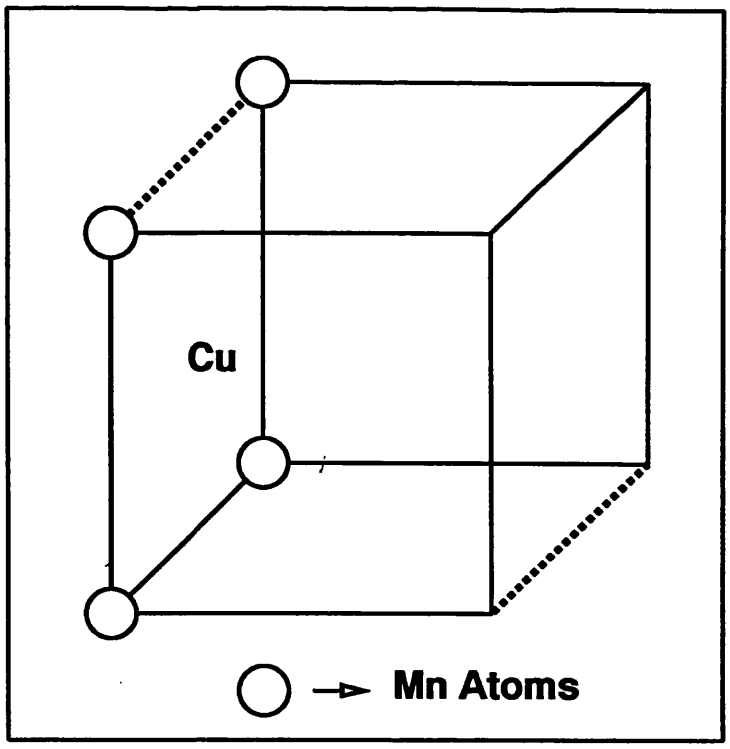

Fig. 6.27 Single Impurity

easily deduce the value of x_c for any small cluster of impurities and further deduce the wavefunction of the bound state, u_j, which satisfies

$$\sum_{j'}[H_{imp}^{-1}]_{jj'}u_{j'} = \sum_{j'}[G^0(\epsilon = 0)]_{jj'}u_{j'} \tag{6.13}$$

for a local basis on which H_{imp} is invertible.

The final technical requirement from our calculation is to deduce the form of the diffuse scattering. This can be shown to be proportional to

$$|\delta S_{\mathbf{k}+\mathbf{Q}}|^2 \alpha \frac{|u_k|^2}{(\epsilon_k)^2} \tag{6.14}$$

in reciprocal space, where $\mathbf{Q}$ is the position of the Bragg scattering from the original magnetism and u_k is the Fourier transform of the bound-state wavefunction.

6-3-1 **Results:**

For an isolated impurity as in Fig(6.27) the lowest values of x_c are 0.95546J and 0.97893J. The reason for two critical points can be understood as follows: an impurity has two nearest neighbour planes, each can be taken independent from another. After the impurities these planes play bonding and antibonding mixtures of transverse distortions trapped in the planes above and below the impurity.

Two impurities in the same z plane as in Fig(6.28) plays similar bonding and antibonding contribution. Again there are two lowest x_c points as 0.87598J and 0.91204J

Two impurities one above the other in the next nearest neighbour z planes as in Fig(6.29), the lowest values of x_c are 0,86115J, 0.96944J and 0.97088J. In this case there are three nearest neighbour planes with the intermediate plane yielding the strongly bound x_c and the two external planes yielding a weaker bonding and antibonding contribution. This way of interpreting the values of x_c is surprisingly powerful, classifying quite exotic clusters by the particular configuration of impurities which neighbour the closest pure planes.

Now let us consider the physical consequences of these results for MnCu. For pure γ-Manganese the c/a ratio is reduced by about 6% and increases to unity with increasing Copper doping[14]. The expected value of x will therefore increase from it's starting value towards unity with Copper concentration. Due to the fact that atomic overlaps are exponential, we might naively expect that the variation in x would be faster than that in c/a, and so variations of larger than 6% might be anticipated. This would in turn suggest that the possibility of a single Copper

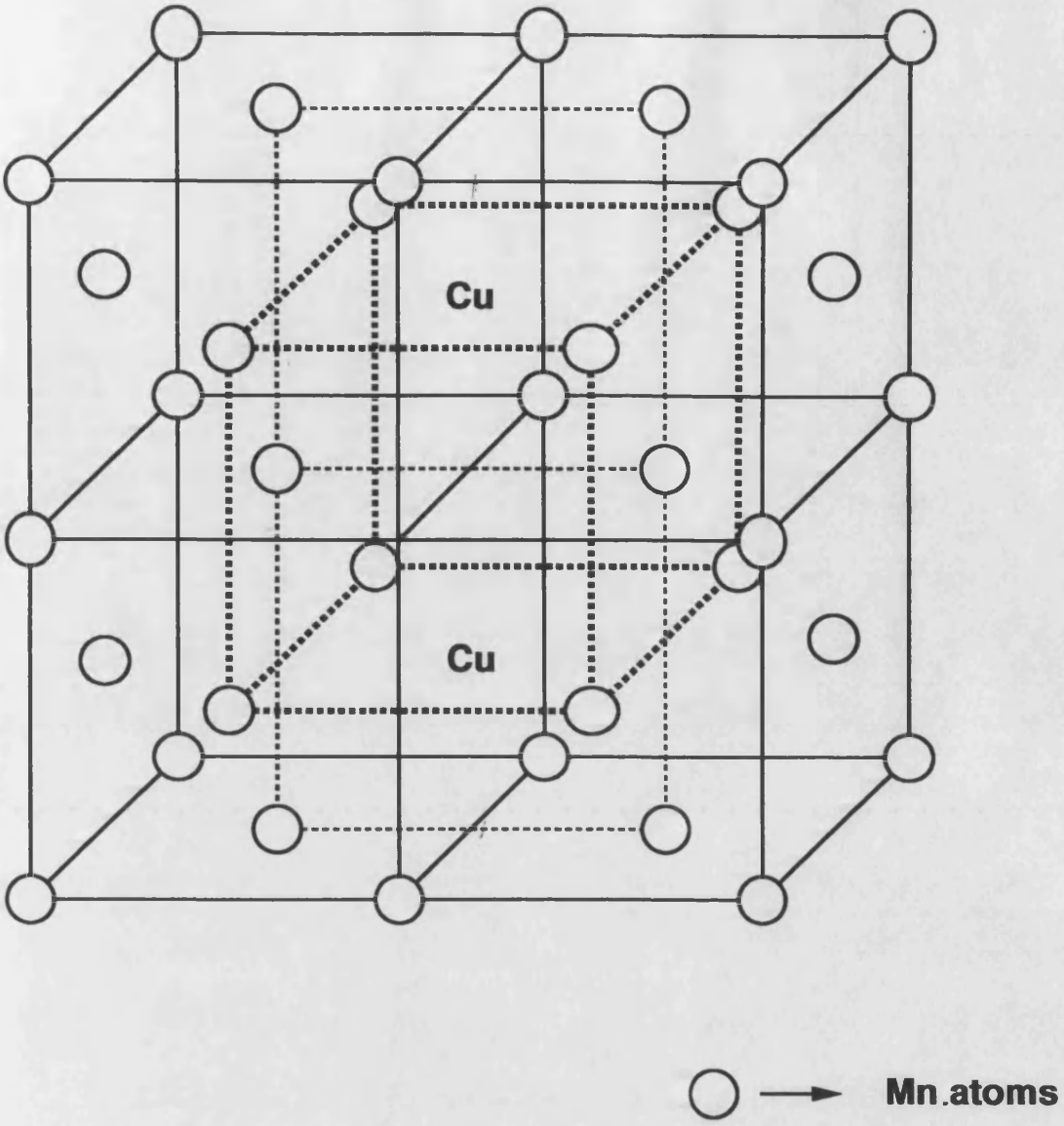

Fig. 6.28 Two impurities in the next nearest neighbour planes

atom trapping a transverse distortion is small but that a pair of nearby impurities might be able to do it. It is consequently possible that a 'phase transition', where the majority of the isolated impurities pick up moments, can be conceived of, as a function of increasing Copper concentration. It should be borne in mind that this assertion is pure conjecture.

The actual value that x_c takes up is dominantly controlled by the few spins

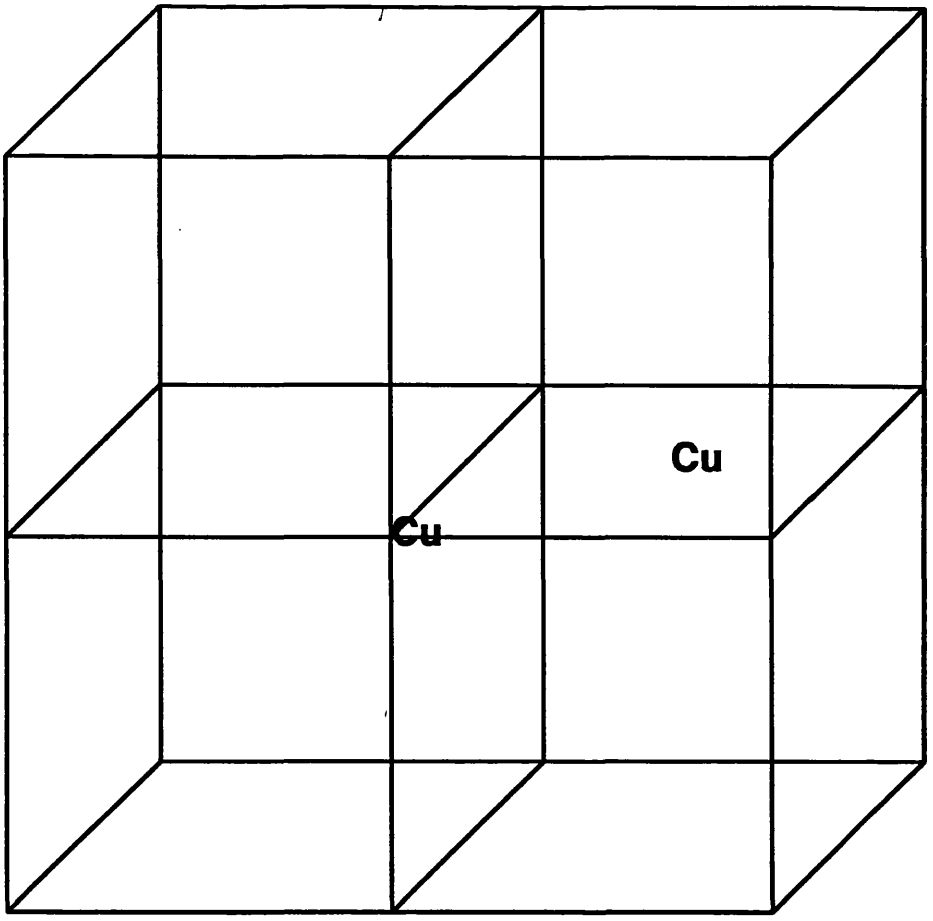

Fig. 6.29 Two Impurities in the same z plane

actually neighbouring the impurity, whereas the magnetic diffuse scattering is dominated by the longer-range tails of the non-collinear impurities which make little contribution to the energetic. Before we move onto an interpretation of what one might expect from the magnetic diffuse scattering off our impurities, firstly we will simply present some of the results. In figure 5.29 we plot the magnetic diffuse profile for the three particular impurity clusters that we have so far considered. The most obvious feature is that the first two configurations, which are more likely to be relevant for anti-clustering impurities, yield scattering as expected at the positions where the new phase appears, whereas for the third configuration, more relevant to clustering systems, there is a huge peak centred on the existing position of the

magnetic Bragg scattering. The point-group symmetries of all three clusters are

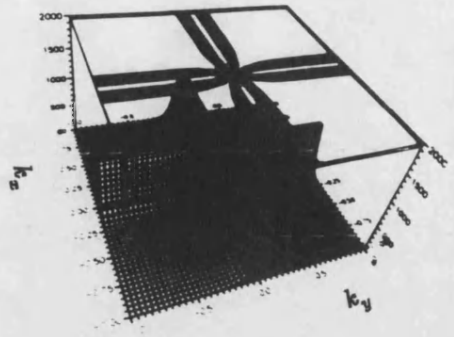

Fig 6.30a A single isolated impurity

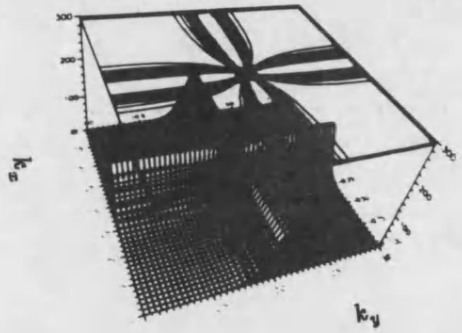

Fig 6.30b Two impurities in the next nearest neighbour planes

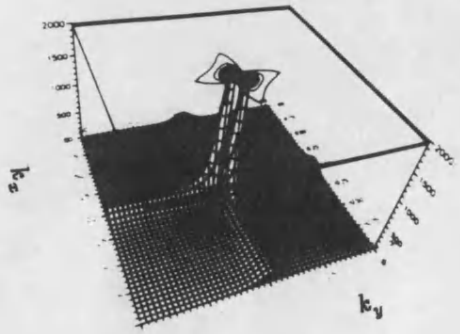

Fig 6.30c Two nearest neighbour impurities in the same plane

different from the ground-state, with the first two being antisymmetric under 90° rotations and the third being antisymmetric under 180° rotations. We have the scattering in the correct place, but not quite of the required form.

The contour plot of the magnetic diffuse scattering profile of the second cluster shows that there is a sharp peak around the magnetic Bragg spot, which corresponds to the rotation of all the spins together when the Cu atoms are introduced Fig(6.31)

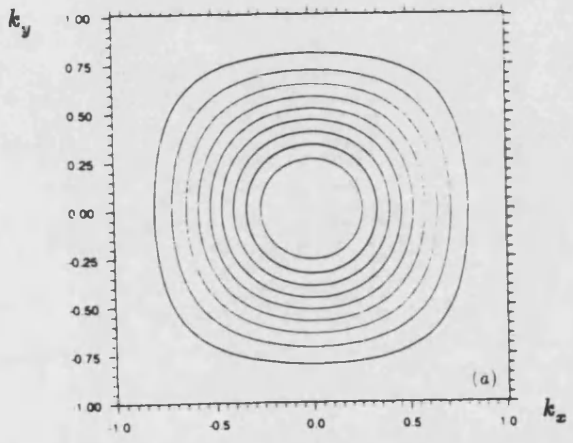

Fig 6.31a Contour Plot of magnetic diffuse scattering: 2 impurities, Clustering

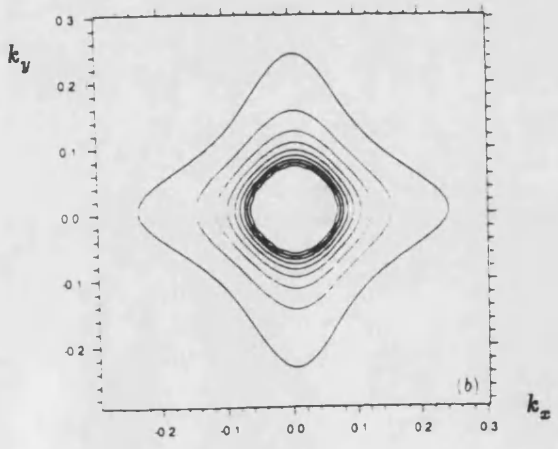

Fig 6.31b Contour Plot of magnetic diffuse scattering: single impurity

In conclusion, we have been able to predict the observed relationship between

nuclear diffuse scattering and magnetic diffuse scattering found in MnCu [30]. The clustering found in MnCu ensures that there will be a preponderance of non-collinear impurities bound to planes with nearest-neighbour copper atoms, and therefore a large amount of scattering near the original magnetic Bragg spots.

Chapter Seven

Conclusion

In this thesis we have been trying to explain the first order magnetic phase transitions in γ-Mn alloys. These alloys show a wealth of antiferromagnetic arrangements of spins as a function of doping concentration. As we mentioned earlier, pure Mn is f.c.c in which the antiferromagnetism is frustrated and this frustration leads to degenerate ground states. This degeneracy can be lifted by alloying and this leads to a possibility of a phase transition at quite modest doping. In order to model these phase transitions in a theoretical way we started with a simple case, namely the two dimensional case. It has been mentioned that somehow these two dimensional lattices are related to f.c.c.

We have used the classical limit of the Heisenberg model throughout this study and in Chapter Two we saw that the spin arrangements of the square and the triangular lattices are not unique. There is more than one spin ordering and this indicates that these lattices are non-bipartite and magnetically they are frustrated (for the square lattice case this result is obtained if the second nearest neighbour interactions are taken into account. If for example only the nearest neighbours are considered, the arrangement of spins would be unique. However, we had to take the second nearest neighbours interactions into account because the square lattices we have considered so far are special projections of f.c.c lattice where some of the nearest neighbours become next nearest neighbours in this projection.). It was pointed out that there is a phase transition as a function of x (which is the ratio of $\frac{J_2}{J_1}$). The exchange couplings J_1 and J_2 depend upon the temperature and the aim was to fix

the temperature and explain this transition in terms of alloying.

In order to investigate the effects of impurities we simply chose a cluster of collinear spin ordering at the degeneracy point and found out the ground state ordering after inputting the impurities. We saw in chapter three that the impurities remove the degeneracy and stabilise the non-collinear arrangement above a certain critical point which is called x_c. We investigated this critical point as a function of cluster size and as a function of impurity concentration. Using Green's functions, we calculated the exact value of x_c. All the results we have obtained indicated that impurities remove the degeneracy and stabilise the non-collinear arrangement as expected.

Although these results are the first indication of a first order AF-AF phase transition caused by alloying, it was not enough. In order to make sure that the alloying caused the first order phase transition we looked at the magnetic diffuse scattering studies of neutrons. The neutron is the most suitable probe for determining the magnetic structure of solids. The magnetic diffuse scattering studies give information about the fluctuations of spins. In chapter four we simply looked at these studies for different size of clusters and for different number of impurities. We saw that the symmetry of the magnetic diffuse scattering for the considered clusters are the same as the symmetry of the non-collinear arrangement. This was another evidence that the paramagnetic impurities trap non-collinear arrangement of spins and remove the degeneracy. However, the considered clusters were very small and they can not be compared with the entire crystal. In other words the phase transitions from these considered clusters do not necessarily indicates that there is a phase

transition for the considered crystal as well. In Chapter Four we said that one can talk about a possibility of a phase transition if the number of clusters is around the percolation threshold that they percolate through the entire crystal and may lead to a phase transition.

The results obtained from chapter three and chapter four showed that the model we have established explains the first order magnetic phase transition in a two dimensional square lattice. In order to make sure that our model works for real materials we had to compare our results with experiments.

In Chapter Five we develop a linearised theory for the classical Heisenberg model which allows us to approximately solve for the local distortion of spins around an impurity in a non-collinear antiferromagnet. Provided that the ratio of disturbed to undisturbed bonds is small, the theory should be applicable. The theory is particularly useful when alloying lifts the degeneracy which is often found in non-collinear magnets.

In Chapter Six we have considered three examples. The first example was MnNi alloys. This alloy shows a wealth of first order antiferromagnetic phase transition as a function of Ni concentration[19]. In order to explain the magnetic phase transition between ordered antiferromagnetic phases we paid attention to two magnetic arrangements of MnNi alloy. These two magnetic arrangements were t_2 or Single Spin Density Wave (SSDW) and t_1 or Double Spin Density Wave (DSDW). As we pointed out in chapter six, these two arrangement can be projected into the two dimensional square lattice without changing the orientations of spins. The projection of t_2 is simply the collinear arrangements of the square lattice and the

projection of t_1 is the non-collinear arrangements of the square lattice. So we have now a square lattice problem. It means that the calculations for the square lattice can be applied to these alloys. One can say that the paramagnetic impurities may cause a phase transition in MnNi alloys if the doping concentration is big enough so that it leads to a creation of many clusters (around the percolation threshold) which can interact with each other and percolate through the entire crystal leading to a phase transition. Since the alloy is MnNi, the clusters should involve a single impurity, because Ni atoms anti-cluster. It is known from Chapter Four that a cluster with a single impurity traps a non-collinear arrangement of spins. So if the created clusters are single impurity clusters then the phase transition is possible. As it was explained in Chapter Six the square lattice is not enough to explain all the observed phases in MnNi alloys. Then we applied the linearisation theory to these alloys in order to have some understanding of all the phase transitions. We saw that the phase transition occurs as a function of Ni concentration, starting from SSDW and ending up to TSDW(triple spin density wave).

The second example was Mn_3Pt alloys. These alloys show a first order phase transition between two ordered antiferromagnetic phases at around 365° K[25]. The alloy crystallises in the Cu_3Au structure with moments of about $3\mu_B$ sitting on the Mn atoms. The Pt atoms have a much smaller moment that we ignored. At low temperatures the moments order in the triangular lattice ground state as we pointed out in chapter six. Each moment is at a relative angle of 120° to each of its nearest neighbours and all the spins are coplanar. At intermediate temperatures there is a second antiferromagnetic phase characterised by twelve directions of spins as shown in Fig(6.13). In order to explain the experimentally observed first order magnetic

phase transition between two ordered antiferromagnetic phases in terms of alloying we developed a linearisation theory which alloys the spins to have an infinitesimal rotation in the presence of impurities. Then we simply replaced either a Mn by Pt or a Pt by Mn at the degeneracy point and found out the polarisation energy. We saw that the replacement of Pt by Mn makes the low temperature phase more stable, whereas the replacement of Mn by Pt makes the intermediate temperature phase more stable which is in agreement with experiments. Thus the alloying lifts the degeneracy and leads to a phase transition as we expected. We must point out here that, although we applied the linearisation theory to both MnNi and Mn_3Pt, it is more convenient to the later alloys because the structure is well ordered and so the experimentally induced compositional changes are small[25,27].

The final example was MnCu alloy. This alloy is different from the first two examples. The phase transition is not observed. Experimentally $\gamma - Mn_{1-x}Cu_x$, a large single crystal with modest, viz about 10%, concentration of impurities have been studied with diffuse scattering[30]. The results are spectacular: clustering of copper atoms occurs very strongly over a long length scale and associated with this clustering is a much-longer range antiferromagnetic impurity associated with the original magnetic symmetry, but perpendicular to the original quantisation direction as in Fig(6.26) of chapter six.

Firstly, the basic idea is that locally some of a secondary phase is trapped. This second phase is associated with scattering at new reciprocal space points which are related to the original by point group symmetries, whereas the observed scattering occurs at the original scattering centre. The scattering is miles away from

where it would naively be expected. This peak is very difficult to understand. As we explained earlier, the peak around the origin (at the original Bragg spot) says that all the spins are rotating together when Cu atoms are introduced. The detailed discussion to this point is given in Chapter Six. It is said that the structure is f.c.c and therefore totally different to the square lattice. In other words we can not apply the results for the square lattice to this alloys. In order to understand this diffuse scattering peak at the original Bragg spot, we elect to use the Heisenberg model, but we include a parameter, x, whose existence can be attributed to the tetragonal distortion.

The magnetic state which is stable finds alternating planes of 'up' and 'down' moments as we travel parallel to the z-axis as in fig(1.2) of chapter one. The z-axis becomes inequivalent to the other Cartesian directions and the magnetism induces a huge tetragonal distortion. This tetragonal distortion is controlled by our parameter x which should be less then unity. Experimentally, additional copper reduces the size of the tetragonal distortion[14], and so we ought to consider the consequences of increasing x in our model.

In order to understand the magnetic phase transition we simply look at the diffuse scattering. As we already mentioned we can explain the experimental diffuse scattering peak (fig(6.25) of chapter six) in a theoretical way by understanding the clustering of Cu atoms.

We conclude that the model we have established, can explain the first order magnetic phase transition between different antiferromagnetic phases provided that the considered system is a frustrated antiferromagnet i.e. has a degenerate ground

state. If this is the case, then the degeneracy can be lifted by alloying leading to a possibility of a phase transition..

Acknowledgements

I would like to express my gratitude to Dr. M W Long for being a very good supervisor to me. He did not only introduce me to this field and let me have part of his knowledge, but he also was a very good friend. His comments were always useful.

Many thanks to Prof. J M F Gunn, Dr. I V Lerner, Dr. D M Bird, and Prof D W Bullett for useful discussions and clarifying my understanding on many topics, to C A Hayward and P A Ewbank for helpful discussions.

Special thanks to Inonu University for the financial support.

References

[1] Slater JC; Quantum Theory Of Matters p293

(McGraw-HILL Book Company New York)

[2] L.D Landau and E.M Lifshitz; Quantum Mechanics p251

(Addision Wesley, 1965)

F. Hund;(1927)Linienspektren und Periodische System... , Springer,Berlin

(Trans. Line Spectra and Periodicity of the Elements) Chap. V

[3] A. Messiah; (1962) Quantum Mechanics Vol.II

(North-Holland Publ. Comp., Amsterdam)

[4] S. Wang; (1966) Solid-State Electronics p475

(McGraw-Hill Book Company)

[5] Krupicka s, and Sternberk J; Elements of Theoretical Magnetism

(ILIFFE Books LTD London)

[6] Martin, D.H Magnetism in Solids p280

(ILIFFE Books LTD London)

Katoni, M et al. (Edited by Flugge, S)

(Vol. XXXVII/2, Molecules, II, Springer, Berlin)

[7] Marrish, A.H; The Physical Principles of Magnetism p280

(John Wiley, New York 1965)

Martin, D.H Magnetism in Solids p298

(ILIFFE Books LTD London)

[8] Anderson P.W (1959) Phys. Rev. **115** p2

[9] Vonsovskii, S.V; 1946 Soviet Physc. JEPT (Engl. trans) **10** p468

Zener, C 1951 Phys. Rev, **81**, p440

Zener, C. and Heikes R.R 1953 Rev. Mod. Phys. **25**, p191

[10] Anderson, P.W ; Magnetism, loc. cit. Vol. I, p25.

[11] Ruderman, M.A and Kittel, C; 1954 Phys. Rev. **96** p99

Kasuya, T; 1956 Prog. Theoret. Phys. (Kyoto) **16** p45

Yosida, K; 1957 Phys. Rev. **106** p893

[12] Friedel, J; 1952 Phil. Mag. **43**, p153.

[13] Frenkel, J; 1928 Z. Phys. **49** p31.

Bloch, F; 1929 ibid **57** p545

[14] Mahan G.D; Many Particle Physics, p53

(Plenum Press-New York and London)

[15] Cowlam N, Bacon G E and Gillott L 1977 J Phys. F:Met Phys. **7** L315

[16] Henion B et al.; 1976 Proc. 2nd Int. Conf. on Neutron Scattering

ed R M Moon (New York: US Department of Commerce) p825

[17] Endoh Y and Ishikawa Y 1971 J. Phys. Soc. Jap. **30** p1614

[18] Yamaoka T, Mekata Y and Takaki H 1974 J. Phys. Soc. Jap. **36** p438

Yamaoka T; 1974 J. Phys. Soc. Jap. **36** p445

[19] Honda N, Tanji Y and Nakagawa Y 1976 J. Phys. Soc. Jap. **41** p1931

Endoh Y and Ishikawa Y; 1971 J Phys Soc Jap **30** p1614

Coles BR; 1977 Physica B+C **91** p167

Makhurane P and Gaunt P; 1969 J Phys C:Solid State **2** p959

[20] Coles BR 1977 Physica B+C **91** p167

Makhurane P and Gaunt P 1969 J. Phys. C: Solid State Phys. **2** p959

[21] Moze O and Hicks T J; 1979 J. Magn. Magn. Mater. **14** p250

[22] Uchishiba H; 1971 J. Phys. Soc. Japan **241** p223

[23] Long M W; 1989 J. Phys.:Condens. Matter **1** p2857

[24] Moze O and Hicks T J; 1982 J. Phys. F:Met.Phys. **12** p1

Long M W; 1990 J. Phys.:Condens. Matter **2** p5383

[25] Kren E et al.; 1968 Phys. Rev. **171** p544

[26] Long M W; 1992 Int. J. Of Modern Phys. B (to appear)

[27] Kren et al.; 1967 J. Appl. Phys. **38** p1265 and [25]

[28] Long M W; 1991 J. Phys.:Condens. Matter **3** p7091

[29] Gaulin B D, Spooner S and Morii Y; 1987 Phys. Rev. Lett. **59** p668

[30] Moze O and Hicks T J; 1992 Phys. Rev. B **46** p915

Tsunoda Y and Cable J; 1992 Phys. Rev. **46** p930

[31] Heisenberg W; 1928 Z. Phys. **49** p619

[32] Fehrenbacher R; 1990 Diplomarbeit, Bodensee Universitat Konnstanz p21

[33] Koester L; 1977 Springer tracts in modern physics, **80**

(Springer-Verlag, Berlin.)

[34] Lovesey S.W; Theory of Neutron Scattering from Condensed Matter

(Clarendon Press. Oxford)

Binney J J, et al.; 1992 The Theory of Critical Phenomena

(Clarendon Press. Oxford)

[35] Long M W and Bayri A; 1993 J.Phys.: Condens Matter **5** L15

[36] Kouvel J S and Kasper J S 1963 J. Phys. Chem. Solids **24** p529

Cade N A and Young W 1977 Adv. Phys. **26** p393

Hirai K and Jo T 1985 J. Phys. Soc. Japan **54** p3567

Long M W and Yeung W 1987 J. Phys. C: Solid State Phys. **20** p5839

[37] Lowde Rd, Harley Rt, Saunders GA, Sato H, Scherm R and Underhill C;

1981 Proc Roy Soc **A74** p87

[38] Long M W and Moze O; 1990 J. Phys. Condens Matter **2** p6013

Long M W; 1990 J. Phys.:Condens. Matter **2** p5383

[39] Crockford D J, Bird D M and Long M W;

1991 J. Physc. Condens matter **3** p8665

Duschanek H et al 1989 Physica B **161** p139

Kubler J, Hock K H, Sticht J and Williams A R;

1988 J. Phys. F: Met. Phys. **18** p 469

Sticht J et al 1989 J. Phys. Condens. Matter **1** 8155

Jo T and Hirai K; 1986 J. Phys. Soc. Japan **55** p2017

Jo T and Hirai K; 1984 J. Phys. Soc. Japan **53** p3183

[40] Samson J H; 1983 Phys. Rev. B **28** p6387

Chana K S et al 1991 J. Phys. Condens. Matter **3** p6455

Heine V et al 1981 J. Phys. F: Met. Phys. **11** p2645

[41] Long M W and Bayri A; 1993 in preparation